LIQUID AIR ENERGY STORAGE: PROCESS OPTIMIZATION AND PERFORMANCE ENHANCEMENT

By

Xiaodong Peng

A thesis submitted to the
University of Birmingham for the
Degree of Doctor of Philosophy

School of Chemical Engineering
College of Engineering and physical Sciences
The University of Birmingham
September 2018

The candidate confirms that the work submitted is his own and that appropriate credit has been given where reference has been made to the work of others.

Abstract

Energy Storage (ES) technologies have a crucial role in electric power networks as they offer remarkable abilities, which enable them to be widely employed to meet the electricity demand-supply mismatch, as well as the intermittent renewable energy sources. Among all technologies, Liquid Air Energy Storage (LAES) aims to large scale operations and has caught the attention of many researchers from the past decade, but the situation is getting more challenging due to its disappointed performance in the current configuration. Therefore, there are urgent needs for the performance improvement to keep the superiority of the LAES in the electricity market.

This thesis concerns the current LAES and the improved LAES technologies, both of which use cryogen (specifically liquid air/nitrogen) as energy carrier for large scale utilizations in power networks. The aim of this study is to increase the system performance of the LAES technology, particularly through developing novel thermodynamic cycles for an increased use of the thermal energy and system optimisation strategies. Experiential results from the LAES pilot plant bring specific issues, which is used to understand possible ways to improve the performance of the LAES. In a standalone LAES configuration, there is ~20-45% of the hot energy generated during the LAES operating which cannot be efficiently used, while the lack of the high-grade cold energy usually occurs, leading to a lower liquid air yield. These thermal energy issues provide an opportunity for increasing the round trip efficiency of the LAES, and hence numerous integrated LAES systems are investigated.

To effectively use the hot sources and hence improve the system performance, three integrated LAES systems are proposed, namely LAES-ORC-VCRC system, LAES-ORC-ARC system and LAES-ORC system. The LAES-ORC-VCRC system consists of a traditional LAES, an Organic Rankine Cycle (ORC) and a Vapor Compression Refrigeration Cycle (VCRC). The LAES-ORC-ARC system drives the Absorption Refrigeration Cycle (ARC) with NH_3-H_2O as the working

medium. Both the VCRC and ARC are used to generate low-temperature cold sources for the ORC cooling. The LAES-ORC system has the simplest configuration but gives the best performance among these three configurations. It is found that all these integrated LAES systems provide obvious improvements to different extents.

External cold sources, such as LNG, can be used to enhance the LAES efficiency, and hence two integrated LAES systems, the LAES-LNG and the LAES-LNG-CS systems are investigated. Both of them extract cryogenic energy from the LNG evaporation for the enhancement of both the air liquification rate and the round trip efficiency. The LAES-LNG system obtains the cold energy directly from the LNG while a cold store (CS) unit is used in the LAES-LNG-CS system to address the instability of the LNG regasification. Thermodynamic analyses show that the LAES-LNG system provides around 15-35% more round trip efficiency than the current stand-alone LAES system, and liquid air yield obtains a significant improvement up to 0.87. Compared with the LAES-LNG system, the LAES-LNG-CS system can produce more electric energy with less amount of LNG.

Acknowledgements

I would like to express my great appreciation to Professor Yulong Ding for the tremendous and continuous guidance of my Ph.D. study. He is the man leading me into the fascinating scientific fields of energy storage. I cannot imagine a better supervisor in my Ph.D. research. It is an honour to have my doctoral training under his patience and advice.

I would also like to express my gratitude to my co-supervisor Dr. Yongliang Li, for caring very much about my work, being so dedicated to his role as my co-supervisor.

I am very grateful to Dr. Xiaohui She. I have been felt extremely thankful for sharing his expertise selflessly. He always helps and inspires me in my Ph.D. study.

A special thanks to my colleagues and visiting scholars in Birmingham Centre for Energy Storage (BCES), Dr. Hui Cao, Dr. Helena Navarro, Dr. Guanghui Leng, Dr. Geng Qiao, Dr. Chuan Li, Mr. Yaoting Huang, Mr. Daniel Smith, Prof. Chun Chang, Prof. Hao Peng, Prof. Yaxuan Xiong and everyone in BCES. It was fantastic for me to have the opportunity to work with all of you.

Finally, a sincere gratitude from deep inside to my family. To my father, thanks for providing me the motivation, sharing your experience willingly. To my mother, thanks for the continues encouragement throughout my work and life. To my sister, thanks for your unfailing support to me. To my beloved girlfriend Ms. Rui Wang, thanks for your unselfish accompany and support since the beginning.

Table of Contents

List of Figures

List of Tables

Abbreviations

ARC	Absorption Refrigeration Cycle
C3MR	propane precooled Mixed Refrigerant cycle
CAES	Compressed Air Energy Storage
CES	Cryogenic Energy Storage
CS	Cold Store
DMR	Dual Mixed Refrigeration
GLU	Gas Liquefication Unit
HEN	Heat Exchanger Network
LAES	Liquid Air Energy Storage
LNG	Liquefied Natural Gas
LPG	Liquefied Petroleum Gas
MAT	Minimum Approach Temperature
MGT	Mirror Gas-Turbine cycle
MHHP	Metal Hydrides Heat Pump
MRC	Mixed Refrigerant Cycle
NPP	Nuclear Power Plant
ORC	Organic Rankine Cycle
PHS	Pumped Hydro Storage
PLU	Power Recovery Unit
SMR	Single Mixed Refrigerant cycle
TES	Thermal Energy Storage
VCRC	Vapor Compression Refrigeration Cycle

Nomenclature

C	Capital cost
C_p	Isobaric heat capacity (kJ/kg·K)
E	Exergy input/output (kJ)
e	Exergy (kJ/kg)
h	Enthalpy (kJ/kg)
$\dot{m}$	Mass flow (kg/s)
NPV	Net present value
P	Pressure (kPa)
PV_I	Present value of investments
PV_S	Present value of savings
Q	Heat load (kJ)
q	Heat flow (kJ)
R	Ratio
S	Entropy (kJ/kg·K)
SIR	Savings to investment ratio
SPP	Simple payback period
T	Temperature (K)
W	Work (kJ)
Y	Liquid air yield
η	Proportion/efficiency
N	Number of years
r_d	Discount rate
r_{in}	Inflation rate

AS	Annual savings
Res. Val.	residual value of the equipment

Subscripts

air	Air
B	Brayton cycle
C	compressor
c, ch	Charging process
d, dis	Discharging process
e	Evaporation/evaporator
E	Evaporator
ex	Exergy
gen	generator
in	Input/inlet
out	Output/outlet
P	Pump
rank	Rankine cycle
RTE	Round trip efficiency
T	Turbine
vap	Refrigerant in VCRC

Chapter 1 Introduction

1.1 Background

Increased worldwide electricity demand and environmental issues have motivated the development of alternative technologies for using renewable resources (hydropower, wind, solar, biomass, tide) to replace the fossil fuels (coal, oil, natural gas) [1,2]. Between 2017 and 2022, the renewable electricity capacity has been forecasted to expand by over 920 GW, with an increase of 43%, therein, China, US and India will account for two thirds of global renewable expansion by 2022 [3]. In China, renewable generation sectors are under construction which will share 36% of all global hydro electricity generation, 40% of world wind generation and 60% of solar PV generation over 2015-2021 [3,4]. The REmap analysis indicates that the share of renewable energy mix in the US will expand to 27% by 2030 through the wind, PV, CSP, biomass and hydro technologies [5]. India has taken a leading role in the renewable energy transformation both regionally and globally, and the REmap analysis indicates that the wind power capacity would reach 185 GW, and the solar PV capacity would increase to approximately 200 GW in India, leading to the potential share of the renewable energy to 60% by 2030 [3,6]. In the European Union, renewable energy, accounting for 80% of new capacity, and wind power is predicted to become a leading source of electricity after 2030 [7]. In the context of the targets proposed by the UK Government, the renewable resources would meet 30% of the primary UK electricity demand by 2020. According to the increased levels of electricity production and demand driven by electrification of heat and transport, it is expected that the electricity sector should be almost entirely decarbonised by 2030 [8]. Figure 1.1 illustrates the global average annual net capacity additions by different resources [7]. One can see that significant efforts have been and continue to be made in increasing the renewable resources penetration.

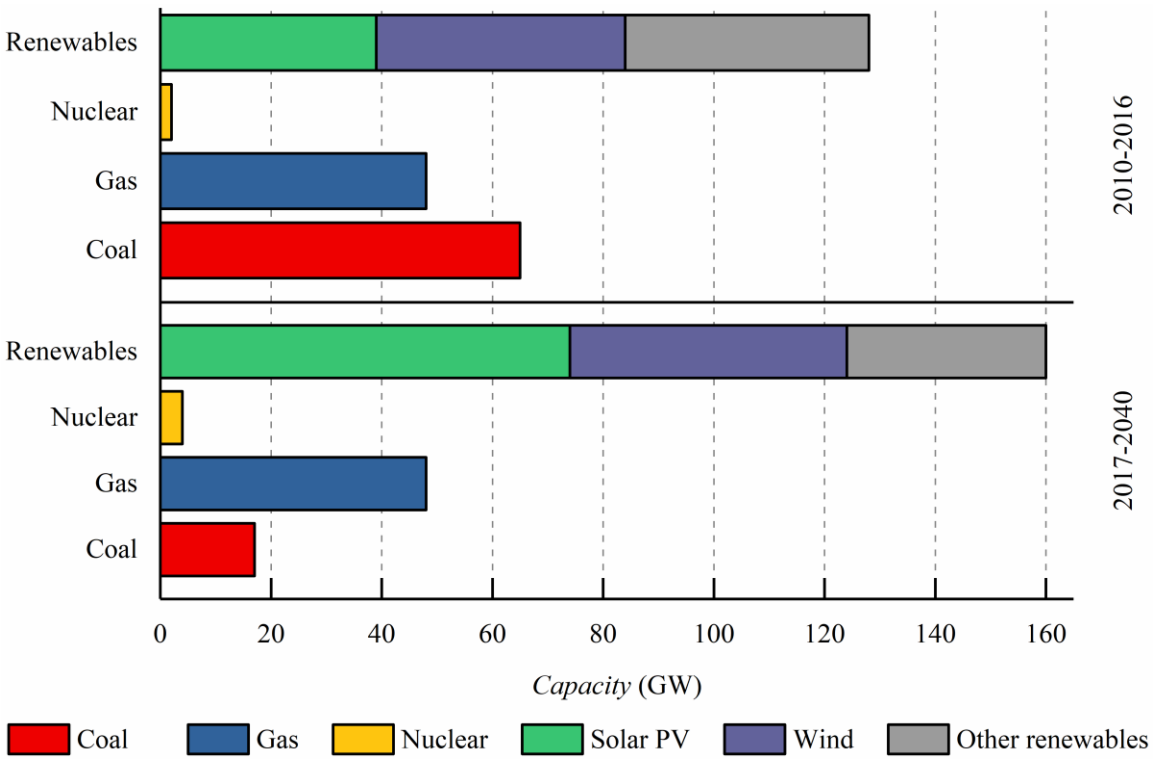

Figure 1.1 Global average annual net power capacity additions by types from 2010 to 2040.

However, the increased utilization of renewable energy faces significant challenges. First, the renewable generation is less predictable due to its nature of intermittence. Solar PV panels or solar collectors require suitable solar radiation which is only possible on daytime and sunny days. Wind turbines need wind to rotate the blades; hydro generation relies on water to fill up and maintain the reservoir. Second, there is significant mismatch between the time-dependent demand of the end-users and the intermittent supply of the renewable energy. Third, the fluctuating renewable energy supply can impact on the state of frequency equilibrium of electricity networks without an extra reserve capacity, particularly when the renewable penetrations exceeds ~10-20% of the total load [9–12].

The mismatch challenge described above becomes more grave due to significant demand changes over different time scales. Figure 1.2 shows the UK electricity demand as a function of time over a 24-hour period, metered half-hourly by the National Grid in 2017 [13]. One can see that there are

significant differences between summer and winter, weekdays and weekends, particularly peak time and off-peak time in a day. The above challenges can be partially addressed by energy storage technologies, for example, the transient fluctuation can be smoothed out by rapid response supercapacitors, batteries or flywheel technologies to maintain the power quality and reliability of an electricity grid [14], whereas the load shifting, over hourly level period or a larger, can be met by the Pumped Hydro Storage (PHS), Compressed Air Energy Storage (CASE) and Liquid Air Energy Storage (LAES).

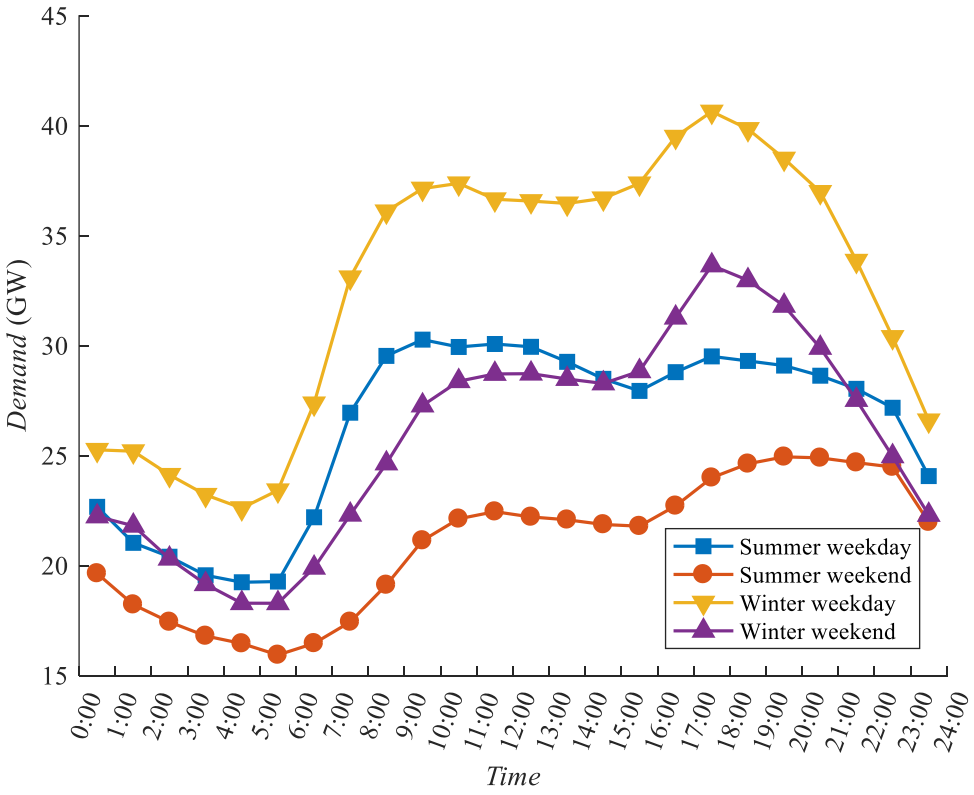

Figure 1.2 Electricity demand profile of UK in 2017 [13].

In the electricity market, prices at peak time often leads to a higher cost to the end-users as a higher demand would strain both the available power generation infrastructure and power transmission infrastructure [15]. In the US, the electricity price at peak time is approximately 3 times more expensive than that at off-peak time; see Table 1.1 [16]. The huge price differences make energy

storage technologies attractive to resolve the mismatch challenge by shifting the peak-load [17], thereby reducing the cost of electricity. Meanwhile, the base load generators can be operated under a steady working condition for most of the time, which can help extend the life-span of the installations.

Table 1.1 Electricity price for US residential customers in 2017 [16].

	Time periods	Price ($/kWh)	
		Winter (Oct.1-May 31)	Summer (June 1-Sept.30)
Off-peak	9 p.m. to 10 a.m. & weekends	0.07516	0.07516
Peak 1	10 a.m. to 1 p.m.	0.23665	0.26429
Peak 2	1 p.m. to 6 p.m.	0.23665	0.28672
Peak 3	6 p.m. to 9 p.m.	0.23665	0.26429

As briefly mentioned above, energy storage technologies provide an avenue to meet the energy supply and demand through the chain of generation, transmission, distribution and end use. Such technologies store the energy in a form that can be either directly used later on or converted into a form that is needed [14,18]. Note that the definition of energy storage is specifically for electrical energy storage, i.e. electrical energy in, electrical energy out. The use of energy storage gives more flexibility on top of other function such as peak shaving, intermittency smoothing and backup generation for electrical networks. There are many energy storage technologies and they can be broadly grouped into the following categories: [14]

- Chemical energy storage, e.g. batteries, hydrogen;
- Mechanical energy storage, e.g. compressed air, pumped hydro, flywheels;
- Thermal energy storage, e.g. sensible heat storage, latent heat storage.

This work concerns Liquid Air Energy Storage (LAES) which is a Thermal Energy Storage (TES) technology and is often termed the Cryogenic Energy Storage (CES) in some literature articles. LAES uses intermittent renewable sources or off-peak electricity to produce liquid air in an air liquefaction (charging) process; the stored liquid air is pumped to a high pressure, heated by a heat source to expand in air turbines to generate electricity in a power recovery (discharging) process. It is mainly for large scale operation, and has attracted significant attention in recent years due to high energy density, a highly competitive capital cost, low maintenance and operational costs, a long life span, no geographical constraints and environmental friendliness [14,19]. The estimated round trip efficiency of the LAES is ~60% using the current configuration. There is therefore a great drive to enhance the round trip efficiency. This forces the main motivation for this Ph.D. study.

1.2 Aims and Objectives

The aim of this study is to increase the round trip efficiency of the LAES technology, particularly through developing novel thermodynamic cycles for an increased use of the thermal energy and system optimisation strategies.

The specific objectives of this study include:

(1) To develop a model for a standalone LAES system and obtain an optimal operation conditions for practical implementation of the LAES technologies.

(2) To perform experiments on the LAES pilot plant and compare the results with the model simulation results.

(3) To study the conversion processes of thermal energy (heat & cold) during the operation of the LAES, and to understand possible ways to improve the performance of the LAES.

(4) To study the LAES efficiency enhancement through integration with processes/cycles, including Organic Rankine Cycle (ORC), Vapor Compression Refrigeration Cycle (VCRC), Absorption Refrigeration Cycle (ARC) and Liquefied Natural Gas (LNG) evaporation process.

1.3 Layout of the Thesis

This thesis consists of 6 Chapters. Chapter 2 gives a summary of the literature closely related to the LAES technologies where the key factors affecting the round trip efficiency, exergy efficiency and other performance indicators of the LAES are also discussed.

Chapter 3 introduces the thermodynamic model and optimisation of complex power/thermal systems, including a generalized method using the Superstructure and Pinch Technology for process and system optimisation.

Chapter 4 presents the experimental results of the world first 350 kW /2.5 MWh LAES pilot plant, as well as the modelling results of a standalone LAES system.

Chapter 5 analyses the enhancement of round trip efficiency enhancement of the LAES through integration with Organic Rankine Cycle (ORC) and Vapor Compression Refrigeration Cycle (VCRC), including an economic analysis on those integration systems.

Chapter 6 considers two different configurations of the integrated LAES with Organic Rankine Cycle (ORC) including optimisation and comparison.

Chapter 7 studies the integration of a large scale LAES plant with LNG terminals, considering two configurations of with and without cold store.

Chapter 8 summaries the main conclusions from this study and gives recommendations for future work.

Chapter 2 Literature Review

This Chapter will briefly explain the principle of the LAES technologies (Section 2.1). The focus is on a summary of the relevant literature closely related to the LAES technologies. This includes gas liquefaction (Section 2.2) and power recovery (Section 2.3); specific configurations and their advantage and disadvantages of those processes and methods to improve the performance of the LAES (Section 2.4). finally, a summary of the literature review is given (Section 2.5).

2.1 Principle of Liquid Air Energy Storage (LAES)

The basic principle of the LAES is shown in Figure 2.1, which consists of a charging cycle and a discharging cycle. The charging cycle, also referred to as a gas liquefication process, runs at off-peak times: the purified air is compressed to a high pressure through multistage compression with compression heat recovered and stored in a heat storage medium, such as thermal oil, hot water or glycol; the compressed air is then cooled in a cold box by recycling air and cold storage medium, such as liquid-phase materials (propane and methanol) and solid-phase materials (rocks and pebbles), containing cold energy recovered from liquid air in the discharging cycle; finally, liquid air is obtained through air expansion in e.g. a cryo-turbine and stored in a liquid air tank at approximately 77 K. The discharging cycle, also known as the power recovery process, works at peak times: the liquid air flowing from the tank is pumped to a high pressure, and then releases cold energy to the cold storage medium in evaporators, which are later used to cool the compressed air in the charging cycle; the air is then heated up by the heat storage medium containing heat recovered in the charging cycle before entering air turbines to generate electricity [20,21]. The details of the gas liquification process and power recovery process will be reviewed in Sections 2.2 and Section 2.3, respectively.

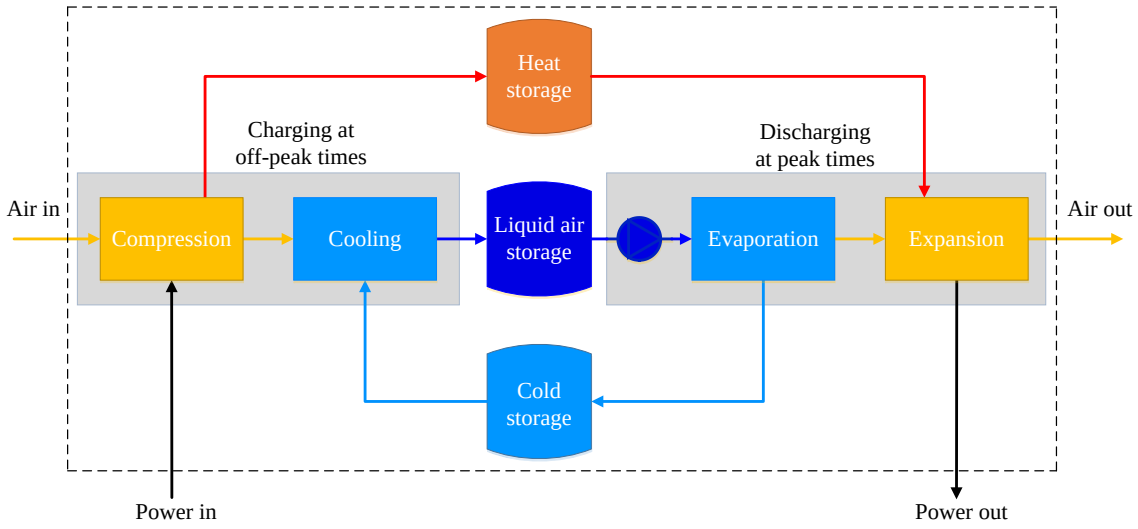

Figure 2.1 Schematic diagram of the basic principle of the LAES.

The use of liquid air as an energy storage medium can be dated back to 20th century, whereas the peak-shaving of a power grid using liquefied air was first proposed by the University of Newcastle upon Tyne in 1977 [22]. The initial idea was to develop the electrical energy storage with a much smaller storage volume than the conventional compressed air energy storage (CAES) system. Subsequent studies, both numerically and experimentally were done by several industrial companies, including Mitsubishi Heavy Industries [23,24] in later 1990s, Hitachi [25–27] in early 2000s, Expansion Energy LLC [28] around 2011. Mitsubishi Heavy Industries proposed a test scale pilot plant to verify the performance of the LAES generator, leading to a relatively low round trip efficiency [23]. The work by Hitachi was focused on integrating LAES system with a regenerator to improve the gas liquification and power generation efficiency. The results from Hitachi indicated that a round trip efficiency of ~70% would be possible for the LAES system as long as the regenerator was efficient [25–27]. Substantial progress in the LAES technology development was done due to a collaborative research between the University of Leeds and Highview Power Storage Ltd from 2005. This collaborative research contributed to the design and construction of the world's first LAES pilot plant (350 kW/2.5 MWh) between 2009 and 2012 [20]. This pilot facility was donated to the University of Birmingham for further research in 2013.

2.2 Gas Liquefaction Process (Charging Cycle)

Gas liquefaction is one key process of the LAES system. A suitable liquefaction process can significantly improve the production, and consume less electric energy at the same time. Gas liquefaction is a process by which the gas is refrigerated to the temperature under its critical point to form a liquid phase at a suitable pressure. As the volume is usually decreased radically from gas phase to liquid phase, which is convenient for gas storage and transportation, liquefaction process is widely used in industrial, medical, biological fields, superconductivity research and in aerospace engineering [29,30]. Some gases, such as carbon dioxide, can be liquefied at atmospheric pressure through simply cooling and pressuring. At a temperature above the critical point, a substance exists in the gas phase only, such as helium, hydrogen and nitrogen whose critical temperature are -268℃, -240℃ and -147℃, respectively [31]. Ordinary refrigeration technologies cannot create such a low temperature environment. Several cycles are therefore needed, such as Linder-Hampson cycle, Cascade refrigerant cycle, mixed refrigerant cycle and expander cycle.

2.2.1 Linder-Hampson cycle

The Linder-Hampson cycle was first proposed by William Hampson and Carl von Linde and was independently patented in 1895 and also be termed the Joule-Thomson (JT) liquefier [32]. The schematic and the *T*-*S* diagram of the Linder-Hampson cycle is shown in Figure 2.2. The purified gas, which is mixed with the uncondensed portion of the gas from the previous cycle, is first compressed by an isothermal compressor (State 1-2); the pressurised gas flows into a counter-flow heat exchanger and is cooled by the uncondensed portion of the gas (State 2-3) and is then depressurised by a Joule-Thomson valve typically (State 3-4). The vapour-liquid mixture is produced after the depressurisation process, therein, the vapour portion of the product is returned to the heat exchanger to cool the high-pressure gas (State 5-1) and then mixed with the purified gas, while the liquid portion is left in the reservoir. Many efforts have been made to improve the performance of the Linder-Hampson cycle. Maytal [33,34] optimized a Linde-Hampson cycle in

terms of the cool-down periods and the maximum liquid rate. He used nitrogen and argon in the experiment and observed that the cool-down period as a function of the setting pressure in the cycle and the resulting flow rate would short the cooldown period; moreover, the optimal mass flow was also determined with the same heat exchanger to maximum the liquid production. Holland et al. [35] presented a small-scale demonstrator and optimized the heat exchanger leading to a minimum temperature of 82 K.

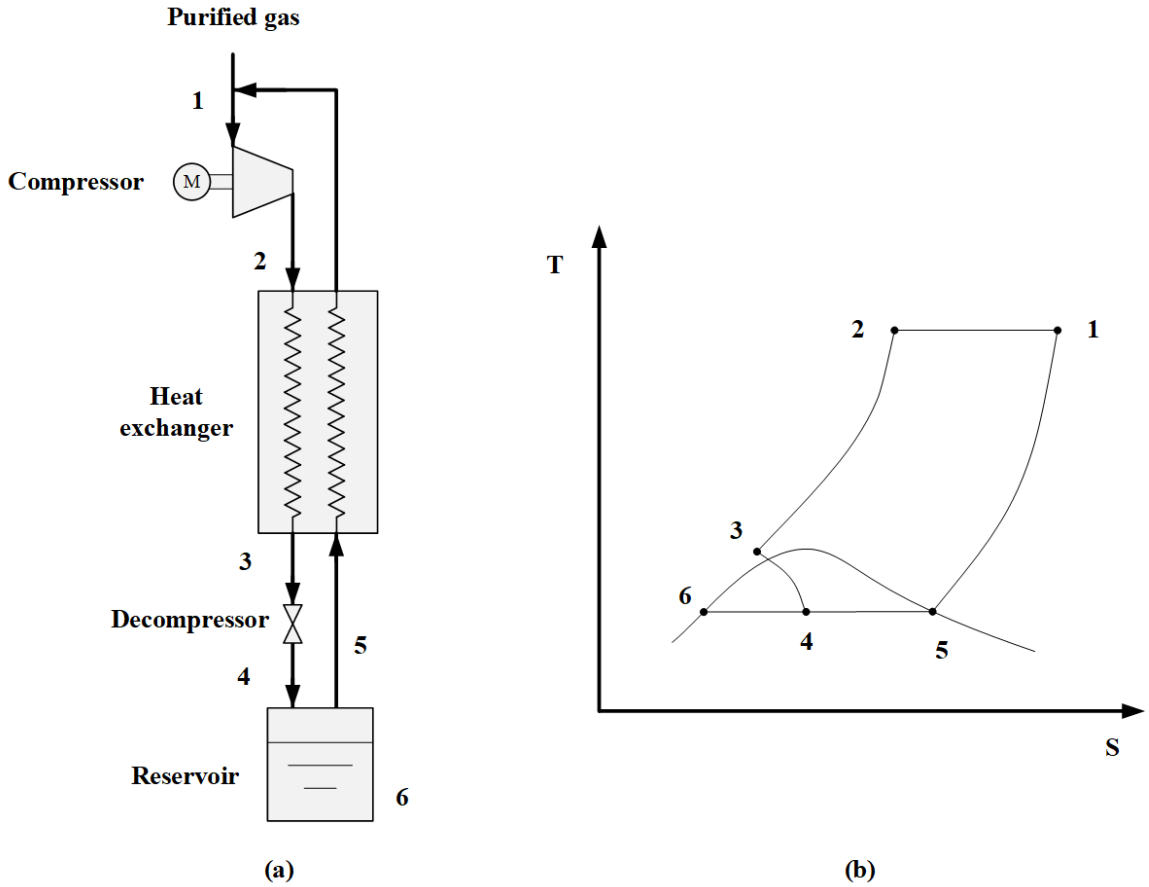

Figure 2.2 Principle of Linder-Hampson cycle: (a) schematic diagram; (b) *T*-*S* diagram.

The advantage of Linde-Hampson cycle is that the configuration is sample and there are no moving parts at the cold end of the heat exchanger. However, many references have claimed that the actual exergy efficiencies of the Linde-Hampson liquefaction cycles are usually under 10% [31,34,36]. The main reasons for the poor thermodynamic performance of the Linde-Hampson cycle include:

- irreversible exergy losses of the throttling expansion process;
- mismatch of the temperature profile between the pressured gas and the returning gas.

The cooling load provided by the vapour portion of the mixture can merely refrigerate a very small fraction of the main mass flow in the heat exchanger. The large temperature difference in the heat transfer process keeps the system away from the thermodynamic reversibility, leading to the low thermodynamic efficiency.

In order to improve the performance of the liquefaction processes, the subsequent liquefication technologies use multiple or mixed refrigerants to cool the pressured gas stage by stage to obtain a better temperature profile match. These include cascade refrigeration cycles and mixed refrigeration cycles, or the use of multiple compression and expansion processes with a single refrigerant instead of the throttling process to generate cold energy.

2.2.2 Cascade refrigeration cycle

The cascade refrigeration cycle offers an additional degree of freedom for temperature profile optimization by choosing a suitable combination of refrigerants [37]. Such a cycle gives a better performance compared to the Linde-Hampson cycle, but its configuration is also more complex: multiple sub-cycles of the cascade cooling are used to create different low-temperature levels with suitable refrigerants, providing a better matched temperature profile. There are many potential options of the refrigerants, such as propane, ethane, methane and nitrogen. Figure 2.3 shows a three-sub-cycle cascade refrigeration cycle using propane, ethane and methane as refrigerants for LNG liquefication [38]. The three sub-cycles are described as follow:

- Propane refrigeration sub-cycle: the propane is pressured by a compressor and is cooled by cooling water in the condenser, then the condensed refrigerant then flows to the JT value and is depressurised to its evaporation pressure; the propane evaporates at the evaporator-

condenser 1, absorbing the heat from the condensing ethane, cooling methane and natural gas, before returning to the propane compressor.

- Ethane refrigeration sub-cycle: the pressured ethane is condensed by the cold energy from propane evaporation, before depressurisation and evaporation in the evaporator-condenser 2; producing cold energy condenses the methane and cools down the natural gas further; finally, the evaporated ethane goes through the ethane compressor.

- Methane refrigeration sub-cycle: after compression, cooling and depressurisation by the compressor, evaporator-condensers and JT valve, respectively, the methane expands and releases cold energy to further cool the natural gas.

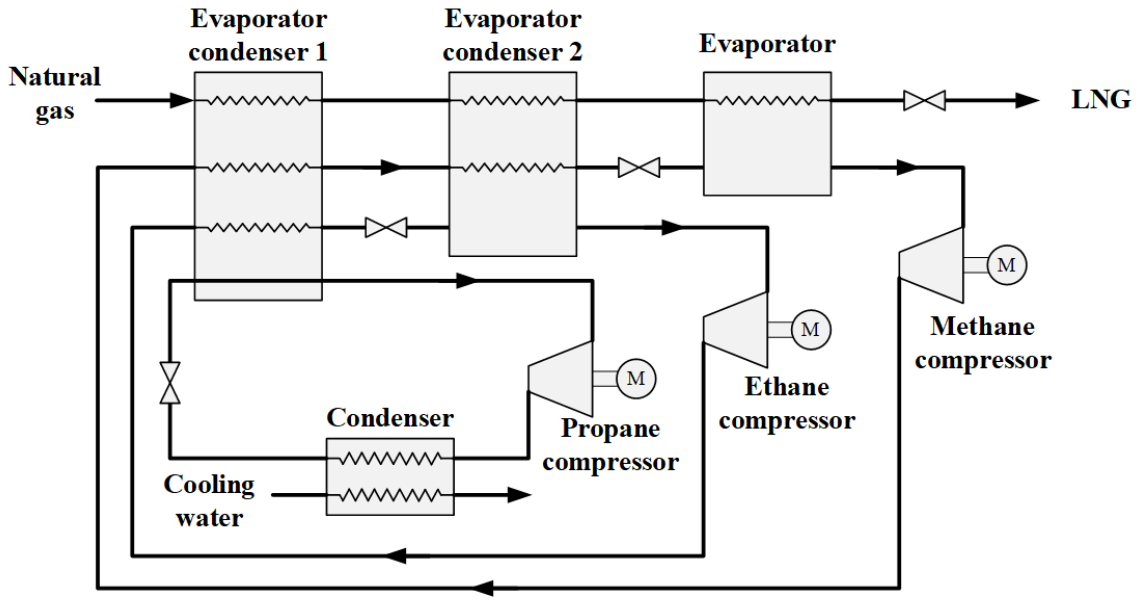

Figure 2.3 Schematic configuration of a three-sub-cycle cascade refrigeration cycle for natural gas liquefication.

Therein, each refrigeration sub-cycle consists multistage compression and expansion processes, normally three stages, leading to a wide temperature range of the cooling power for every single refrigerant. Figure 2.4 (a) illustrates a three-stage refrigeration cycle for a single refrigerant. Under such a configuration, each refrigerant is evaporated at three different pressures, giving three

different evaporation temperatures, as shown in Figure 2.4 (b). This may lead to a higher thermodynamic efficiency than that with only one evaporation temperature.

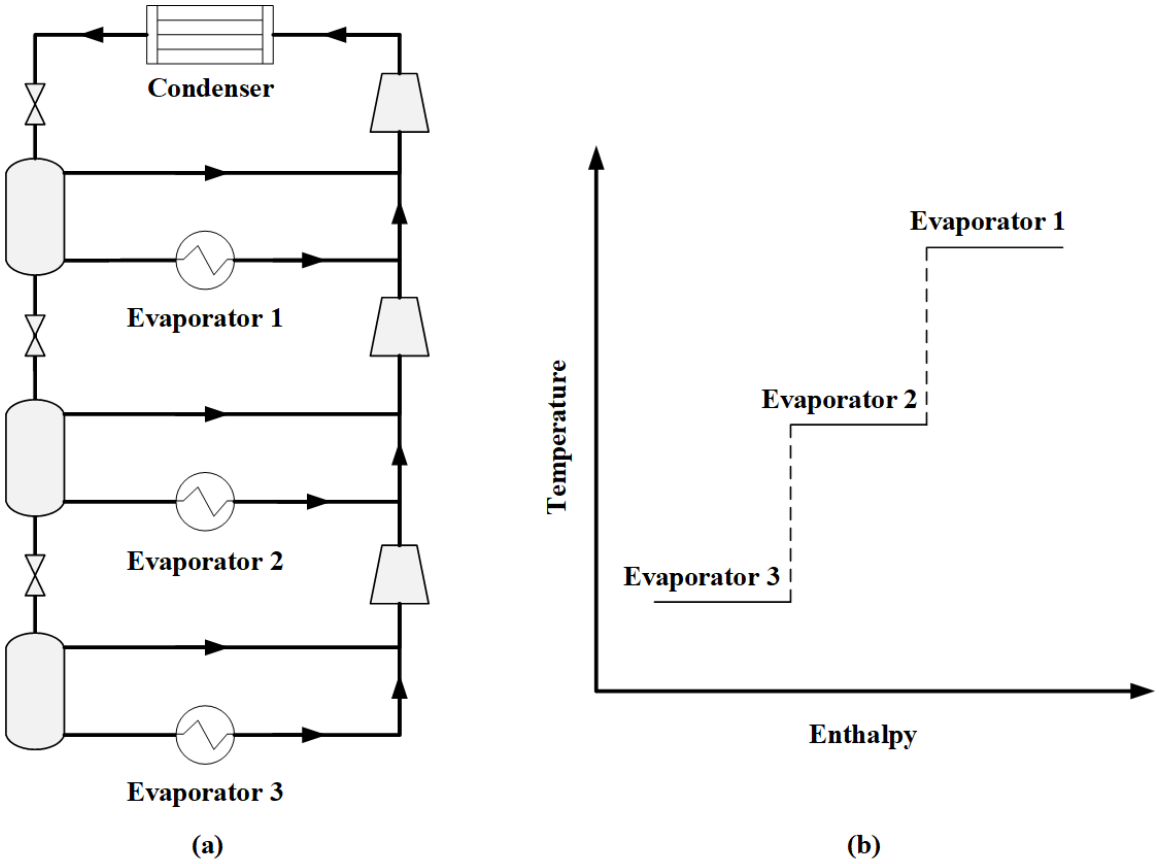

Figure 2.4 Principle of a three-stage refrigeration cycle for a single refrigerant; (a) schematic design; (b) evaporation temperature profile.

The refrigeration sub-cycles using different refrigerants can produce low-grade cold (233-203 K) by the propane refrigeration sub-cycle, mid-grade cold (193-163 K) by the ethane refrigeration cycle and high-grade cold (118-113 K) by the methane refrigeration cycle [39]. The wide cooling temperature range gives a better match of the temperature profile between the feed gas and the refrigerants. This is shown in Figure 2.5, which illustrates that the mean temperature difference between the pressurised natural gas and the refrigerant is smaller than that of the Linde-Hampson cycle, leading to a decrease in the exergy losses in the heat exchanger. As a result, the cascade refrigeration cycle requires much less power than the Linde-Hampson cycle.

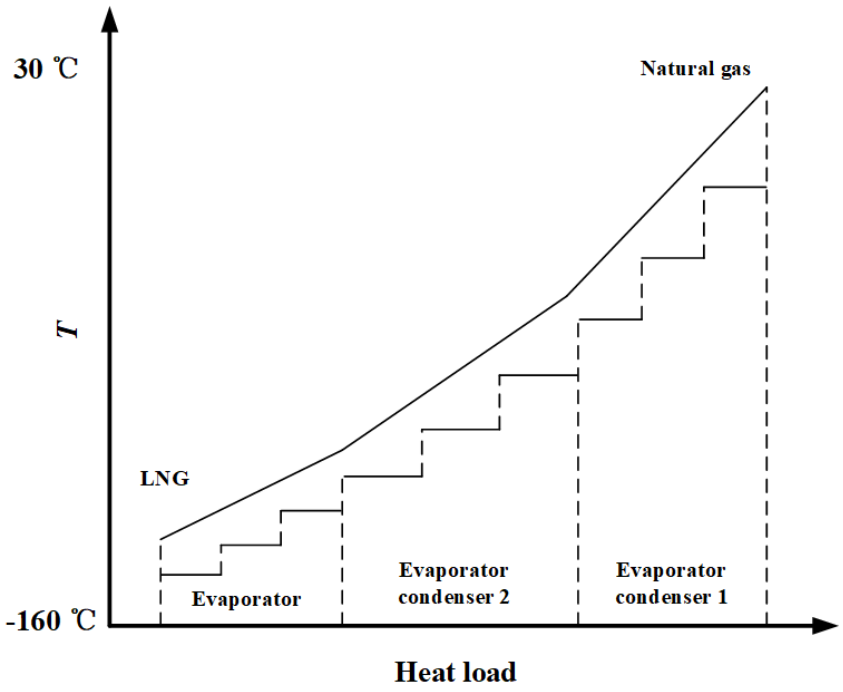

Figure 2.5 Cooling curve of three-sub-cycle cascade refrigeration cycle for LNG liquefication.

The cascade refrigeration cycle gives a higher thermodynamic efficiency than the Linde-Hampson cycle. It is reported the exergy efficiency of the multistage cascade refrigeration cycle for nitrogen and natural gas liquefaction processes ranges from 35% to 55% [38,40–43]. Additionally, the cascade refrigeration cycle has relatively low surface area requirements for heat exchange.

Cascade refrigeration cycle needs a complex configuration, and hence has several disadvantages as follow:

- The properties of refrigerants (propane, ethane, methane or nitrogen) determine the refrigeration temperature range, and hence it is not applicable for liquefying very low boiling point gases such as hydrogen and helium [44]. Although Valenti et al. [45] proposed an innovative liquefier using four cascading helium sub-cycles to liquify hydrogen , the system may not give a reasonable exergy efficiency;

- Cascade refrigeration cycle consists of numerous refrigeration sub-cycles and each of sub-cycle has its own compressor and refrigerant storage, and hence a comparatively high costs of both capital and maintenance [46]. Economic analyses have shown that the cascade refrigeration cycle is more suitable for large-scale offshore LNG production.

New technologies have emerged over the last decade for cascade refrigeration cycle based on integrated cascade refrigeration cycle with power generator using low-temperature waste heat. For example, Lizarte et al. [47] proposed a standalone refrigeration system with organic Rankine cycle for a power generation, achieving highest *COP* of 0.79 and exergy efficiency of 31.6% . Jiang et al. [48] investigated an innovative cascade refrigeration cycle for power and refrigeration cogeneration using R245fa as a refrigerant, and obtained an exergy efficiency of the system ranging from 30.1% to 41.8%.

2.2.3 Mixed refrigeration cycle

Mixed refrigerant cycle (MRC) are also commonly considered for natural gas liquefaction [38]. Such cycles use a single mixed refrigerant (SMR) instead of the multiple pure refrigerants in a cascade refrigerant cycle. The refrigerant in the MRC refrigeration cycle is usually a mixture of non-polar molecules and hence the phase change occurs continuously over a range of temperature between the dew point and bubbles point. Table 2.1 [49] gives some typical refrigerants used in LNG liquefaction. It has been shown that the mixed refrigerant can smooth the cooling curve and match it well by a non-constant temperature phase change process, as illustrated in Figure 2.6 [50].

Table 2.1 A list of some mixed refrigerants [49].

	Pressure setting (bar)	Composition (wt %)	Refrigerant flow rate (kmol/s)	Shaft work (kW)
1	4.0/46.0	CH_4, 15.7; C_2H_6, 46.4; C_3H_8, 3.5; C_4H_{10}, 14.7;	4.0	34852.3

		N_2, 19.8		
2	4.0/45.0	CH_4, 18.7; C_2H_6, 45.1; C_3H_8, 0.0; C_4H_{10}, 18.1; N_2, 18.2	3.8	32610.6
3	3.8/43.0	CH_4, 20.1; C_2H_6, 42.4; C_3H_8, 4.5; C_4H_{10}, 17.1; N_2, 15.9	3.6	30912.6
4	3.8/42.0	CH_4, 21.7; C_2H_6, 39.8; C_3H_8, 2.7; C_4H_{10}, 21.5; N_2, 14.3	3.4	28763.9

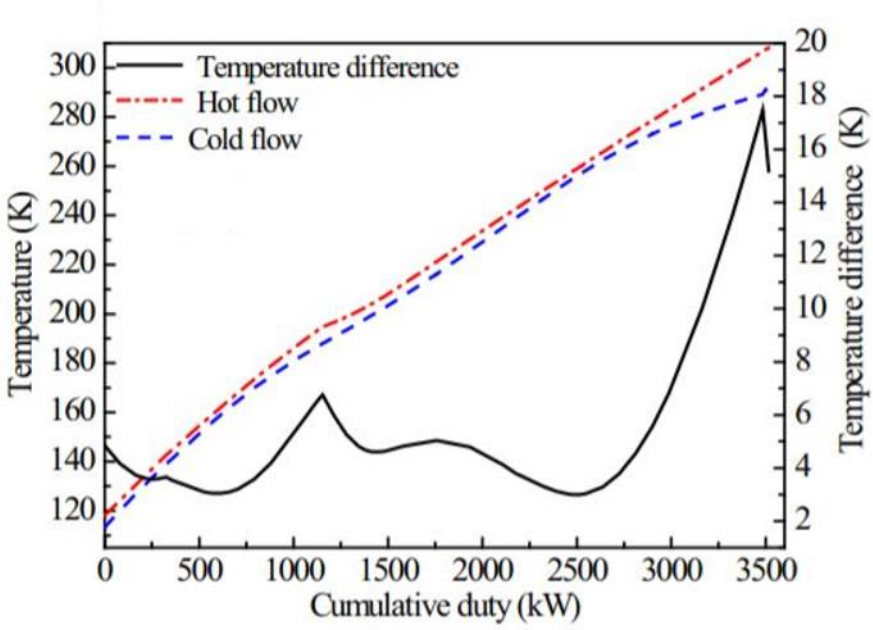

Figure 2.6 Composite curves for a mixed refrigerant cycle [50].

Due to the wide cooling temperature range (approximately from ambient down to -160 ℃), the refrigerant has to be compressed to an extremely high working pressure in the MRC. However,

such a high pressure is not easy to reach due to the mechanical restrictions. It is also inefficient to justify in terms of the system performance. Practically, self-cooling multi-stage MRC is often implemented for natural liquefication or other cryogenic processes, as shown in Figure 2.7. The three stages can be explained as follow:

- The evaporated refrigerant is compressed and partially condensed by cooling water or cooling air in the condenser and then enters the separator 1 and heat exchanger 1, followed by the depressurisation at the JT valve, part of refrigerant returns to the heat exchanger 1, absorbing heat from the high-pressure mixed refrigerant and hot stream; the hot stream undergoes the first cooling; the rest part of refrigerant enters the second stage;

- The high-pressure mixed refrigerant from stage 1 flows into the separator 2 and heat exchanger 2 for further condensation continuously; similarly, part of the refrigerant is depressurised enthalpically to supply cooling duty and the rest enters the third stage; the hot stream undergoes the second cooling and its temperature reduces further;

- Before depressurisation and evaporation, the high-pressure mixed refrigerant from stage 2 is condensed for the last time in the heat exchanger 3; the hot stream undergoes the third cooling by the evaporated refrigerant; the resulting refrigerant returns to the compressor and start the new cycle.

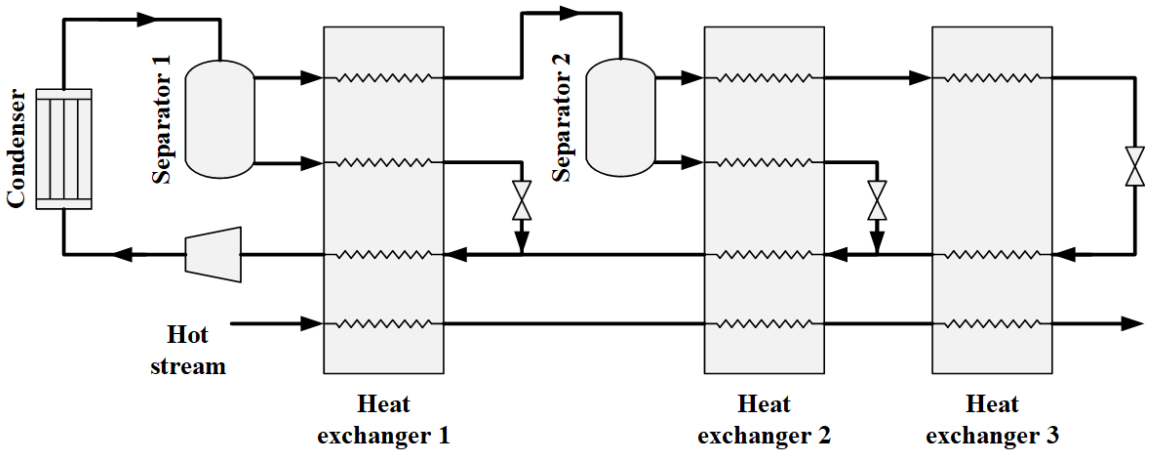

Figure 2.7 Schematic configuration of self-cooling three-stage MRC.

It should be noticed that both the hot and cold refrigerants in the recuperative heat exchangers are two-phase mixtures so as the high-pressure refrigerant condenses continuously with changes in both the quality and composition [38]. Followed by such a self-cooling method, the high-pressure refrigerant is continuously cooled down and therefore can reach a lower temperature and/or a lower vapor fraction after the multiple stages. The mixed refrigerant can smooth the cold curve and match the hot curve well through its non-constant temperature phase change process. Ideally, constant temperature difference between the hot stream and the mixed refrigerant is expected to occur in the cryogenic heat exchangers to give as high exergy efficiency as possible. However, it requires accurate working pressure control and suitable refrigerant composition for different liquefication processes. This is impractical and costly in the majority of cases. The exergy efficiency of a MRC is normally lower than that of a cascade refrigeration cycle under similar conditions [46].

Innovative technologies emerge over the past decade for MRC applying to the natural gas liquefaction refer to combine or modify MRC with the cascade refrigeration cycle.

New developments have been made over past decade to use the MRC in natural gas liquefication. These include propane precooled mixed refrigerant (C3MR) cycle [46,51–54], dual mixed refrigeration (DMR) cycle [55–57] and AP-X cycle. C3MR is developed through adding the C3 (propane) refrigeration cycle to the MRC to pre-cool the feed gas. The feed gas is cooled down to

approximate -30 ℃ by a C3 heat exchanger before liquefied at -160 ℃ in the MRC heater exchanger [54]. In the DMR cycle, an alternative mixed refrigerant (rather than C3) is used to provide cold energy for initial cooling of the feed gas and pre-cooling of the original mixed refrigerant [55–57]. Nibbelke et al. [58] compared the C3MR cycle with DMR cycle in terms of the LNG and LPG production rates. Their results showed that the DMR cycle gives 15% more capacity than the C3MR cycle, and the DMR cycle has 11% more exploitable power than the C3MR cycle. The AP-X LNG process is developed by Air Products successfully and applied to large trains. Such a process uses C3 for precooling, a MRC for liquefaction, and a closed nitrogen refrigeration loop for sub-cooling [59,60]. Figure 2.8 shows the liquefication capacity of the various technologies, one can see that the technologies summarised in this sub-section dominate the gas liquefaction capacity in the worldwide market, and this trend will maintain till 2022.

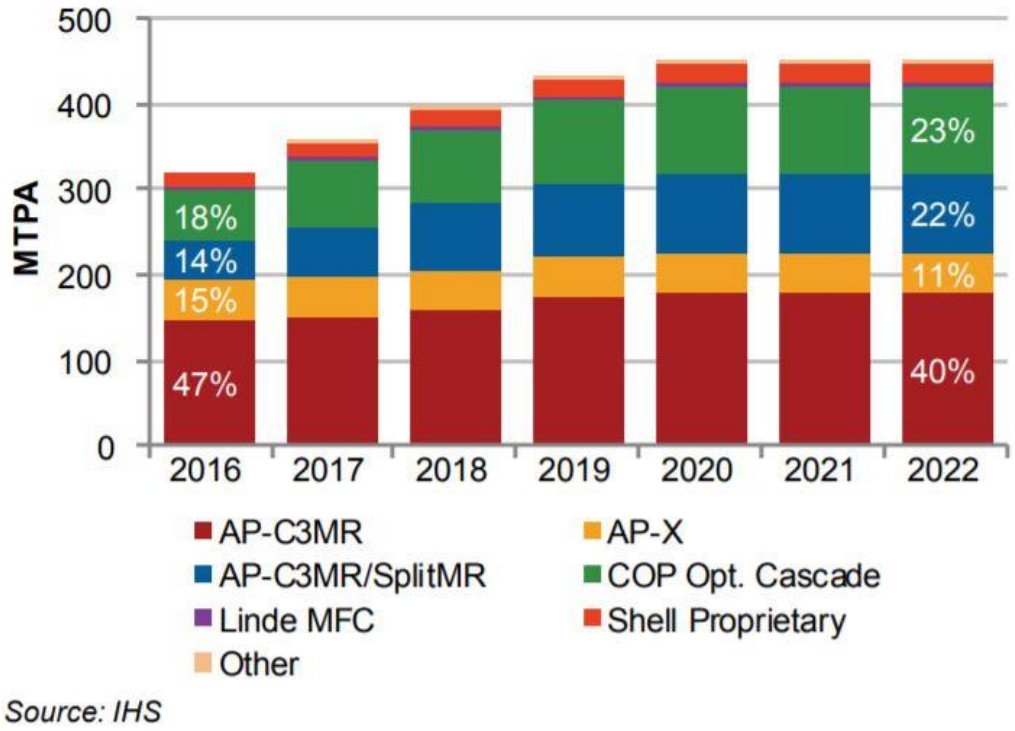

Figure 2.8 Liquefaction capacity by type of process, 2016-2022 [61].

2.2.4 Expander refrigeration cycle

Expander refrigeration cycle uses one or more isentropic processes through expansion devices, expanders or turbines for instance, rather than the isenthalpic processes in the cascade refrigeration cycle and MRC. The expansion devices can produce a temperature much lower than that generated by an isenthalpic throttling process. Theoretically, due to the adiabatic expansion of high-pressure refrigerants through expanders or turbines, the internal energy of the refrigerants can be discharged in the form of work, which greatly improves the efficiency of the refrigeration cycle. Expander refrigeration cycles have attracted more attention in recent years in the cryogenic field due to several advantages over the cascade refrigeration cycle and MRC, such as wide working temperature, rapid response time, which have economical implications for intermittent operations of liquefaction plants [46,62].

The so-called reversed-Brayton refrigeration cycle is the simplest configuration among all expander refrigeration cycles [63]. Such a cycle is well suitable for small-scale liquefaction with cooling capacity ranging from ~30 to ~220 kW and the lowest temperature of 120 k. Figure 2.9 gives a schematic of the reversed-Brayton refrigeration cycle. The refrigerants for this cycle can be selected from a wide range of candidates, such as methane, ethane, treated pressurized natural gas and nitrogen. In this cycle, the refrigerant firstly is compressed, followed by a heat rejection in a condenser. An isentropic expansion then occurs in the expander after further cooling in the recuperative heat exchanger. The expansion leads to a large temperature drop in the refrigerant, and also shaft work. The cold refrigerant then flows into the liquefying heat exchanger to remove both the sensible and latent heat of the feed gas. The warm, low-pressure refrigerant is then recompressed in the compressor to complete the cycle. It has been reported that the reversed-Brayton refrigeration cycle gives an attractive efficiency (FOM) ranging from 0.25 to 0.35 at various cooling capacities [38,64]. Economically, the reversed-Brayton refrigeration cycles have a reasonable capital investment due to the sample configuration.

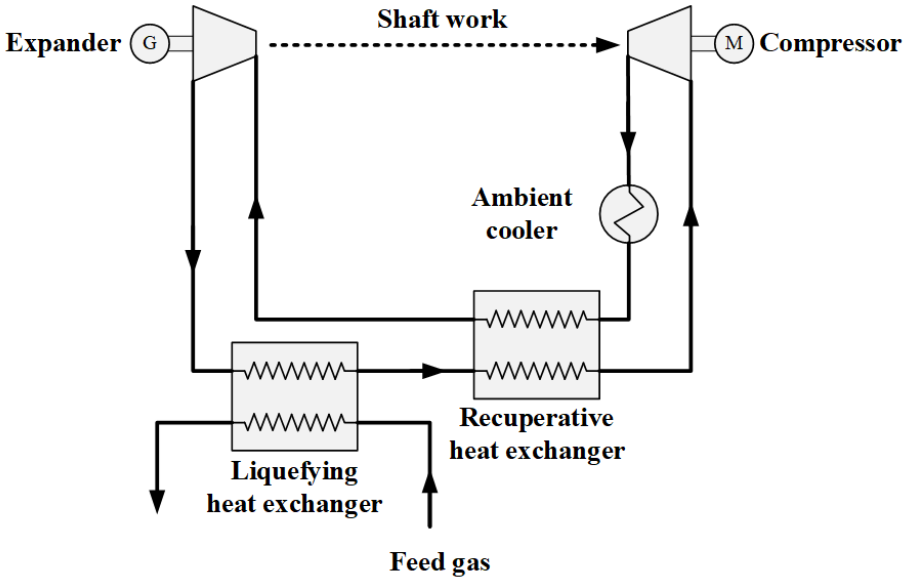

Figure 2.9 Schematic configuration of the liquefaction system with reversed-Brayton refrigeration cycle [63].

However, the reversed-Brayton refrigeration cycles have a clear disadvantage of a comparatively wide temperature difference in the both liquefying and recuperative heat exchanging process, leading to a relatively higher power consumption. Therefore, a multiple-stage reversed-Brayton refrigeration cycle has been proposed to increase the performance of the expander refrigeration cycle. Jorge proposed and patented [65] a dual expander refrigeration cycle for LNG liquefaction in 2001. The natural gas goes through two independent expander refrigeration cycles with two different refrigerants. The first refrigerant is chosen from methane, ethane or natural gas, while the second is nitrogen. As a result, cold and hot stream temperature curves are more closely matched, leading to a significantly reduced temperature gradients and thermodynamic losses [65].

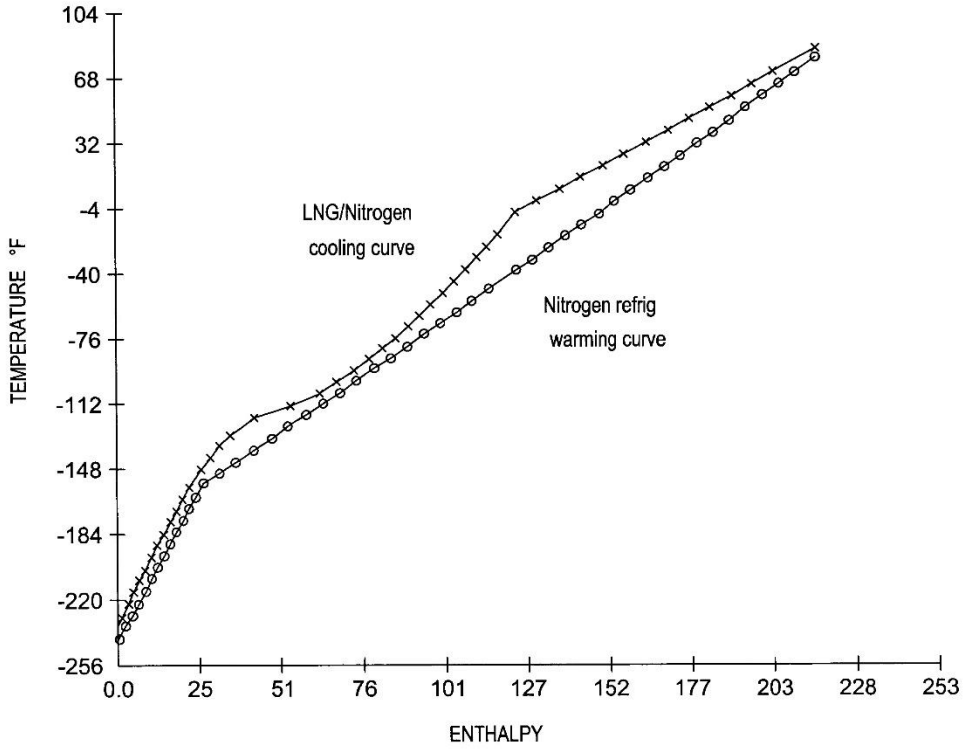

Figure 2.10 Composite curves of the dual independent expander refrigeration cycle.

Claude refrigeration cycle is an alternative method for gas liquefication. This cycle was invented by Georges Claude in 1902 for liquefying hydrogen or helium [36,66–69]. The refrigerants, which are the feed gases themselves, are small molecule gases, such as helium and neon. Such small molecule gases and their mixtures gives better heat transfer properties than the other refrigerants [70].

Figure 2.11 shows schematically a Claude refrigeration cycle which split into three refrigeration processes as follow:

- Pre-cooling stage: the feed gas, for example, helium goes through an isothermal compression process, rejecting heat to the returning helium heat in the heat exchanger 1; therein, an additional nitrogen refrigeration cycle can be utilized in the pre-cooling stage

and making the temperature drop to 80 K, which compared with the process without liquid nitrogen refrigeration cycle, can have a liquefaction rate increased by 2 to 3 times.

- Two-expansion cooling stage: part of the helium flows to expander 1 & expander 2 where a large enthalpy drop occurs providing main cold energy for the entire liquefaction process; the expanded gas, like a refrigerant, returns to heat exchanger and further cooling down the feed gas.

- Throttling refrigeration stage: the helium with temperature dropping down to below the critical temperature, is depressurised by a throttling value or a cryogenic expander, leading to liquid-vapor mixture; the liquid helium is separated as a liquid product and the vapour phase returns the heat exchanger.

It should be mentioned that compared with the throttling value, the two-phase expander has an advantage of improving the liquefaction rate by 3-5%, due to shaft work generation by the expander while supplying cold energy [71].

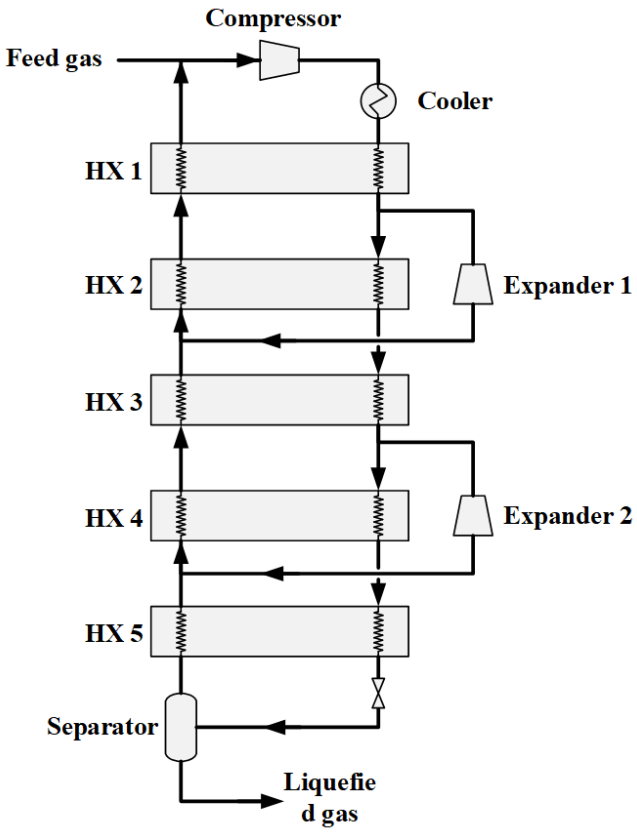

Figure 2.11 Schematic configuration of 2-expander Claude cycle [70].

Efforts have been made to improve the performance of the Claude refrigeration cycle over the past decades. Thomas et al. [69] investigated the losses at different stages of the Claude cycle, for optimising operating conditions, including pressure ratios, mass flow distribution on the expander and the heat exchanger, and temperature profile in the heat exchanger. Kanoglu et al. [68] proposed an integrated Claude cycle that used geothermal energy to drive an absorption refrigeration cycle for hydrogen pre-cooling. The cooling power produced by the absorption refrigeration cycle can pre-cool the hydrogen down to -26.9 ℃, leading to a reasonable *COP* of 0.162 and a relatively high exergy efficiency of 67.9. Chang et al. [72] optimized the Claude refrigeration cycle by improving the exergy efficiency of the heat exchangers and controlling pressure, obtaining a maximum Figure Of Merit (FOM) of 0.294 for an optimised cycle for offshore floating plants. It should be noted that

the FOM is defined as the reversible work input divided by the actual work input in some literature articles [72,73].

A Collins refrigeration cycle is similar to a Claude refrigeration cycle. In such a cycle, an independent refrigerant, differing from the feed gas, is used to make mainly cooling power for liquefying the feed gas. The advantage of the Collins refrigeration cycle is that the lowest temperature of the cooling power produced by the refrigeration cycle is not limited by the boiling point of the feed gas, thus, the exergy efficiency of Collins refrigeration cycle can be higher than that of the Claude refrigeration cycle [74].

Both Claude refrigeration cycle and Collins refrigeration cycle have a complex configuration with multiple cryogenic expanders which have shorter lifespans, so the costs in terms of capital and maintenance tend to be often comparatively high. These issues could be resolved by further design optimization.

2.3 Power Recovery Process (Discharging Cycle)

Power recovery from the LAES refers to the process that the stored cryogenic energy in form of liquid phase is extracted and converted back to electrical energy. A suitable power generation brings not only a higher output but a reasonable exergy efficiency. In this section, four cryogenic power generation cycles are reviewed: direct expansion cycle, Rankine cycle, Brayton cycle and Combined cycle. In the direct expansion cycle, the cryogen, which plays the role of the ‘fuel’, is pumped up to over its critical pressure, which is then heated to approximately atmospheric temperature by the ambient heat, followed by superheating and expansion processes to generate power. In the Rankine cycle, cryogen is used as a heat sink while the atmosphere or waste heat is used as a heat source. The temperature difference between the heat source and heat sink drives the working fluid to generation power. In the Brayton cycle, a compressor is employed to compress the working fluid, the cryogen is used to low the temperature of the working fluid before entering

the compressor so that less work is required in the compression process, further increasing the cycle efficiency. The combined cycle uses the direct expansion process and either the Rankine cycle or the Brayton cycle to enhance the overall performance.

2.3.1 Direct expansion cycle

Direct expansion cycle is one of the simplest configurations for the cryogenic power generation where the mechanical power is produced from the energy stored in the cryogen [75]. A cryogenic heat engine employs cryogens as a heat sink and the atmosphere as a heat source [75–79]. The potential of cryogenic energy for power generation has been under investigation by Knowlen [77] at University of Washington as an alternative to electrochemical batteries for zero-emission vehicles. The cryogen, which normally selected from liquid air and liquid nitrogen, plays the role of 'fuel' for the cryogenic power generation. A schematic of such a direct expansion cycle is shown in Figure 2.12. The cryogen 'fuel', stored in the tank, is pumped to a certain level above the inlet pressure of the expander to make up pressure losses in the heat exchangers, followed by heating up by the returning exhaust, ambient environment and possibly other heat sources if available; the resulting high pressure gas is expanded by multiple expansion processes, producing shaft power for electricity generation; finally the exhaust is released to the environment through a heat recovery heat exchanger for effective energy utilization.

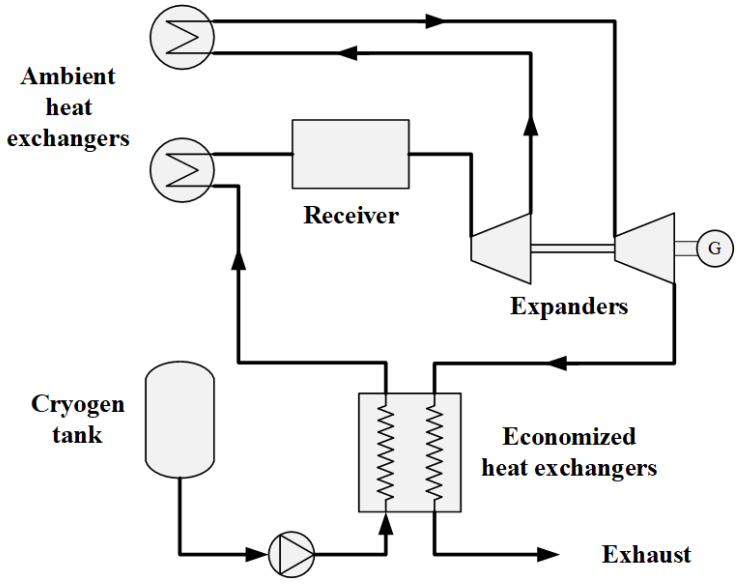

Figure 2.12 Schematic configuration of the direct expansion cycle.

The advantages of the direct expansion cycle include:

- The cryogenic power generation is a zero-emission system; the flue comes from the atmosphere while the pollutants are removed before the cryogen condensation [78];
- The configuration is simple, compact, endurable, as the system does not employ any combustion unit.

However, the direct expansion cycle is an inefficient cycle for cryogenic power generation as it does not fully use the cryogenic exergy when it is evaporated, and a huge amount of cold energy is discarded into the environment. Many efforts have been made to improve the energy efficiency, leading to two methods being developed: energy storage and combined cycle. The energy storage method is to recover the cold energy from the cryogen evaporation process instead of the use of atmosphere heating process, and the recovered cold could be used in the refrigeration process to decrease the cost of the gas liquefaction [78,80], see Figure 2.13. The combined cycle recovers the cold energy from the cryogen and directly use the cold as a heat sink for other power generation cycles, such as the closed loop Rankine cycle and Brayton cycle, see Section 2.3.4. for more details.

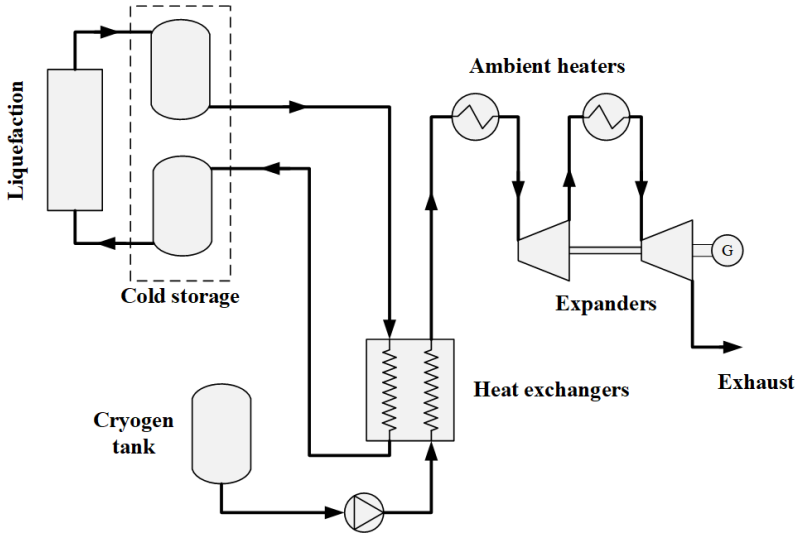

Figure 2.13 Schematic configuration of the direct expansion cycle with energy storage unit.

2.3.2 Rankine cycle

The Rankine cycle could avoid the drawbacks of the direct expansion cycle and give more efficient exergy utilizations. The Rankine cycle often uses the cold exergy from a LNG evaporation process as the heat sink for power generation [81–86]. Figure 2.14 (a) shows a sample of Rankine cycle, which absorbs the evaporation heat from the environment and rejecting the heat in the condenser to reheat and evaporate LNG. The temperature difference between the ambient and LNG temperature drives the indirect working fluid to generate power through the Rankine cycle [81–83]. To recover both the latent heat and the sensible heat of the cryogen, a material which has a slightly higher phase change point than that of the cryogen is often selected as a working fluid for the Rankine cycle. Propane has a boiling point of -42.6 ℃ at the atmospheric pressure and is usually selected as the working fluid to absorb the cryogenic exergy of the LNG in the Rankine cycle. However, Due to large temperature differences between the propane and the LNG in the evaporator-condenser and the lack of cold recovery in the evaporator, the overall energy efficiency is less than ~20%. Additionally, the power generation using Rankine cycle cannot reach below -90 ℃ as the working fluid is in the both gaseous and liquid state and cryogenic energy transferred

to the working fluid is in the form of sensible heat and latent heat, leading to a great irreversibility in the heat exchanger and high exergy losses [87].

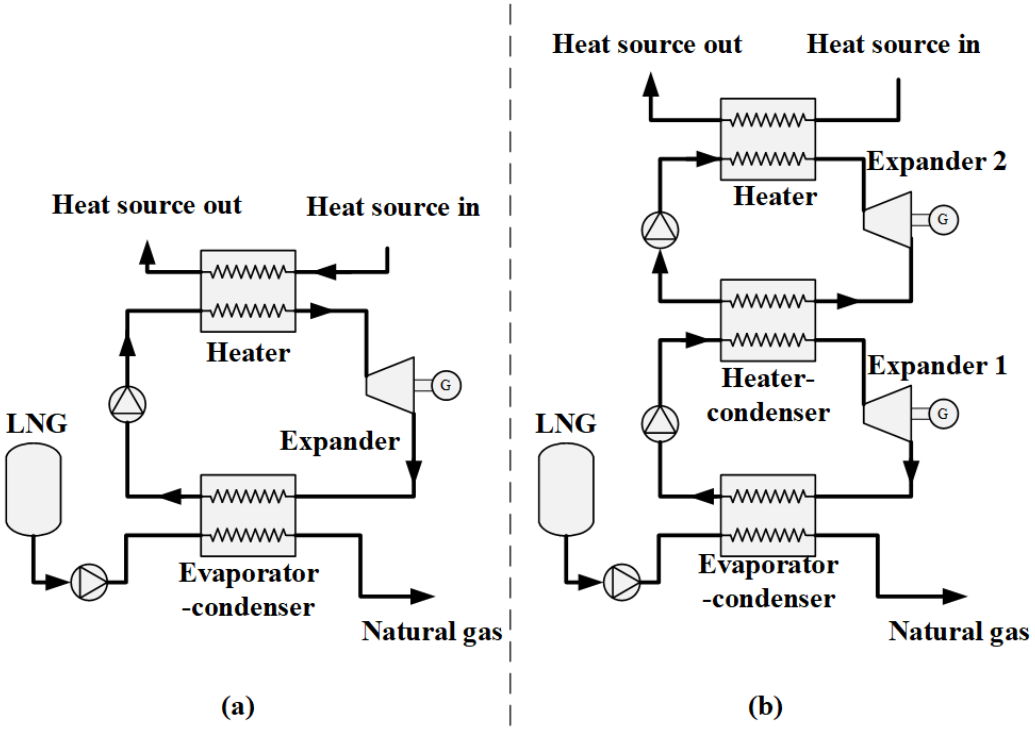

Figure 2.14 Schematic configurations of the Rankine cycle; (a) simplest Rankine cycle; (b) 2 stage cascade Rankine cycle.

To effectively use the cryogenic energy extracted from the LNG evaporation and minimize the temperature difference between the working fluid and the LNG, Bisio and Tagliafic [85,86] proposed several configurations based on the cascade Rankine cycle, as shown in Figure 2.14 (b). In such a configuration, methane and ethene, with a lower phase change point, serve as a working fluid in the first Rankine cycle, while propane, water and ethane are used in the subsequent Rankine cycles. Therefore, this method improves the cryogenic energy efficiency by decreasing the temperature difference across the evaporator-condenser and hence minimizes the exergy loss when heat transfer occurs. However, Bisio and Tagliafic also found that it is not always the case that more cascade configurations gives a higher efficiency because the system complexity can weaken the operation stability [86]. It is also concluded that a promising configuration is the one employing

three cascade Rankine cycles with a much higher heat source temperature than the ambient temperature, reaching a maximum exergy efficiency of 64%.

Increasing the gas temperature before expansion can effectively improve the output power of an expander in the Rankine cycle. Deng et al. [88] and Zhang et al. [89] used CO_2 as a working fluid and designed a combustor before the expander, where the high-pressure working fluid is mixed with part of natural gas from the LNG evaporation process, leading to more shaft work produced for electricity generation. Such a cogeneration system results in a good thermodynamic performance with the energy and exergy efficiencies over 60% and 50%, respectively. CO_2 is generated by fuel combustion, which is mostly recovered as a liquid phase, and therefore, this Rankine cycle could obtain the ability of CO_2 capture.

Waste heat can be produced during the charging process of the LAES system. Thus, there is an enormous potential to enhance the system output power by effectively utilizing waste heat. Organic Rankine Cycle (ORC) is not a new concept, which is mainly focused on the low-grade heat as heat source, such as industrial exhaust [90,91], biomass [92] and geothermal [93]. The ORC uses such a configuration as the conventional Rankine cycle as shown in Figure 2.14 (a) but an organic working fluid instead of the ones mentioned above. Organic fluids can be widely selected, as shown in Table 2.2, and organic fluids lead to a higher cycle efficiency at low-temperature low-pressure conditions. These make the ORC more economically feasible for small plants [92]. It has been concluded that thermal efficiency of a standalone ORC ranges from 10% to 25%, however, the round trip efficiency of a combined system with the ORC is significantly higher than the conventional system [94].

Table 2.2 Properties of typical working fluids used in ORC [94].

Working fluid	Molecular mass (kg/kmol)	Critical temperature (K)	Critical pressure (MPa)	Boiling point (K)
R245fa	134.05	427.2	3.64	288.05
R245ca	134.05	447.57	3.925	298.28
R141b	116.95	479.96	4.46	305.2
R123	152.93	456.83	3.662	300.97
R236ea	152.04	412.44	3.502	279.34
Butane	58.122	425.12	3.796	272.6
R32	52.02	78.10	5.780	-51.60
R134a	102.03	101.06	4.059	-26.07
R124	136.48	122.28	3.624	-11.96
R11	137.37	471.11	4.408	296.86

2.3.3 Brayton cycle

The Brayton cycle uses a gas compressor to pressurise the working fluids instead of a pump in the Rankine cycle. The cryogenic exergy from the cryogens such as LNG and liquid air is used to cool down the gas at the inlet of the compressor, leading to a significant decrease of the specific compression work. It is mainly because that the temperature is related to the specific volume (v) of the gas and further affects the compression work based on the following equation:

$$w_{compression} = \int v \cdot dp \tag{2.1}$$

Figure 2.15 presents two configurations of the Brayton cycle for the exploitation of the cryogenic energy: an open Brayton cycle and a closed Brayton cycle. These two configurations are often considered for use in LNG evaporation process.

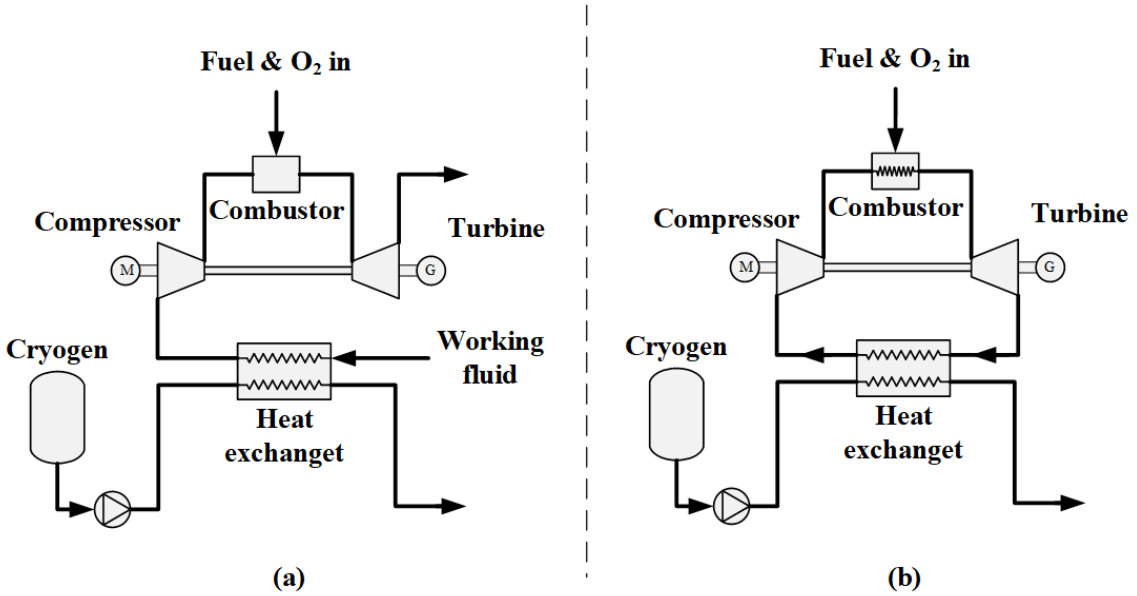

Figure 2.15 Schematic configurations of the Brayton cycle; (a) open cycle; (b) closed cycle.

The open Brayton cycle, as shown in Figure 2.15 (a), refers to a gas open cycle where the cryogenic energy from the cryogen cools down the working fluid before being compressed, and a coaxial arrangement of compressor and turbine is implemented in the cycle. The feasibility of this method was studied by Kim and Ro [87], using LNG cold energy to cool down the air at the compressor inlet. They found that the environment temperature and humidity had a dramatic effect on the output power: an increase of ~10 ℃ in the environment temperature led to a 6% drop in the output power, while the use of dry air gave a maximum increase of 8% in output power.

In the closed Brayton cycle as shown in Figure 2.15 (b), the expanded working fluid returns to the hot side of the heat exchanger, forming a closed loop. Thus, the working fluid can be cooled to a temperature of below -140 ℃ as the working fluid is in the gaseous state throughout the Brayton cycle and cryogenic energy transferred to the working fluid is in the form of sensible heat [87,95,96].

The temperature profiles between the cryogen and working fluids in the closed Brayton cycle have closer match than the Rankine cycle, as illustrated in Figure 2.16. This contributes to the reduction of irreversibility in the heat exchanger and the increase of the exergy efficiency [97].

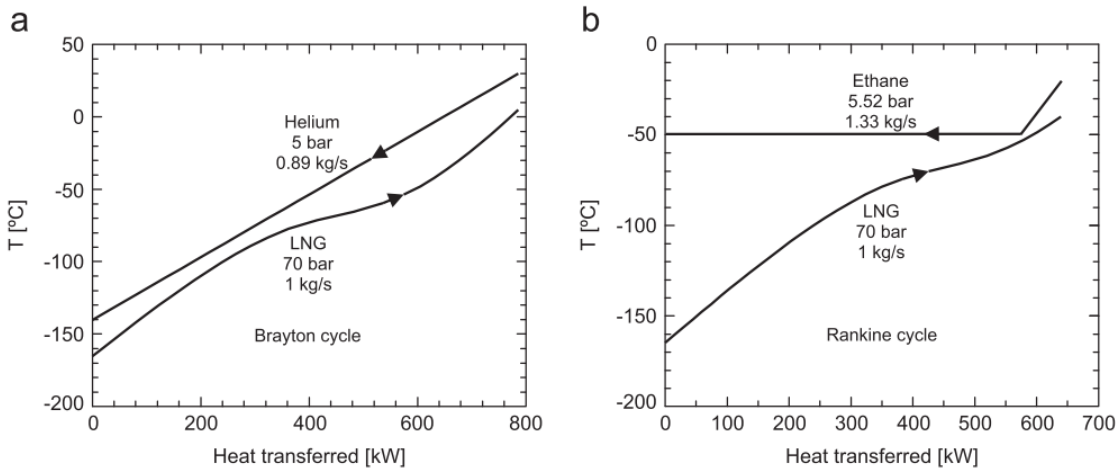

Figure 2.16 Composite curves of the LNG and the working fluid in (a) closed Brayton cycle; (b) Rankine cycle [97].

Efforts have been made to improve the performance of the Brayton cycle in recent years. For example, a multi-stage compression process with inter-stage cooling has been investigated by many researchers. Bisio et al. [86] proposed a closed Brayton cycle with two-stage compression, for which the LNG is split into two streams for inter-stage cooling to decrease the power consumption of the compressor. Kaneko et al. [98] proposed an improved Brayton cycle, namely mirror gas-turbine cycle (MGT), for which LNG is used to cool the working fluid at the outlet of turbine and at the inlets of the compressors continuously. They reported that 7-20% of the exhaust energy can be converted to useful work by a three inter-stage cooling process, whereas the thermal efficiency of the turbine can be improved by over 25% [98].

2.3.4 Combined cycle

A Combine cycle integrates the Rankine cycle, the Brayton cycle or both. Such a method effectively uses the available cryogenic exergy, which would otherwise be discarded to the environment, to

convert energy to useful work. In a typical combined cycle, the cryogen is pumped up to the supercritical state and then transfers the cryogenic exergy to the working fluid to produce one part of output power, followed by a direct expansion cycle to discharge the rest part of output power.

Figure 2.17 presents three typical combined cycles for the LNG evaporation process. Figure 2.17 (a) consists of a 2-stage cascading Rankine cycle and a direct expansion cycle, the top Rankine cycle could be operated with steam, ammonia or ethane, while the bottom cycles could use butane, propane or propylene as the working fluid which have a low phase change point. Kaneko et al. [99] developed an integrated system with a simplest Rankine cycle and a direction expansion cycle in a large-scale LNG terminal, which had reached 1100 MW by 2009. Oliveti et al. [100] proposed an integrated plant that employed a steam based closed Rankine cycle, an intermediate ammonia based closed Rankine cycle and a natural gas based direct expansion cycle. A waste incinerator was used to supply heat to the steam based Rankine cycle. They reported that the thermodynamic efficiency increased to 28.8%, the output power increased to 27.8 MW, meanwhile the proposed plant would allow for a reduction of 60% in water consumption. Meng et al. [101] analysed a cascading system for recovering the LNG cold with a metal hydrides heat pump (MHHP) as the heat source. The results showed that the proposed system gave a higher thermal and exergy efficiency, varying respectively from 44-60% and 56-70% with the change of the heat source temperature. Shi et al. [102] investigated a combined system using ammonia-water mixtures as the working fluid, and found that the net electrical efficiency and exergy efficiency could be 33% and 48% respectively, while the waste heat recovery efficiency could reach 86.57%.

Figure 2.17 (b) shows a schematic diagram of a combined cycle which integrates the closed Brayton cycle with the direct expansion cycle. The direct expansion is also called the open cycle, where the feed gas is combusted after mixing with fuel and oxygen. Such a combined cycle could be implemented to effectively increase the working fluid temperature at the gas turbine inlet of the Brayton cycle, leading to an increasing in the overall net output power. In this configuration, the

heat exchange between the cryogen and the working fluid occurs through a sensible heat discharging process, thus enables a higher cryogenic exergy recovery. Dispenza et al. [103,104] proposed a combined cycles similar to the configuration shown in Figure 2.17 (b), which is fed by natural gas in the gas turbine cycle, and helium or nitrogen in the Brayton cycle. They concluded that a higher thermodynamic efficiency of over 50% could be achieved by using helium as the working fluid at a low compression ratio. Bisio et al. [85,86] investigated a combined cycle with the nitrogen as the working fluid in the Brayton cycle. A two-stage compression with inter-cooling was used to minimize the power consumption of the compressors. They found that the combined cycles gave an overall exergy efficiency of 46%.

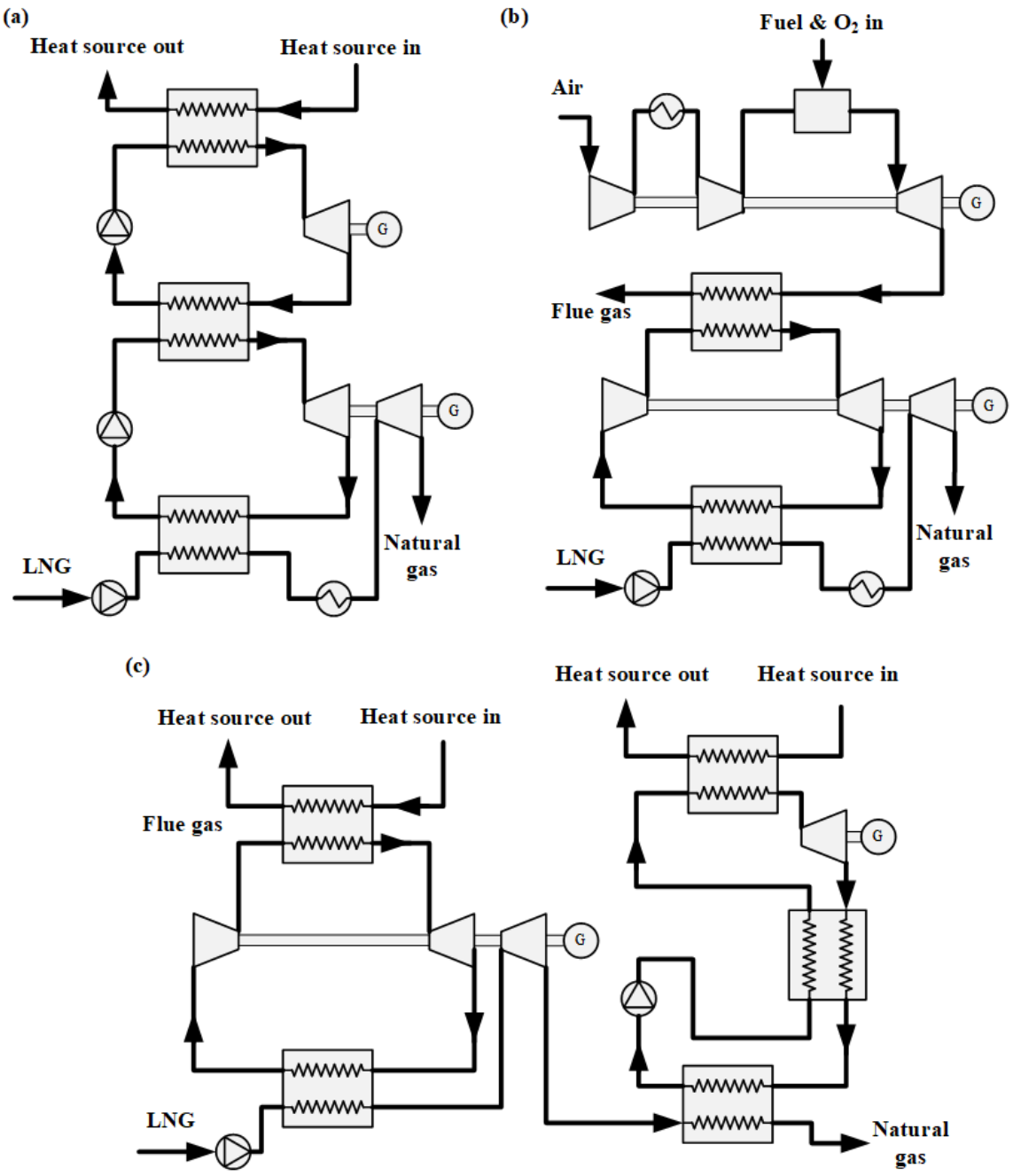

Figure 2.17 Schematic configurations of combined cycles; (a) Rankine cycle and direct expansion cycle; (b) gas open cycle with intercooling, closed Brayton cycle and direct expansion cycle; (c) closed Brayton cycle, Rankine cycle and direct expansion cycle.

Figure 2.17 (c) presents an example of a complex cycle consisting of the Rankine cycle, the Brayton cycle and the direct expansion cycle, as studied by Bai et al. and Hisazumi et al. [105,106]. The high-grade cold is used to cool the low-pressure working fluid before compression in the closed

Brayton cycle, while low-grade cold is used to liquefy the working fluid in a regenerative Rankine cycle. Such a configuration takes full advantage of the LNG cold energy, leading to temperature profiles matching closer both in the Brayton cycle and in the Rankine cycle. This could therefore decrease the irreversibility for the heat exchanger and effectively increase of the exergy efficiency for the whole cycle.

A significant amount of efforts has been made to study combined cycles. Table 2.3 gives some examples of the exergy recovery using the combined cycles.

Table 2.3 A summary of combined cycles for the utilization of the exergy of LNG.

Cycle type	Working fluid	Heat source	Thermal efficiency	Exergy efficiency	Ref.
D+R	propane	Waste heat	-	-	[98]
D+R	Steam-ammonia	Waste heat	28.8%	39.48	[99]
D+R	Ethylene-propane	Waste heat	44-60%	56-70%	[101]
D+R	Ammonia-water	Waste heat	33%	48%	[102]
D+B+O	Helium or nitrogen	Combustion	52%	-	[103,104]
D+B+O	Nitrogen	Combustion	58%	64%	[85,86]
D+R+B	Nitrogen, ammonia-water	Waste heat	53%	60%	[105]
D+R+B	Freon mixture, natural gas	Waste heat	53-63%	56%	[106]
D+R	R134a	Solar	22.3%	10.6%	[107]
D+B+O	Nitrogen, natural gas	Combustion	75%	52%	[108]

*D: Direct expansion cycle; R: Rankine cycle; B: Brayton cycle; O: Open gas cycle

2.4 Methods to improve the LAES performance

The LAES was developed on the basis of mature technologies of the gas liquefaction and power generation as reviewed earlier in this chapter. The expected round trip efficiency of a large scale standalone LAES is reported to be in a range of 50-60% [109]. The efficiency enhancement has been a subject of considerable research in the past few years. In this section, three main methods of efficiency improvement are discussed, including system configuration optimization, enhanced

thermal energy storage and system integration. The system configuration optimization enhances the performance through re-configuration to obtain a more optimized system, appraising the working parameters for the LAES. The enhanced thermal energy storage refers to the effective energy recovery through thermal energy storage devices. System integration refers to the integration of the LAES system with other industrial processes for an enhanced overall system efficiency.

2.4.1 System configuration & optimization

The gas liquefaction and the power recovery are the two key processes that determine the performance of the LAES. The round trip efficiency is a critical factor in system performance. For the sake of understanding, the definition of the round trip efficiency is first given here: the round trip efficiency refers to the fraction of electrical energy put into the energy storage system that can be retrieved.

A considerable effort has therefore been made to improve the system performance. Morgan et al. [110] studied the LAES performance enchantment by optimizing the gas liquefaction process with the conventional two-turbine Claude operated in parallel as shown in Figure 2.18. This cycle has a pinch in the cold box which limits the effective utilization of the cold energy. To resolve this problem, a three-turbine cycle was proposed to replace the single cold turbine [111], leading to an estimated round trip efficiency increase from 47% to 57%. Abdo et al. [112] compared the Linde-Hampson cycle, Claude cycle and the Collins cycle for the cryogenic energy storage system. Their results showed the system power outputs are similar for both, while the Claude cycle behaved better the on cost-benefit ratio. Borri et al. [113] analysed a small-scale air liquefaction cycle for LAES applications in a microgrid. The Linde-Hampson cycle, Claude cycle and Kapitza liquefaction cycle were studied, and the results demonstrated that a conservative final optimal configuration of an air liquefier can be considered as a two-stage compression Kapitza liquefaction cycle, leading to a maximum 25% of performance improvement with an operating pressure of 38-45 bar.

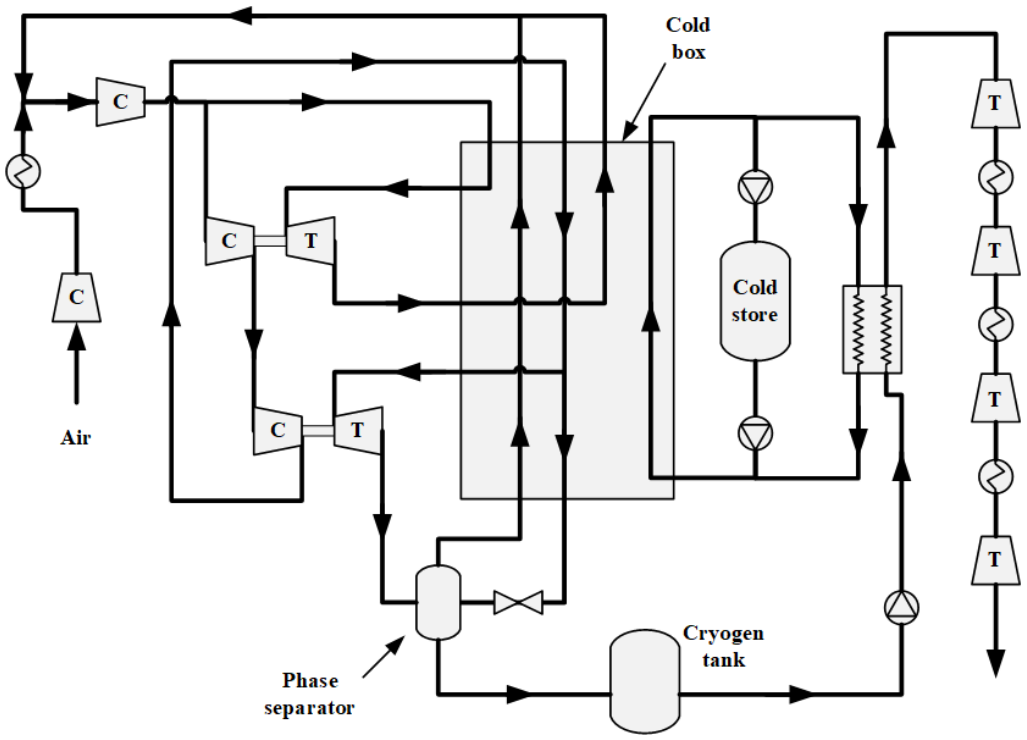

Figure 2.18 Schematic configuration of the LAES with conventional two-turbine Claude cycle [110].

Guizzi et al. [114] studied the effect of isentropic efficiencies of turbines, pressure losses and pinch-point temperatures of heat exchangers on the performance of a standalone LAES system. Every 5 K increase of the pinch point in the heat exchanger leads to a round trip efficiency drop of 2%. They also reported that a round trip efficiency in the range 54-55% for the standalone LAES can indeed be achieved. External heat sources are commonly considered for use in power generation to increase the power output of the LAES. Chino et al. [115] proposed a LAES system with a combustor, where, a gas mixture of the compressed air, natural gas and oxygen is ignited, leading to a temperature increase of the compressed air at the inlet of the gas turbine. The output power was shown to be significantly increased compared with the conventional LAES with a combustor. Cold recovery has been studied for reuse in the gas liquefication at the same time. Their results showed a higher round trip efficiency of 70% than the standalone LAES (~60%). Antonelli et al. [116] compared the LAES with and without fuel combustion, as shown in Figure 2.19. Natural gas

is used as the fuel in the case with fuel combustion. Their results showed that the LAES with the use of fuel combustion here could achieve the highest round trip efficiency of 76% and the fuel efficiency of 105%, respectively. Krawczyk et al. [117] performed a thermodynamic analysis on both the CAES and the LAES with fuel combustion as heat sources, where the compressed air is overheated to 1300 ℃ before expansion for generating power. Their results showed that the LAES system gave a 15% higher round trip efficiency than the compressed air energy storage (CAES). The heat transfer optimization for either the cold side or hot side has not been considered for the LAES, which is one of the reasons that the proposed LAES has a lower round trip efficiency than others with fuel combustion. However, external heat sources often give extra operating costs and CO_2 emissions, through the output power can be improved significantly. As a result, a careful balance between the efficiency improvement and costs (both economical and environmental) is needed.

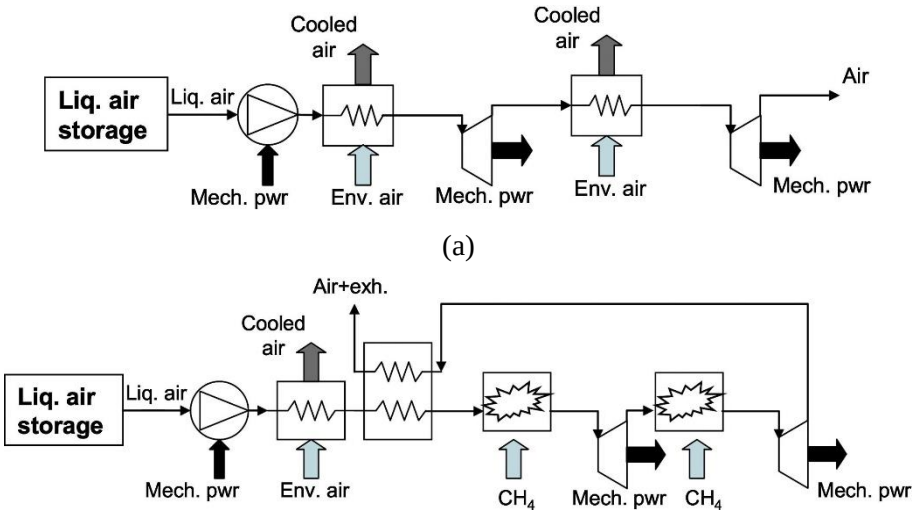

Figure 2.19 Schematic configurations of the LAES (a) without fuel combustion; (b) with combustion [116].

Another possible way to increase efficiency is to combine the conventional LAES with the other cycles. Figure 2.20 (a) shows a hybrid LAES combined with the organic Rankine cycle. The cold exergy from the liquid air expansion process plays the role of the heat sink for the ORC. The

exhaust from the gas turbine (after combustion with methane) can be used as the heat source and drives the working fluid of R134a, which is evaporated at 10 bar and condensed at 0.3 bar, respectively. Antonelli et al. [116] found that the LAES combined with the ORC could achieve a highest round trip efficiency of 77%. Antonelli et al. also designed a hybrid LAES combined with an open Brayton cycle, as shown in Figure 2.20 (b). The cold energy from the liquid air evaporation is used in a recuperation Brayton cycle where the working fluid is cooled to a low temperature to minimize the specific power consumption of the compressor. The round trip efficiency of such a hybrid system could achieve a highest value of 90%, making this process very attractive for LAES performance improvement. However, the hybrid LAES also faces the same issues of an extra operating cost and CO_2 emissions as the external heat source mentioned above. As a result, a LAES without combustion appears to be more attractive.

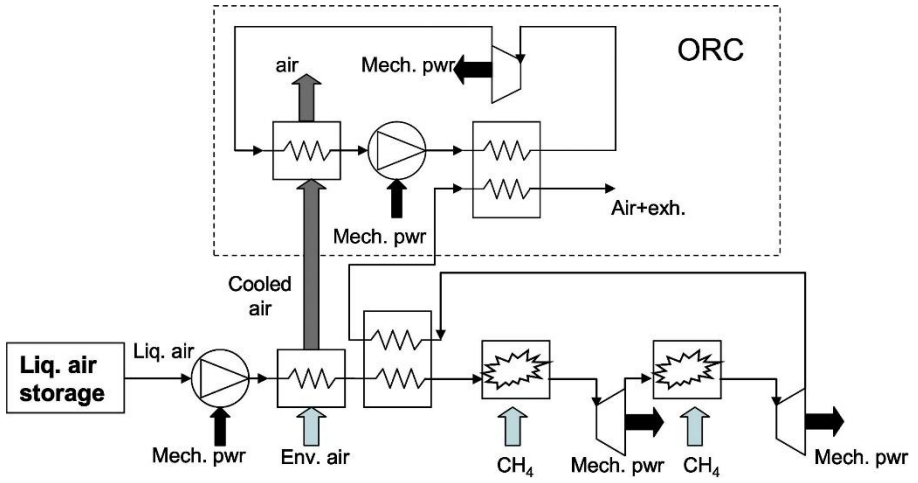

(a)

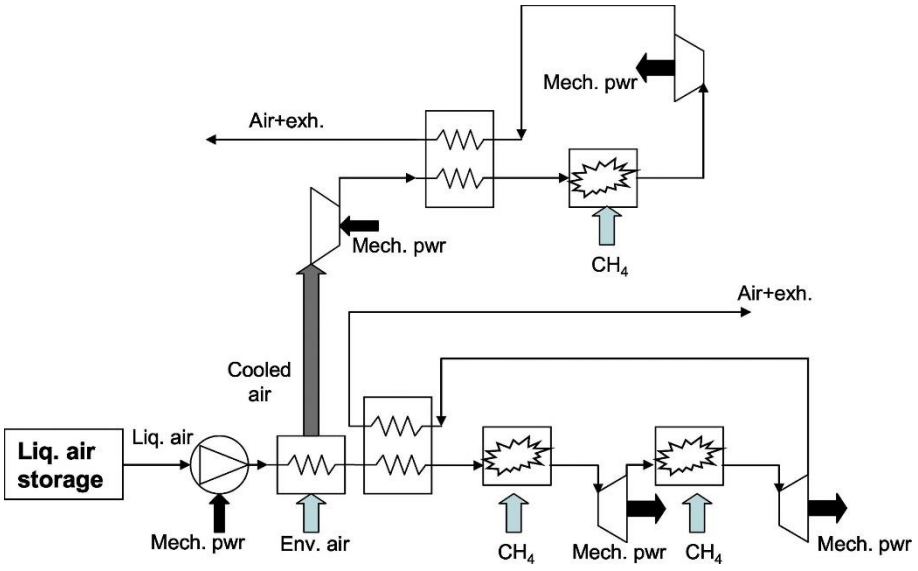

(b)

Figure 2.20 Schematic configurations of the hybrid LAES (a) with organic Rankine cycle; (b) with open Brayton cycle [116].

Kantharaj [118,119] proposed a hybrid energy storage system involving compressed air and liquid air to avoid the pressurised vessel for compressed air storage, and they found that the round trip efficiency of the hybrid system could reach 53%. Hamdy et al. [120] improved the standalone cryogenic energy storage system by utilizing the cold from liquid air evaporation to drive an indirect Rankine cycle. This additional cycle increased the specific power output of the discharging process by up to 25% and reached a round trip efficiency of 40%.

2.4.2 Enhanced thermal energy storage

A standalone LAES system implies that such a system does not rely on any external heat or cold source for the charging and discharging processes. The standalone LAES usually utilises a thermal energy storage to recovery heat and cold respectively from the compression and expansion processes. The temperature of compression heat can be in the range of 150-300 ℃ or wider, depending on the number of compression stage and compression ratio, whereas the cold energy produced in the liquid air evaporation process can be approximately -150 ℃. Thermal energy storage (TES) technologies could have a great role to play in the efficient use of compression heat and expansion cold, addressing the energy mismatch between demand and supply during charging and discharging of the LAES operation [121,122]. Packed bed is the most studied method for the TES, which serves as a direct contact heat exchanger and an energy storage device. Meanwhile it is relatively inexpensive method with a high reliability. It is thus possible to be a suitable thermal storage device to recover both heat and cold during the LAES operation. Figure 2.21 shows a schematic diagram of a pack bed based TES. The charge and discharge of the packed bed can be described mathematically in the following [123–125]:

Gas phase temperature:

$$\varepsilon\rho_a c_{p,a}\left(\frac{\partial T_a}{\partial t}+u_a\frac{\partial T_a}{\partial \chi}\right)=\varepsilon k_a\frac{\partial^2 T_a}{\partial \chi^2}+\frac{6(1-\varepsilon)h}{d_p}(T_s-T_a)+h_w(T_w-T_a) \tag{2.2}$$

Solid phase temperature:

$$(1-\varepsilon)\rho_a c_{p,s}\frac{\partial T_s}{\partial t}=(1-\varepsilon)k_s\frac{\partial^2 T_s}{\partial \chi^2}+\frac{6(1-\varepsilon)h}{d_p}(T_a-T_s) \tag{2.3}$$

The above equations upon combination with mass and momentum equations, can be solved numerically to give temperature profiles as a function of time.

Clearly, the above equations assume a one-dimensional system. More sophisticated treatments of packed bed systems can be found in the literature [126–128].

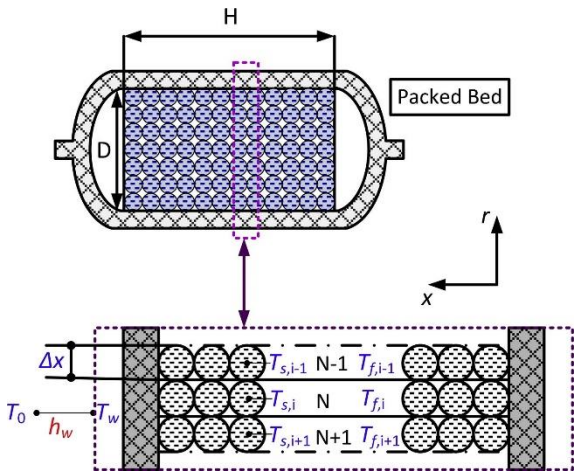

Figure 2.21 A schematic illustration of a packed bed TES [129].

Efforts have been made on enhancing the LAES performance including a packed bed heat exchanger in the LAES system. For example, Peng et al. [129,130] used packed-beds to store heat generated during air compression and analysed the thermodynamic performance of the LAES as shown in Figure 2.22. A two-stage compression process was considered, and the compression heat was recovered and stored in two packed-bed regenerators in the charge step. In the discharging time, the evaporated liquid air extracts the heat from the solid particles by direct contact with the storage medium in the packed beds. They concluded that a round trip efficiency of 50-60% could be achieved by using the packed bed TES system.

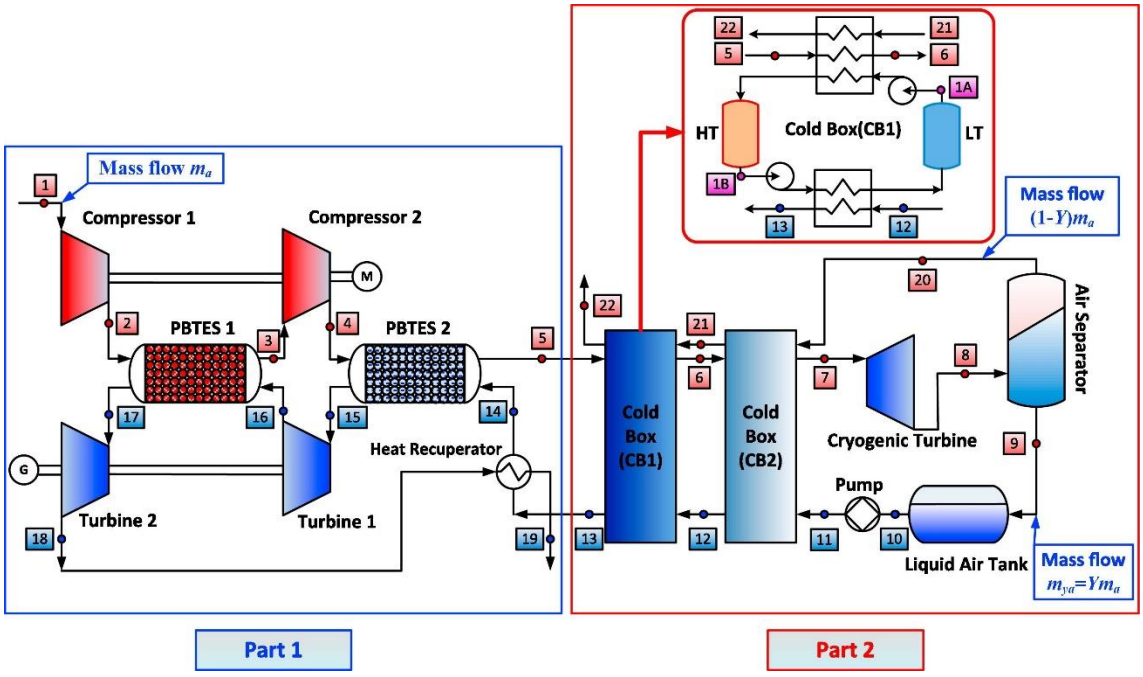

Figure 2.22 Schematic of the novel LAES system comprising packed bed TES [130].

Sciacovelli et al. [131] performed a dynamic study on a LAES system with a rated power of 100 MW and a storage capacity of 300 MWh in a direct-contact storage device packed with pebbles and rocks to improve the efficiency of cold recovery. A stand-alone LAES was investigated, comprising a packed bed TES to recover cold energy from evaporation of liquid air, a diathermic hot thermal store is for storing compression heat. Their results showed that a round trip efficiency of 50-60% could be achieved. Although a packed bed TES is regarded as a viable solution to cold energy recovery in the LAES system, it introduces dynamic effects due to thermal front propagation in the packed bed. They found that this issue leads to a maximum value of 25% for outlet temperature increase near the end of the discharge stage.

2.4.3 System integration

The LAES is a flexible energy storage system that can be integrated with external thermal energy sources for performance enhancement. For example, a natural gas combustor can significantly increase the shaft work of a gas turbine in the discharging cycle [115–117]; and refrigeration cycle

can be used to produce cold energy for pre-cooling compressed air to increase the production rate of the liquid air, or to cool the compressed air at the inlets of the compressors to minimise the specific power consumption. The integrated LAES system couples the LAES to industrial processes mechanically and geographically, where the LAES serves the industrial processes through conserving and releasing the electrical energy. The industrial processes can provide the required cold or heat energy in return for the LAES. Thanks to most thermal energy could not be fully used in the industrial processes, the costs of the external energy is shared by both sides.

Many efforts have been made on LAES integration with various processes, such as solar power generation, wind power generation, nuclear power generation, LNG regasification. For example, Li et al. [132] proposed the integration of the LAES with nuclear power plants (NPPs), as shown in Figure 2.23. The integrated system can give significant load shifting of the NPPs. When the demand is much lower than the rated power of the NPP, the NPP is still operated at its rated power and the excessive power is used to drive the charging cycle of the LAES to produce liquid air. When the demand is much higher than the rated power, the discharging cycle is launched and the stored energy in form of liquid air is converted back to electrical energy. The round trip efficiency of the integrated LAES system is reported to be over 70% while the net output power of the integrated LAES-NPP system could be as high as 2.7 times that of the rated NPP power.

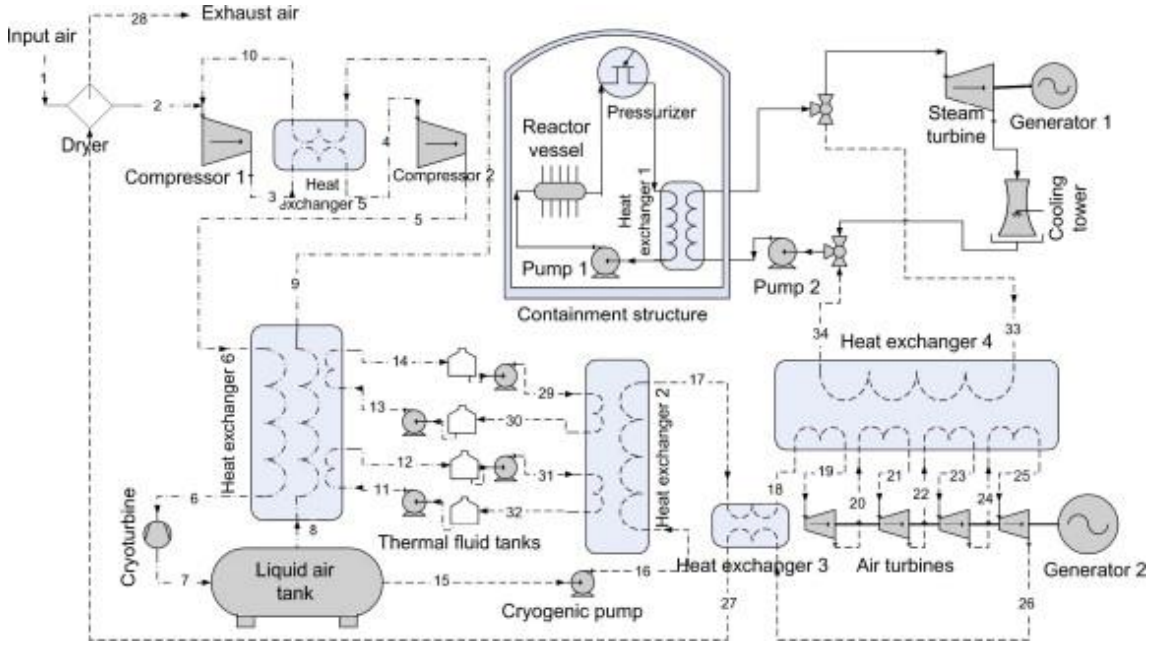

Figure 2.23 Schematic of the LAES system integrated with nuclear power generation [132].

Lee et al. [133] studied the integration of a cryogenic energy storage system with a liquified natural gas (LNG) regasification process. The heated natural gas drives multi-turbines to generated additional work to decrease power consumption of air compressors. Their results suggested a significantly higher exergy efficiency of 94.2% and 61.1% respectively for the air storage process and the release process. Kim et al. [134] proposed a distributed energy generation system by combining the LAES with LNG regasification. The cold energy from the LNG regasification process is used to meet partial cold need for the air liquefaction whereas natural gas combustors are used to increase the specific output power of the gas turbine. they found that the round trip efficiency and exergy efficiency could reach 64.2% and 70% respectively.

2.5 Summary of the Literature Review

The LAES technology attracted more attentions over the past decade due to the advantages of high energy density, no geographical constraints, highly competitive capital costs, relatively low maintenance and operational costs, a long-life span, and environmental friendliness. The LAES

was originally aimed for large grid scale electrical energy storage. The technology consists mainly of two processes of air liquefaction (charge) through refrigerating and air expansion (discharge).

There are a few of gas liquefaction processes. Linder-Hampson cycle is not suitable for large-scale gas liquefaction such as the LAES due to poor thermodynamic performance. Due to the high exergy efficiency and good performance, the cascade refrigerant cycle, MRC and their combinations dominantly have taken ~90% of the large-scale gas liquefaction market worldwide. However, these refrigeration technologies do not work well for intermittent operation needed for the LAES. Expander refrigeration cycles enable an intermittent operation due to rapid response time both for startup and shutdown. Many efforts have been made to optimise the expander refrigeration cycles and results have been shown an exergy efficiency of 60-70%. However, little has been done on liquefaction cycles with the cold storage devices or the use of external cold source for performance improvements.

Numerous studies have been done on low-temperature power generation. These studies can be classified into direct expansion cycle, Rankin cycle, Brayton cycle and combined cycle. It is illustrated that combined cycles have been shown to be the most efficient and flexible among all cycles. The combined-Rankine cycles are most suitable for cases with low-grade heat sources while the combined-Brayton cycles perform better with high temperature heat sources.

A significant number of studies have been done on the performance improvement of the LAES, and the following is a list of the findings:

- The studied LAES systems with decent performance usually rely on external energy sources. External heat sources or cold sources provide a significant improvement in the system performance, but little has been done on quantification of the energy requirement.

- Low-grade Waste heat could be recovered during the LAES charging process, if some alternative ways of reusing low-grade heat can be employed, there may be potentials in LAES performance enhancement.

- The cold energy is not efficient used in current LAES and LNG integrated systems as the refrigerant temperature can be lower if temperature range could be widened. It may not only obtain a better temperature profile match, but also increase the liquid air yield to a higher level (currently ~0.71). If LNG turbines could be used to replace the LNG combustors, there is no more natural gas consumption during the charging process, and a higher round trip efficiency could be achieved at the same time.

- Different LAES configurations have been studied, but little has been done on optimization, there are still rooms for improvements both on system configurations and components.

The present work aims to address the gaps as summarised above through a comprehensive analysis the LAES with a specific attention on thermal energy generation and utilization. The results of the analyses provide a guidance to the improvement of performance of the LAES. By optimizing each component of the LAES system, one finds that a standalone LAES can give a decent performance without external thermal energy. A novel integrated LAES is then proposed to effectively use the external energy sources to further improve the LAES performance.

Chapter 3 Methodologies

In this chapter, methods used in this research are introduced, including the Pinch technologies and the thermal property reference.

3.1 Pinch technology

3.1.1 Introduction to the pinch technologies

The transfer of heat either from one process stream to another (interchanging) or from a utility stream to a process stream is commonly involved in many industrial processes. Two of the targets in any industrial process design are to maximize the process-to-process heat recovery and to minimize the energy utility requirements [135]. To meet these goals, an appropriate heat exchanger network (HEN) is required.

The so-called Pinch technologies, devised by Linnhoff in late 1978, enables a systematic analysis of the overall plant [136–138]. The Pinch technology was further developed for the HEN design by Linnhoff and Hindmarsh [139], which uses thermodynamic principles to achieve utility savings by using better process heat integration, maximizing heat recovery and reducing external utility loads [140]. The Pinch technology gradually evolves to an integral part of the overall strategy for process design and optimization, known as process synthesis or process integration. The Pinch technologies have been extended to address problem in other applications, such as capital cost, mass pinch and water pinch, which are out of this research and will not be discussed further [141].

The use of the Pinch technologies in dealing with the HEN or other industrial processes simply relies on the first and second laws of thermodynamics. The first law provides an energy equation for calculating the enthalpy changes of streams through heat exchangers while the second law determines the direction of energy flow (always from hot to cold stream in the absence of any work

input). In a practical process, a Minimum Approach Temperature (MAT) must be maintained between the ‘hot stream’ and ‘cold stream’ in the HEN.

The Pinch technology will convert the streams in the HEN to lines called hot and cold composite curves. The composite curves can be used to demonstrate that heat recovery limits exist in the HEN topologies, which are independent of the area of the individual exchanger units in the network [142]. The Composite curve of a heat exchange process is illustrated in Figure 3.1 (a) which shows the opportunity for heat recovery as well as the minimum net hot and cold utility requirements. The position of closest temperature approach between hot and cold streams is defined as the process pinch point where the temperature difference should not be lower than MAT. The performance of the process is then limited by this constraint. It has been reported that any change in process parameters due to modification of de-bottlenecking will change the pinch position and thus affect the hot and cold utility requirements, as shown in Figure 3.1 (b).

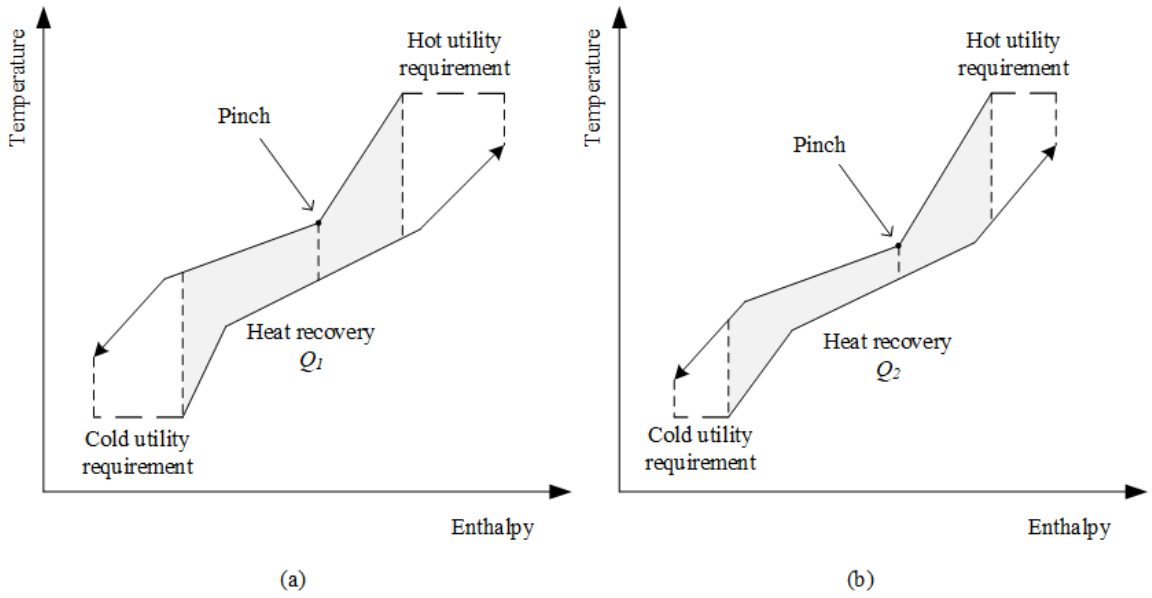

Figure 3.1 Composite curves of the hot and cold streams in HEN; (a) original performance; (b) optimal performance.

3.1.2 Heat exchanger optimization using the Pinch technology

The use of the Pinch technologies in this work is mainly for the optimisation of the performance of heat exchanger (HEX) in the LAES system, to achieve a good exergy efficiency for both the heat exchangers and the cold box, which are two important units of the storage system. The optimization process can be summarised as follow [141]:

(1) Establishment of the mass and energy conservation equations;

(2) Extract the stream data from the equations;

(3) Select an appropriate Minimum Approach Temperature (MAT), then calculate the utility requirements and the pinch points;

(4) Examine how the process changes, modify stream data affect the targets;

(5) Once decided whether to implement process changes and what utility levels are used, design a HEX heat within the process;

(6) Design the utility systems to supply the remaining hot and cold utility requirements, and modify the heat exchanger network if necessary;

(7) Reproduce the process based on the above modifications, return to step (2) to study if a further improvement is possible.

An example for a systematic design and optimisation procedure is shown in Figure 3.2. The thermodynamic properties of the streams (compressed air, cold air, propane and methanol) are obtained for solving the conservation equations. The Pinch technology is used in the optimisation process leading to eventually an optimal heat exchanger network (HEN).

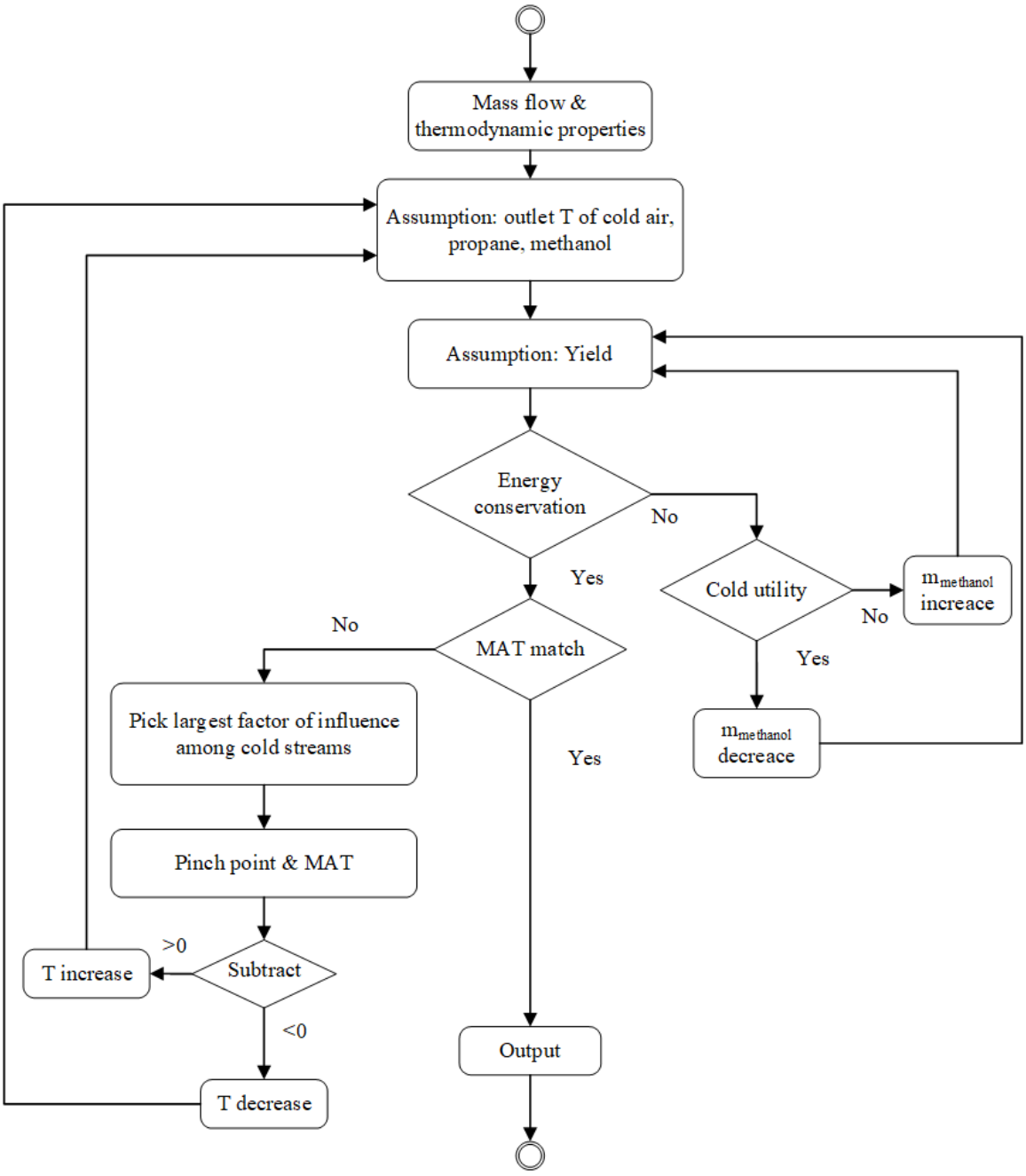

Figure 3.2 An example of a systematic design and optimisation for a multi-stream cold box in the LAES system.

One can see that the optimisation process is essential to the systematic design although it is a complex and time-consuming process, an effective and efficient optimisation technique is required to obtain the best configuration and an optimal setting of parameters.

3.2 Thermodynamic properties

The ideal gas law is the simplest equation that relates to the state parameters of a gas, which is an approximation for veal gases at low pressures and above a moderate temperature:

$$PV = nRT \tag{3.1}$$

where P is the absolute pressure, T is the absolute temperature, n is the number of moles of a gas and R is the ideal gas constant.

This study concerns a complex environment often with high pressures and/or low temperatures. This implies an inaccurate estimation of the thermodynamic properties using the idea gas law. In the same time, the simulation involves a huge amount of computation which could lead the accumulation of minor inaccuracies into a huge one, leading to reliability reduction of the data. Therefore, accurate thermodynamic properties are prerequisite for a valid thermodynamic simulation for this study.

As a result of the above, a commercial program named REFPROP is implemented for the thermodynamic property calculations, which is based on the most accurate pure fluid and mixture models currently available. The REFPROP program was developed by the US National Institute of Standards and Technology (NIST) and can provide tables and plots of the thermodynamic and transport properties of industrially important fluids and their mixtures including refrigerants and hydrocarbons.

For the thermodynamic properties of pure fluids, three models are implemented in the REFPROP: (1) the equations of state (Helmholtz energy); (2) the modified Benedict-Webb-Rubin equation of state; (3) the extended corresponding states (ECS) model. For the calculation of mixtures, the REFPROP program employs a model that applies the mixing rules to the Helmholtz energy and a departure function is used to account for the deviation from an ideal mixture. These models,

implemented in a suite of FORTRAN subroutines, written in a structured format, and internally documented with extensive comments, have been tested on a variety of compilers [143].

The thermodynamic property of pure fluids or mixtures can be accessed by other software environments, such as MATLAB used in this study, through the use of a provided dynamic link library (DLL). The calling sequence for both pure substances and mixtures can be described as:

$$\text{Result=refpropm(prop\_req, spec1, value1, spec2, value2, substance1)} \quad (3.2)$$

$$\text{Result=refpropm(prop\_req, spec1, value1, spec2, value2, mixture1)} \quad (3.3)$$

$$\text{Result=refpropm(prop\_req, spec1, value1, spec2, value2, substance1, substance2, … , x1, x2, …)} \quad (3.4)$$

where prop_req is the requested properties, spec1 and spec2 are the known properties. Each property is represented by a character when calling the sequence, as illustrated in Table 3.1.

Table 3.1 Acronyms for the properties in REFPROP sequence calling.

Spec	Property	Spec	Property
A	Speed of sound [m/s]	R	d(rho)/dP (constant T) [kg/kPa]
B	Volumetric expansivity [1/K]	S	Entropy [J/(kg K)]
C	Cp [J/(kg K)]	T	Temperature [K]
D	Density [kg/m3]	U	Internal energy [J/kg]
E	dP/dT [kPa/K]	V	Dynamic viscosity [Pa*s]
F	Fugacity [kPa]	W	d(rho)/dT (constant p) [kg/(m^3 K)]
G	Gross heating value [J/kg]	X	Liquid phase & gas phase comp. (mass fraction.)
H	Enthalpy [J/kg]	Z	Compressibility factor
I	Surface tension [N/m]	+	Liquid density of equilibrium phase

J	Isenthalpic Joule-Thompson coefficient [K/kPa]	-	Vapor density of equilibrium phase
K	Ratio of specific heats (Cp/Cv)	!	dH/d(rho) (constant T) [(J/kg)/(kg/m^3)]
L	Thermal conductivity [W/(m K)]	@	dH/dT (constant rho) [J/(kg K)]
M	Molar mass [g/mol]	#	dP/dT (constant rho) [kPa/K]
N	Net heating value [J/kg]	$	Kinematic viscosity [cm^2/s]
O	Cv [J/(kg K)]	%	Thermal diffusivity [cm^2/s]
P	Pressure [kPa]	^	Prandtl number
Q	Quality (vapor fraction) (kg/kg)		

Chapter 4 Experiments and Simulations: Liquid Air Energy Storage

4.1 Introduction

The world's first pilot plant (350 kW/2.5 MWh) was established and tested by Highview Power Storage in collaboration with University of Leeds from 2009 to 2012. It was relocated at University of Birmingham for further testing and academic research in 2013 [144].

In this chapter, the testing results from the 350 kW pilot plant including the cold store are analysed, and simulation work is carried out and validated using testing data from the pilot plant experiments. Meanwhile the performance of the cold store is tested, and the results will be fed back to the simulation work to study the effect of thermal loss of the cold store on the LAES performance.

4.2 The 350 KW Pilot Plant

4.2.1 System description

Figure 4.1 shows a picture of the relocated LAES pilot plant. The plant consists of a Gas Liquefication Unit (GLU), the energy stores (cold, heat & liquid gas) and a Power Recovery Unit (PRU). Note the followings for the relocated pilot plant at Birmingham:

- Liquid nitrogen is used instead of the liquid air as the GLU was not connected mainly due to cost issues.
- Pebbles are used as the cold energy storage medium to recover the cold from the liquid nitrogen evaporation process.
- A water-glycol mixture is used as a heat transfer medium to heat the gas before expanding at the turbine, which takes heat from a hot water store with a temperature of ~80. The hot

water is from the university CHP system. The reason for such an arrangement is that the pilot plant does not have a compression heat recovery unit.

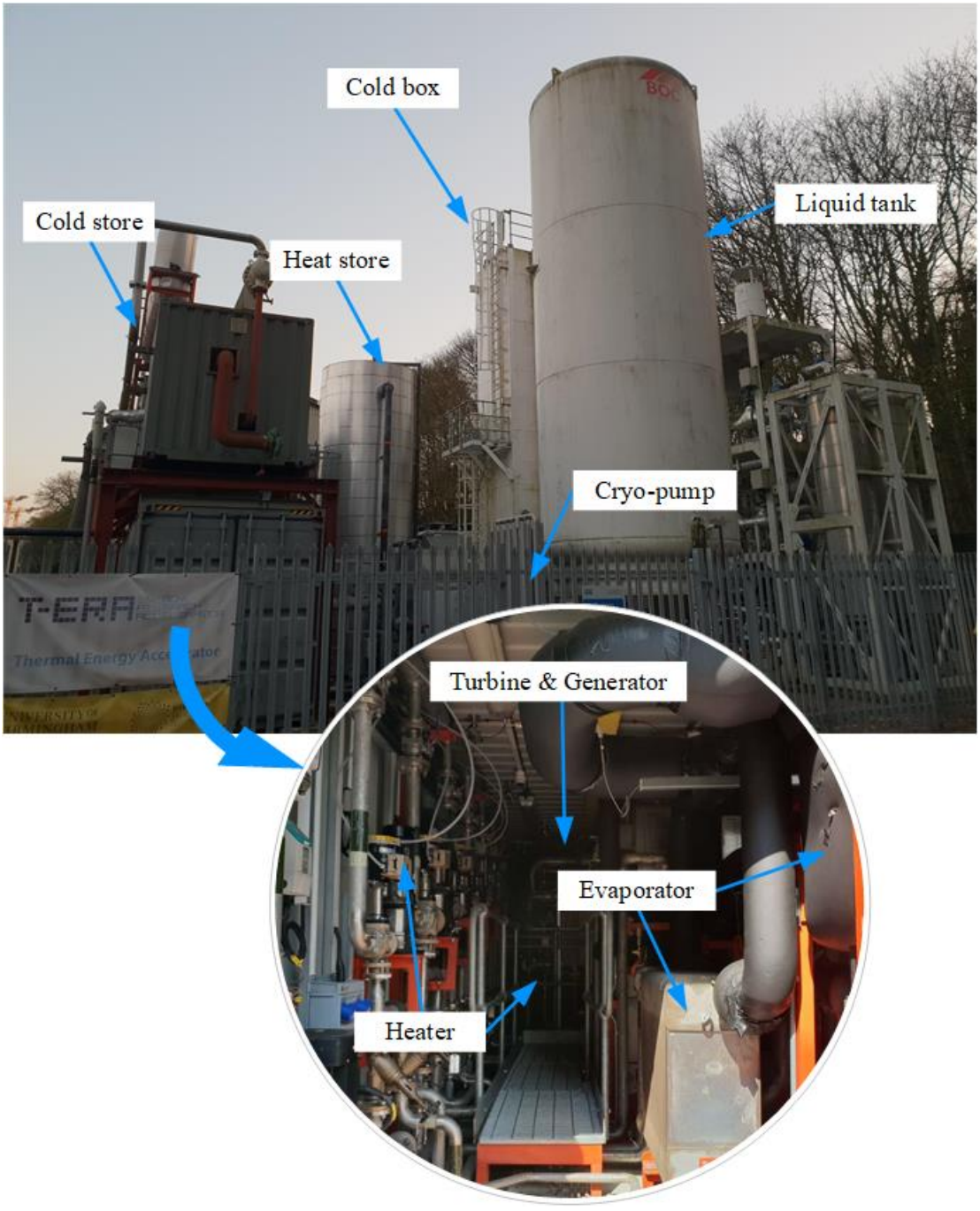

Figure 4.1 A picture of the 350 kW LAES/CES pilot plant showing some main components/units.

The configuration of the PRU of the LAES plant is illustrated in Figure 4.2. When electricity is needed, the PRU is started. Liquid nitrogen from the storage is pumped to a high pressure (above the critical pressure), heated by the hot water-glycol mixture before entering the 4-stage turbine with inter-stage heating to generate electricity. The exhausted gas then flows back to evaporators where the cold energy from the liquid nitrogen is captured and stored in cold store.

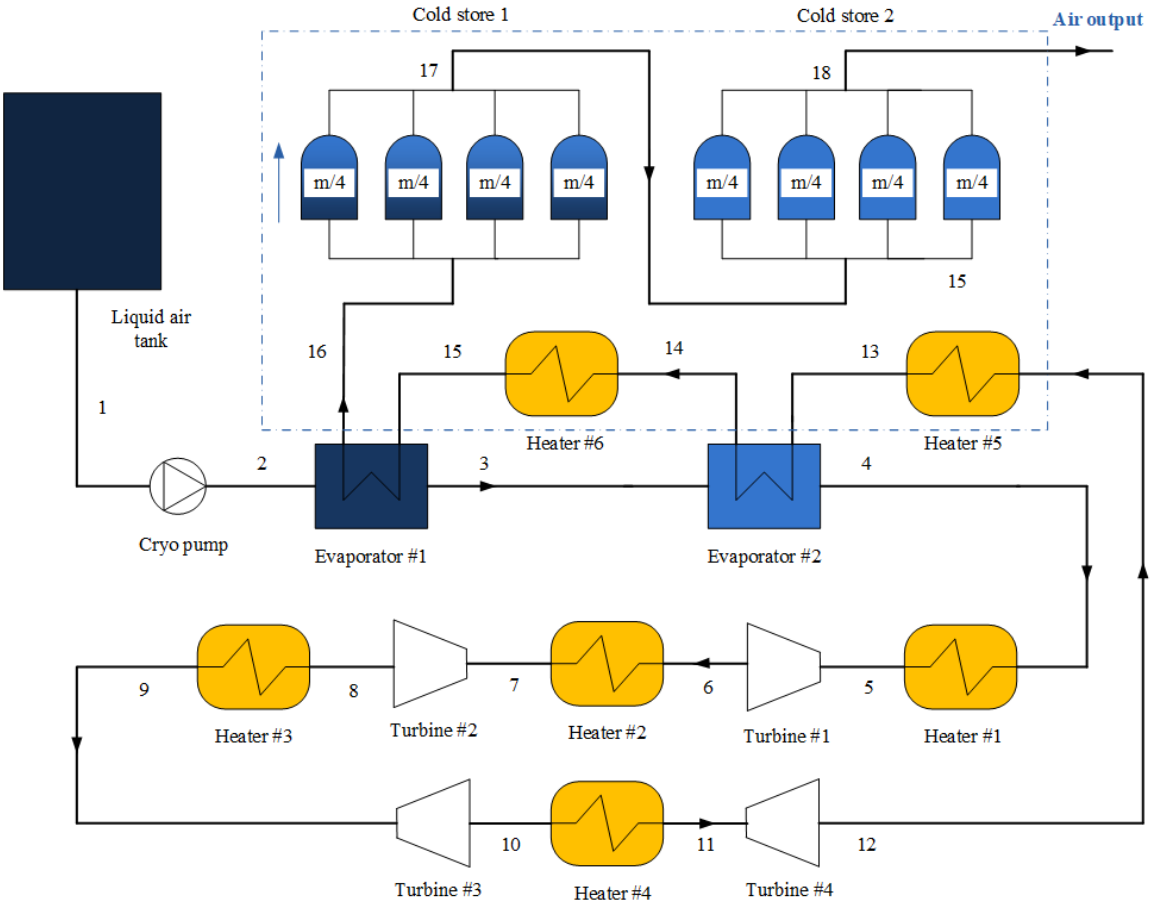

Figure 4.2 Layout of the 350 kW PRU for LAES.

4.2.2 Experimental results

The experimental parameters are listed in Table 4.1. The pressure and mass flow rate of the liquid nitrogen are controlled by charging the rotating speed of the cryo-pump. However, the cryogenic valve cannot be 100% opened during the experiment due to some safety requirements of the University. Thus, the maximum speed of the cryo-pump in this study is ~85% of the maximum.

During the experiment, the output power, mass flow rate and pressure are collected at least 3 times under each set of operating conditions.

Table 4.1 Working parameters of the PRU for LAES/CES.

Parameters	Value
Testing ambient temperature	10 ℃
Liquid nitrogen storage pressure	8 bar
Liquid nitrogen temperature	-196 ℃
Hot water store temperature	80 ℃
Glycol based heat transfer fluid temperature	65 ℃
Initial temperature of cold store	10 ℃
Power rating	350 kW
Max inlet pressure of turbine	60 bar

4.2.2.1 Factors affecting the net output power

The net output power is affected by several factors. Figure 4.3 shows the effect of the mass flow rate of the liquid nitrogen on the net output power. One can see a nearly linear relationship between the mass flow rate of liquid nitrogen and the power output. The rated power of 350 kW was not achieved due to the value restriction as mentioned above. The variance of the net output power increases from ~4.5 kW to ~10 kW as the mass flow rate increases from ~0.5 to ~1.6 kg/s. This is mainly due to the growing rotating speed of the cryo-pump, which may have led to the inaccuracy of thermocouples installed at the cryogenic valve and cryo-pump.

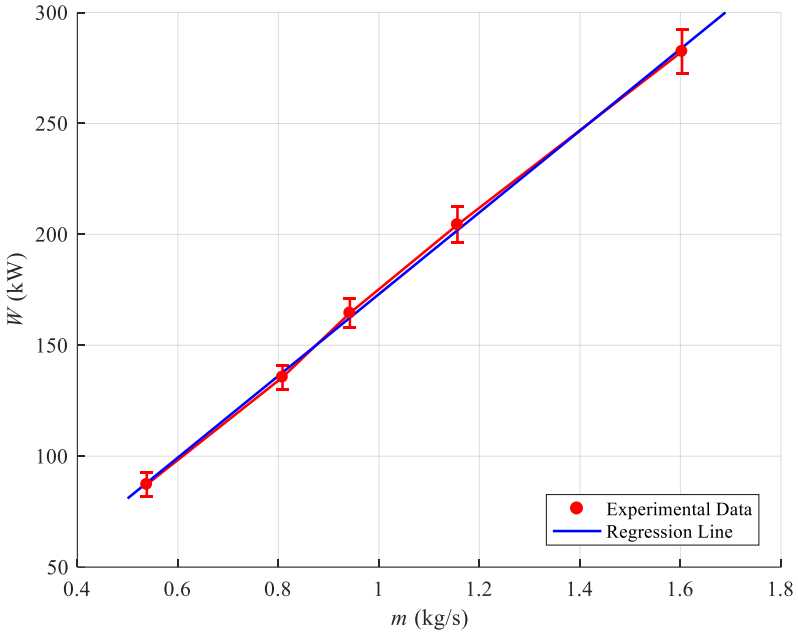

Figure 4.3 Effect of mass flow rate of the liquid nitrogen on the net output power of the pilot plant; temperature of the heated nitrogen heated by glycol based heat transfer fluid at $T_{nitrogen}$ =55°C.

The pressure of the nitrogen is controlled by the cryo-pump as well. Figure 4.4 shows how the liquid nitrogen pressure correlates to the mass flow (Figure 4.4 (a)) and to the output power (Figure 4.4 (b)). The linear relationships indicate an easy and simple control of the power output through adjusting the pump rotating speed.

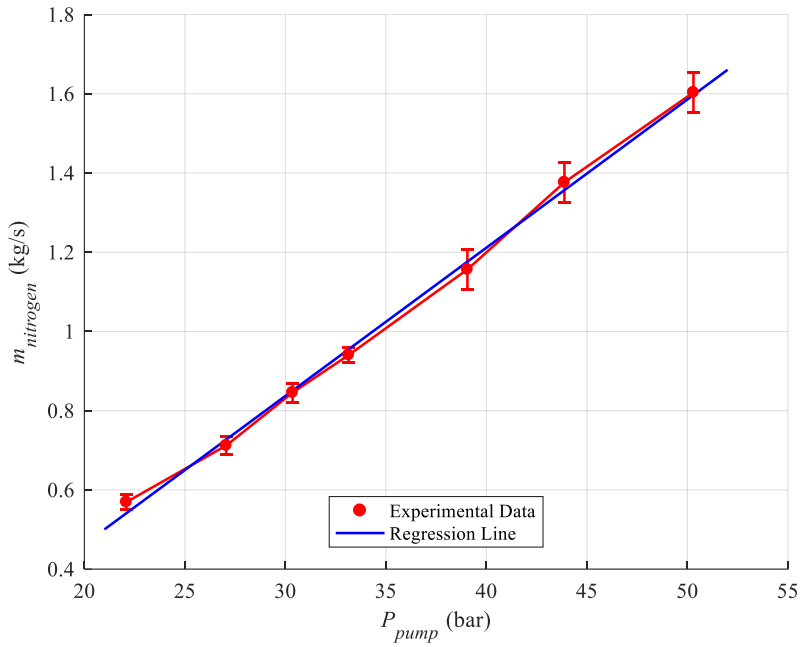

(a)

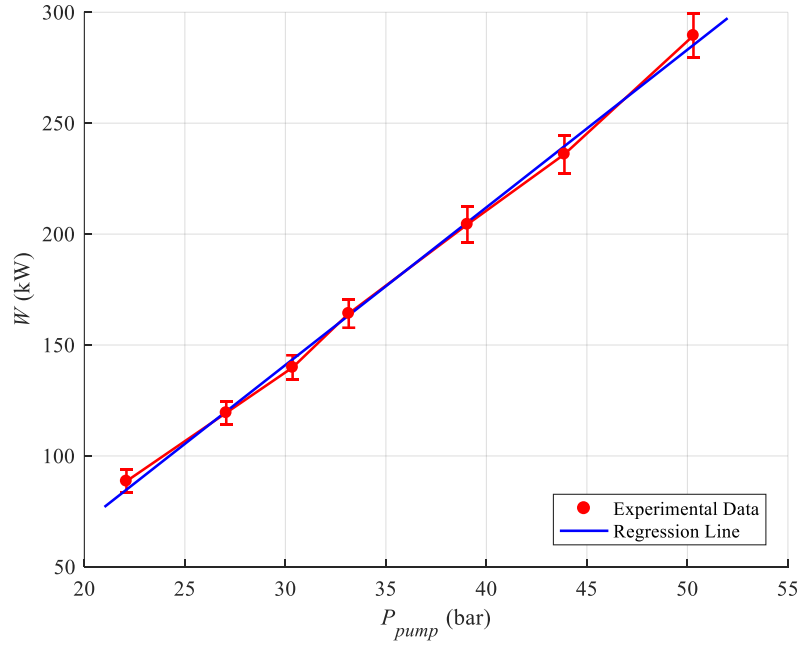

(b)

Figure 4.4 Effect of the pressure of the liquid nitrogen on (a) mass flow rate of liquid nitrogen and (b) net output power of PRU; temperature of the nitrogen heated by glycol based heat transfer fluid at $T_{nitrogen}$ =55°C;

Both hot water and glycol based heat transfer fluid play a role for the inter-stage reheating of the nitrogen during expansion in the turbine. This simulates the effect of the use of compression heat or external heat sources. The inter-stage reheating temperature is varied by adjusting the mass flow rate of the heat transfer fluid (see Figure 4.2). Figure 4.5 illustrates that the inter-stage reheating temperature significantly affects the output power: an increase of 1℃ contributes to an increase of ~1 kW in output power of the PRU of the LAES. As a result, there is an enormous potential for the LAES system to use waste heat including the compression heat and other industrial processes, as well as renewables (e.g. solar thermal).

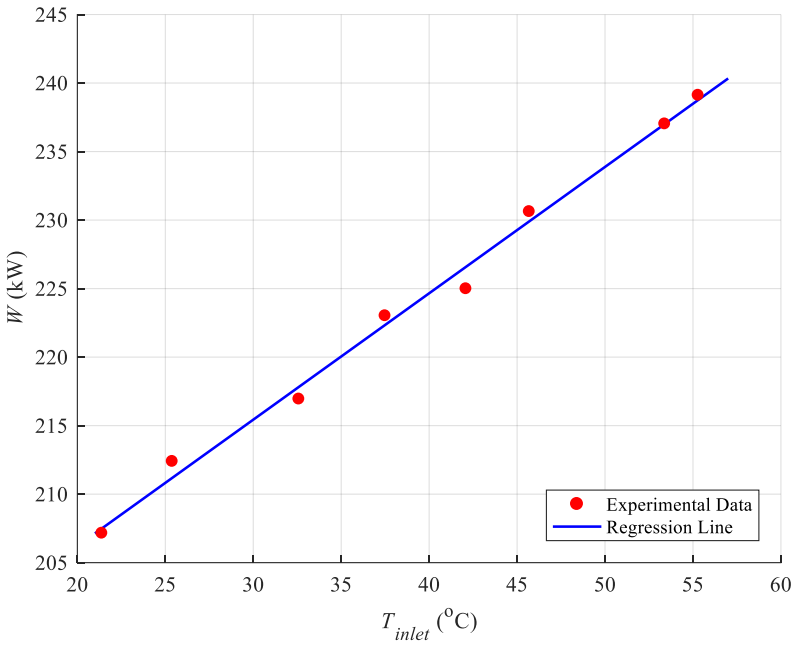

Figure 4.5 Effect of turbine inlet temperature on output power of the PRU ($m_{nitrogen}$=1.37 kg/s).

4.2.2.2 Time evolution of the discharging cycle of the LAES system

During the discharging process, the delivered power of the LAES could follow the variation of electricity demand by adjusting the power output. The response time of such a system is crucial for the energy storage as a rapid response time would be needed to meet the variation timely and efficiently. Figure 4.6 shows the time evolution of the nitrogen mass flow rate against the output

power. One can see that the pilot plant PRU can bring ~70% of the rated power output in 120 seconds while maintaining a smoothing power supply for at least 12 minutes under this specific set of testing conditions. The results also suggest a small mass flow of liquid nitrogen is needed in the discharging cycle due to the requirement of a minimum speed of 3000 rpm for the turbines before synchronizing with an electricity generator.

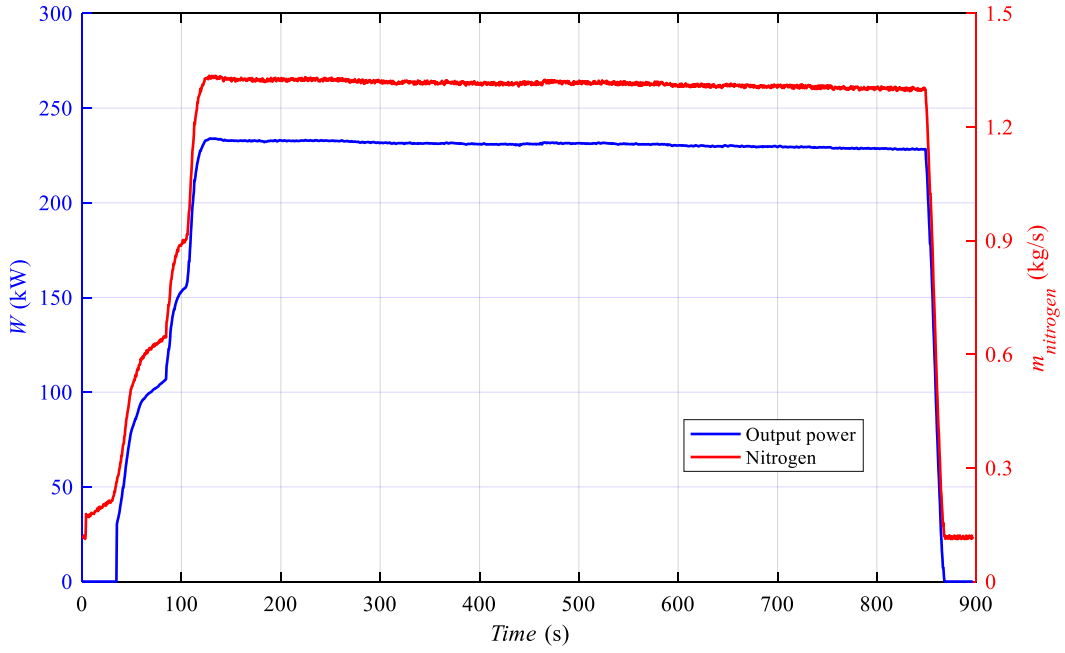

Figure 4.6 Power output of the LAES pilot plant power during a discharge cycle.

4.2.2.3 Configuration and performance of the high-grade cold store

In the discharging process, liquid nitrogen is evaporated, releasing cold energy is carried by the nitrogen gas from the last stage turbine, recovered by the secondary stream of the evaporator (State 15-16 in Figure 4.2). The cold energy flows to the packed bed where the cold energy is stored, as shown in Figure 4.7 (a). The high-grade cold store consists 8 cells of cylinder shape with a diameter of 0.6 meter and a height of 2 meters, filled with pebbles. Five thermocouples are installed at a equal distance from bottom to top of each packed bed cell.

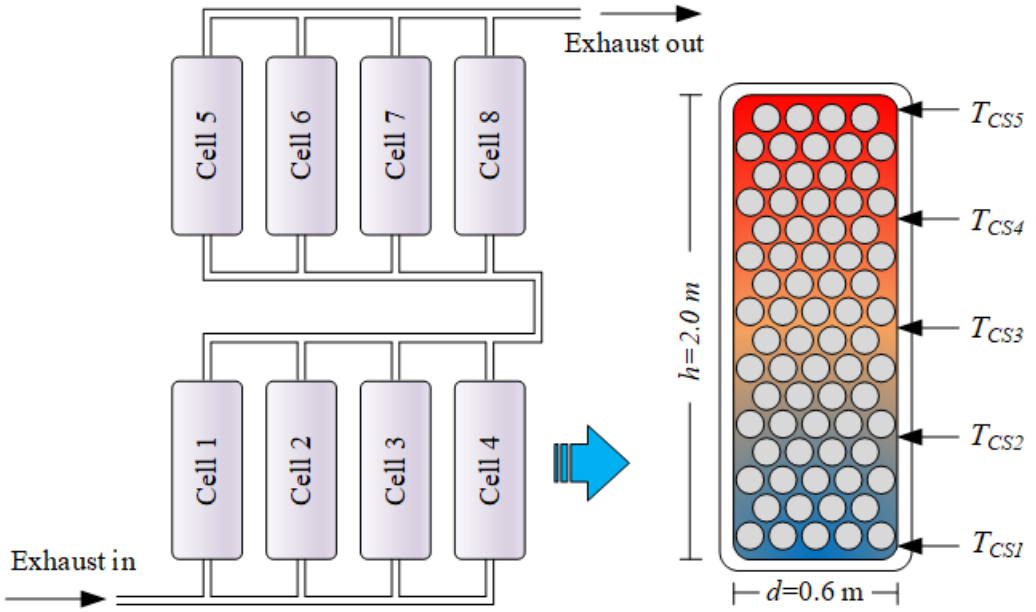

(a)

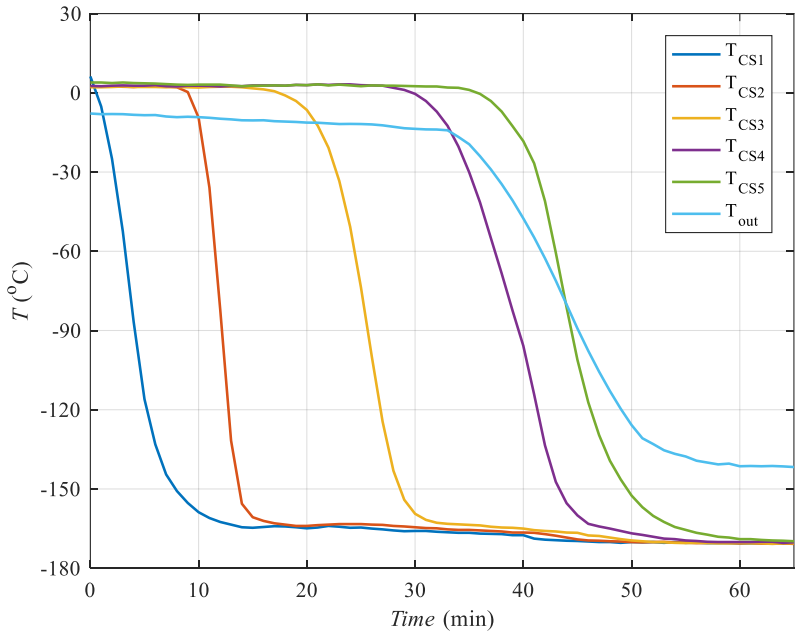

(b)

Figure 4.7 Performance of the packed bed cold store; (a) a schematic arrangement of the cells; (b) temperature evolution of the cold store bed during a discharging cycle.

The performance of the packed bed cold store in the discharging process can be evaluated by the temperature profiles from the five thermocouples. Figure 4.7 (b) illustrates the time evolution of

the temperature distribution in the cells. The profiles (T_{CS1}-T_{CS5} in Figure 4.7) are typical of a packed bed thermal storage system with the propagation of a thermal front, also named as thermocline in reference [145,146]. It can be seen that the cells are fully charged in ~60 minutes. The outlet temperature of the cold store starts to drop after ~30 minutes of charging and finally reduces to around -140 ℃, indicating that the cold energy is not fully captured. Therefore, although packed bed based thermal stores are a viable for cold energy storage in the LAES system, improvements could be achieved through minimising the loss of cold energy.

4.3 Thermodynamic model for the LAES system

A thermodynamic model of the LAES system has been developed to predict the performance of the pilot plant, which also enables further research on the performance optimization of the LAES system. The results indicated that there are urgent needs for reducing the cold energy losses for experimental PRU during the discharging cycle. Also, little attention has been paid on the effect of the cold and hot energy losses on the LAES performance. These will be studied here using a simulation model. It will be shown that the cold energy has much more effect on the LAES performance than the hot energy does; the cold energy loss can lead to a decreased round trip efficiency, which is ~7 times that caused by the hot energy loss. It will also be shown that the recovered cold energy from liquid air PRU is insufficient to achieve the maximum liquid air yield in the charging process, and the difference is ~18%, indicating that external cold sources could significantly increase the round trip efficiency. Unlike the cold energy, ~20-45% of the compression heat cannot be used efficiently in the discharging process, which could also be explored for increasing the round trip efficiency of the LAES.

4.3.1 System description

The configuration of a standalone LAES is shown in Figure 4.8, which consists of a charging process and a discharging process. The charging process often runs at off-peak times: the purified

air is compressed to a high pressure through multistage compression with compression heat recovered and stored with thermal oil; the compressed air is then cooled in the cold box by recycling air and cold storage fluids (propane and methanol) containing cold recovered from liquid air in the discharging cycle. Finally, liquid air is obtained through air expansion in a cryo-turbine and stored in a liquid air tank at approximately 77 K. The discharging process usually works at times of peak electricity demand: the liquid air from the storage tank is pumped to a high pressure, and then releases cold energy to the cold fluids (propane and methanol) in two evaporators, which are later used to cool the compressed air in the charging process; the air is then heated by the hot thermal oil containing heat recovered in the charging cycle before entering air turbines to generate electricity.

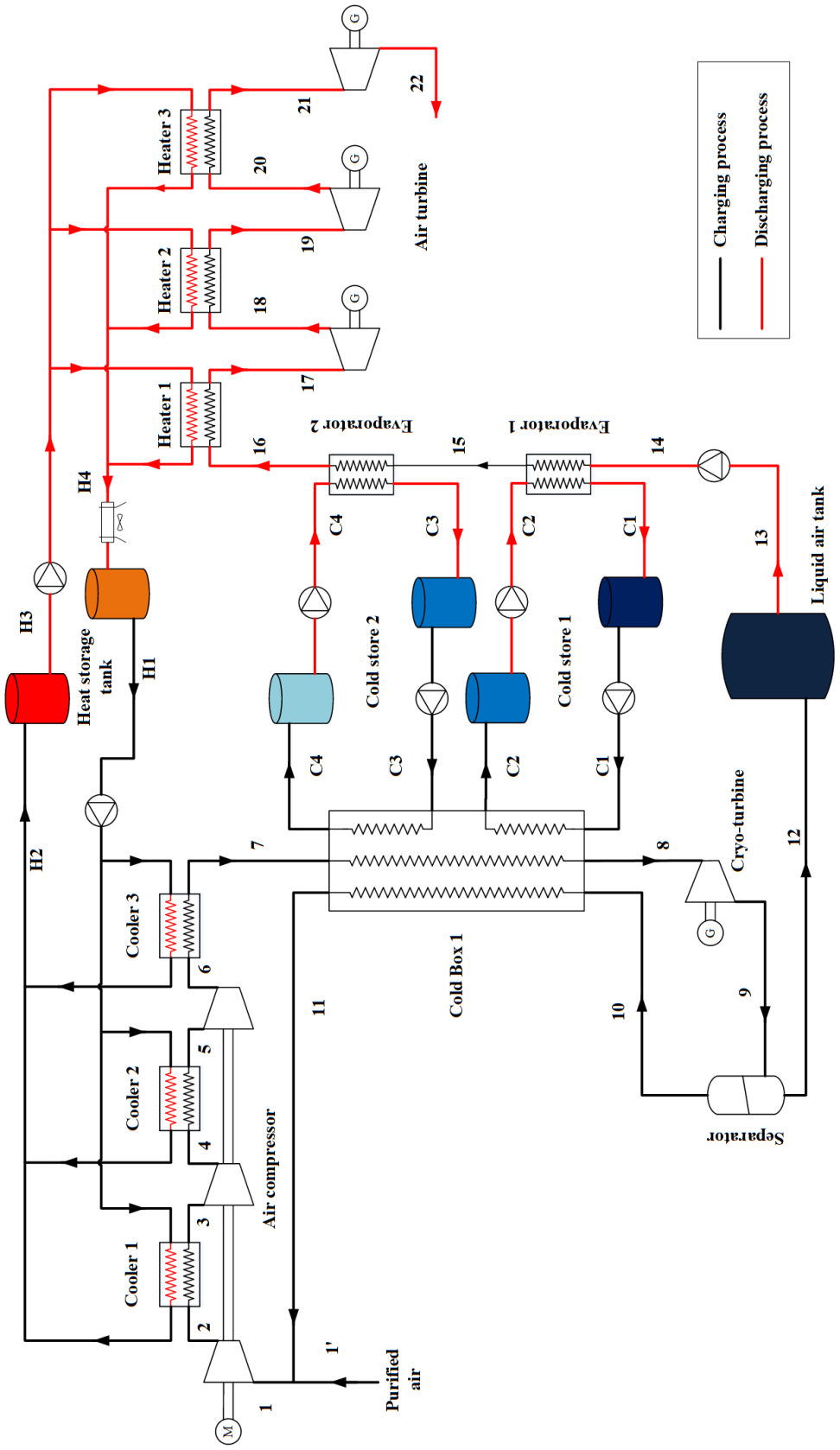

Figure 4.8 Layout of a standalone LAES system.

4.3.2 System model and validation

The entire system is complex. To simplify the system analysis, several assumptions are made as follows:

- The system is in a steady state, and neither dynamic nor transient effects are considered in this part of analyses;
- There is no heat loss through the system components unless otherwise specified.

4.3.2.1 System model

In the charging process of the LAES, dehumidified air is compressed to a high pressure by a multi-stage air compressor, and the air outlet enthalpy at each stage is:

$$h_{i+1} = h_i + \frac{(h_{i+1,s} - h_i)}{\eta_C} \tag{4.1}$$

where, h_i is the specific enthalpy at State *i*; and the subscript *i* refers to 1, 3 or 5; η_c is the isentropic efficiency of the air compressor; and subscript *s* represents the isentropic compression process.

The compressed air (State 7) is cooled down by the recycling air and cold storage fluids (propane and methanol) in the cold box, and the outlet conditions (State 8) are calculated based on energy conservation and pinch point limitation:

$$\begin{aligned} m_{air,c} \cdot (h_7 - h_8) = (1-Y) \cdot m_{air,c} \cdot (h_{11} - h_{10}) + m_{propane,c} \cdot (h_{C2} - h_{C1}) \\ + m_{methanol,c} \cdot (h_{C4} - h_{C3}) \end{aligned} \tag{4.2}$$

$$\gamma = \frac{m_{12}}{m_{air,c}} \tag{4.3}$$

where, $m_{air,c}$, $m_{propane,c}$ and $m_{methanol,c}$ are the mass flow rates of air, propane and methanol in the charging process, respectively; γ is the liquid air yield.

The compressed air after cooling (State 8) expands in the cryo-turbine to the ambient pressure with part of air liquefied. The outlet enthalpy of the two-phase air is:

$$h_9 = h_8 - \eta_{c,T} \cdot (h_8 - h_{9,s}) \tag{4.4}$$

where, $\eta_{c,T}$ is the isentropic efficiency of the cryo-turbine, subscript *s* refers to isentropic process.

In the discharging process, liquid air leaving the liquid air tank (State 13) is pumped to a high pressure, and its outlet enthalpy is calculated by:

$$h_{14} = h_{13} + \frac{(h_{14,s} - h_{13})}{\eta_{pump}} \tag{4.5}$$

where, η_{pump} is the isentropic efficiency of the pump.

The cold energy of the liquid air is recovered through transferring to propane and methanol in the evaporator 1 and evaporator 2, respectively. The outlet conditions of the cold storage fluids could be determined using the energy conservation equations and the pinch point limitation:

$$m_{air,d} \cdot (h_{15} - h_{14}) = m_{propane,d} \cdot (h_{C2} - h_{C1}) \tag{4.6}$$

$$m_{air,d} \cdot (h_{16} - h_{15}) = m_{methanol,d} \cdot (h_{C4} - h_{C3}) \tag{4.7}$$

where, $m_{air,d}$, $m_{propane,d}$ and $m_{methanol,d}$ are the mass flow rates of air, propane and methanol in the discharging process, respectively.

In the multi-stage air turbine, the high-pressure air enters each stage to generate electricity. The outlet enthalpy of the air of each stage is given by:

$$h_{i+1} = h_i - \eta_T \cdot (h_i - h_{i+1,s}) \tag{4.8}$$

where, η_T is the isentropic efficiency of the air turbine; subscript *i* refers to 17, 19 or 21.

The round trip efficiency of the LAES, η_{RTE}, is defined as the ratio of the net output work of the discharging process ($W_{air,out}$) to the net input work consumed to produce liquid air in the charging process ($W_{air,in}$):

$$\eta_{RTE} = \frac{W_{air,out}}{W_{air,in}} \tag{4.9}$$

$$W_{air,out} = (h_{17} - h_{18}) + (h_{19} - h_{20}) + (h_{21} - h_{22}) - (h_{14} - h_{13}) \tag{4.10}$$

$$W_{air,in} = \frac{m_{air,c} \cdot ((h_2 - h_1) + (h_4 - h_3) + (h_6 - h_5) - (h_8 - h_9))}{m_{12}} \tag{4.11}$$

The exergy efficiency of the charging process of the LAES, $E_{eff,c}$, is defined as the ratio of exergy output ($E_{out,c}$) to exergy input ($E_{in,c}$):

$$E_{eff,c} = \frac{E_{out,c}}{E_{in,c}} \tag{4.12}$$

$$E_{out,c} = Y \cdot m_{air,c} \cdot e_{12} + m_{oil,c} \cdot e_{H2} \tag{4.13}$$

$$E_{in,c} = W_{air,in} + m_{propane,c} \cdot (e_{C1} - e_{C2}) + m_{methanol,c} \cdot (e_{C3} - e_{C4}) \tag{4.14}$$

where, $m_{oil,c}$ is the total mass flow rate of thermal oil in the charging process; and e is the specific exergy.

The exergy efficiency of the discharging process of the LAES, $E_{eff,d}$, is calculated by:

$$E_{eff,d} = \frac{E_{out,d}}{E_{in,d}} \tag{4.15}$$

$$E_{out,d} = W_{air.out} + m_{propane,d} \cdot (e_{C1} - e_{C2}) + m_{methanol,d} \cdot (e_{C3} - e_{C4}) \tag{4.16}$$

$$E_{in,d} = m_{air,d} \cdot e_{13} + m_{oil,d} \cdot e_{H2} \tag{4.17}$$

where, $m_{oil,di}$ is the mass flow rate of thermal oil in the discharging process.

4.3.2.2 Model validation

Before performing thermodynamic analyses, the system model was validated by comparing with the available numerical data in the literature. Figure 4.9 compares the performance of LAES of this study and that obtained by Guizzi et al. [114], for a discharging pressure of 6.5 MPa. The maximum deviation between the two sets of data is 4.2% for the LAES. The simulation results match well with the reference data. Hence, the system model is acceptable for the following simulation.

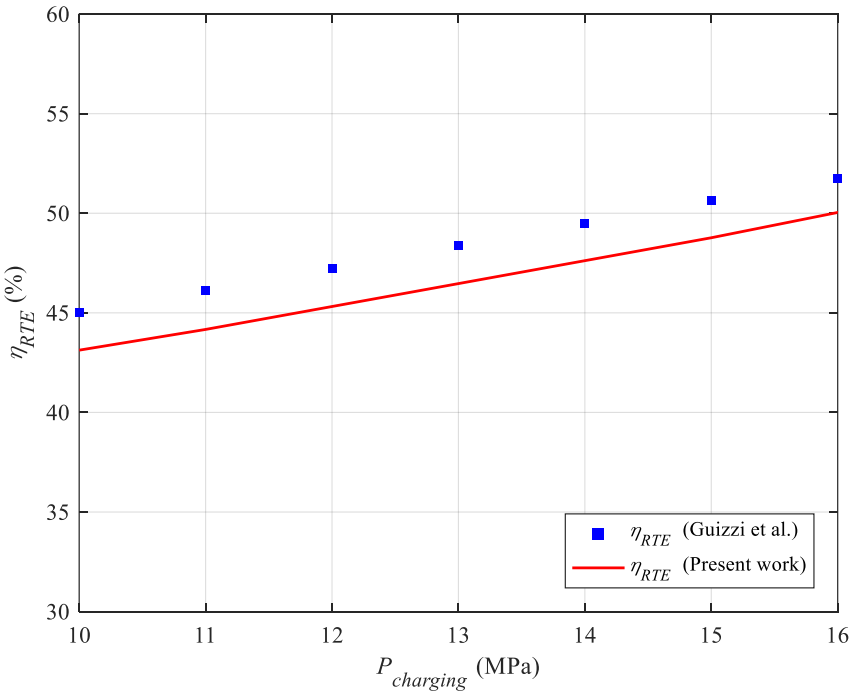

Figure 4.9 Model validation by comparing with the literature data of Guizzi et al. [114].

4.3.3 Results and discussions

Table 4.2 lists the operating conditions used for the analyses of the standalone LAES system.

Table 4.3 gives the data at each point/state of the LAES system for a given set of working conditions of P_c=14 MPa; P_d=8 MPa. The simulations used after CO_2 and water removal with 78.12% nitrogen, 20.96% oxygen and 0.92% argon and the energy consumption of the removal process is included in the consumption of the air compression. The calculations were done in the MATLAB environment, with the thermal properties of air, propane, methanol obtained for REFPROP 8.1, and

the thermal properties of thermal oil from the ASPEN plus database. Note that isentropic efficiency of 90% can be achieved in industry, and actually this value has been widely used in the LAES literature [130,132,133,147–149].

Table 4.2 Default parameters of the LAES.

Parameter	Value	Unit
Ambient Temperature	293	K
Ambient Pressure	100	kPa
Thermal oil temperature	293	K
Minimum propane temperature	95	K
Minimum methanol temperature	214	K
Ammonia evaporation temperature	250	K
Pinch point of Cooler	2	K
Pinch point of Heater	5	K
Pinch point of Cold box	5	K
Pinch point of Evaporator	2	K
Relative pressure drops of heat exchanger	1%	
Isentropic efficiency of Compressor	85%	
Isentropic efficiency of Turbine	90%	
Isentropic efficiency of Cryo-turbine	75%	
Isentropic efficiency of Pump	75%	

Table 4.3 Stream Data of a standalone LAES system (P_c=14 MPa; P_d=8 MPa).

	$\dot{m}/\dot{m}_{air,ch}$	T [K]	P [MPa]	h [kJ/kg]	Fluids
1	1.000	293.00	0.100	293.27	air

2	1.000	493.58	0.519	496.62	air
3	1.000	303.00	0.514	302.42	air
4	1.000	510.69	2.669	513.39	air
5	1.000	303.00	2.643	297.81	air
6	1.000	513.23	13.721	513.10	air
7	1.000	303.00	13.584	277.80	air
8	1.000	100.08	13.448	-77.40	air
9	1.000	79.88	0.110	-92.59	air
10	0.161	82.45	0.110	79.60	air
11	0.161	270.44	0.109	270.55	air
12	0.839	79.66	0.110	-124.88	air
13	0.839	79.66	0.110	-124.88	air
14	0.839	83.13	8.000	-112.91	air
15	0.839	212.00	7.920	176.41	air
16	0.839	291.00	7.841	273.83	air
17	0.839	479.89	7.762	478.88	air
18	0.839	331.71	1.801	329.22	air
19	0.839	479.89	1.783	481.80	air
20	0.839	333.15	0.414	333.14	air
21	0.839	479.89	0.410	482.59	air
22	0.839	333.54	0.095	334.11	air
H1	1.917	293.00	0.100	422.83	thermal oil
H2	1.917	489.89	0.100	759.34	thermal oil
H3	1.487	489.89	0.100	759.34	thermal oil
H4	1.487	328.17	0.100	473.08	thermal oil

Table 4.4 presents the system performance of the LAES under the working conditions in Table 4.2. The net input work per unit mass of liquid air in the charging process is ~731.9 kJ/kg, whereas the net output work per unit mass of liquid air in the discharging process approaches 434.7 kJ/kg,

leading to the round trip efficiency of 59.40% for the LAES system. The ratios of the stored exergy in the liquid air tank, the cold store and the hot store are 50.63%, 33.28% and 16.09% respectively.

Table 4.4 Simulation results of the LAES (P_c=14 MPa; P_d=8 MPa).

Items	LAES	
	charging	discharging
Net work per unit mass of liquid air (kJ/kg)	731.9	434.7
Exergy efficiency	0.84	0.81
Exergy loss	31.96%	
Liquid air yield	0.840	
Stored exergy ratio in liquid air store	50.63%	
Stored exergy ratio in cold store	33.28%	
Stored exergy ratio in hot store	16.09%	
Round trip efficiency	59.40%	

The composite curves for key heat transfer components shown in Figure 4.10 illustrate that the temperature gradients of the working fluids in each of components match well with the constraints at the pinch points, suggesting very effective heat exchange. Figure 4.11 shows the *T-s* diagrams of the charging cycle, discharging cycle, ORC cooled by the ambient water and the ORC-ARC.

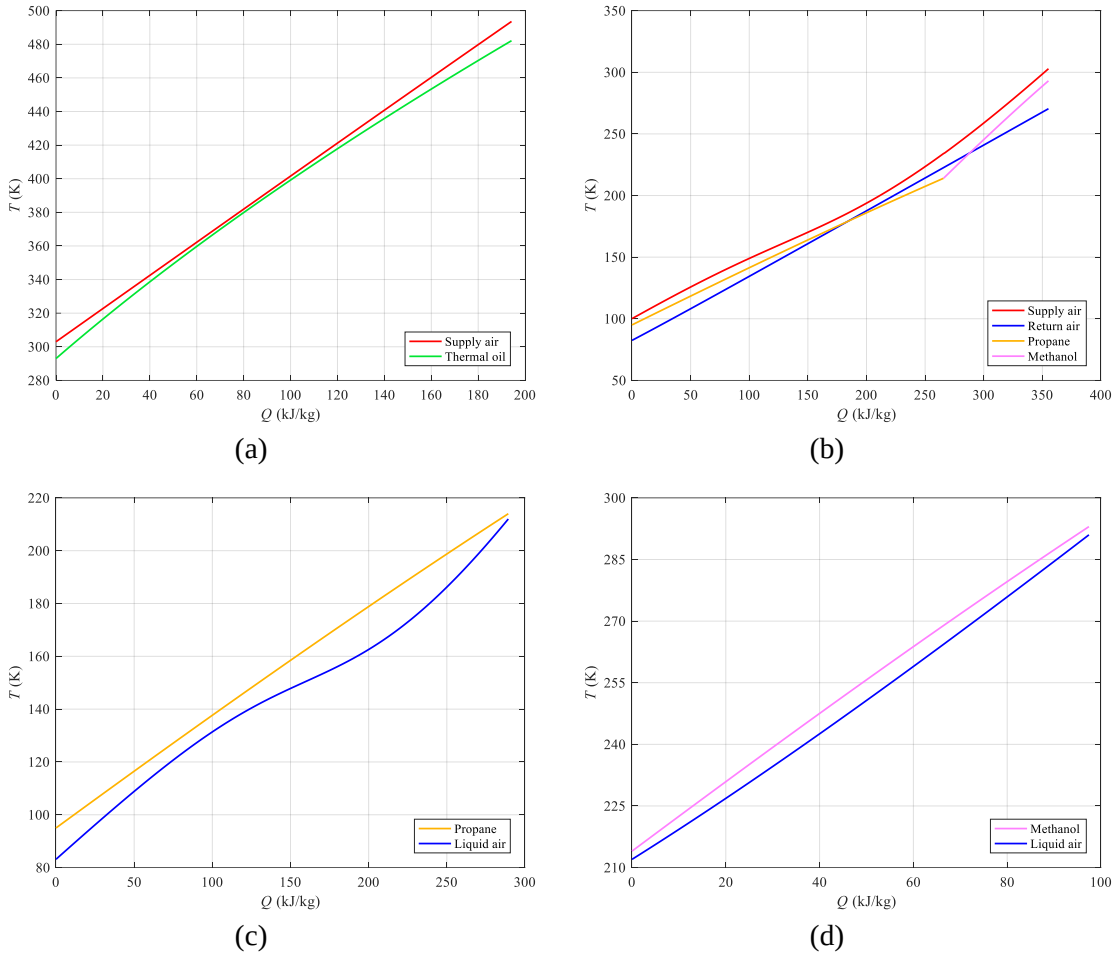

Figure 4.10 Composite curves of heat exchangers: (a) Cooler; (b) Cold box; (c) Evaporator 1; (d) Evaporator 2.

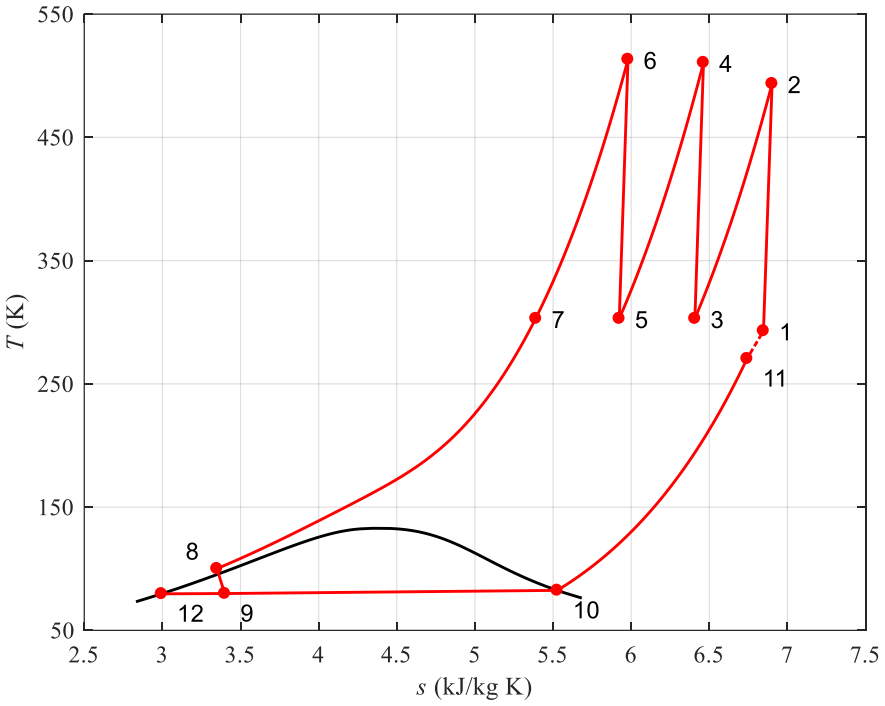

(a)

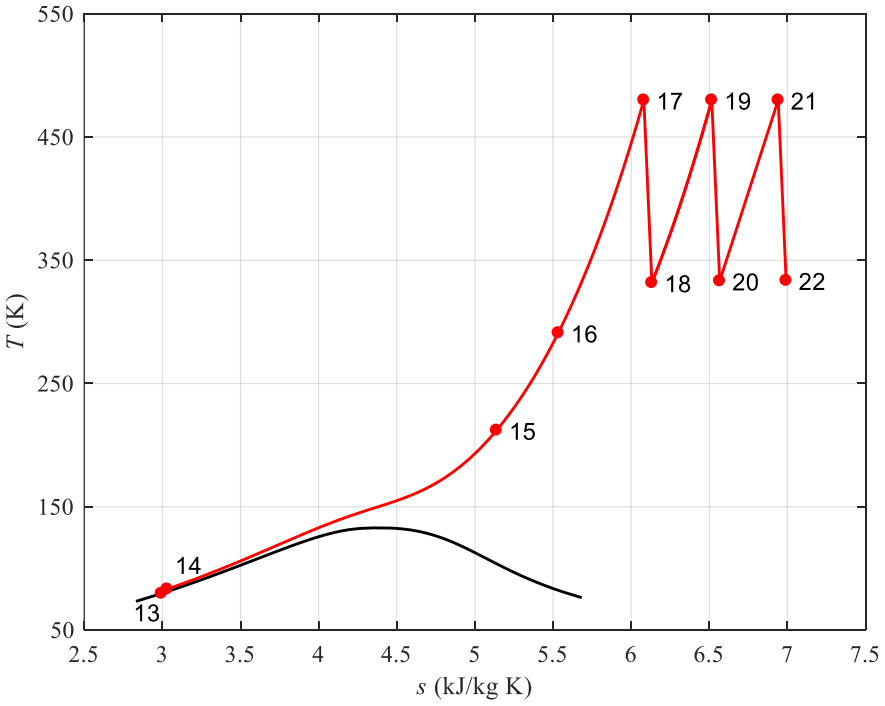

(b)

Figure 4.11 *T*-*s* diagrams: (a) charging process; (b) discharging process (P_c=14 MPa; P_d=8 MPa).

4.3.4 Effects of design parameters on the LAES performance

4.3.4.1 Influence of charging and discharging pressures

Figure 4.12 shows the effect of the charging pressure on the LAES performance. One can see that an increase in the charging pressure results in a significant increase in liquid air yield and a maximum value of ~0.84 occurs at a charging pressure of 14 MPa beyond which there is a little further increase. However, the electricity consumption of compressors shows a continuous increase. The exergy efficiency of the charging process increases gradually with the increase in the charging pressure, whereas the dependence of the round trip efficiency on the charging pressure shows a maximum at ~14MPa. This is because the liquid air yield is almost constant when the charging pressure is above 14 MPa, whereas a further increase in the charging pressure leads to an increase of net work consumption of compressors and hence the decrease of the round trip efficiency.

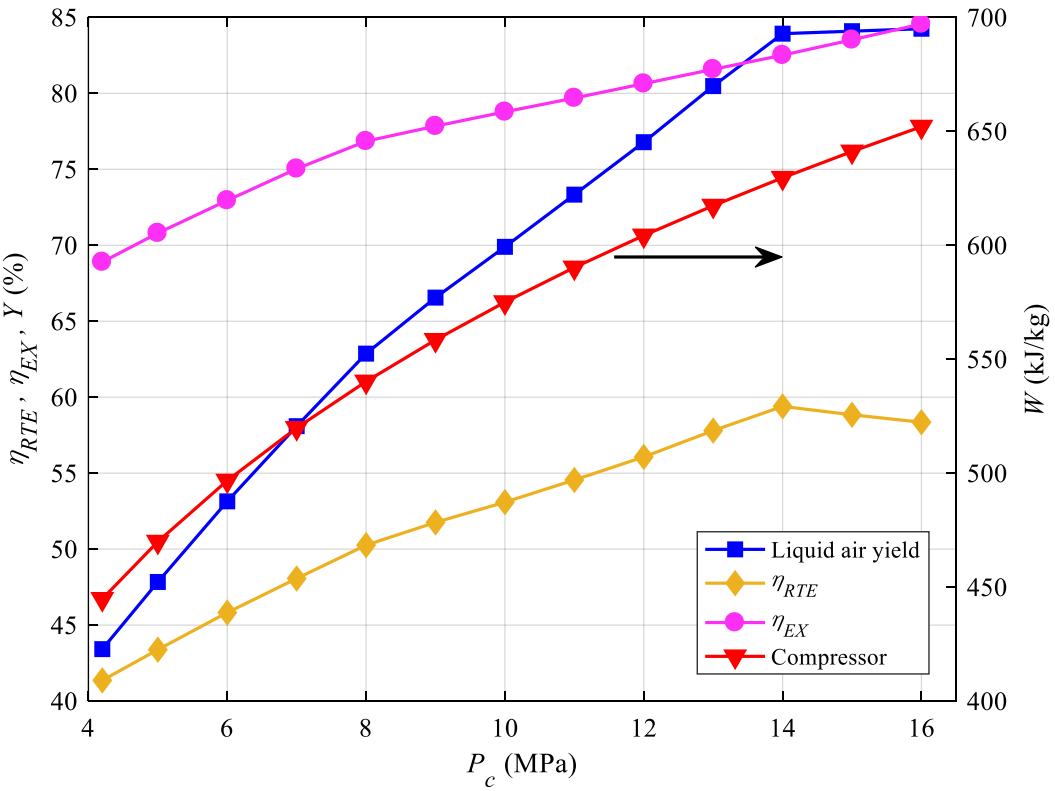

Figure 4.12 Influence of charging pressure on the LAES performance (P_d=8 MPa).

The round trip efficiency of the LAES at different discharging pressures is shown in Figure 4.13. When the charging pressure is relatively low at ~4-8 MPa, the discharging pressure does not show much effect on the round trip efficiency. This is due to the balance between the decrease of liquid air yield and the increase of output power. When the charging pressure is in the range of ~8-14 MPa, the round trip efficiency decreases gradually with increasing discharging pressure, due to the extent of the decrease of the liquid air yield exceeding the extent of the increase of output work. When the charging pressure is above 14 MPa, round trip efficiency reaches the maximum and a high discharging pressure is beneficial to the LAES performance.

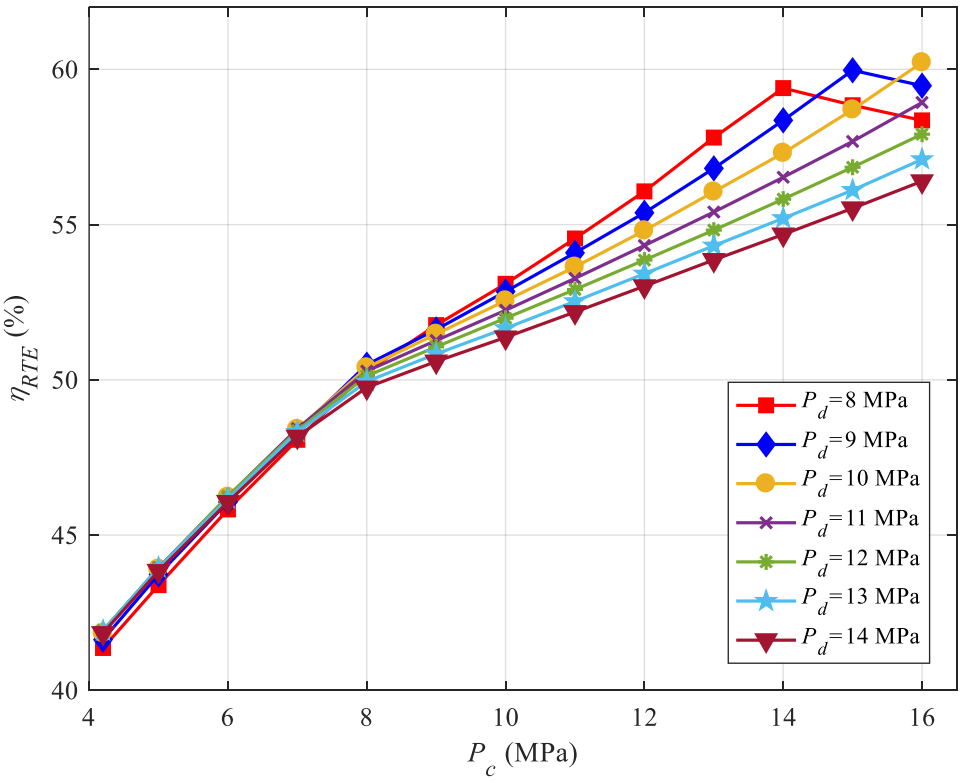

Figure 4.13 Influence of discharging pressure on the LAES with different charging pressures.

4.3.4.2 Influence of thermal losses of the heat and cold storage

Thermal dissipation to the environment is inevitable during energy storage processes. In the LAES, hot energy is stored in the thermal oil while the cold energy is stored with propane and methanol.

Energy losses lead to temperature decrease of the thermal oil and temperature increase of the propane and methanol, but the amount of fluids (thermal oil, propane and methanol) does not change. Figure 4.14 illustrates the effect of energy losses of the fluids on the round trip efficiency of the LAES with a charging pressure of 14 MPa and a discharging pressure of 8 MPa. The round trip efficiency of the LAES drops from 59.4% to 58.1% as the heat energy loss increases from 0 to 5%, while it decreases significantly to 50% as the cold energy loss increases to 5%. The energy losses of hot and cold energy can both decrease the performance of the LAES, but the extent of decrease caused by the cold energy losses is ~7 times that by the hot energy losses under a given operating conditions. Excellent thermal insulation of the stores is therefore essential to minimize the part of energy losses for the LAES system.

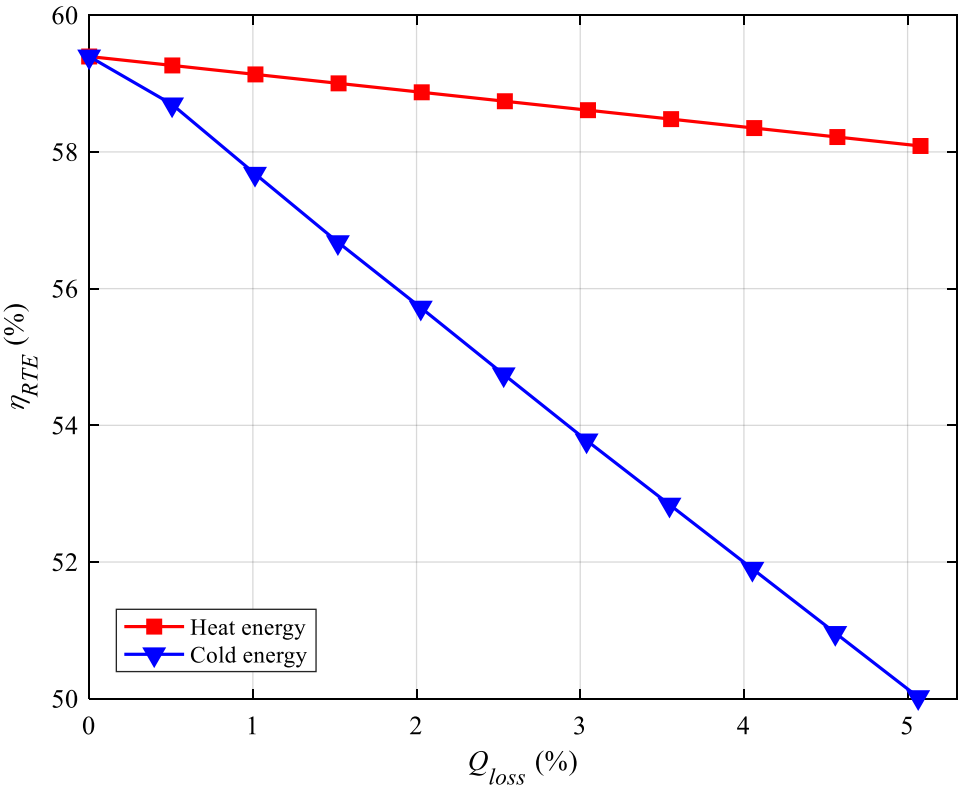

Figure 4.14 Influences of energy losses of the hot fluid (thermal oil) and cold fluids (propane and methanol) during storage processes on the LAES (P_c=14 MPa, P_d=8 MPa).

4.3.4.3 Influence of cold recovery of liquid air

Cold recovery of liquid air in the discharging process is crucial to cool the compressed air to a low temperature in the charging process. In this study, propane and methanol are used to respectively recover and store the high grade and low-grade cold energy from the liquid air, respectively. As the compressed air has a lower specific heat capacity at medium temperatures (above ~220 K), it is easy to be cooled in this temperature range. However, it has a much higher specific heat capacity at low temperatures (~100 K) which requires a higher grade of cold energy to be cooled down [132], as shown in Figure 4.15 (a). Cold methanol and propane can be used to cool the compressed air respectively to a medium temperature and a low temperature. The effect of the cold methanol flow rate on the liquid air yield of the LAES is shown in Figure 4.15 (b), which indicates that external free cold sources with the same energy grade as methanol have little effects on neither liquid air yield nor the round trip efficiency of the LAES. On the other hand, the cold propane, which will be shown in Figure 4.16, has a significant effect on the LAES performance.

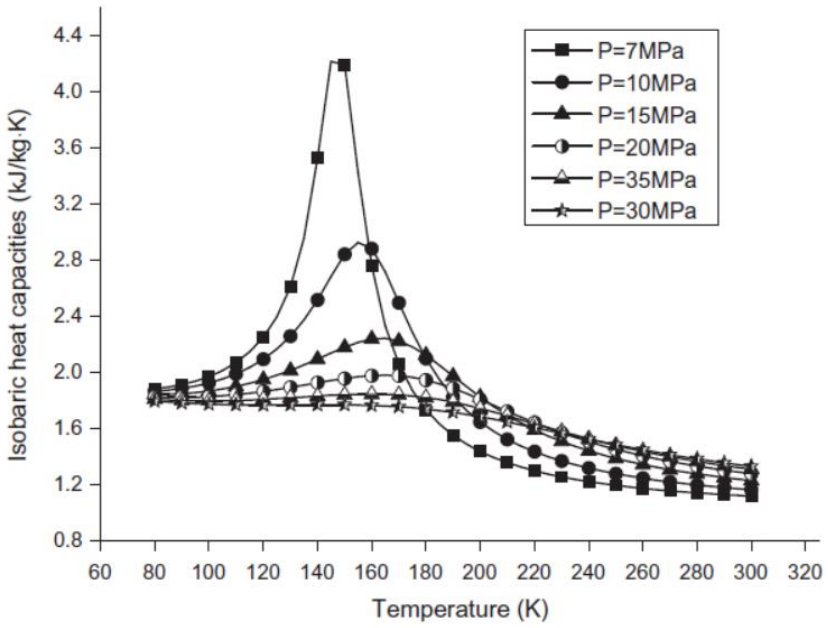

(a)

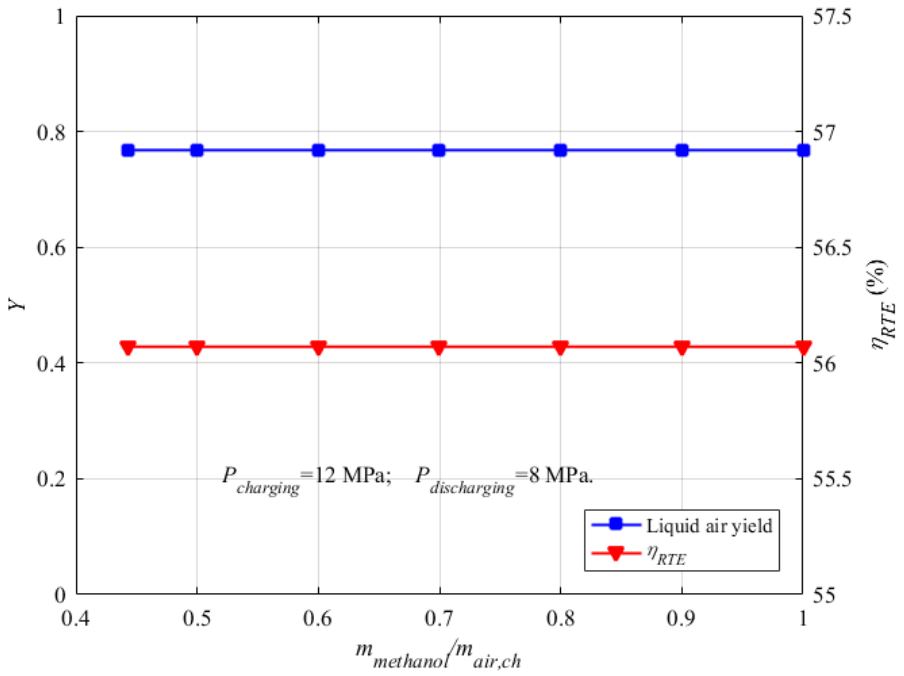

(b)

Figure 4.15 Effect of low-grade cold energy; (a) Isobaric heat capacity of air as a function of temperature at different [132]; (b) effect of cold methanol on the liquid air yield of the LAES.

The dashed lines in Figure 4.16 indicate the maximum amounts of cold propane that can be produced by using the cold recovered from the evaporation of liquid air under different charging

pressures. An increase in the amount of cold propane increases the liquid air yield till the maximum and then any further increase contributes less to the yield, as shown in Figure 4.16 (a). This is because the gaseous air has been cooled to the lowest temperature limited by the pinch point in the heat exchanger, and a further increase in the cold propane flow does not give further effect. It is noted that the maximum amount of cold propane produced in the evaporating liquid air is ~10.7-17.8% lower than the optimal value. This implies that a further improvement on the liquid air yield can be meet by external (free) high grade cold sources, such as cold energy from LNG evaporation. The round trip efficiency of the LAES shows a similar trend to the liquid air yield and it is possible to achieve 60.5% if external cold sources could be implemented (Figure 4.16 (b)).

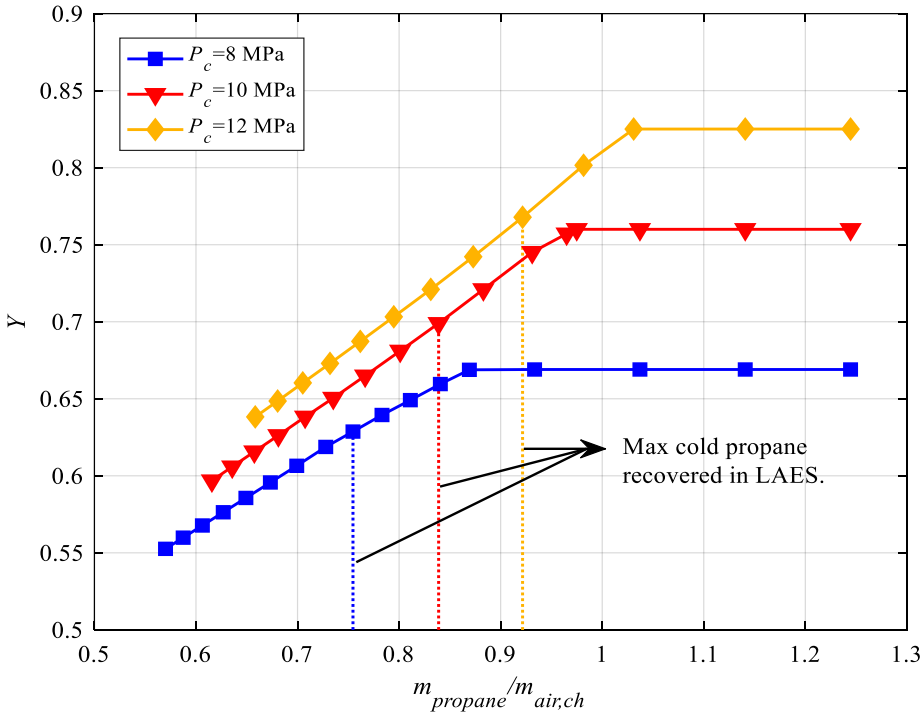

(a)

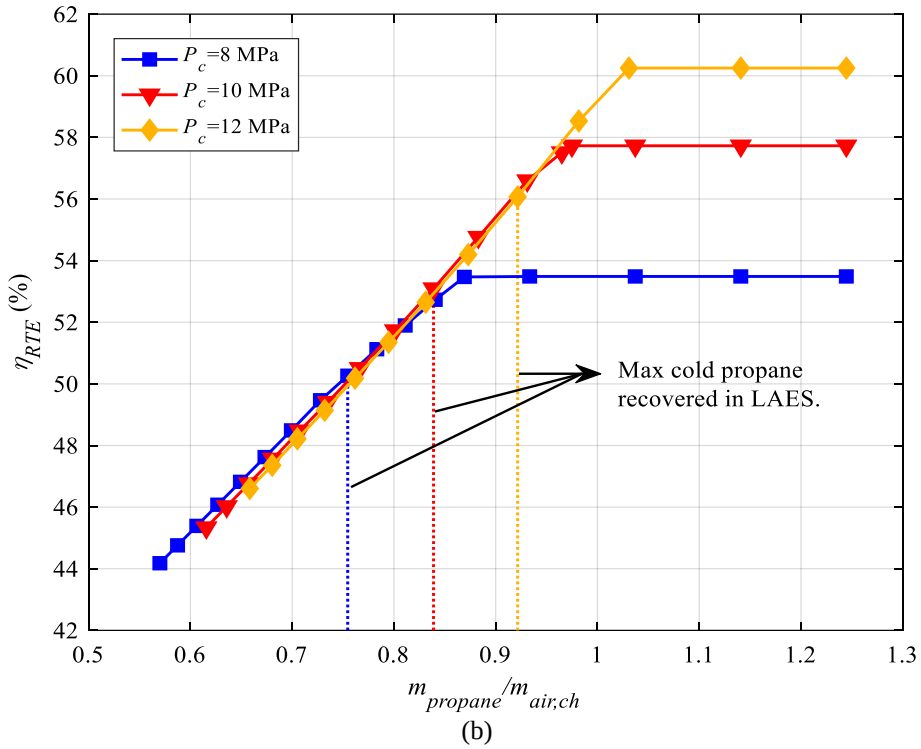

(b)

Figure 4.16 Insufficient high-grade cold energy (propane) to achieve the largest liquid air yield (a) and round trip efficiency (b) of the LAES (P_d=8 MPa).

4.3.4.4 Influence of heat recovery of compressed air

In the charging process, ambient air is compressed to a high pressure, accompanied with compression heat generation. Recovery of such heat is important for enhancing the LAES performance. In this work, thermal oil is used to store the heat for use in the discharging process, and sensitivity analysis is carried out under different charging and discharging pressures. Figure 4.17 shows the results of how much compression heat is excess during the LAES operation. One can see that some 20-45% of the compression heat cannot be used efficiently. This opens an opportunity to improve the system performance by using the compression heat. A heat pumped system can be used to increase the temperature of the thermal oil by using amount of external power in the charging process of the LAES system, leading to an increase in the output power in the discharging process. The compression heat can also be used to drive the other power generation,

the examples, such as LAES-ORC system, LAES-ORC-VCRC system and LAES-ORC-ARC system, will be discussed in later chapters.

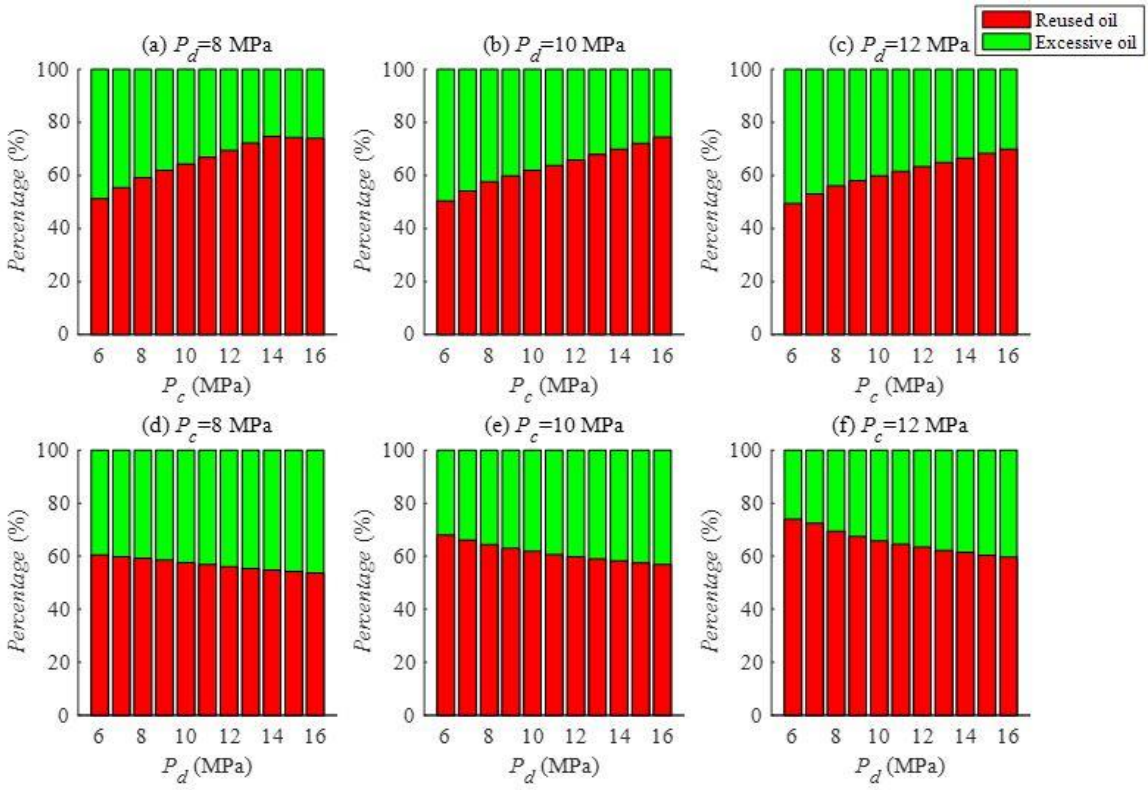

Figure 4.17 Excess compression heat (hot thermal oil) in the LAES with different charging and discharging pressures.

4.4 Conclusions of Chapter 4

This chapter first presents the detailed configuration of the world first LAES pilot plant, and some real experimental data including factors affecting the net output power, start-stop performance, and the cold store. A steady state thermodynamic model was then described for a standalone plant consisting of thermal (hot and cold) energy stores. The model was then validated with the literature data before a detailed sensitivity analyses was carried out.

The main conclusions are as follows:

- The experimentally measured output power correlates well with the mass flow rate, for a given set of pressure and temperature before turbine. The inter-stage reheating temperature significantly affects the output power: an increase of 1℃ contributes to an increase of ~1 kW in output power.
- The pilot plant LAES gives an excellent dynamic response, which could bring ~70% of maximum power output in 2 minutes.
- The modelling results show that energy losses of the cold and hot energy stores significantly affect the performance of a standalone LAES. The round trip efficiency of the LAES drops from 59.4% to 58.1% when the hot energy loss increases from 0 to 5%. The effect of the cold energy loss is significantly larger: the round trip efficiency reduces to 50% when the cold energy loss increases to 5%, which is ~7 times that caused by the hot energy losses under a given set of operating conditions. Therefore, good thermal insulation of the stores is needed, particularly for the cold store, to ensure a good round trip efficiency.
- High-grade cold energy recovered from the evaporation of liquid air in the discharging process is insufficient to achieve the maximum liquid air yield in the charging process, which provides an opportunity for the use external cold sources, such as waste cold from the regasification of liquified natural gas.

- There is ~20-45% of compression heat in the charging process which cannot be efficiently used in the discharging process. The use of such excessive heat provides more opportunities to increase the round trip efficiency of the LAES.

Chapter 5 Integration of the LAES with Organic Rankine Cycle (ORC) and Vapor Compression Refrigeration Cycle (VCRC)

5.1 Introduction

As mentioned in previous chapters, very little has been done on the effective utilization of heat of compression in the LAES for the round trip efficiency enhancement. The heat of compression from the charging process has been configured for full use to increase the output power of the turbine in the discharging process. This, as demonstrated in Chapter 4, if harvested and stored in an efficient way even using current configuration, cannot be fully used in the discharging process and there is ~20-45% of excess heat depending on the system parameters. A new configuration, termed the LAES-ORC-VCRC system, is proposed for more efficient utilization of the excess heat. Such a configuration consists of a traditional LAES, an organic Rankine cycle (ORC) and a vapor compression refrigeration cycle (VCRC). Thermodynamic analyses are performed on the newly proposed system. Comparisons are made between the LAES-ORC-VCRC and the LAES with different charging and discharging parameters. The results show that new system configuration has a significant improved round trip efficiency and the discharging exergy efficiency, compared with the conventional LAES system. An economic analysis will also be performed on the integrated LAES-ORC-VCRC system with a project life-span of 15 years. The results are compared with the use of the single ORC.

5.2 The LAES-ORC-VCRC System

5.2.1 System description

Figure 5.1 shows the newly proposed LAES-ORC-VCRC system. The system consists of a charging cycle, a discharging cycle, an organic Rankine cycle (ORC), and a vapor compression refrigeration cycle (VCRC). The charging cycle is the same as the traditional LAES, whereas the

discharging cycle, the organic Rankine cycle and the vapor compression refrigeration cycle can be regarded as an integrated or a coupled discharging cycle of the new LAES system. The main feature of the LAES-ORC-VCRC is that the stored heat of compression is split into two streams; one stream is used in the discharging cycle (similar to the LAES) and the other stream is used in the organic Rankine cycle.

At off-peak hours, excess electricity is used to liquefy air. In this process, ambient air is cleaned first to obtain purified air (State 1) and compressed to a high pressure (State 8) with the heat of compression harvested and stored in a heat storage tank using thermal oil as the storage medium with a 2-tank arrangement. The compressed air is then cooled down by cold energy captured during the discharging process and stored in cold storage tanks 1 and 2 (State 10) using methanol and propane as both cold storage media and heat transfer fluids, respectively. Finally, liquid air (State 24) is produced through expansion.

At peak hours, the discharging cycle, the organic Rankine cycle and the vapor compression refrigeration cycle work simultaneously to generate electricity. In the discharge cycle, liquid air (State 24) is pumped to high pressure (State 25) and transfers the cold energy to propane and methanol through heat exchange with recovered cold energy stored in the cold storage tanks 1 and 2 (both with a 2-tank arrangement). The air (State 27) is then heated up by one stream of the heat of compression through heat exchange with the thermal oil stored in the heat storage tank, expand and produce electricity.

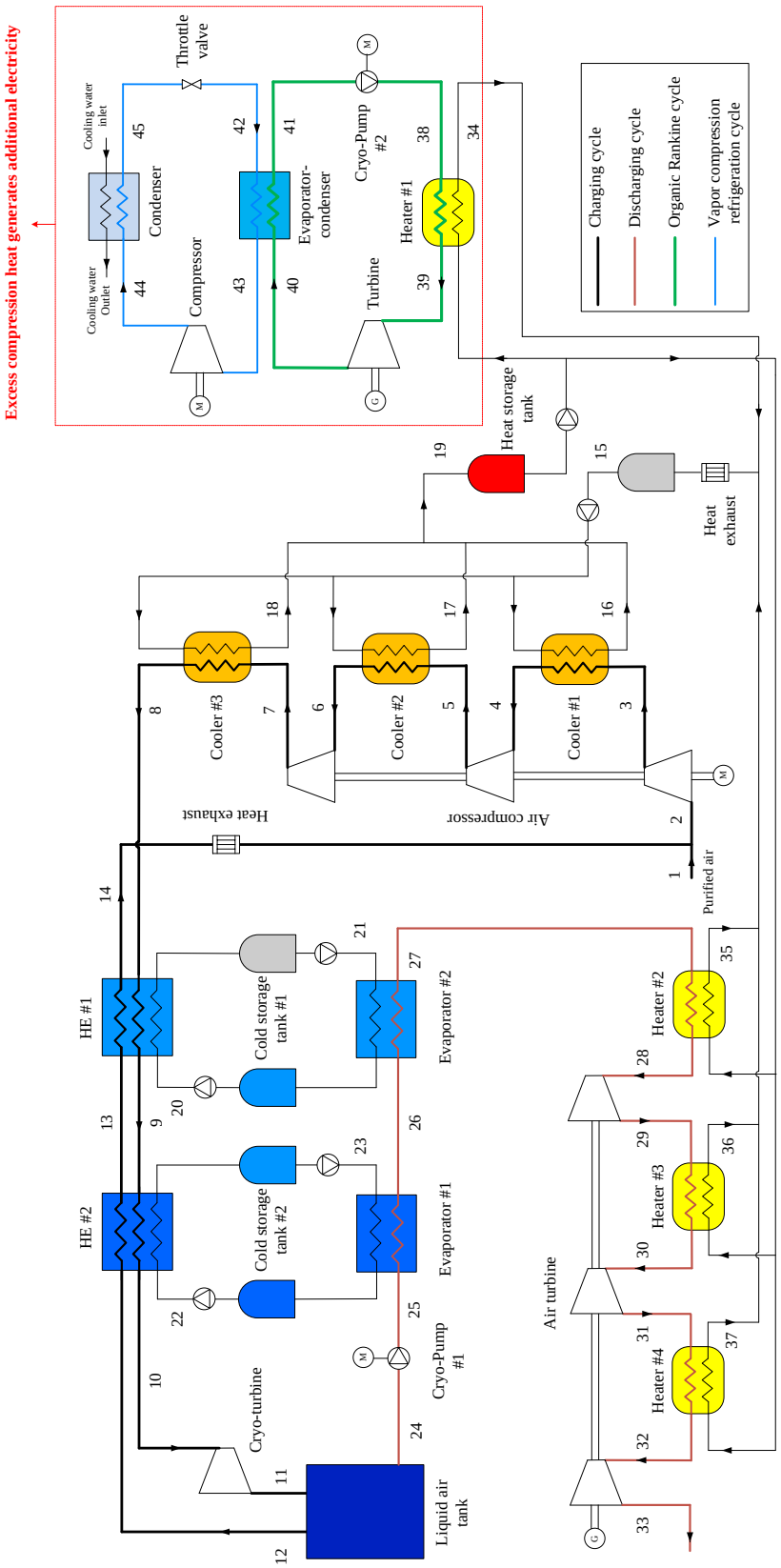

Figure 5.1 A schematic diagram of the LAES-ORC-VCRC system.

In the organic Rankine cycle, the excess heat of compression stored in heat storage tank is used to heat the high-pressure working fluid (State 38) to produce additional electricity through expansion of the working fluid (State 39). The low-pressure working fluid (State 40) is condensed to State 41, pumped to high pressure (State 38) to complete the cycle. The vapor compression refrigeration cycle consumes electricity to produce cold energy (State 42) for condensing the working fluid (State 40) in the organic Rankine cycle.

5.2.2 System model

Round trip efficiency and exergy efficiency are two key performance indexes for the evaluation of the LAES system. They are explained in the following sub-sections.

5.2.2.1 Round trip efficiency

The round trip efficiency is defined as the power output in the discharging cycle divided by the power input in the charging cycle.

In the charging cycle, the net power input is given by:

$$W_{air,in} = m_{air,c} \cdot ((h_3 - h_2) + (h_5 - h_4) + (h_7 - h_6) - (h_{10} - h_{11})) \tag{5.1}$$

where $m_{air,c}$ is the air mass flow rate of the charging process, and h_i is the specific enthalpy with i corresponding to State i shown in Figure 5.1.

In the discharging cycle, the net power output is:

$$W_{air,out} = m_{air,d} \cdot ((h_{28} - h_{29}) + (h_{30} - h_{31}) + (h_{32} - h_{33}) - (h_{25} - h_{24})) \tag{5.2}$$

$$m_{air,d} = Y \cdot m_{air,c} \tag{5.3}$$

where $m_{air,d}$ is the mass flow rate of liquid air in the discharging process, and Y is the liquid yield.

In the vapor compression refrigeration cycle, the net power input is as follows:

$$W_{vap,in} = m_{vap} \cdot (h_{44} - h_{43}) \tag{5.4}$$

where m_{vap} is the mass flow rate of the refrigerant.

In the organic Rankine cycle, the net power output is:

$$W_{rank,out} = m_{rank} \cdot ((h_{39} - h_{40}) - (h_{38} - h_{41})) \tag{5.5}$$

where m_{rank} is the mass flow rate of the working fluid in the organic Rankine cycle.

The round trip efficiency of the LAES is defined as:

$$\eta_{RTE,LAES} = \frac{W_{air,out}}{W_{air,in}} \tag{5.6}$$

The round trip efficiency of the LAES-ORC-VCRC is calculated by:

$$\eta_{RTE,LAES-ORC-VCRC} = \frac{W_{air,out} + W_{rank,out} - W_{vap,in}}{W_{air,in}} \tag{5.7}$$

The round trip efficiency improvement can therefore be given by:

$$\eta_{RTE,imp} = \frac{\eta_{RTE,LAES-ORC-VCRC} - \eta_{RTE,LAES}}{\eta_{RTE,LAES-ORC-VCRC}} \tag{5.8}$$

5.2.2.2 Exergy efficiency

The exergy efficiency of the charging process gives an indication of the ability of the process to produce liquid air with a given power input, whereas the exergy efficiency of the discharging process shows the ability of the process to generate output power with a given amount of liquid air.

The output exergy of the charging cycle is calculated by:

$$E_{air,c,out} = m_{air,l} \cdot e_{24} + m_{oil} \cdot (e_{19} - e_{15}) \tag{5.9}$$

$$m_{oil} = R_{oil} \cdot m_{air,c} \tag{5.10}$$

where m_{oil} is the mass flow rate of cold thermal oil, R_{oil} is the ratio of mass flow rate of the cold thermal oil to the air in the charging process, and e_i is the specific exergy at i^{th} State as shown in Figure 5.1.

The input exergy of the charging cycle is:

$$E_{air,c,in} = W_{air,in} + m_{propane} \cdot (e_{22} - e_{23}) + m_{methanol} \cdot (e_{20} - e_{21}) \tag{5.11}$$

where $m_{propane}$ and $m_{methanol}$ are the mass flow rates of propane and methanol in the cold storage tanks 2 and 1, respectively.

The exergy efficiency of the charging cycle is given by:

$$\eta_{ex,air,c} = \frac{E_{air,c,out}}{E_{air,c,in}} \tag{5.12}$$

The output exergy of the discharging cycle is calculated by:

$$E_{air,d,out} = W_{air,out} + m_{propane} \cdot (e_{22} - e_{23}) + m_{methanol} \cdot (e_{20} - e_{21}) \tag{5.13}$$

The input exergy of the discharging cycle is:

$$E_{air,d,in} = m_{air,d} \cdot e_{24} + m_{oil,d} \cdot (e_{19} - e_{15}) \tag{5.14}$$

$$m_{oil,d} = R_{oil,d} \cdot m_{air,c} \tag{5.15}$$

where $m_{oil,dis}$ is the mass flow rate of hot thermal oil used in the discharging cycle, and $R_{oil,dis}$ is the mass flow ratio of hot thermal oil to the air in the charging process.

The exergy efficiency of the discharging cycle can therefore be defined as:

$$\eta_{ex,air,d} = \frac{E_{air,d,out}}{E_{air,d,in}} \tag{5.16}$$

The exergy efficiency of the organic Rankine cycle is calculated by:

$$\eta_{ex,rank} = \frac{W_{rank,out}}{(m_{oil} - m_{oil,d}) \cdot (e_{19} - e_{15}) + m_{vap} \cdot (e_{42} - e_{43})} \tag{5.17}$$

where m_{oil}-$m_{oil,d}$ represents the mass of the thermal oil in the hot storage tank that store excess heat for heating up the working fluid of the organic Rankine cycle.

The exergy efficiency of the vapor compression refrigeration cycle is defined as:

$$\eta_{ex,vap} = \frac{m_{vap} \cdot (e_{42} - e_{43})}{W_{vap,in}} \tag{5.18}$$

The exergy efficiency of the integrated or coupled discharging cycle in the LAES-ORC-VCRC system, including the discharging cycle, the organic Rankine cycle and the vapor compression refrigeration cycle, can be given by:

$$\eta_{ex,coup,d} = \frac{W_{air,out} + m_{propane} \cdot (e_{22} - e_{23}) + m_{methanol} \cdot (e_{20} - e_{21}) + W_{rank,out} - W_{vap,in}}{m_{air,d} \cdot e_{24} + m_{oil} \cdot (e_{19} - e_{15})} \tag{5.19}$$

The exergy efficiency of the discharging cycle of the LAES is:

$$\eta_{ex,air,d,LAES} = \frac{E_{air,d,out}}{m_{air,c} \cdot e_{24} + m_{oil} \cdot (e_{19} - e_{15})} \tag{5.20}$$

5.2.2.3 Economic performance indexes

In order to evaluate the economic benefit of the use of an organic Rankine cycle (ORC) and a vapor compression refrigeration cycle (VCRC) in the LAES-ORC-VCRC, an economic analysis is performed with the life cycle costs estimated using annualized cash flows [150]. The details are given in the following:

The present value of investments (PV_I) is:

$$\mathrm{PV_I} = \sum_{t=0}^{N-1} \mathrm{I}_t \cdot \left(\frac{1+r_{in}}{1+r_d}\right)^t - \frac{\mathrm{Res.\ Val.}}{(1+r_d)^N} \tag{5.21}$$

The present value of savings (PV_S) is:

$$PV_S = \sum_{t=1}^{N} AS_t \cdot \frac{1}{(1+r_d)^t} \tag{5.22}$$

where, N is the number of years of the project life-span; r_d is the discount rate; r_{in} is the inflation rate; AS is the annual savings; and Res. Val. is the residual value of the equipment.

The net present value (NPV) is the life cycle net savings of the project and is calculated by:

$$NPV = PV_S - PV_I \tag{5.23}$$

The savings to investment ratio (SIR) is a parameter indicating the profitability of a project, and is defined as:

$$SIR = \frac{PV_S}{PV_I} \tag{5.24}$$

The Simple Payback Period (SPP), expressed in years, refers to the length of time that it takes for a project to recoup its initial investment:

$$SPP = \frac{\text{Capital cost}}{\text{Savings/year}} \tag{5.25}$$

5.3 Results and discussion

The model described in Section 5.2 is solved by using the following assumptions:

- Air consisting of nitrogen (78.12%), oxygen (20.96%) and argon (0.92%);
- Pure propane and methanol used as the cold storage media;
- Dowtherm G used as the heat storage oil;
- R134a as the refrigerant in the vapor compression refrigeration cycle;
- A default discharging pressure of 12 MPa used in organic Rankine cycle;
- Various working fluids (R32, R502, CO_2 and R134a) considered with R32 as the default working fluid unless otherwise specified.

The properties of the thermal oil were obtained from Aspen Plus 8.8 software package, whereas the properties of other fluids came from REFPROP 8.0. The calculations were done in the MATLAB environment with other parameters used as the basis of the calculations listed in Table 5.1.

Table 5.1 Working parameters and assumptions of the LAES-ORC-VCRC system.

Ambient air temperature (K)	293
Ambient pressure (kPa)	100
Liquid air storage pressure P_{24} (kPa)	100
Thermal oil temperature T_{15} (K)	293
Methanol temperature T_{21} (K)	293
Propane temperature T_{23} (K)	214
Cooling water temperature (K)	290
Temperature difference at pinch point in Evaporator and Evaporator-condenser (K)	2
Temperature difference at pinch point in HE, Heater and Cooler (K)	5
Isentropic efficiency of compressor	0.89
Isentropic efficiency of turbine	0.9
Isentropic efficiency of cryo-turbine	0.8
Isentropic efficiency of cryo-pump	0.7

Table 5.2 shows the calculated results at each state of the LAES-ORC-VCRC system with a typical set of working conditions:

Table 5.2 Parameters at different states in the LAES-ORC-VCRC system.

State	T (K)	P (MPa)	m (kg/s)	Media
1	293	0.1	108.9	Air
2	293	0.1	180	Air
3	467.9	0.448	180	Air
4	309	0.448	180	Air
5	493.5	2.008	180	Air
6	309	2.008	180	Air
7	495.3	9	180	Air
8	309	9	180	Air
9	223.8	9	180	Air
10	128.7	9	180	Air
11	79.5	0.1	180	Air
12	81.6	0.1	71.1	Air
13	216.9	0.1	71.1	Air
14	302.4	0.1	71.1	Air
15	293	0.1	351	Thermal oil
16	445.6	0.1	117	Thermal oil
17	468.3	0.1	117	Thermal oil
18	477.7	0.1	117	Thermal oil
19	463.7	0.1	351	Thermal oil
20	207.7	0.1	63.2	methanol
21	293	0.1	63.2	methanol
22	87.2	0.1	108.9	propane
23	214	0.1	108.9	propane
24	78.8	0.1	108.9	Air

25	84.6	12	108.9	Air
26	205.2	12	108.9	Air
27	289.5	12	108.9	Air
28	458.1	12	108.9	Air
29	304.9	2.433	108.9	Air
30	458.1	2.433	108.9	Air
31	307.2	0.493	108.9	Air
32	458.1	0.493	108.9	Air
33	307.8	0.1	108.9	Air
34	303.2	0.1	130.8	Thermal oil
35	295.5	0.1	73.4	Thermal oil
36	328.3	0.1	73.4	Thermal oil
37	331.6	0.1	73.4	Thermal oil
38	291.4	12	91.5	R32
39	456.6	12	91.5	R32
40	288.7	1.1	91.5	R32
41	282.9	1.1	91.5	R32
42	280.8	0.383	161	R134a
43	282.8	0.383	161	R134a
44	305.7	0.703	161	R134a
45	295	0.703	161	R134a

In the charge process, air is first compressed to 9 MPa with a compression ratio of 4.48, with the heat of compression transferred and stored in the thermal oil, then cooled down to 128.7 K before expansion in the cryo-turbine, leading to almost 60.5% of the air being liquefied.

In the discharge process, liquid air is pumped to 12 MPa, heated up by the cold storage media for capturing cold for use in the charge process, and then superheated by the hot thermal oil stored in the heat storage tank before expansion in the turbine; the superheating of the air uses 62.7% of the stored heat of compression with the 37.3% excess heat used for the organic Rankine cycle (the reason for this split will be explained in Section 5.3.1)

The performance of each cycle is shown in Table 5.3. One can see that the LAES-ORC-VCRC system has a round trip efficiency that is 10.3% higher than the LAES system. Figure 5.2 are the composite curves for key heat exchanging components, illustrating that the temperature gradients of the working fluids of each of the components match well with the constraints at the pinch points and hence ensuring effective heat exchange. Figure 5.3 shows the *T-s* diagrams of the charging and discharging cycles in the LAES system.

Table 5.3 Performance of main cycles in the LAES-ORC-VCRC system.

	Charging cycle	Discharging cycle	Organic Rankine cycle	Vapor compression refrigeration cycle
Net Power (MW)	94.88	47.77	7.1	2.3
Exergy efficiency	0.827	0.839	0.644	0.531
Liquid yield	0.605			
Round trip efficiency	LAES-ORC-VCRC: 55.5%; LAES: 50.3%			

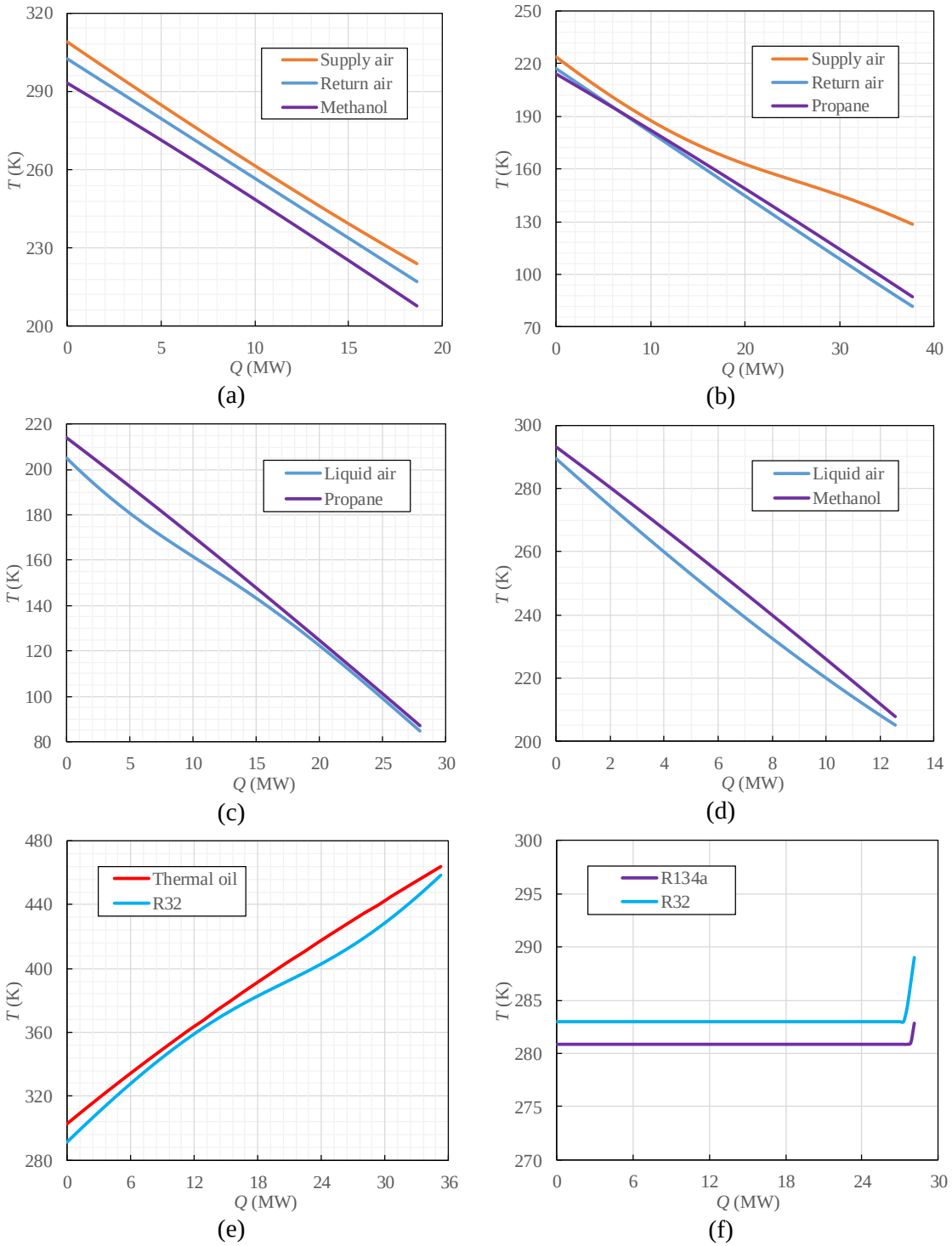

Figure 5.2 Composite curves of heat exchangers: (a) HE #1; (b) HE #2; (c) Evaporator #1; (d) Evaporator #2; (e) Heater #1; (f) Evaporator-condenser.

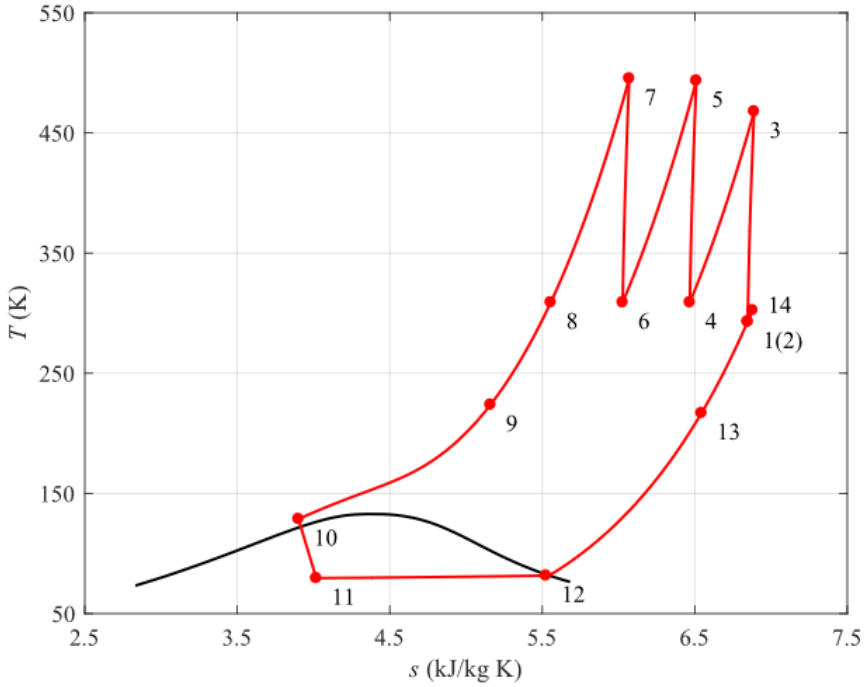

(a)

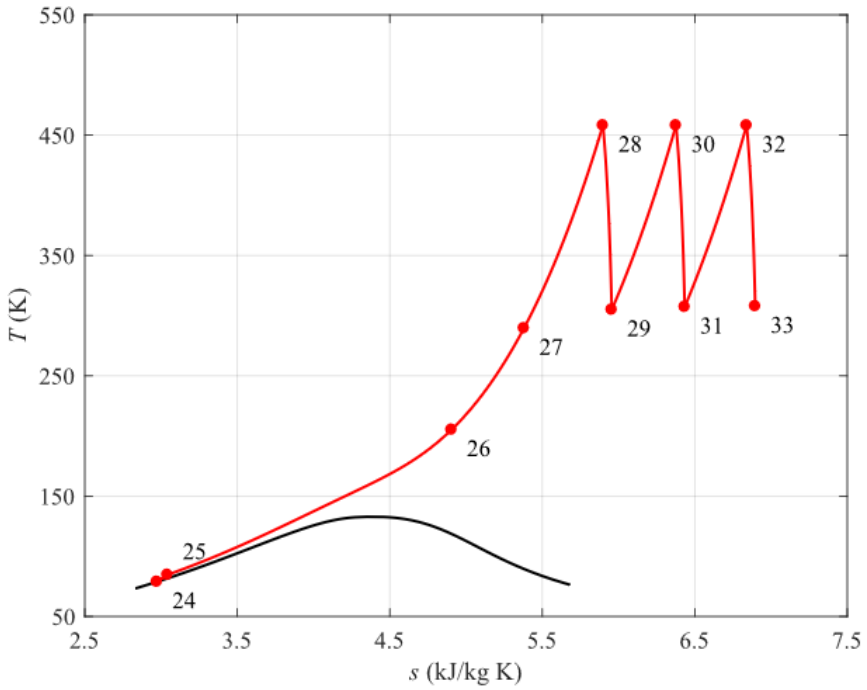

(b)

Figure 5.3 *T*-*s* diagrams of the charging cycle (a) and discharging cycle (b) in the LAES system.

5.3.1 Excess heat of compression in the LAES system

In the charging cycle, cold thermal oil cools down the compressed air, harvesting and storing the heat for use in the discharge process (cold oil becomes hot oil). The mass flow ratio (R_{oil}) of the oil to air is important for the LAES system. A lower R_{oil} would achieve a higher temperature when capturing the heat of compression, which is beneficial for increasing the output power during the discharging cycle. On the other hand, it will lead to an increase in the power consumption of the compressor in the charging cycle as a smaller R_{oil} may not fully cool down the compressed air. A higher R_{oil} gives a lower temperature of the oil, which, although is good for cooling down the compressed air and reducing the power consumption for the compression process, is not a good option for increasing the output power at the discharge process. An optimal R_{oil} therefore exists, as illustrated in Figure 5.4 (a), which shows that, for given discharging pressure (P_d=12 MPa in this case), the round trip efficiency of the LAES ($\eta_{RTE,trad}$) increases with increasing R_{oil}, reaches a peak, and then decreases with a further increase in the R_{oil}. The peak round trip efficiency is a function of the charging pressure (P_c).

In the discharging cycle, hot oil heats the high-pressure cold air before expansion. The mass flow ratio ($R_{oil,d}$) of the oil to the air also affects the system performance of the LAES, as illustrated in Figure 5.4 (b). One can see that, for a given charging pressure, an increase in $R_{oil,d}$ leads to an increase in $\eta_{RTE,trad}$ first, reaches a plateau beyond which little change occurs with further increase in the $R_{oil,d}$, due to mainly the pinch point in the heat exchangers. There is therefore an optimal $R_{oil,d}$ as well. At a charging pressure of 10 MPa, the optimal $R_{oil,d}$ increases with increasing discharging pressure; at P_d =12 MPa, the optimum $R_{oil,d}$ is 1.32 (hot oil stored R_{oil} is 2.07 in this case). These results indicate that the stored heat of compression should not be fully used for the conventional discharging cycle as in the LAES system.

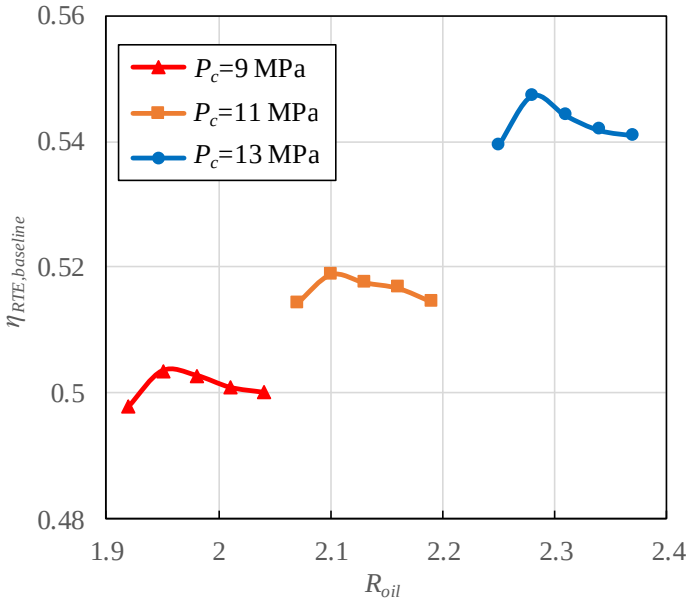

(a) P_d=12 MPa

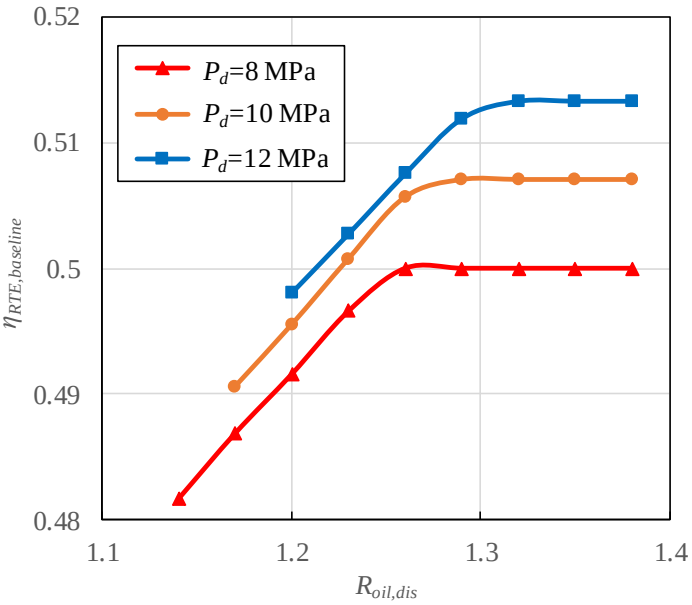

(b) P_c=10 MPa

Figure 5.4 Effect of mass flow ratios of thermal oil in the charging cycle (a) and discharging cycle (b) on the LAES system.

It is clear from the above that there is excess heat of compression in the LAES system. Figure 5.5 shows the ratio of excess heat to the total harvested and stored heat ($R_{oil,excess}$) at different charging pressures (P_c) and discharging pressures (P_d). As can be seen there is approximately 20-40% excess

heat. Given P_c = 10 MPa, the $R_{oil,excess}$ increases from 30% to 39% when P_d increases from 6 to 14 MPa. This is mainly due to decreasing liquid air yield with increasing discharging pressure, which consumes less heat for heating the air before expansion in the discharging cycle. At a higher P_c = 14 MPa, $R_{oil,excess}$ is lower than that at P_c = 10 MPa, due to an increased liquid air yield and hence consumption of more heat in the discharging cycle. As the charging process normally occurs at a pressure lower than 10 MPa, the ratio of excess heat can be even higher. This part of heat cannot be efficiently used in the LAES.

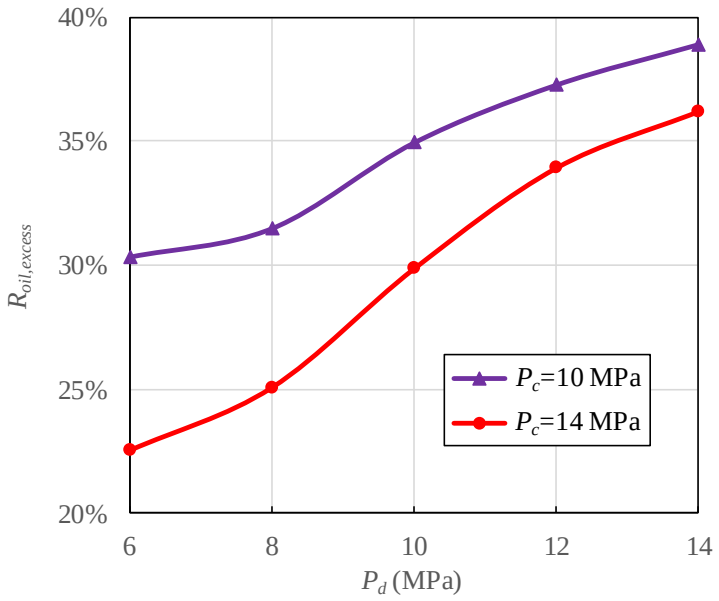

Figure 5.5 Excess heat of compression stored in thermal oil in the LAES system.

To make full use of the excess heat of compression, one possible solution is to use more stages of expansion in the discharging cycle. As shown in Figure 5.6 (a), one can see that an increase in the number of expansion stages significantly decreases the excess heat of compression, and there will be no excess heat of compression when the stages of expansion increases to 5.

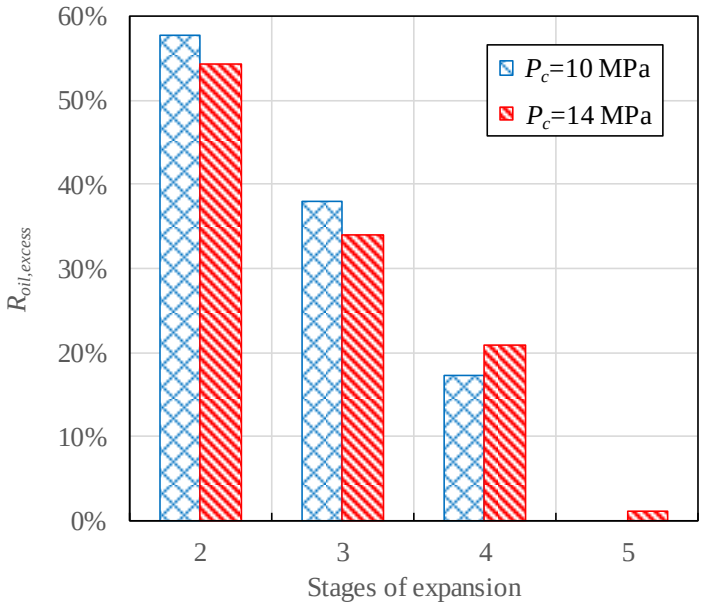

(a)

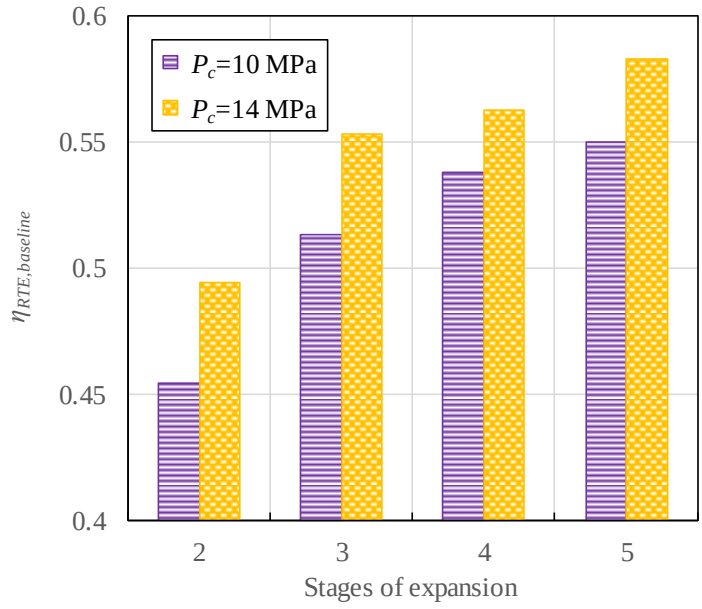

(b)

Figure 5.6 Effect of stages of expansion in the discharging cycle on the excess heat of compression (a) and round trip efficiency (b) in the LAES system (P_d=12 MPa).

The round trip efficiency of the LAES is affected by the number of expansion as shown in Figure 5.6 (b); when the stage number of expansion increase from 3 to 5, the round trip efficiency increases relatively by 5.4% and 7.2% for the charging pressure at 14 and 10 MPa, respectively. The improvement seems to be slight which is mainly due to the lower inlet pressure of the last two

turbines, leading to a low output power using the excess heat of compression. It is proposed to the use the excess heat in the organic Rankine cycle in the LAES-ORC-VCRC system, which, as will be shown, can lead to a much higher increase in the round trip efficiency.

5.3.2 Effects of charging pressure on the performance of the LAES-ORC-VCRC

Figure 5.7 shows the effect of the charging pressure (P_c) on the LAES-ORC-VCRC performance. One can see that the round trip efficiency of the LAES-ORC-VCRC system increases from 56.3% to 60% when P_c increases from 9 to 13 MPa; see Figure 5.7 (a). This is mainly due to an increased liquid yield and hence a decrease in power consumption of the compressor per unit mass of liquid air. At a P_c higher than 13 MPa, the change to the round trip efficiency becomes less due to a change in the specific heat capacity of air. Figure 5.7 (a) indicates that the round trip efficiency of the LAES-ORC-VCRC system is some 9-12% higher than that of the LAES under the conditions of this study.

The liquid yield and exergy efficiency are shown in Figure 5.7 (b). An increase in the charging pressure (P_c) from 9 to 15 MPa leads to a significant increase in the liquid yield (Y) from 0.605 to 0.789. This is due to the fact that a higher P_c will decrease the specific heat capacity of the air in the low temperature range (below 170 K), leading to more air to be liquefied. Exergy efficiency of the charging cycle, $\eta_{ex,air,c}$, is also seen to increase from 0.827 to 0.873 as P_c increases from 9 to 15 MPa. This is due to a combination of the results from an increased liquid yield and the power consumption of the compressor.

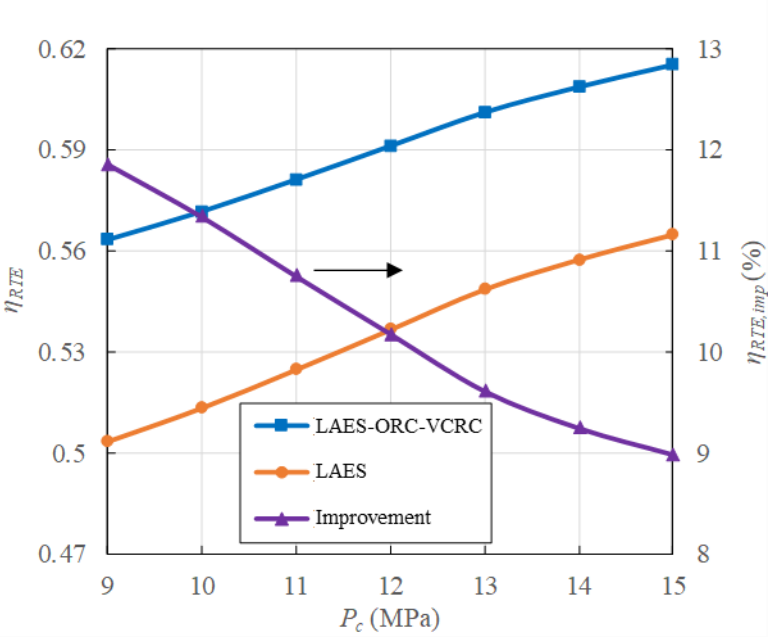

(a)

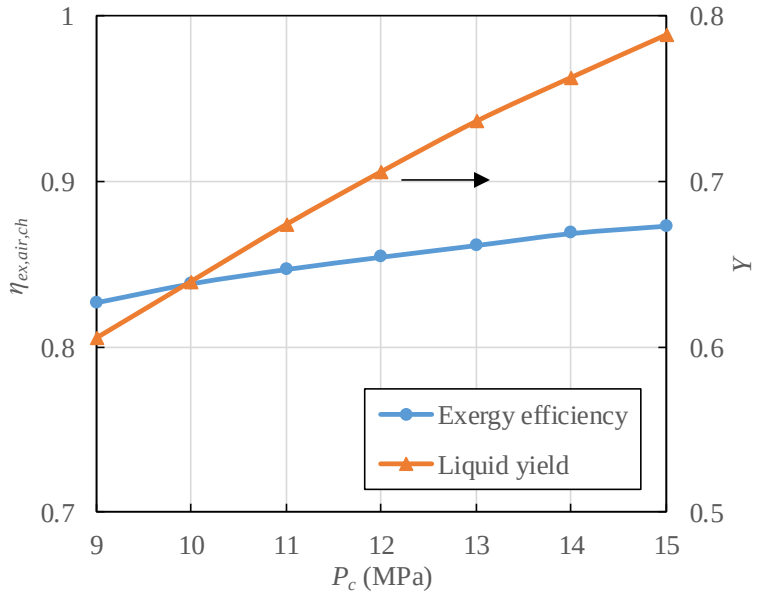

(b)

Figure 5.7 Effect of charging pressure on the round trip efficiency (a), and charging exergy efficiency and liquid yield (b) of the LAES-ORC-VCRC system (P_d=12 MPa).

5.3.3 Effects of discharging pressure on the performance of the LAES-ORC-VCRC system

Figure 5.8 shows the effect of discharging pressure (P_d) on the LAES-ORC-VCRC performance. One can see that the round trip efficiency of the LAES-ORC-VCRC increases first with increasing

P_d, peaks at ~13 MPa with an efficiency of 58.8%, followed by a decrease in the efficiency with further increase in the discharging pressure, exhibiting an optimal discharging pressure at 13 MPa; see Figure 5.8 (a). This is mainly due to a combination of the increased output power with the increased pressure and less cold recovery from liquid air at the high discharging pressure hence less unfavourable for the air liquefaction in the charging cycle. Figure 5.8 (a) also shows that the round trip efficiency of the LAES-ORC-VCRC is approximately 10-12% higher than that of LAES.

Figure 5.8 (b) compares the exergy efficiency of the discharging cycle of the LAES-ORC-VCRC ($\eta_{ex,air,d}$), the integrated / coupled discharging cycle of the LAES-ORC-VCRC ($\eta_{ex,coup,d}$), and the discharging cycle of the LAES ($\eta_{ex,air,d,trad}$). As can be seen that, over the range of P_d studied in this work (8-15 MPa), there is a peak for all the three exergy efficiencies at ~13 MPa and there exists a small extent of pressure dependence: $\eta_{ex,air,d}$ = 0.825-0.844 (peak value = 0.844); $\eta_{ex,coup,d}$ = 0.802 to 0.821 (peak value =0.821); showing an enhancement of the exergy efficiency by 9.1-10.6% through the effective allocation of heat of compression in the LAES-ORC-VCRC. The $\eta_{ex,coup,d}$ is ~6.5% on average higher than $\eta_{ex,air,d,trad}$, illustrating a higher round trip efficiency of the LAES-ORC-VCRC system.

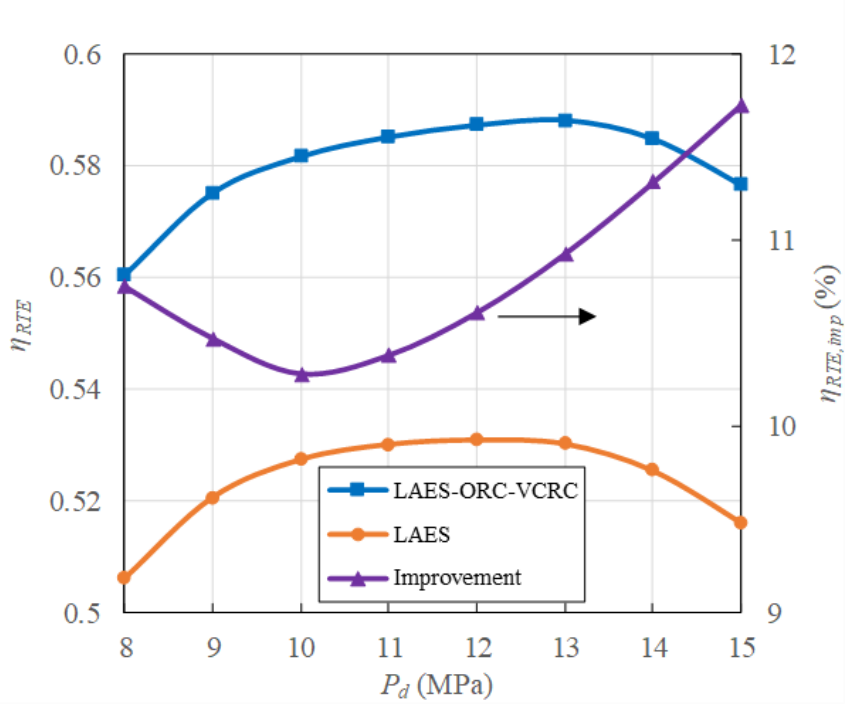

(a)

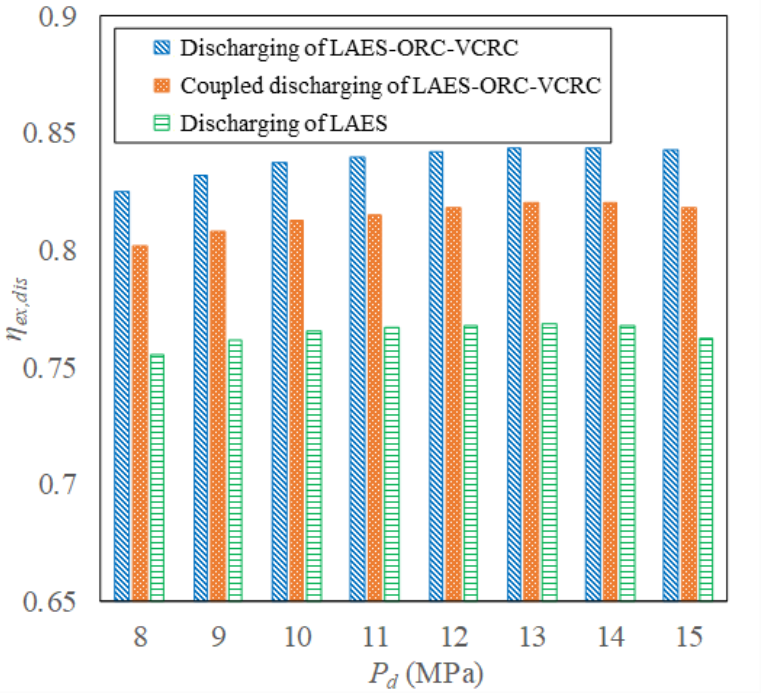

(b)

Figure 5.8 Effect of discharging pressure on the round trip efficiency (a), and discharging exergy efficiency (b) of the LAES-ORC-VCRC system (P_c=12 MPa).

5.3.4 Effects of the turbine inlet pressure of the organic Rankine cycle on the LAES-ORC-VCRC

Figure 5.9 shows the effect of the turbine inlet pressure of the organic Rankine cycle ($P_{rank,T,in}$) on the round trip efficiency of the LAES-ORC-VCRC ($\eta_{RTE,LAES\text{-}ORC\text{-}VCRC}$). Various working fluids (R32, CO_2, R502 and R134a) are considered as the working fluids for the organic Rankine cycle to compare their performances. Except for the use of CO_2, the other three working fluids show a similar performance with the round trip efficiency of the LAES-ORC-VCRC between 0.577 and 0.588 and there appear to be an optimal inlet pressure of the organic Rankine cycle between 9 and 11 MPa: $\eta_{RTE,LAES\text{-}ORC\text{-}VCRC}$ = 0.577 - 0.588 for R32 with optimal $P_{rank,T,in}$ = 11 MPa; $\eta_{RTE,LAES\text{-}ORC\text{-}VCRC}$ = 0.579 - 0.583 for R502 with optimal $P_{rank,T,in}$ = 10 MPa; and $\eta_{RTE,LAES\text{-}ORC\text{-}VCRC}$ = 0.581 - 0.585 for R134a with the optimum $P_{rank,T,in}$ = ~9 MPa. The use of CO_2 as a working fluid shows a completely different performance. First, a strong effect of turbine inlet pressure is seen on the round trip efficiency; when $P_{rank,T,in}$ increases from 9 to 14 MPa, $\eta_{RTE,LAES\text{-}ORC\text{-}VCRC}$ increases significantly from 0.541 to 0.557. Second, there is no optimal operating inlet pressure and a high $P_{rank,T,in}$ is beneficial for the performance of the LAES-ORC-VCRC. Third, R32, R502 and R134a give a better performance than CO_2 and are therefore favourable working fluid candidates for this type of applications.

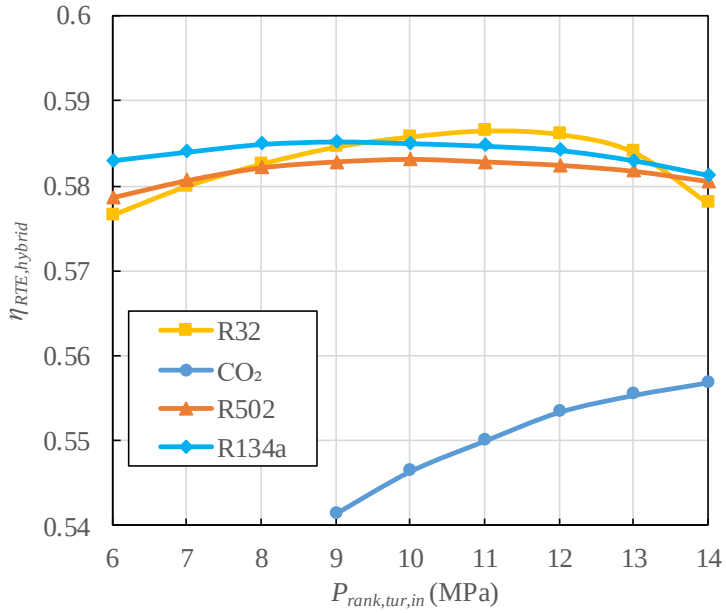

Figure 5.9 Effect of turbine inlet pressure of the organic Rankine cycle on the LAES-ORC-VCRC system (P_c = 12MPa; P_d = 12 MPa).

5.3.5 Effects of the turbine outlet pressure of the organic Rankine cycle on the LAES-ORC-VCRC

The effect of the outlet pressure of the turbine of the organic Rankine cycle ($P_{rank,T,out}$) on the round trip efficiency of the LAES-ORC-VCRC ($\eta_{RTE,LAES\text{-}ORC\text{-}VCRC}$) is shown in Figure 5.10. There is clearly an optimal outlet pressure at which the LAES-ORC-VCRC has the highest round trip efficiency for each of the three favourable working fluids: $\eta_{RTE,LAES\text{-}ORC\text{-}VCRC}$ = 0.586 at the optimal $P_{rank,T,out}$ of ~1.8 MPa for R32; $\eta_{RTE,LAES\text{-}ORC\text{-}VCRC}$ = 0.582 at the optimal pressure of $P_{rank,T,out}$ = ~1.2 MPa for R502; $\eta_{RTE,LAES\text{-}ORC\text{-}VCRC}$ = 0.585 at the optimal pressure of $P_{rank,T,out}$ = ~0.7 MPa for R134a.

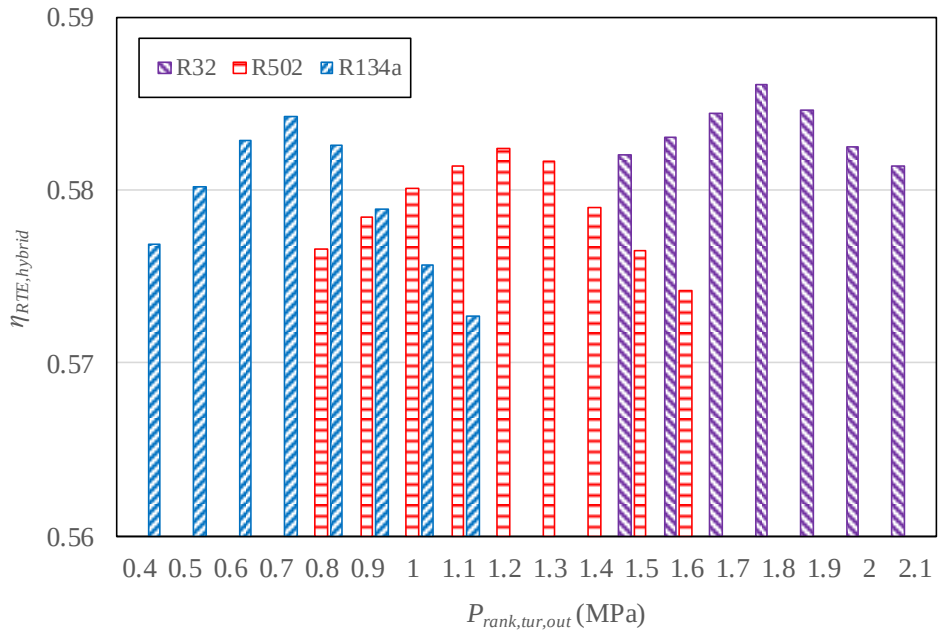

Figure 5.10 Effect of turbine outlet pressure of the organic Rankine cycle on the LAES-ORC-VCRC system (P_c=12 MPa; P_d=12 MPa).

5.3.6 Economic evaluation of the use of the ORC and VCRC in the LAES-ORC-VCRC system

As detailed in the previous sections, the LAES-ORC-VCRC gives a much higher round trip efficiency than the LAES, so it would be of interest to evaluate the economic benefits of the use of the organic Rankine cycle (ORC) and the vapor compression refrigeration cycle (VCRC) in the LAES-ORC-VCRC. In the analyses, the VCRC is set to work at off-peak times, using cheap electricity to generate cold energy and to store the cold in the Evaporator-condenser which works as a latent heat energy storage device; and the ORC is set to work at peak times using the excess heat of compression and the stored cold energy to generate (more expensive) electricity.

A 5 MW/40 MWh LAES plant is considered with a project life-span of 15 years and 300 days/year (P_c = 10 MPa; P_d = 12 MPa; $P_{rank,T,in}$ = 11 MPa). Water is chosen as the energy storage medium with liquid-solid phase changes in the Evaporator-condenser for storing the cold. The cost of components in the ORC and VCRC is shown in Table 5.4. For a complete financial analysis, additional costs, such as mechanical costs, electrical costs, site works and commissioning costs, are

considered to be 25% of the initial capital cost [151]. The UK domestic rates of electricity of $181/MWh in the daytime and $80.6/MWh in the midnight are used in the assessment [152].

Table 5.4 Component cost summary (net present cost) of the ORC and VCRC in the project life-span.

Component	Capital ($)	Replacement ($)	O&M ($)	Residual value ($)
Turbine	855,130	-	42,757	-16,453
Evaporator-condenser	34,450	58,027	3,101	-663
Cryo-pump #2	22,500	37,899	2,025	-433
Heater #1	64,144	108,043	5,773	-1,234
Compressor	57,216	-	2,861	-1,101
Condenser	35,073	59,076	3,157	-675
Cooling tower	25,200	19,998	1,512	-485

Note: Capital and replacement costs are from the manufacturers.

Table 5.5 shows the results of the economic analysis, where the inflation rate is taken as 2.6% and a discount rate of 5% is used. One can see that the economics of the combination of the ORC and VCRC (ORC+VCRC) is excellent with a payback period of 2.7 years and a savings to investment ratio of 3.08. It is more economical than the use of the ORC with ambient temperature water cooling, which has a payback period of 3.1 years and a savings to investment ratio of 2.78.

Table 5.5 Economic analysis results of the single ORC and the combination of the ORC and VCRC (ORC+VCRC).

Performance indexes	ORC+VCRC	ORC
Electricity (MW)	ORC (output): 0.823 VCRC (input): 0.375	ORC (output): 0.58

Total present value of investment ($)	1,690,324	1,513,517
Total present value of savings ($)	5,213,113	4,204,509
Net present value ($)	3,522,788	2,690,991
Savings to investment ratio	3.08	2.78
Simple payback period (years)	2.7	3.1

The effects of the inflation and discount rates on the economic benefit have also been considered both for the single ORC and the combination of the ORC and VCRC (ORC+VCRC). The results are shown in Figure 5.11. The discount rate has a more significant effect on the economic benefit, compared with the inflation rate. With a given inflation rate of 2%, the net present value (NPV) of the ORC+VCRC decreases dramatically from $4,282,261 to $2,012,197 as the discount rate increases from 3% to 11%; accordingly, the savings to investment ratio (SIR) of the ORC+VCRC decreases significantly from 3.5 to 2.26. In addition, higher inflation rate will slightly decrease the NPV and SIR.

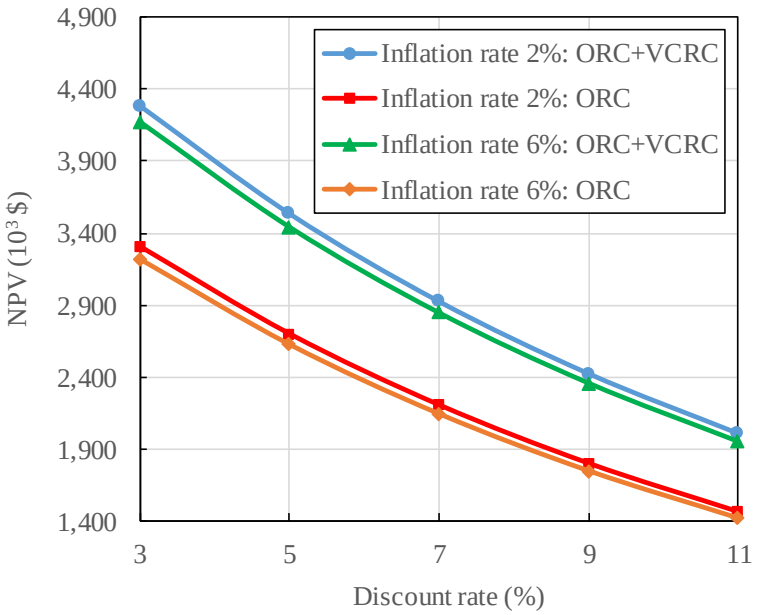

(a)

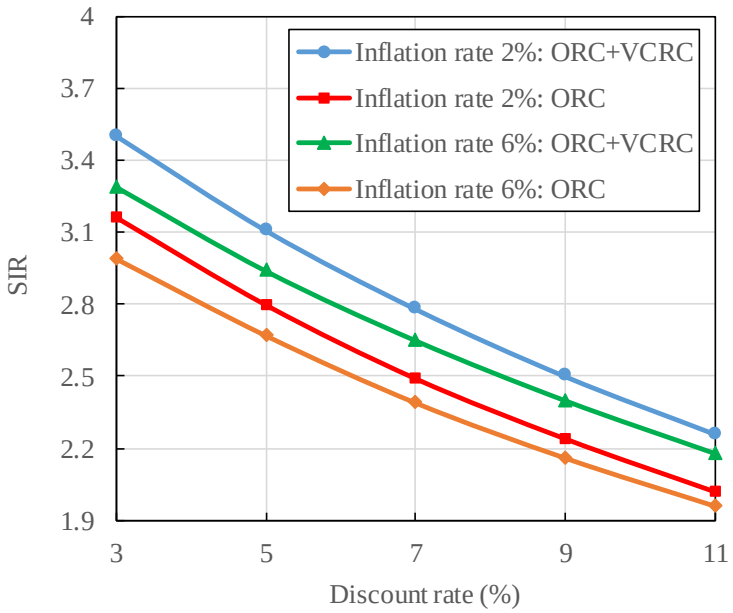

(b)

Figure 5.11 Effect of inflation rates and discount rates on the net present value (a) and savings to investment ratio (b).

5.4 Conclusions of Chapter 5

In the current liquid air energy storage system (LAES), heat of compression is recovered and stored in the charging cycle. The stored heat is only used for improving the output power of the turbine in the discharging cycle. The heat of compression cannot be efficiently used in the LAES system and there is ~20-40% excess heat. A new LAES-ORC-VCRC system is therefore proposed, which consists of a LAES, an organic Rankine cycle (ORC) and a vapor compression refrigeration cycle (VCRC).

The main conclusions are as follows:

- The round trip efficiency of the LAES-ORC-VCRC could be higher than 60%, which is 9-12% higher than that of the LAES;

- The exergy efficiencies of the discharging cycle and the integrated/coupled discharging cycle of the LAES-ORC-VCRC are ~9.6% and ~6.5% higher on average than that of the discharging cycle of the LAES, respectively;
- There is an optimal discharging pressure of 13 MPa for the air expansion to give the highest round trip efficiency under the conditions studied in this work;
- R32, R502 and R134a outperform CO_2 as a working fluid and are regarded as favourable working fluid candidates for the organic Rankine cycle;
- For the favourable working fluids in the organic Rankine cycle, there exists an optimal turbine inlet pressure at 11 MPa, which gives the highest round trip efficiency of the LAES-ORC-VCRC;
- An economic analysis using a project life-span of 15 years shows that the combination of the ORC and VCRC has an excellent economic performance with a payback period of 2.7 years and a savings to investment ratio of 3.08. It is more economical that the use of ORC with the ambient temperature water cooling;
- The discount rate has a much more significant effect on the economic benefit than the inflation rate. As the discount rate increases from 3% to 11%, the savings to investment ratio decreases significantly from 3.5 to 2.26. A higher discount rate or inflation rate decreases both the net present value and the savings to investment ratio.

The above conclusions suggest that the LAES-ORC-VCRC would be both technically and economically feasible.

Chapter 6 Integration of LAES with Organic Rankine Cycle for compression heat utilization

6.1 Introduction

This chapter proposes the use of the excess heat to drive an Organic Rankine Cycle (ORC) for power generation. Two configurations, LAES-ORC and LAES-ORC-ARC, are considered, where ARC refers to Absorption Refrigeration Cycle. In the LAES-ORC configuration, the working fluid of the ORC is cooled by the ambient, while in the LAES-ORC-ARC configuration, it is cooled by a low-temperature cold source from an ARC using part of the excess heat. Thermodynamic analyses are performed on the two configurations, and comparisons are made among the LAES, LAES-ORC and the LAES-ORC-ARC with different charging and discharging parameters.

6.2 The integration of Liquid Air Energy Storage with Organic Rankine Cycle

6.2.1 System description

The basic principle of the LAES is shown in Figure 2.1, which consists of a charging cycle and a discharging cycle. The charging cycle runs at off-peak times: the purified air is compressed to a high pressure through multistage compression with compression heat recovered and stored in thermal oil; the compressed air is then cooled in a cold box by recycling air and cold fluids (propane and methanol) containing cold recovered from liquid air in the discharging cycle; finally, liquid air is obtained through air expansion in a cryo-turbine and stored in a liquid air tank at approximately 77 K. The discharging cycle works at peak times: the liquid air flowing from the tank is pumped to a high pressure, and transfers cold energy to the cold fluids (propane and methanol) in two evaporators, which are used later to cool the compressed air in the charging cycle; the air is then heated by the hot thermal oil containing heat recovered in the charging cycle before entering air turbines to generate electricity.

The analyses in Chapter 4 show that the amount of cold energy recovered in the discharging cycle is not enough to fully cool the compressed air in the charging cycle (see Section 4.3.4.3), whereas the compression heat generated in the charging cycle is in excess and cannot be used efficiently in the discharging cycle (see Section 4.3.4.4). To make a full use of the excess heat for generating power, two configurations are considered. The first configuration, denoted as LAES-ORC, is shown Figure 6.1; all the excess heat is used to heat the working medium in the Organic Rankine Cycle (ORC), which is then cooled down by ambient cooling water at 293 K. The second configuration, denoted as LAES-ORC-ARC, is shown in Figure 6.2; the excess heat is split into two streams: one is to heat the working medium in the ORC, and the other drives the ARC with NH_3-H_2O as the working medium, to generate low-temperature cold sources for cooling the working medium of the ORC. Here, a serial arrangement of ARCs is proposed to realize a cascading use of the excess heat.

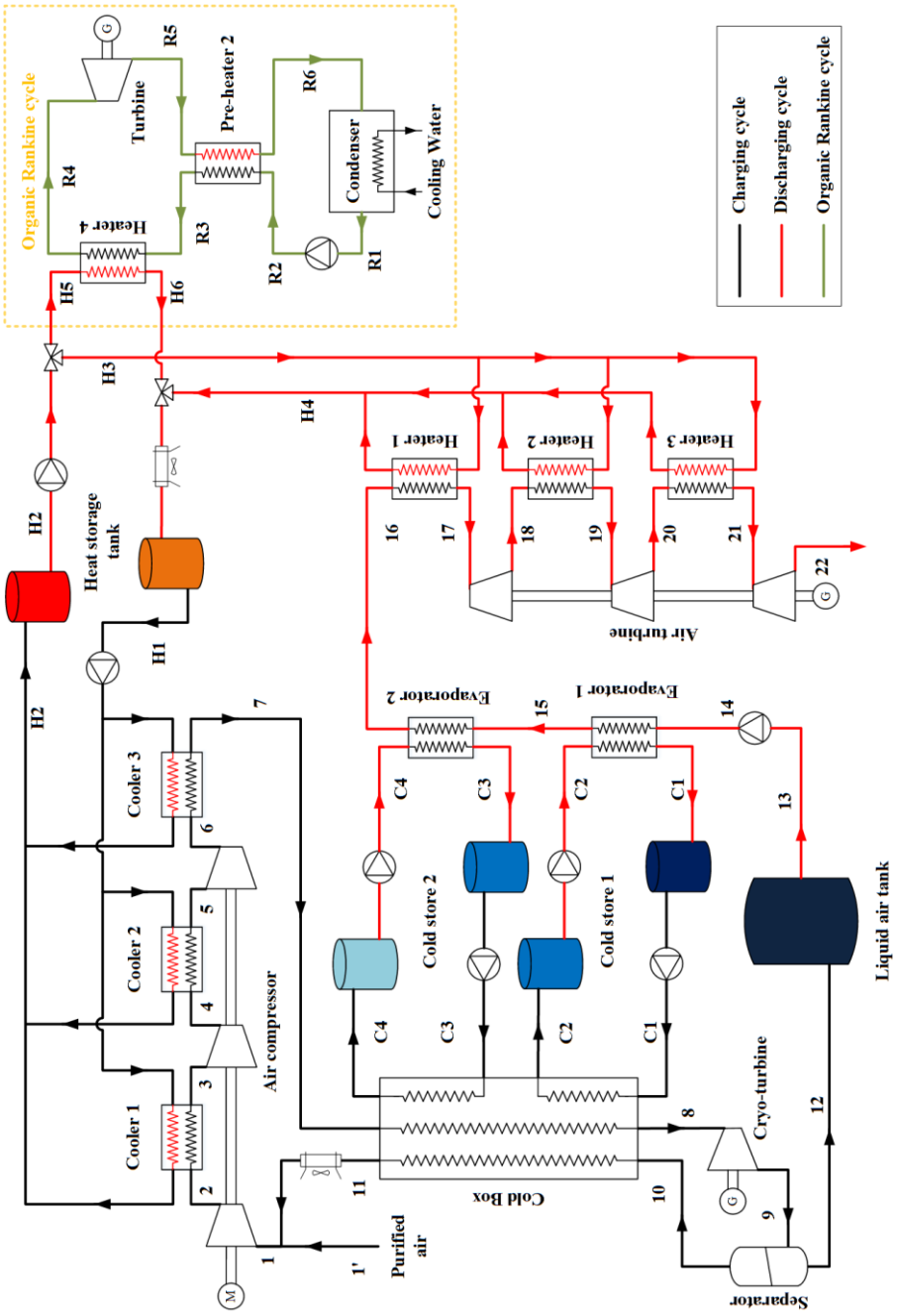

Figure 6.1 Layout of the LAES-ORC system.

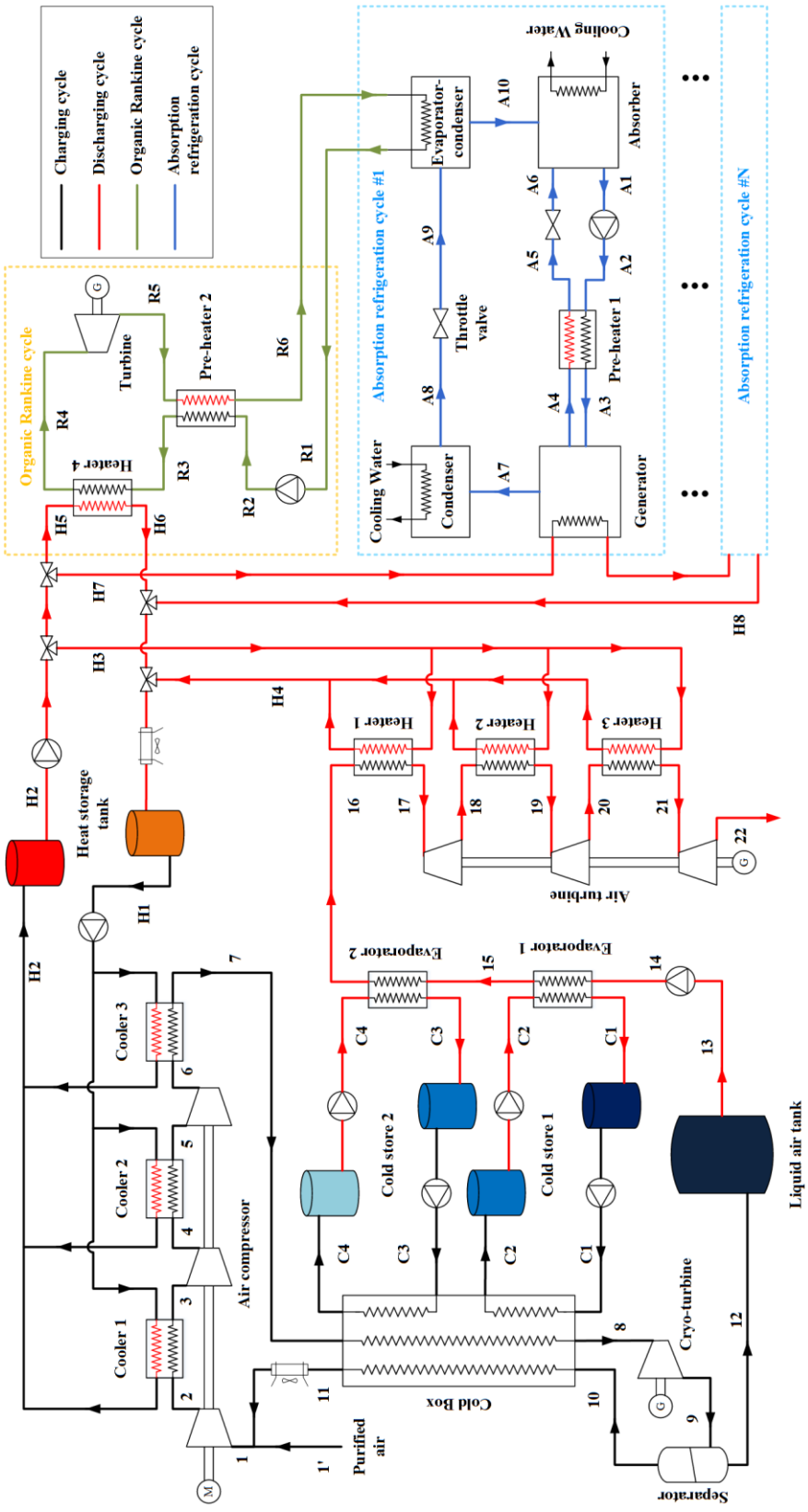

Figure 6.2 Layout of the LAES-ORC-ARC system.

For the ORC, R134a is chosen as the working medium, which has been shown to have a better performance even when the turbine inlet pressure is low, see Figure 5.10. Thermodynamically, for a given heat source, a lower temperature cold source will give to a higher specific output power, as shown in Figure 6.3. Ambient water can be used as a free cold source for the ORC. To achieve a low-temperature cold source without consuming electricity, heat can be used to drive the ARC. The LAES-ORC configuration uses the ambient water as a cold source of the ORC, a low specific output power is therefore expected and the mass flow rate of the working medium (R134a) is high since all the excess heat is used as a heat source. The ORC of the LAES-ORC-ARC configuration has a low-temperature cold source by consuming part of the excess heat, a high specific output power is expected. The mass flow rate of the working medium (R134a) in this configuration is lower because only part of the excess heat is used as the heat source for the ORC, and to heat the working medium (R134a) to the same temperature, the mass flow rate of the working medium (R134a) should be lower due to energy conservation.

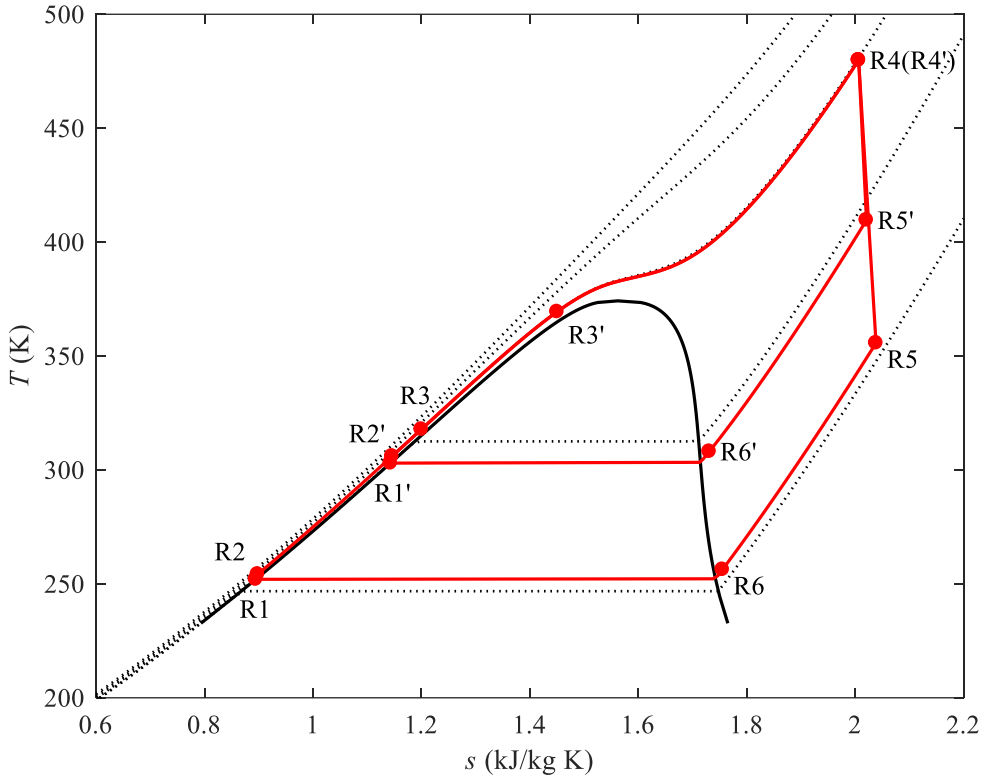

Figure 6.3 Effect of cold source temperature on an Organic Rankine Cycle with R134a as the working fluid.

6.2.2 System model and validation

The entire system is complex. To simplify the system analysis, several assumptions are made:

- The system is in a steady state, and neither dynamic nor transient analyses are considered;
- There is no heat loss from the system components unless otherwise specified;
- In the ORC, R134a is condensed to a saturated state in the evaporator-condenser;
- In the ARC, the refrigerant (NH3) leaving the condenser is saturated and it goes through an isenthalpic process in the throttle valve; the ammonia-water solution at the outlet of the generator and absorber is saturated.

6.2.2.1 System model

Both the LAES-ORC system and LAES-ORC-ARC configuration are developed based on a standalone LAES system, as described in Section 4.3. The thermodynamic models for compressor, cold box, cryo-turbine, cryo-pump, and turbine are the same as described there, see Equation 4.1 to Equation 4.8, and round trip efficiency and exergy efficiency are calculated in the same was as illustrated by Equation 4.9 to Equation 4.17.

The Organic Rankine Cycle (ORC) uses R134a which is condensed to a liquid (State R1) and then pumped to a high pressure, and the outlet enthalpy is given by:

$$h_{R2} = h_{R1} + \frac{(h_{R2,s} - h_{R1})}{\eta_{pump}} \tag{6.1}$$

The high pressure R134a is heated by the thermal oil to a high temperature (State R4) before entering the turbine to generate electricity. The outlet enthalpy of R134a is calculated by:

$$h_{R5} = h_{R4} - \eta_T \cdot (h_{R4} - h_{R5,s}) \tag{6.2}$$

The ORC works together with the discharging cycle of the LAES to produce peak time electricity. The equivalent output work of the ORC per unit mass of liquid air can be given as:

$$W_{orc,out} = \frac{m_{orc} \cdot ((h_{R4} - h_{R5}) - (h_{R2} - h_{R1}))}{m_{air,d}} \tag{6.3}$$

where, m_{orc} is the mass flow rate of R134a in the ORC.

In the Absorption Refrigeration Cycle (ARC) uses ammonia-water solution, which is heated up by thermal oil in the generator to give the heat source:

$$Q_{gen} = m_{\mathrm{A4}} \cdot h_{\mathrm{A4}} - m_{\mathrm{A3}} \cdot h_{\mathrm{A3}} + m_{\mathrm{A7}} \cdot h_{\mathrm{A7}} \tag{6.4}$$

$$m_{\mathrm{A7}} = m_{\mathrm{A3}} - m_{\mathrm{A4}} \tag{6.5}$$

The refrigerant NH_3 evaporates to generate cold energy in the ARC for condensing R134a in the ORC. The outlet enthalpy of the fluids can be calculated by using energy conservation:

$$m_{\mathrm{A9}} \cdot (h_{\mathrm{A10}} - h_{\mathrm{A9}}) = m_{orc} \cdot (h_{\mathrm{R6}} - h_{\mathrm{R1}}) \tag{6.6}$$

The gaseous NH_3 is absorbed by the ammonia-water solution in the absorber, and the cooling capacity required, Q_{abs}, is determined by:

$$Q_{abs} = m_{\mathrm{A10}} \cdot h_{\mathrm{A10}} - m_{\mathrm{A1}} \cdot h_{\mathrm{A1}} + m_{\mathrm{A6}} \cdot h_{\mathrm{A6}} \tag{6.7}$$

The low pressure ammonia-water solution (State A1) is pumped to a higher pressure. To fully use the stored heat in the thermal oil, several ARCs can work in series, and the equivalent input work of the ARC per unit mass of liquid air can be given by:

$$W_{arc,in} = \frac{1}{m_{air,d}} \cdot \sum_{i=1}^{n} m_{\mathrm{A1},i} \cdot (h_{\mathrm{A2},i} - h_{\mathrm{A1},i}) \tag{6.8}$$

where, n represents the n^{th} stage of the ARC.

The round trip efficiency of the LAES-ORC can then be calculated by:

$$\eta_{RTE,orc} = \frac{W_{air,out} + W_{orc,out}}{W_{air,in}} \tag{6.9}$$

The round trip efficiency of the LAES-ORC-ARC is given by:

$$\eta_{RTE,orc,arc} = \frac{W_{air,out} + W_{orc,out} - W_{arc,in}}{W_{air,in}} \tag{6.10}$$

The enhancement of the round trip efficiency for the LAES-ORC and LAES-ORC-ARC, with respect to the LAES, can then be respectively given by:

$$\eta_{RTE,imp,orc} = \frac{\eta_{RTE,orc} - \eta_{RTE}}{\eta_{RTE}} \tag{6.11}$$

$$\eta_{RTE,imp,orc,arc} = \frac{\eta_{RTE,orc,arc} - \eta_{RTE}}{\eta_{RTE}} \tag{6.12}$$

6.2.2.2 Model validation

Before comprehension thermodynamic analyses, the model is first validated by comparing with numerical data in the literature. The comparison for the LAES system has been shown in Figure 4.9 (Chapter 4) and will not be repeated here. Figure 6.4 (a) compares the ARC results between the present work and Du et al. [153], with ammonia-water as the working medium. One can see a very good agreement with the maximum deviation of 1.7% for the ARC. Figure 6.4 (b) gives a performance comparison of the ORC between the present work and Su et al. [154], with a turbine inlet pressure of 5 MPa with R134a as the working medium. Again, an excellent agreement is seen with the maximum deviation of 0.1% for the ORC. Hence, the system model is acceptable for the following simulation.

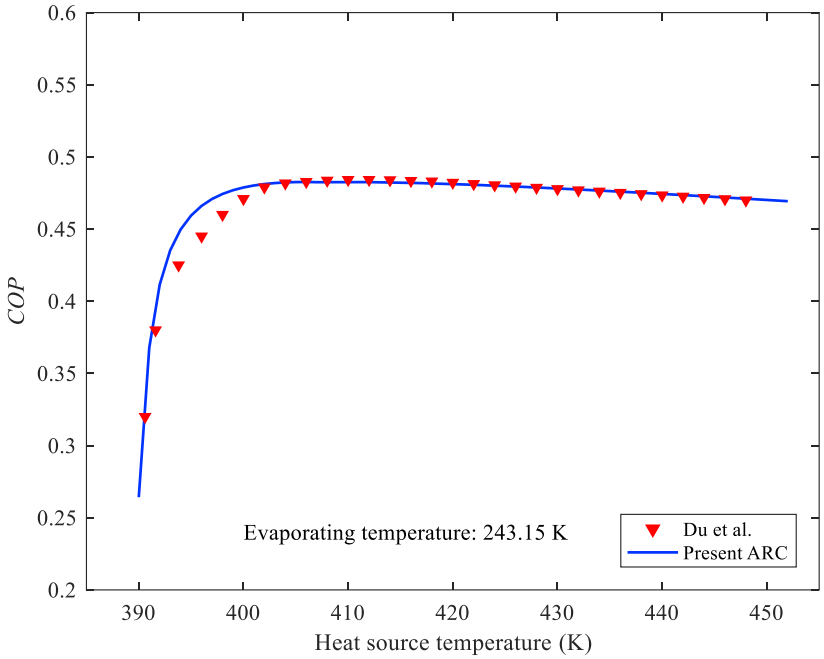

(a) ARC

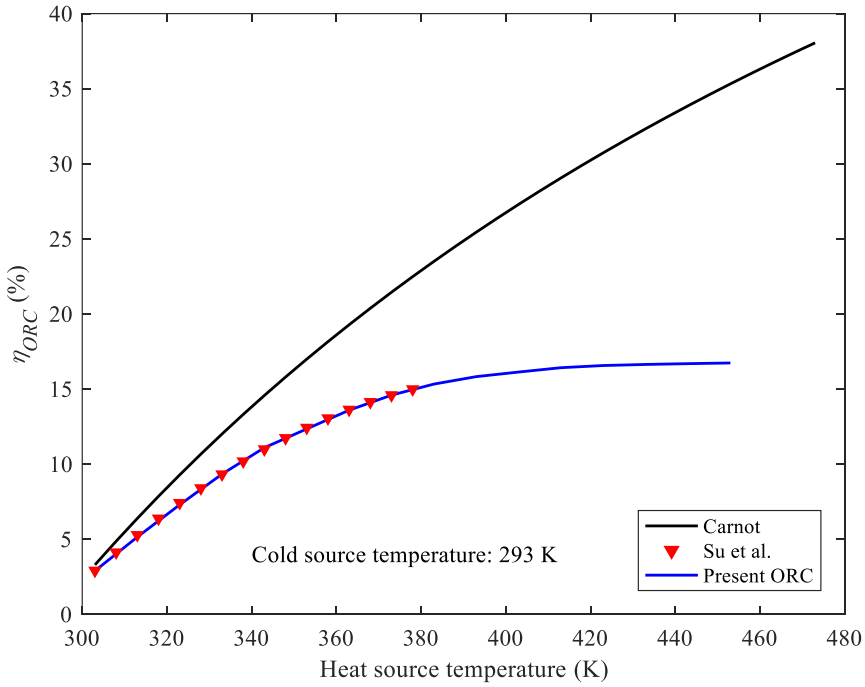

(b) ORC

Figure 6.4 Comparison of the modelling results of this work with the data of the ARC with Du et al. [153] and the ORC with Su et al. [154].

6.3 Results and discussions

6.3.1 System performance of the LAES, LAES-ARC and LAES-ARC-ORC.

Table 6.1 lists the operating parameters used for the analyses of the LAES, the ORC and the ARC cycles. Table 6.2 presents the data at each point/state of the LAES under a given set of working conditions, which has an excess compression heat of 33.27%. To make use of such excess heat, the ORC with ambient water cooling at 293 K was analysed (Table 6.3) and the ORC with a low-temperature cold source at 250 K was also analysed (Table 6.4). The cold sources for the ORC was obtained by ARC which consumed 69% of the excess heat and the rest of the heat was used as the heat source for the ORC. The calculations were done in the MATLAB environment, with the thermal properties of air, propane, methanol, ammonia and R134a obtained by using REFPROP 8.1, and the thermal properties of thermal oil from ASPEN plus.

Table 6.1 Default parameters of the LAES-ORC and the LAES-ORC-ARC.

Parameter	Value	Unit
Ambient Temperature	293	K
Ambient Pressure	100	kPa
Thermal oil temperature	293	K
Minimum propane temperature	95	K
Minimum methanol temperature	214	K
Cooling water temperature	293	K
Ammonia evaporation temperature	250	K
Pinch point of Cooler	2	K
Pinch point of Heater	5	K
Pinch point of Cold box	5	K
Pinch point of Evaporator	2	K

Relative pressure drops of heat exchanger	1%
Isentropic efficiency of Compressor	85%
Isentropic efficiency of Turbine	90%
Isentropic efficiency of Cryo-turbine	75%
Isentropic efficiency of Pump	75%

Table 6.2 Stream Data of the LAES.

	$\dot{m}/\dot{m}_{air,ch}$	T [K]	P [MPa]	h [kJ/kg]	Fluids
1	1.000	293.00	0.100	293.27	air
2	1.000	493.58	0.519	496.62	air
3	1.000	303.00	0.514	302.42	air
4	1.000	510.69	2.669	513.39	air
5	1.000	303.00	2.643	297.81	air
6	1.000	513.23	13.721	513.10	air
7	1.000	303.00	13.584	277.80	air
8	1.000	100.08	13.448	-77.40	air
9	1.000	79.88	0.110	-92.59	air
10	0.161	82.45	0.110	79.60	air
11	0.161	270.44	0.109	270.55	air
12	0.839	79.66	0.110	-124.88	air
13	0.839	79.66	0.110	-124.88	air
14	0.839	83.13	8.000	-112.91	air
15	0.839	212.00	7.920	176.41	air
16	0.839	291.00	7.841	273.83	air

17	0.839	479.89	7.762	478.88	air
18	0.839	331.71	1.801	329.22	air
19	0.839	479.89	1.783	481.80	air
20	0.839	333.15	0.414	333.14	air
21	0.839	479.89	0.410	482.59	air
22	0.839	333.54	0.095	334.11	air
H1	1.917	293.00	0.100	422.83	thermal oil
H2	1.917	489.89	0.100	759.34	thermal oil
H3	1.487	489.89	0.100	759.34	thermal oil
H4	1.487	328.17	0.100	473.08	thermal oil

Table 6.3 Stream data of the Organic Rankine Cycle cooled by the ambient water.

	$\dot{m}/\dot{m}_{air,ch}$	T [K]	P [MPa]	h [kJ/kg]	Fluids
R1	0.412	303.00	0.767	241.51	R134a
R2	0.412	306.04	5.000	245.93	R134a
R3	0.412	369.42	4.950	349.00	R134a
R4	0.412	479.89	4.901	576.62	R134a
R5	0.412	409.66	0.782	523.63	R134a
R6	0.412	308.10	0.775	419.93	R134a
H5	0.430	489.89	0.100	759.34	thermal oil
H6	0.430	371.57	0.100	541.25	thermal oil

Table 6.4 Stream data of the Organic Rankine Cycle cooled by the Absorption Refrigeration Cycles.

	$\dot{m}/\dot{m}_{air,ch}$	T [K]	P [MPa]	h [kJ/kg]	Fluids
R1	0.127	252.00	0.126	172.15	R134a
R2	0.127	254.23	5.000	176.61	R134a
R3	0.127	317.82	4.950	262.78	R134a
R4	0.127	479.89	4.901	576.62	R134a
R5	0.127	355.71	0.129	475.78	R134a
R6	0.127	256.29	0.128	389.28	R134a
H5	0.134	489.89	0.100	759.34	thermal oil
H6	0.134	321.10	0.100	462.61	thermal oil
A1(1)	0.241	298.00	0.162	2.80	strong Sol.
A2(1)	0.241	298.12	1.029	4.06	strong Sol.
A3(1)	0.241	359.32	1.019	299.364	strong Sol.
A4(1)	0.216	373.00	1.009	341.41	weak Sol.
A5(1)	0.216	300.22	0.999	11.84	weak Sol.
A6(1)	0.216	300.38	0.162	11.84	weak Sol.
A7(1)	0.025	388.00	1.009	1862.84	ammonia
A8(1)	0.025	298.00	0.999	460.10	ammonia
A9(1)	0.025	250.00	0.165	460.10	ammonia
A10(1)	0.025	252.00	0.165	1581.21	ammonia
A1(2)	0.181	298.00	0.162	2.80	strong Sol.
A2(2)	0.181	298.12	1.029	4.06	strong Sol.
A3(2)	0.181	356.55	1.019	270.92	strong Sol.
A4(2)	0.179	359.00	1.009	282.55	weak Sol.

A5(2)	0.179	300.22	0.999	12.77	weak Sol.
A6(2)	0.179	299.44	0.162	12.77	weak Sol.
A7(2)	0.002	366.00	1.009	1808.63	ammonia
A8(2)	0.002	298.00	0.999	460.10	ammonia
A9(2)	0.002	250.00	0.165	460.10	ammonia
A10(2)	0.002	252.00	0.165	1581.21	ammonia
H7	0.296	489.89	0.100	759.34	thermal oil
H8	0.296	359.00	0.100	520.82	thermal oil

Table 6.5 presents the performance comparison of the LAES, LAES-ORC and the LAES-ORC-ARC under the working conditions listed in Table 6.1. The net input work per unit mass of liquid air in the charging process is ~731.9 kJ/kg, whereas the net output work per unit mass of liquid air in the discharging process approaches 434.7 kJ/kg, leading to a round trip efficiency of 59.40%, 62.65% and 61.33% for the LAES, LAES-ORC and the LAES-ORC-ARC, respectively.

Table 6.5 Comparison of the LAES, LAES-ORC and the LAES-ORC-ARC.

Items		Net work per unit mass of liquid air (kJ/kg)	Exergy efficiency	Liquid air yield	Round trip efficiency
LAES	charging	731.9	0.84	0.84	59.40%
	discharging	434.7	0.81		
LAES-ORC	charging	731.9	0.84	0.84	62.65%
	discharging	434.7	0.81		
	ORC	23.9	NA		
LAES-ORC-ARC	charging	731.9	0.84	0.84	61.33%
	discharging	434.7	0.81		
	ORC	15.2	NA		
	ARC	1	NA		

The composite curves for key heat transfer components are shown in Figure 6.5, which illustrate that the temperature gradients of the working fluids in each of the components match well with the constraints at the pinch points, suggesting very effective heat exchange. Figure 6.6 shows the *T*-*s* diagrams of the charging cycle, discharging cycle, ORC cooled by the ambient water and the ORC-ARC.

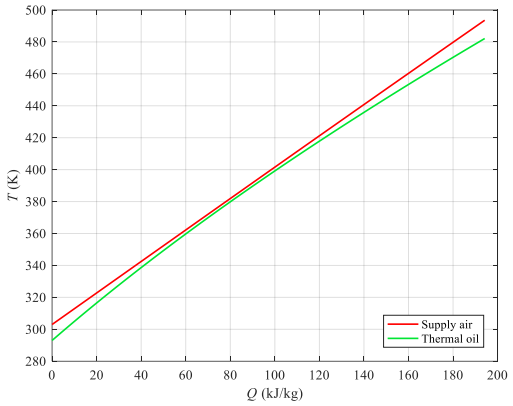

(a)

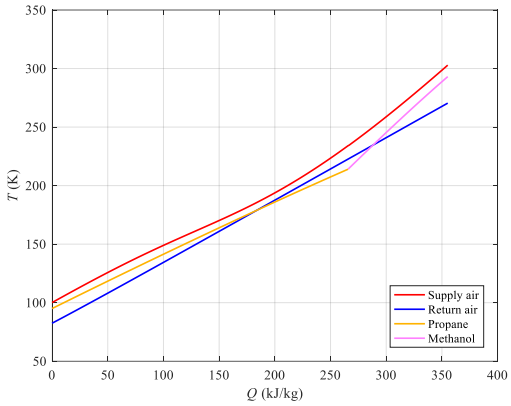

(b)

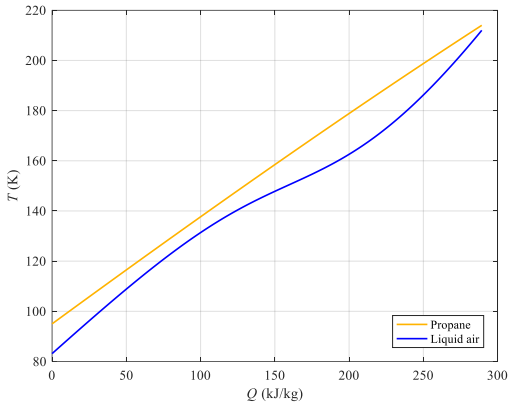

(c)

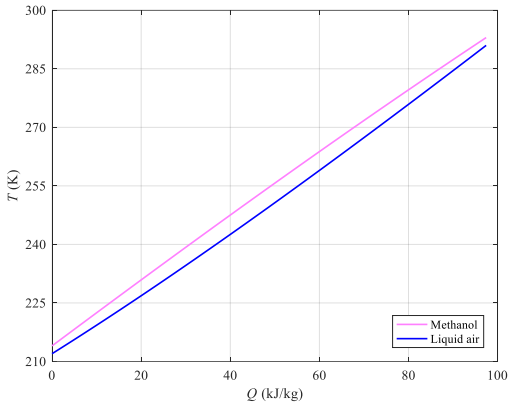

(d)

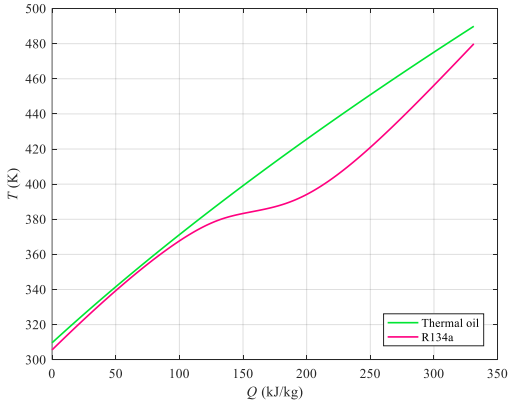

(e)

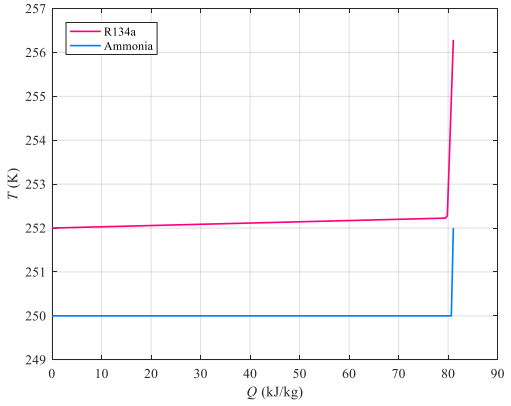

(f)

Figure 6.5 Composite curves of heat exchangers: (a) Cooler; (b) Cold box; (c) Evaporator 1; (d) Evaporator 2; (e) Heater 4; (f) Evaporator-condenser.

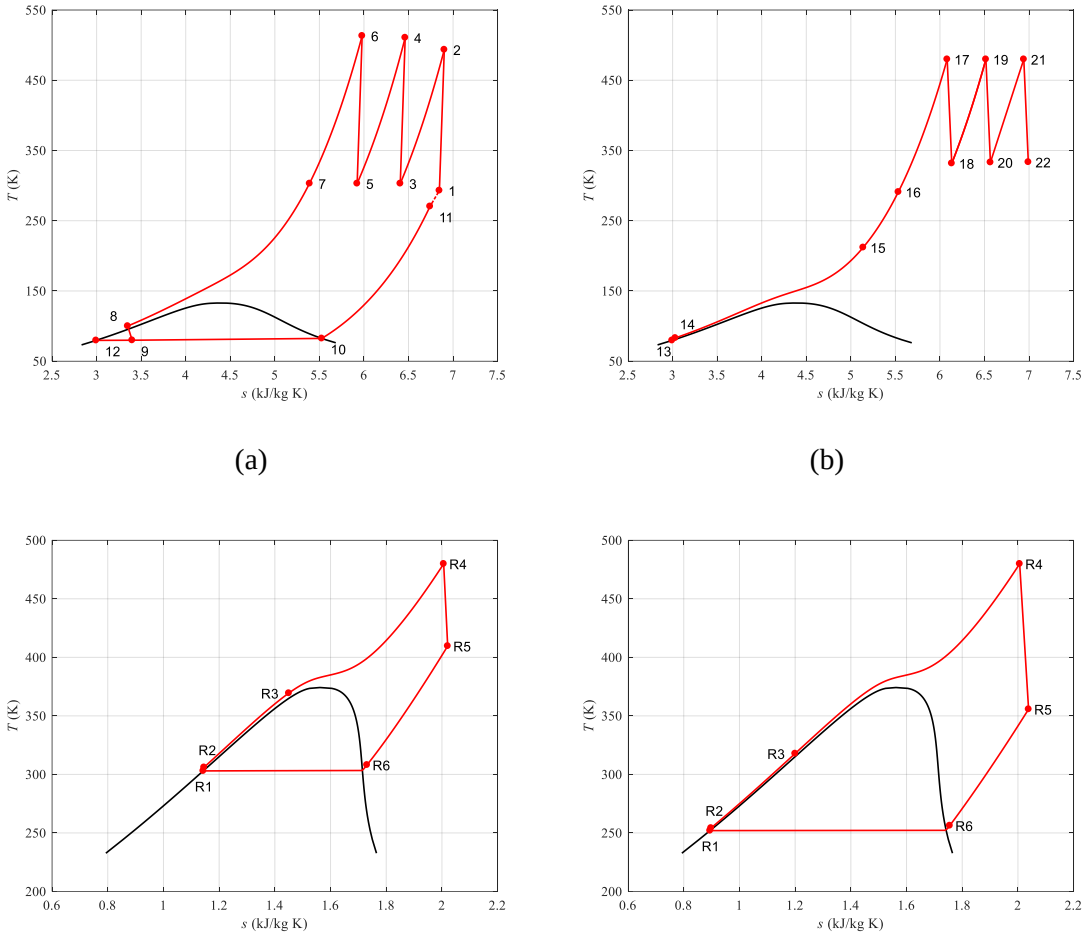

Figure 6.6 *T-s* diagrams: (a) charging process; (b) discharging process; (c) ORC with ambient water cooling; (d) ORC integrated with Absorption Refrigeration Cycles.

In order to obtain more low-temperature cold energy without consuming electricity, and also make full use of the excess heat, two ARCs in series are implemented in the LAES-ARC-ORC. The heat source temperature of the second ARC is ~30 ℃ lower than that of the first ARC. Figure 6.7 shows the effect of heat source temperature on the *COP* of the ARC at different evaporating temperatures, suggesting the existence of an optimal heat source temperature.

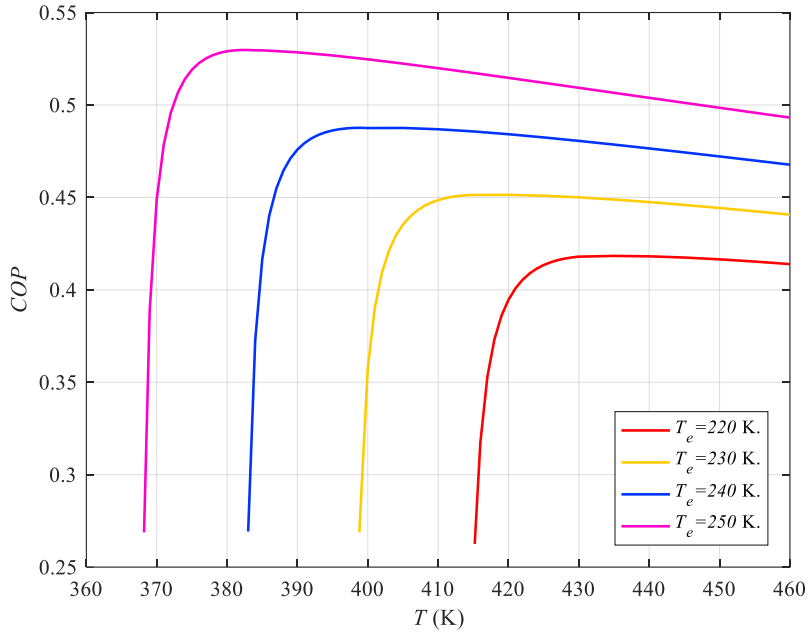

Figure 6.7 Effect of heat source temperature on *COP* of the Absorption Refrigeration Cycle.

6.3.2 Comparison between LAES, LAES-ORC and LAES-ORC-ARC configurations.

6.3.2.1 Effect of the charging pressure on the system performance

Figure 6.8 compares the performances of the LAES, LAES-ORC and LAES-ORC-ARC under different charging pressures (P_c). Once can see that both the LAES-ORC system and LAES-ORC-ARC system have a much higher round trip efficiency than the LAES system, showing an enhancement of 5.5-17.6% and 3.2-13.1%, respectively, and the lower the charging pressure, the higher the enhancement. The results also show that the LAES-ORC is more efficient than the LAES-ORC-ARC with the round trip efficiency of the LAES-ORC reaching 62.7%.

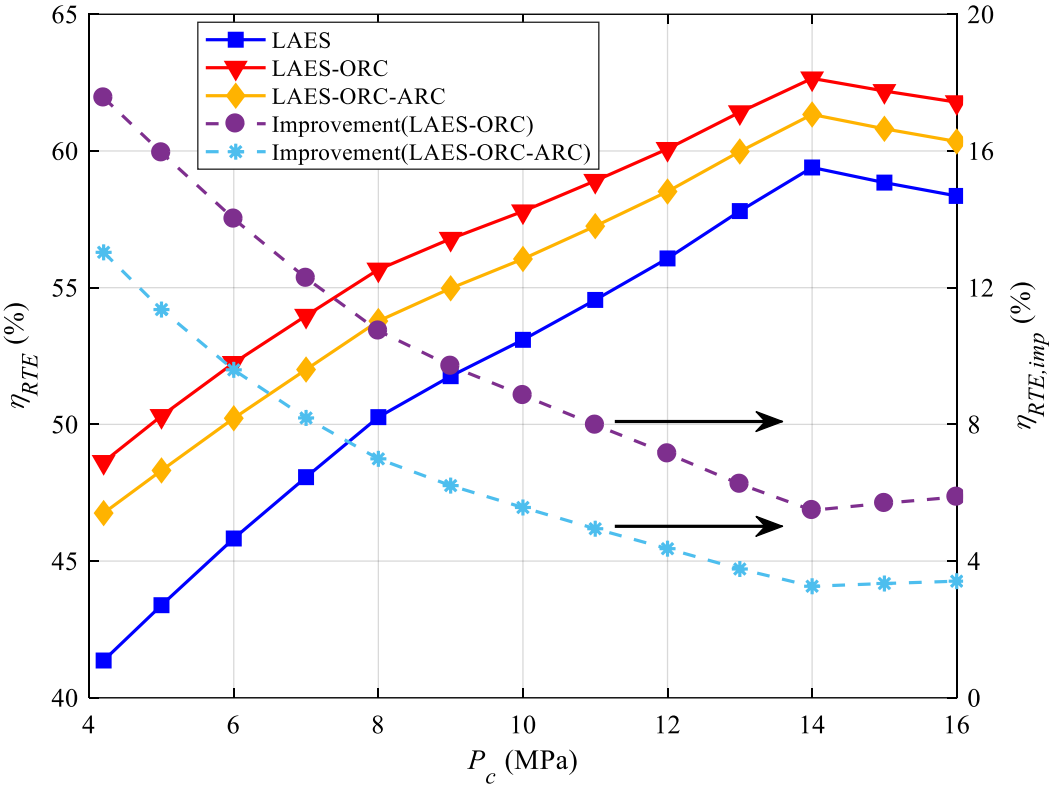

Figure 6.8 Comparison among the LAES, LAES-ORC and the LAES-ORC-ARC under different charging pressures (P_d=8 MPa).

6.3.2.2 Effect of the discharging pressure on the system performance

Figure 6.9 compares the performance of the LAES, LAES-ORC and LAES-ORC-ARC under various discharging pressures (P_d). One can see that the round trip efficiency increases first, reaches a peak, and then decreases with increasing discharging pressure. It is because the increased discharging pressure increases the specific output work of air turbines, but the high-grade cold energy recovered from the liquid air decreases due to the decreased air specific heat capacity at low temperatures. This leads to a decrease in the liquid air yield during the charging process and the increased input work per unit mass of liquid air. The results shown in Figure 6.9 clearly demonstrated that the round trip efficiency of the LAES-ORC and LAES-ORC-ARC is 5.5-9.0%

and 3.2-5.3% higher than that of the LAES, respectively, and a higher discharging pressure results in a higher performance improvement.

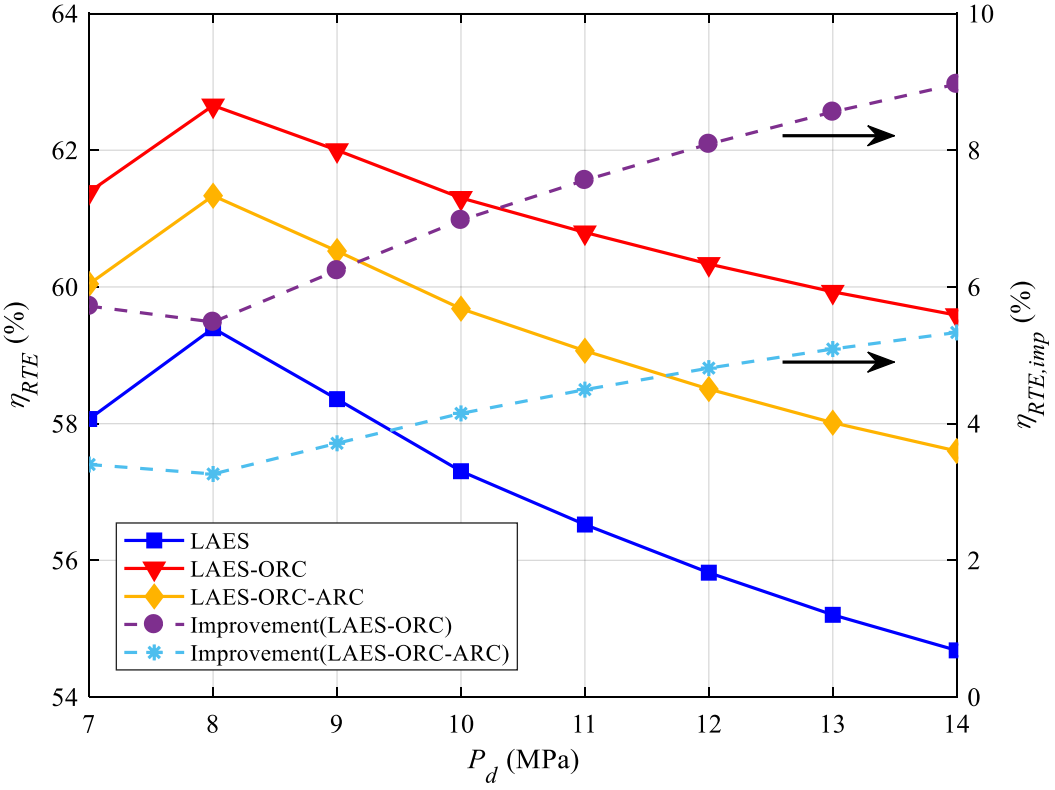

Figure 6.9 Comparison among the LAES, LAES-ORC and the LAES-ORC-ARC under various discharging pressures (P_c=14 MPa).

6.3.2.3 Effect of the turbine inlet pressure of the ORC on the system performance

Figure 6.10 shows a comparison between the LAES-ORC and LAES-ORC-ARC configurations under various turbine inlet pressures (P_{ORC}) of the Organic Rankine Cycle (ORC). Overall, the effect of the P_{ORC} is relatively small. An increase in the ORC turbine pressure from 5 to 12 MPa only leads to an increase in the round trip efficiency of the LAES-ORC from 62.7% to 63.4%, and any further pressure increase yields little benefit. For the LAES-ORC-ARC, the effect of P_{ORC} on the round trip efficiency is negligible under the conditions of this study. The results also indicate

that the LAES-ORC configuration gives a higher round trip efficiency than the LAES or the LAES-ORC-ARC configuration.

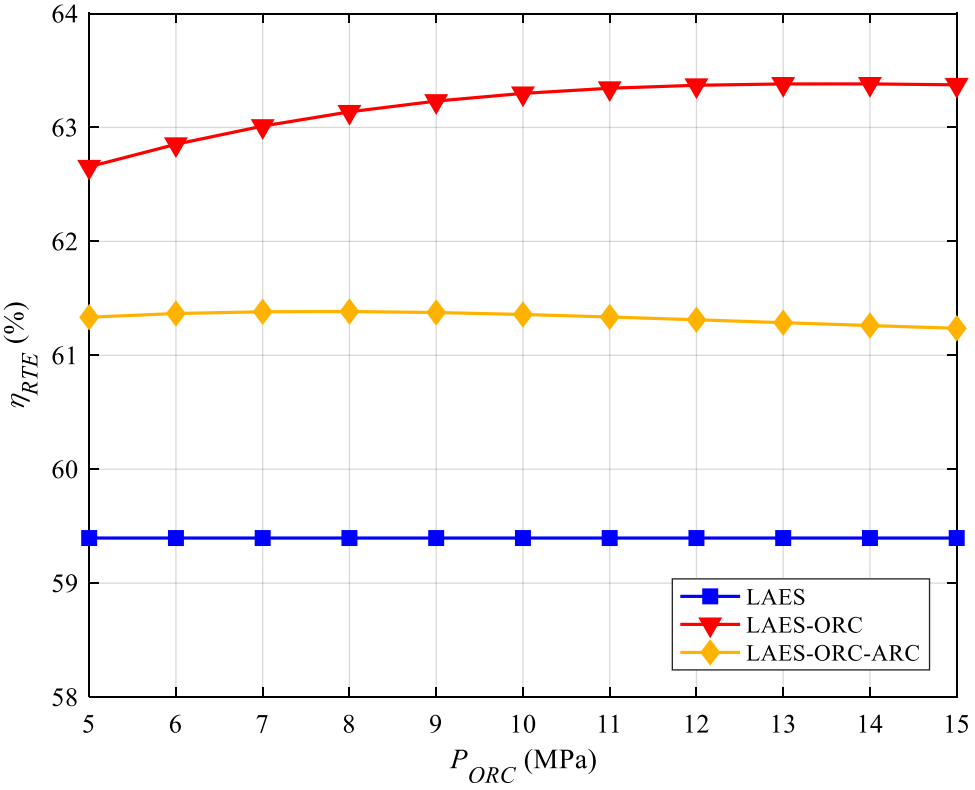

Figure 6.10 Effect of turbine inlet pressure of the ORC on the LAES-ORC and LAES-ORC-ARC (P_c=14 MPa; P_d=8 MPa).

6.3.2.4 Effect of the evaporation temperature of Absorption Refrigeration Cycle on the LAES-ORC-ARC system performance

The effect of evaporation temperatures (T_e) of the ARC on the round trip efficiency of the LAES-ORC-ARC system is shown in Figure 6.11. A minimum occurs in the round trip efficiency over the temperature range studied. This is mainly because a lower temperature cold source contributes to a larger temperature difference between the heat source and cold source in the ORC, and hence more net output work could be obtained; whereas a higher evaporation temperatures results in a higher *COP* of the ARC (as shown in Figure 6.7), leading to the generation of the same amount of

cold energy with less heat and hence more heat for heating the working medium in the ORC. it can be speculated that if the evaporation temperature of the ARC was to increase to the ambient temperature, the ARC would stop working and the LAES-ORC-ARC becomes the LAES-ORC.

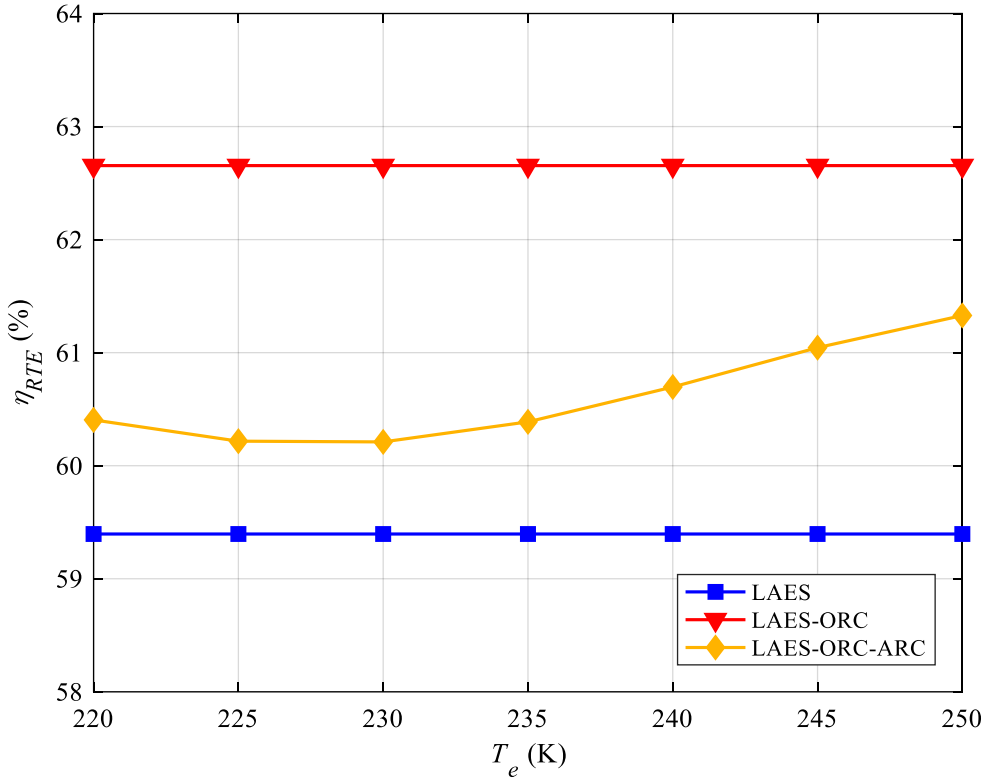

Figure 6.11 Effect of evaporation temperature of the Absorption Refrigeration Cycle on the LAES-ORC-ARC (P_c=14 MPa; P_d=8 MPa; P_{ORC}=5 MPa).

6.4 Conclusions of Chapter 6

The LAES generates heat energy during air compression in the charging process, whereas the power recovery (discharging) process produces high-grade cold energy during the liquid air evaporation. The recovery and utilization of both the cold and hot energy are crucial to the performance of the LAES. This chapter examines the integrated use of ORC and ARC and compares the performance of those integrated system with the LAES system. The main conclusions are as follow:

- The integrated LAES-ORC and LAES-ORC-ARC systems are more efficient than the standalone LAES system with highest improvements of ~17% and ~13% respectively for the round trip efficiency.
- There is an optimal set of pressure of 8 MPa for ORC turbine to give the highest round trip efficiency to the LAES-ORC system while that of 12 MPa for LAES-ORC-ARC system to reach the maximum. Changes of the ORC performance affects less on both the output power and round trip efficiency of the LAES-ORC, compared with LAES-ORC-ARC.
- There is an optimal evaporation temperature of ~225 K for ARC to provide the highest round trip efficiency to the LAES-ORC-ARC system.
- Although both the LAES-ORC system and LAES-ORC-ARC system could achieve a round trip efficiency over 60%, the LAES-ORC shows a better performance than the LAES-ORC-ARC and has a simpler configuration. The LAES-ORC system is more efficient than the LAES-ORC-ARC system.

Chapter 7 Integration of LAES with Liquefied Natural Gas (LNG) regasification process

7.1 Introduction

It has been concluded in Chapter 4 that the high-grade cold energy recovered from the evaporation of liquid air in the discharging process is ~18% in short for achieving the maximum liquid air yield in the charging process. As a result, external cold sources, such as waste cold energy from the regasification of the Liquified Natural Gas (LNG). Guided by understanding, this chapter aims to study how high-quality cold sources could improve liquid air yield and the roundtrip efficiency. Natural Gas (NG) currently provides ~21% of global energy demand [155] and is expecting to grow owes to several advantages including clean, easy to transport and store and high energy density [156,157]. LNG is a cryogenic liquid form of natural gas produced by cooling the gas to approximately 112 K at atmospheric pressure and therefore suitable for long-distance transportation via cargo ships or vehicles [158,159]. Open Rack Vaporizers (ORV) [158] and Submerged Combustion Vaporizers (SCV) [158,160] are two most commonly used vaporizers for LNG regasification. Both vaporizers utilize seawater as a heat source and all cryogenic energy is emitted to the open sea directly, which causes not only serious energy losses but environmental issues [158,161]. Therefore, the LNG regasification process brings opportunities to use LNG cryogenic energy through integration with other industrial processes, such as cryogenic energy electricity production [162–166], low temperature CO_2 capture [167,168], cold storage system [169,170] and air separation process [171,172].

Integration of the LAES system with the LNG regasification process is studied here with an aim to increase the yield of liquid air and enhance the overall roundtrip efficiency. Sensitivity analysis and exergy efficiency analysis are performed on the integration system. A comparison among the

integration system (LAES-LNG), integration system with cold store (LAES-LNG-ES) and LAES is made under same operating conditions.

7.2 A proposed LAES-LNG system and LAES-LNG-CS system.

7.2.1 System descriptions and assumptions.

Figure 7.1 shows a schematic diagram of the proposed LAES-LNG system, which is composed of an air charging cycle, air discharging cycle, LNG cycle and a Brayton cycle. The air charging cycle operates at off-peak hours: purified air enters the multistage compressor to increase the pressure with the compression heat recovered and stored in the thermal oil; the high pressure air then enters the cold box where it is cooled down by the cold energy from LNG and cold air; and finally, the compressed cold air expands in the cryo-expander, with part of air liquefied to be stored in the liquid air tank.

The LNG cycle works at off-peak time together with the air charging cycle: LNG is pumped to a high pressure, with cold energy transferred to the compressed air through heat exchange. It should be noted that this assumption is not reasonable. In practice, LNG regasification is often unsteady, depending on the demand on the natural gas. As a result, a more practical cycle would include a cold store to store LNG cold energy and the cold store is integrated with the LAES. Thus, this direct integration of LNG is for the first approximation and in a way that the LNG cycle serves as a cold store.

The air discharging cycle works at peak hours: liquid air from the liquid air tank is pumped to a pressure above its critical pressure; the high pressure air releases part of the cold energy to propane which also acts as a storage medium for reused in the air charging cycle, and the rest of the cold energy is used to drive a Brayton cycle using nitrogen (N2) as the working medium; the high pressure air then enters turbine set to generate electricity, in which the air is superheated by the stored thermal oil to enhance the work output.

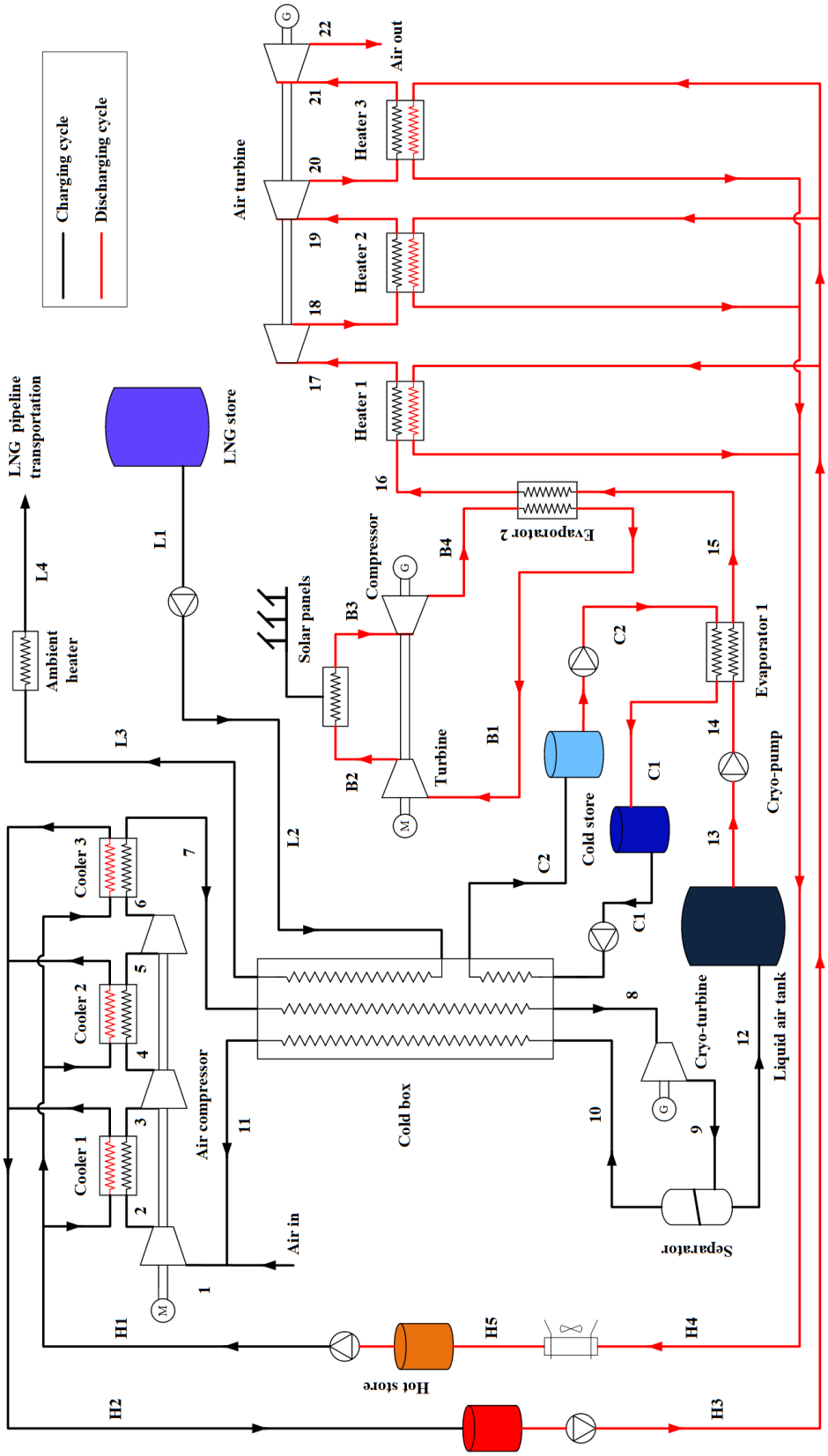

Figure 7.1 Schematic diagram of the LAES-LNG system.

However, it can be found that the LNG regasification process is limited by the charging process of the LAES system during the off-peak hours, but the reality is the LNG regasification is operated according to the needs of users. Thus, to increase the flexibility and feasibility of the LAES-LNG system, an extra low-grade cold store (CS) is implemented to recover the cold energy released from the LNG evaporation, named as the LAES-LNG-CS system, as shown in Figure 7.2.

In the LNG cycle, LNG is pumped to a high pressure and evaporates at Evaporator 3, where the cryogenic fluid (pressured propane) from the low-grade cold store recovers and stores the cold for air liquefication. After warming up by the ambient, the evaporated natural gas (NG) then enters each stage of turbine to generate electricity, which can be used to decrease the work consumption of the compressor in charging process or increase the net output work of in the discharging process.

The air charging cycle of the LAES-LNG-ES system is similar as that of the LAES-LNG system but only the low-grade refrigerant is replaced from LNG to pressured propane. In the air discharging process, the rest of cold energy from liquid air evaporation would be recovered and stored by low-grade cold store to instead of the Brayton cycle.

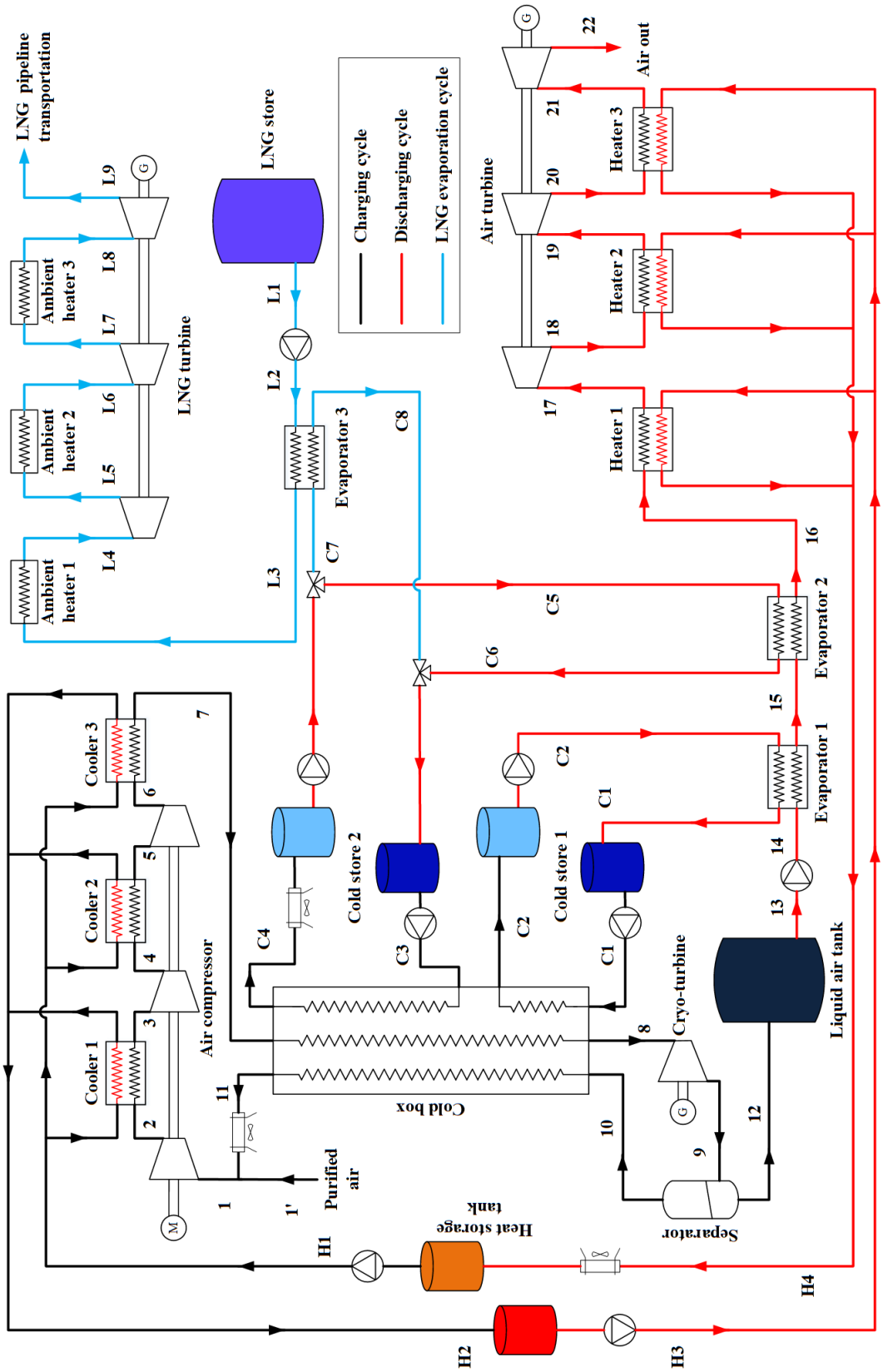

Figure 7.2 Schematic diagram of the LAES-LNG-CS system.

Natural gas in the primary transportation pipeline is set to 7 MPa to meet the requirements of long-distance distribution. The major chemical ingredient of NG and LNG is methane, which ranges between 87.0% and 99.8% [161]. Therefore, methane is assumed to the one and only constituent of LNG and NG in the simulation. The simulation of the integrated LAES system is implemented in the MATLAB environment; the thermal properties of air, propane, nitrogen and methane are obtained from REFPROP 8.1, while thermal properties of thermal oil come from ASPEN plus.

7.2.2 Performance indexes

7.2.2.1 Round trip efficiency

As discussed in previous chapters, the round trip efficiency of a standalone LAES system can be simply defined as the net output work in the discharging cycle divided by the net input work in the charging cycle. For convenient, it is reproduced here:

$$\eta_{RTE,LAES} = \frac{W_{out}}{W_{in}} = \frac{m_d w_d}{m_c w_c} \tag{7.1}$$

where w_c represents the net input work per unit mass of air in the charging cycle; w_d represents the net output work per unit mass of air in the discharging cycle; m_c and m_d are the mass flow rates of air in the charging cycle and in the discharging cycle, respectively.

The specific net input of the charging cycle w_c is the difference between the total work consumption of three compressors (w_C) and the specific net work of cryogenic air expander (w_E):

$$w_c = w_C - w_E = (h_2 - h_1) + (h_4 - h_3) + (h_6 - h_5) - (h_8 - h_9) \tag{7.2}$$

The specific net output of the discharging cycle is the difference between the specific output of three turbines (w_T) and the specific work consumption of the cryogenic pump (w_P):

$$w_d = w_T - w_P = (h_{17} - h_{18}) + (h_{19} - h_{20}) + (h_{21} - h_{22}) - (h_{14} - h_{13}) \tag{7.3}$$

In the integration LAES-LNG system, the round trip efficiency is defined in a similar way:

$$\eta_{RTE,LAES-LNG} = \frac{W_{out}}{W_{in}} = \frac{m_{13} w_d + m_{B1} w_B}{m_1 w_c} \tag{7.4}$$

where w_B represent the specific net output work of the Brayton cycle, which is calculated by taking the difference between specific electricity output of the turbine and specific electricity input of the compressor:

$$w_B = (h_{B3} - h_{B4}) - (h_{B2} - h_{B1}) \tag{7.5}$$

The specific net work of LNG pump can be neglected as it is part of the LNG receiving terminals.

In the LAES-LNG-CS system, the round trip efficiency can be expressed in 3 types depending on the operation period of the LNG cycle. If the LNG cycle is operated at off-peak time, the round trip efficiency can be described as follow:

$$\eta_{RTE,LAES-LNG-CS,off\text{-}peak} = \frac{W_{out}}{W_{in}} = \frac{m_{13} w_d}{m_1 w_c - m_{L1} w_L} \tag{7.6}$$

where w_L is the specific net output of the LNG cycle, it can be calculated as:

$$w_L = (h_{L4} - h_{L5}) + (h_{L6} - h_{L7}) + (h_{L8} - h_{L9}) - (h_{L2} - h_{L1}) \tag{7.7}$$

At peak time, the round trip efficiency can be described as follow:

$$\eta_{RTE,LAES-LNG-CS,peak} = \frac{W_{out}}{W_{in}} = \frac{m_{13} w_d + m_{L1} w_L}{m_1 w_c} \tag{7.8}$$

If the LNG cycle runs whole day, the round trip efficiency can be described as follow:

$$\eta_{RTE,LAES-LNG-CS,full} = \frac{W_{out}}{W_{in}} = \frac{m_{13} w_d \cdot t_{peak,LAES} + m_{L1} w_L \cdot t_{peak,LNG}}{m_1 w_c \cdot t_{off\text{-}peak,LAES} - m_{L1} w_L \cdot t_{off\text{-}peak,LNG}} \tag{7.9}$$

where $t_{off\text{-}peak,LAES}$ and $t_{off\text{-}peak,LNG}$ are the time of the LAES system and LNG cycle operated at off-peak hour, while $t_{peak,LAES}$ and $t_{peak,LNG}$ are the time of the LAES system and LNG cycle operated at peak hour respectively. It should be explained that the value of the mass flow of the LNG m_{L1} is only controlled by demand of the users. Exaggerated m_{L1} may lead to round trip efficiency becoming negative, which is meaningless for evaluating the performance. Thus, m_{L1} is chosen based on the cold energy released from LNG cycle just meets the required cold energy for air liquefication.

7.2.2.2 Exergy efficiency

In the proposed LAES-LNG system, the exergy input of the charging cycle consists of a few components of the net power input of compressors, the exergy of LNG and the exergy of propane (cold store), while the exergy output includes the exergy of liquid air, the exergy of high-temperature thermal oil and the net work of cryogenic air expander. They can be mathematically expressed by:

$$E_{in,c} = m_1 w_C + m_{L1}(e_{L2} - e_{L3}) + m_{C1}(e_{C1} - e_{C2}) \tag{7.10}$$

$$E_{out,c} = m_{12} e_{12} + m_{H1}(e_{H2} - e_{H1}) + m_8 w_E \tag{7.11}$$

In the discharging cycle, the exergy input includes the exergy of liquid air, the exergy of thermal oil and the net work of cryogenic pump, while the exergy output consists of the net work of turbines, cold exergy recovered by propane and the net output work generated by Brayton cycle. Thus, the exergy input and exergy output of the discharging cycle are:

$$E_{in,d} = m_{13} e_{13} + m_{H3}(e_{H3} - e_{H5}) + m_{13} w_P \tag{7.12}$$

$$E_{out,d} = m_{13} w_T + m_{C1}(e_{C1} - e_{C2}) + m_{B1} w_B \tag{7.13}$$

Similarly, in the proposed LAES-LNG-CS system, the exergy input of the charging cycle consists of a few components of the net power input of compressors, the exergy of pressured propane (low-grade cold store) and the exergy of propane (high-grade cold store):

$$E_{in,c} = m_1 w_C + m_{C3}(e_{C3} - e_{C4}) + m_{C1}(e_{C1} - e_{C2}) \tag{7.14}$$

The exergy output is mathematically expressed same as Eq. 7.11.

In the discharging cycle of the proposed LAES-LNG-CS system, the exergy input is same expressed as Eq. 7.12, while the exergy output consists of the net work of turbines, cold exergy recovered by propane (high-grade cold store) and cold exergy recovered by pressured propane (low-grade cold store). Thus, the exergy input and exergy output of the discharging cycle are:

$$E_{out,d} = m_{13} w_T + m_{C1}(e_{C1} - e_{C2}) + m_{C6}(e_{C6} - e_{C7}) \tag{7.15}$$

In both LAES-LNG system and LAES-LNG-CS system, the exergy efficiency of the charging cycle and that of the discharging cycle can be respectively defined as:

$$\eta_{ex,c} = \frac{E_{out,c}}{E_{in,c}} \tag{7.16}$$

$$\eta_{ex,d} = \frac{E_{out,d}}{E_{in,d}} \tag{7.17}$$

7.3 Results and discussions

The entire system is complex. To simplify the system analysis, several assumptions are made as follows:

- The system is in a steady state, and neither dynamic nor transient analyses are considered;
- The kinetic and potential energy changes of air are neglected;
- There is no heat loss or pressure loss through the system components unless otherwise specified.

In the LAES, the air consists of nitrogen (78.12%), oxygen (20.96%) and argon (0.92%) while pressured nitrogen is considered as the mainly working medium in the Brayton cycle. The calculations were done in the MATLAB environment, with the thermal properties of air, propane, methanol, ammonia and R134a obtained by using REFPROP 8.1, and the thermal properties of thermal oil from ASPEN plus.

7.3.1 Simulation results of the LAES-LNG system

A large-scale LAES-LNG system with power output of 10MW is simulated in this research, whose operating time is consisted of 8 hours for the charging cycle at off-peak hours and 8 hours for discharging cycle in an entire day. The default values of parameters of LAES-LNG system are given in Table 7.1.

Table 7.1 Default parameters of the LAES-LNG system.

Parameter	Value
Ambient temperature	298 K
Ambient pressure	0.1 MPa
Pinch point in coolers	2.0 K
Pinch point in cold box	5.0 K
Pinch point in evaporators	2.0 K
LNG feed temperature	111.5 K
Pumped LNG pressure	7.0 MPa
Pressure drop	1%
Isentropic efficiency of compressor	85%
Isentropic efficiency of turbine	90%
Isentropic efficiency of pump	75%
Isentropic efficiency of cryogenic expander	75%

Turbine inlet pressure in Brayton cycle	3.5 MPa
Compressor inlet pressure in Brayton cycle	10.0 MPa

The setting pressure of charging cycle and discharging cycle are 10 MPa and 8 MPa respectively and the optimized performance of LAES-LNG system is shown in Table 7.2, in terms of net work for charging and discharging cycles, mass flow rate of each cycles, exergy efficiencies, roundtrip efficiency and liquid air yield. For comparison purposes, the result of the LAES system are also given in Table 7.2.

Table 7.2 Performance results of LAES-LNG and traditional LAES.

Items	LAES-LNG		LAES	
	Charging	Discharging	Charging	Discharging
Net power (MW)	13.15	10.00	18.84	10.00
Air mass flow rate (kg/s)	23.17	20.14	28.82	20.14
Exergy efficiency	86.14%	69.92%	78.78%	80.67%
LNG mass flow rate (kg/s)	11.28		-	
Liquid air yield	0.8693		0.6989	
Round trip efficiency	76.05%		53.09%	

From Table 7.2, one can see that for net output power of 10 MW, both the LAES-LNG and conventional LAES system consume the same quantity of liquid air. However, the LAES-LNG system consumes ~19.6% less electric energy than the LAES during air liquification, and hence the roundtrip efficiency increases from 53.09% to 76.05%. The significant drop of exergy efficiency of LAES-LNG discharging cycle is because some of the recovered cold energy is used to drive the

Brayton cycle whose performance is limited by its relatively lower thermal efficiency of approximately 50% with a low-temperature heat source.

The stream data of the 10 MW LAES-LNG system is listed in Table 7.3 and Table 7.4 respectively for the charging cycle and discharging cycle, and Table 7.5 for other processed and cycles including the thermal fluid, the cold fluid, the LNG and the Brayton cycle. The temperature-Entropy diagrams (*T*-*S*) for energy storage and release processed, the LNG cycle and the Brayton cycle are illustrated in Figure 7.3.

Table 7.3 Stream data for the LAES-LNG system in the charging cycle.

	$\dot{m}$ [kg/s]	T [K]	P [MPa]	H [kJ/kg]	Fluid
1	23.17	293.00	0.10	293.27	Air
2	23.17	476.96	0.46	479.55	Air
3	23.17	303.00	0.46	302.54	Air
4	23.17	493.41	2.13	495.63	Air
5	23.17	303.00	2.11	298.94	Air
6	23.17	495.30	10.00	494.55	Air
7	23.17	303.00	9.90	283.74	Air
8	23.17	95.66	9.80	-87.92	Air
9	23.17	79.83	0.11	-98.63	Air
10	3.03	82.45	0.11	79.60	Air
11	3.03	255.23	0.11	255.25	Air
12	20.14	79.66	0.11	-124.88	Air

Table 7.4 Stream data for the LAES-LNG system in the discharging cycle.

	$\dot{m}$ [kg/s]	T [K]	P [MPa]	H [kJ/kg]	Fluid
13	20.14	79.66	0.11	-124.88	Air
14	20.14	83.13	8.00	-112.91	Air
15	20.14	127.51	7.92	-22.34	Air
16	20.14	279.09	7.84	260.15	Air
17	20.14	466.24	7.76	464.35	Air
18	20.14	321.95	1.80	319.17	Air
19	20.14	466.24	1.78	467.68	Air
20	20.14	323.47	0.41	323.34	Air
21	20.14	466.24	0.41	468.57	Air
22	20.14	323.88	0.10	324.37	Air

Table 7.5 Stream data for thermal oil, propane, LNG cycle and Brayton cycle.

	$\dot{m}$ [kg/s]	T [K]	P [MPa]	H [kJ/kg]	Fluid
H1	43.80	293.00	0.10	422.83	Thermal oil
H2	43.80	476.24	0.10	731.89	Thermal oil
H3	36.76	476.24	0.10	731.89	Thermal oil
H4	36.76	329.06	0.10	474.41	Thermal oil
H5	36.76	298.00	0.10	429.70	Thermal oil
C1	23.45	90.63	0.10	-186.73	Propane
C2	23.45	130.63	0.10	-108.94	Propane
L1	11.28	111.51	0.10	-0.56	Methane

L2	11.28	114.86	7.00	21.12	Methane
L3	11.28	219.91	6.93	577.54	Methane
L4	11.28	298.00	6.93	840.37	Methane
B1	29.14	133.00	3.47	86.45	Nitrogen
B2	29.14	180.96	10.00	124.53	Nitrogen
B3	29.14	373.00	9.90	376.55	Nitrogen
B4	29.14	284.17	3.50	286.54	Nitrogen

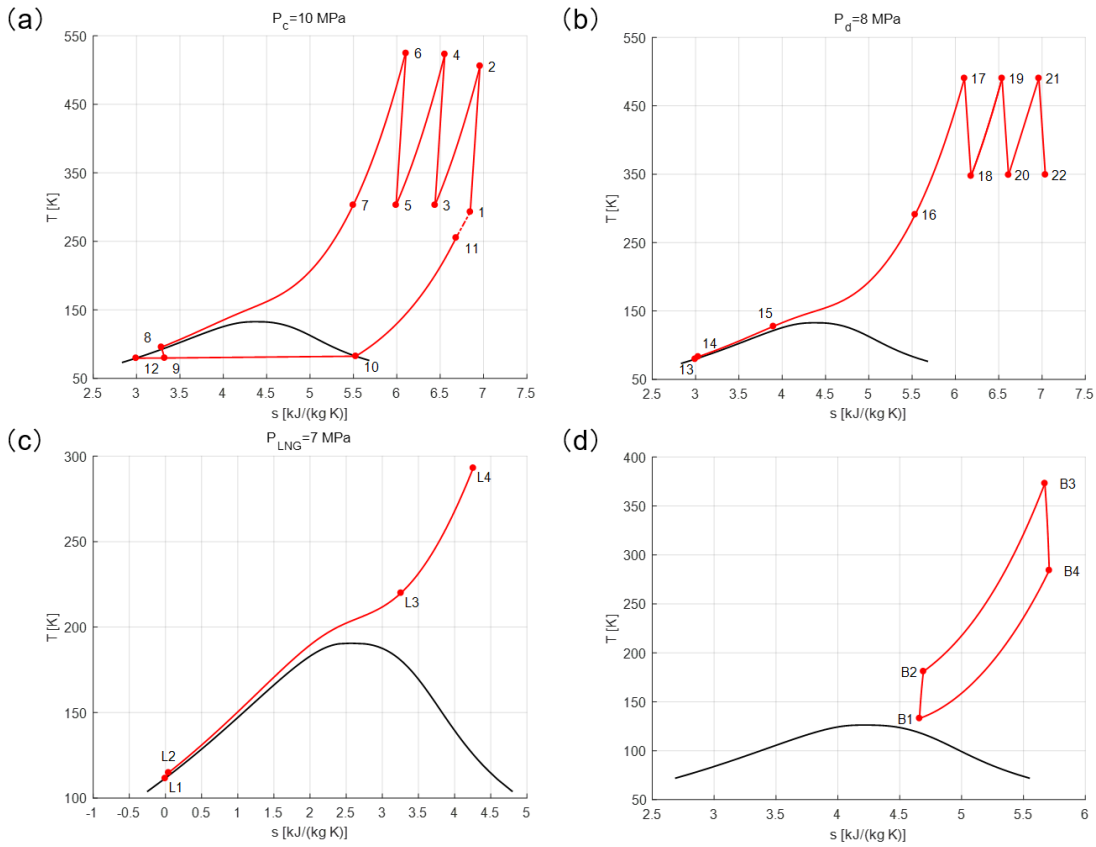

Figure 7.3 *T-S* diagrams for LAES-LNG, (a) energy storage section; (b) energy release section; (c) LNG cycle; (d) Brayton cycle.

7.3.2 Influence of LNG amount on the LAES-LNG performance

Figure 7.4 illustrates how the mass flow rate of the LNG input affects the LAES-LNG system performance, including the liquid air yield, the roundtrip efficiency, the exergy efficiency of the energy storage process and the supplied air temperature at the cold box outlet. The horizontal axis represents the mass flow rate ratio of the LNG to the supplied air through liquification. An increase in the LNG mass flow increases the liquid air yield, roundtrip efficiency and exergy efficiency first until a mass flow rate of ~0.48, beyond which little benefit can be seen. There is an even a slight decrease in the exergy efficiency at a mass flow ratio above ~0.48. These can be explained by Eq. 7.10, Eq. 7.11 and Eq. 7.16 that a further increase in LNG flow rate results in an increase in the exergy input but with no change in exergy output. On the other hand, the air temperature at the cold end of the cold box shows a sharp drop first, followed by a relative lower rate of drop till a minimum is reached, beyond which little effect is seen with a further LNG increase in the mass flow ratio. The initial quick drop of the mass flow ratio lasts to a ratio of ~0.19, which is due to the LNG can be well heated and fully exchanges heat with the air, evidenced by the temperature at hot end of cold box reaching to near-ambient temperature. When the mass flow ratio exceeds 0.19, the LNG temperature at the hot end of the cold box starts to drop. At the same time, liquid air yield, roundtrip efficiency, exergy efficiency and supplied air temperature change at a relatively slow rate until they reach their respective maxima.

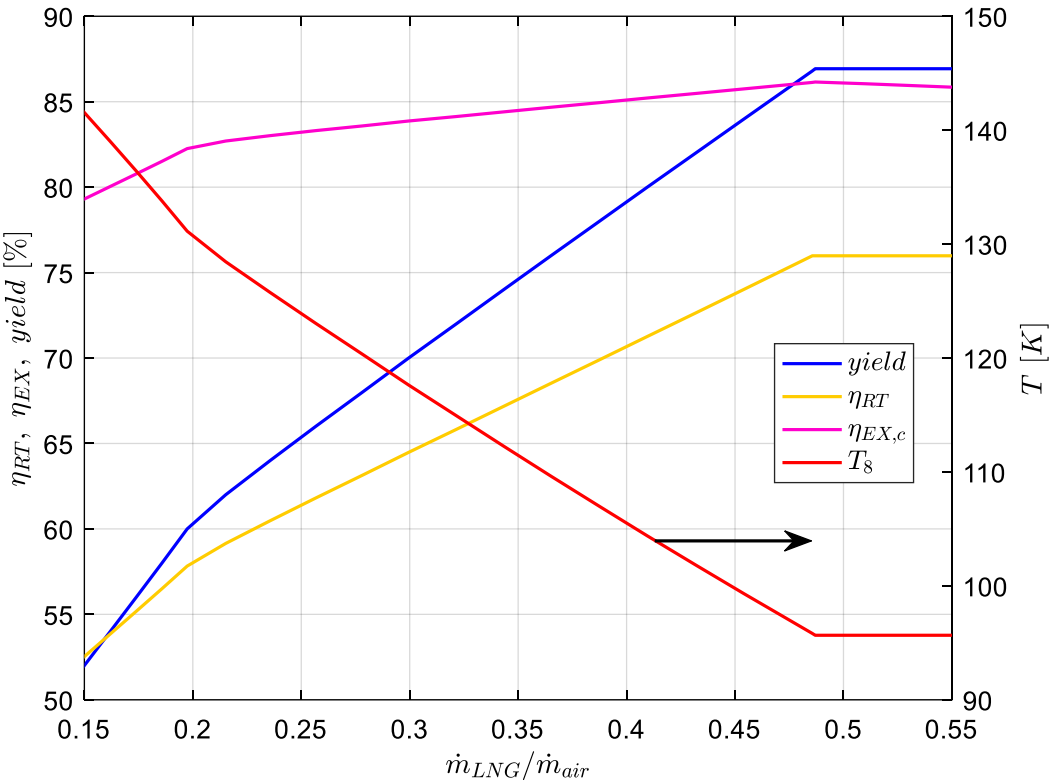

Figure 7.4 Influence of LNG flow to the cold box on liquid air yield, roundtrip efficiency, exergy efficiency of the energy storage process and supplied air temperature at cold box outlet; charging pressure $P_{charging}$ =10 MPa.

7.3.3 Influence of the mass flow and expansion pressure on performance of the Brayton cycle.

The Brayton cycle in LAES-LNG system acts as a cold energy user during liquid air evaporation, which can generate extra electrical energy in the discharging cycle. Figure 7.4 illustrates that specific net output power of the Brayton cycle as a function of the working fluid mass flow rate ratio and expansion pressure during LAES discharging process. Here the mass flow ratio is defined as the ratio of the working fluid flow rate to the liquid air mass flow rate. The specific net work is with respect to the liquid air mass flow rate.

The following observations can be made from Figure 7.4:

- For a given expansion pressure. the specific net work increases first with the mass flow rate ratio in a linear fashion, reaches a maximum, then decreases with further increase in the mass flow rate ratio, also in a linear manner.
- The mass flow rate ratio, at which the maximal specific network occurs, decreases with increasing expansion pressure.
- The peak specific net work is a function of the expansion pressure and these appears to be a maximum at expansion pressure of ~2.0-2.5 MPa (see dotted line on Figure 7.4) with a mass flow rate ratio of ~1.42-1.54.

The effect of the mass flow rate ratio on the specific net work for a given expansion pressure is related to the balance between the net work increase due to increased mass flow in the turbine and the work consumption increase of the compressor.

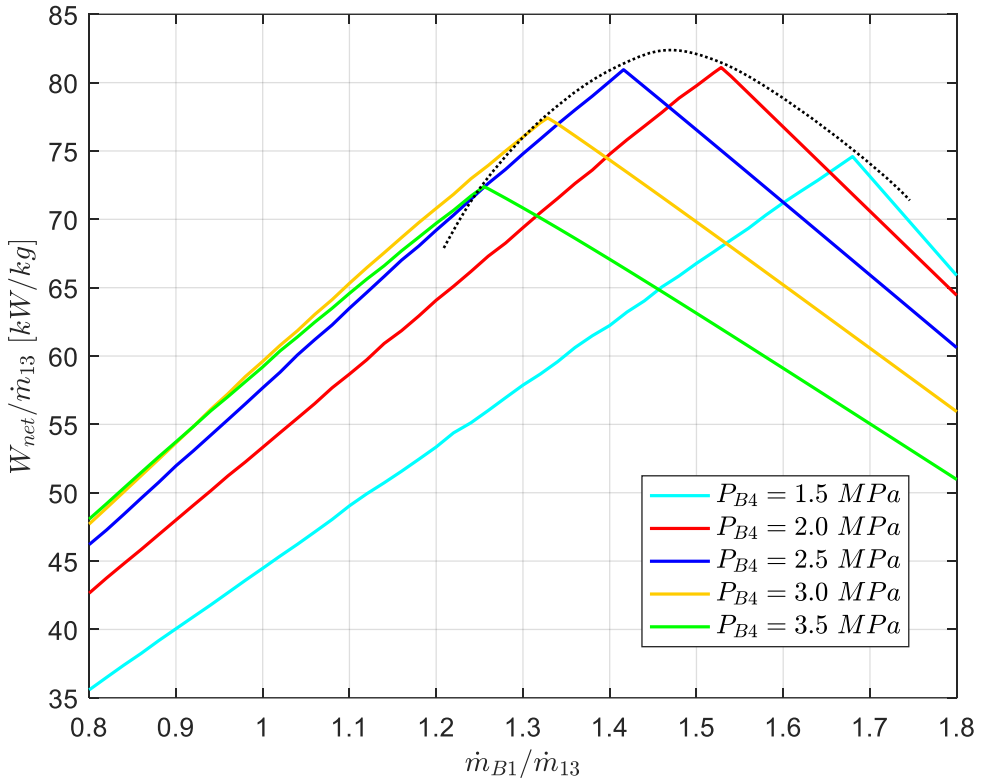

Figure 7.5 Influence of the working fluid flow rate flow on the net output power of the Brayton cycle in energy release process of the LAES-LNG system; cold source temperature T_{15}=127.51 K; hot source temperature T_{B3}=373.0 K.

7.3.4 Influence of charging pressure on performance of the LAES-LNG system

The effect of the charging pressure (P_6) on the LAES-LNG system performance is shown in Figure 7.6 (a) for the roundtrip efficiency and liquid air yield change and Figure 7.6 (b) for the exergy efficiency during both charging and discharging processes. From Figure 7.6 (a), one can see that, for a given discharging pressure, the liquid air yield increases slightly with increasing charging pressure (dash lines) but the round trip efficiency decreases. This can be explained by the fact that the output power of LAES-LNG system is almost unchanged because of little benefits to the liquid air yield, while the power consumption of compressor increases due to charging pressure increasing. Figure 7.6 (a) also shows that, for a given charging pressure, a lower discharging pressure gives a higher liquid air yield but a higher round trip efficiency.

Attention is now paid to Figure 7.6 (b). Note that although the change in charging pressure cannot influence the performance of discharging cycle directly and vice versa, the temperature, pressure and amount of the working mediums, including liquid air, propane and thermal oil, are influenced by the charging pressure or the discharging pressure, and hence the effect is indirect. Look first at the solid lines, one can see that, for a given discharging pressure (P_{14}), the exergy efficiency of the charging cycle increases with increasing charging pressure (P_6), varying from ~72% to ~85%. This is due to the sufficient cold energy supply from LNG evaporation, the increased charging pressure increases the liquid air yield. Meanwhile, the increased charging pressure also leads to a temperature increase of the thermal oil. However, the effect of the discharging pressure is small for a given charging pressure. Looking at the dash lines, one can see that the exergy efficiency of discharging cycle in LAES-LNG is much lower than that of the standalone LAES as the Brayton cycle is implemented in discharging cycle. The standalone LAES uses an energy storage unit to store both high-grade cold energy and low-grade cold energy from liquid air evaporation, while LAES-LNG only stores and reuses high-grade cold energy and low-grade cold energy is used in the Brayton cycle as a cold source. Thus the lower energy conversion efficiency of the Brayton cycle leads to the lower exergy efficiency of discharging cycle in LAES-LNG than that in the LAES. It also can be found that the exergy efficiency significantly increases first with discharging pressure (P_{14}), then slightly increases with further increase in the P_{14}. This is because the increased discharging pressure not only increases the outpower of the turbine, but also leads to a temperature increase of the propane, which decreases the amount of the cold energy from the liquid air evaporation. When the discharging pressure reaches a specific given value, the extent of the effect caused by the decreased cold energy increases significantly and hence decreases the growth rate of the exergy efficiency.

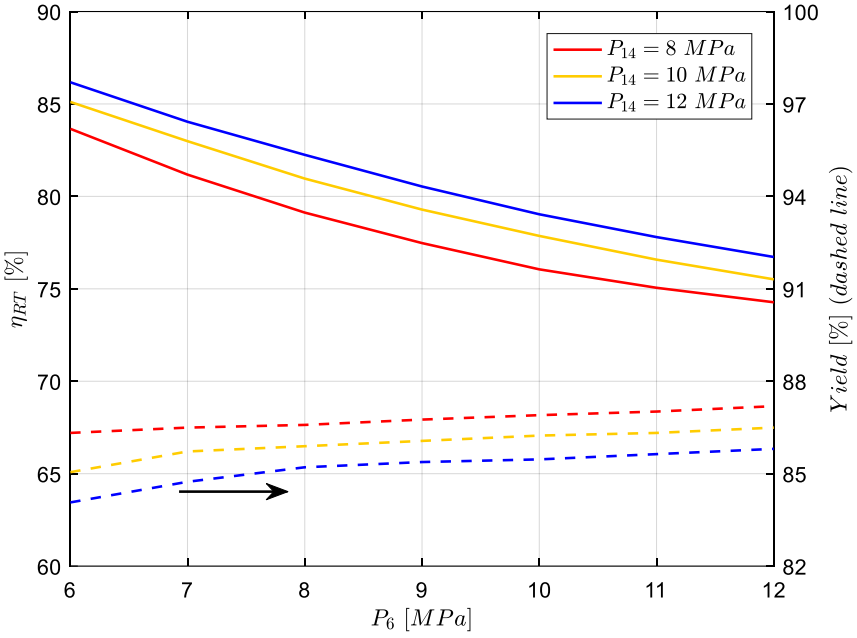

(a)

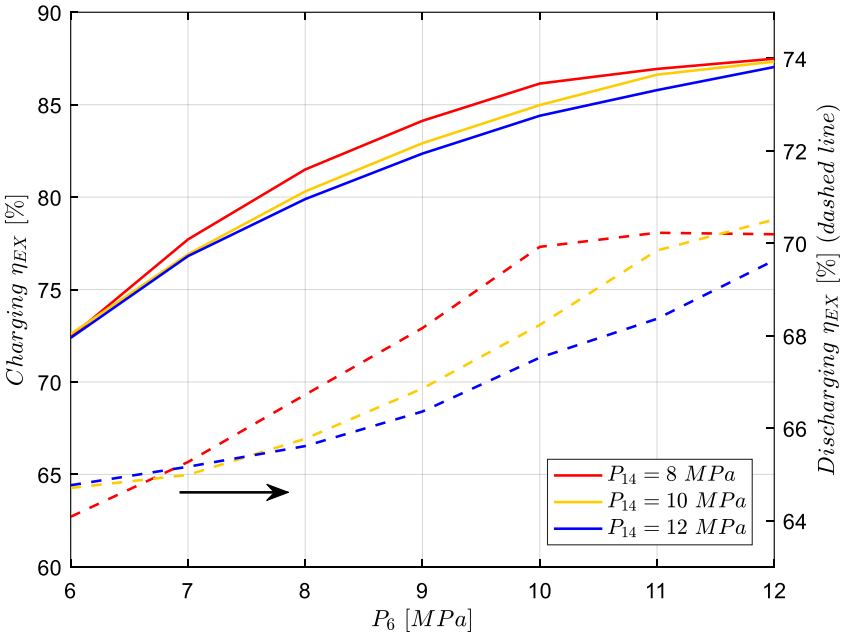

(b)

Figure 7.6 Influence of charging pressure on the performance of the LAES-LNG system; (a) round trip efficiency and liquid air yield; (b) exergy efficiency of the charging and discharging cycles.

The charging pressure of LAES-LNG system can also influence the optimum configuration of the cold box in terms of the entropy generation, as illustrated in Figure 7.7, which shows the heat exchange diagrams for the cold box at different charging pressures. An increase in the charging pressure (P_6) gives a higher utilization ratio of the high-grade cold (propane), as illustrated by the vertical of dash line shown in Figure 7.7, which means the more cold energy can be recovered from liquid air evaporation. The outlet LNG temperature from the cold box increases significantly due to the pressure increases, leading to a better utilization of the cold energy from the LNG.

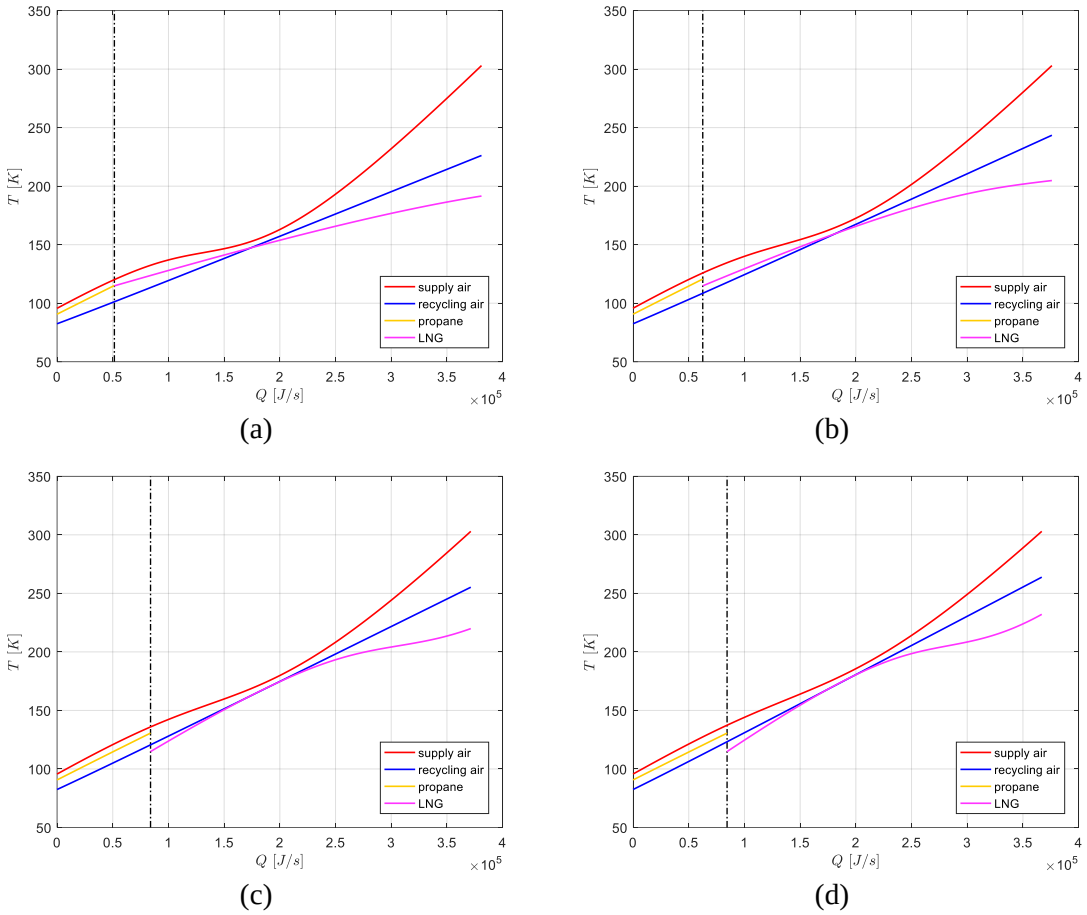

Figure 7.7 Optimal heat exchange diagrams for the cold box at P_{14} =8 MPa; (a) P_6=6 MPa; P_6=8 MPa; (c) P_6=10 MPa; (d) P_6=12 MPa.

7.3.5 Influence of discharging pressure on the LAES-LNG system

Figure 7.8 (a) illustrates the roundtrip efficiency and liquid air yield as a function of the discharging pressure (P_{14}) in the energy storage part of the LAES-LNG system. An increase in the discharging pressure results in an increase in the roundtrip efficiency, with a scale of approximately 1% per 1 MPa increase. Higher pressure ratios contribute to a larger net output of the turbine and hence the increase in the roundtrip efficiency is shown by Eq. 7.2 represented. It should be noticed that the discharging pressure cannot directly affect the liquid air yield, but the change in the discharging pressure directly affects the temperature of propane when recovering and storing the cryogenic energy. Such stored cold is used in the charging process and hence the indirect effect is illustrated as dashed lines in Figure 7.8 (a), the increasing discharging pressure results in a slight drop in the liquid air yield, with approximately 0.33% decrease per 1 MPa pressure increase.

Figure 7.8 (b) shows the effect of the discharging pressure on the exergy efficiency of the charging process and the discharging process of the LAES-LNG system respectively. One can observe that the increase in discharging pressure gives a small extent of changes (decrease) to the exergy efficiency of charging process of the LAES-LNG system, which is less than ~3%. The exergy efficiency of the discharging process shows an increasing trend first, reaches a maximum before reduces with a further increasing in the discharging process. The peak for P_6=8 MPa does occur but at a discharging pressure below 6 MPa, so it is not shown on the figure. Clearly, a higher charging pressure of the LAES-LNG system gives to a higher optimal exergy efficiency. The results shown in Figure 7.8 (b) also indicates that it is not feasible to increase the exergy efficiency significantly by only increasing the discharging pressure.

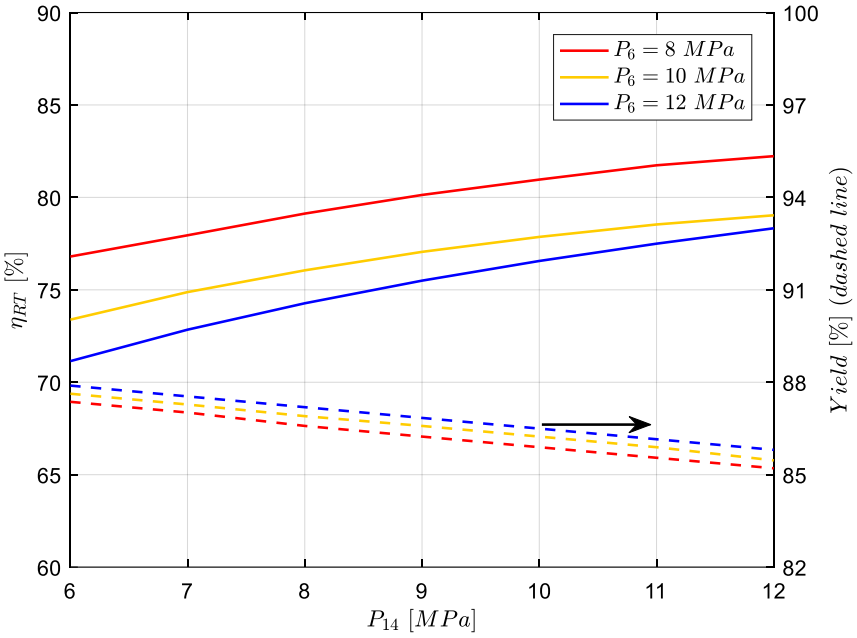

(a)

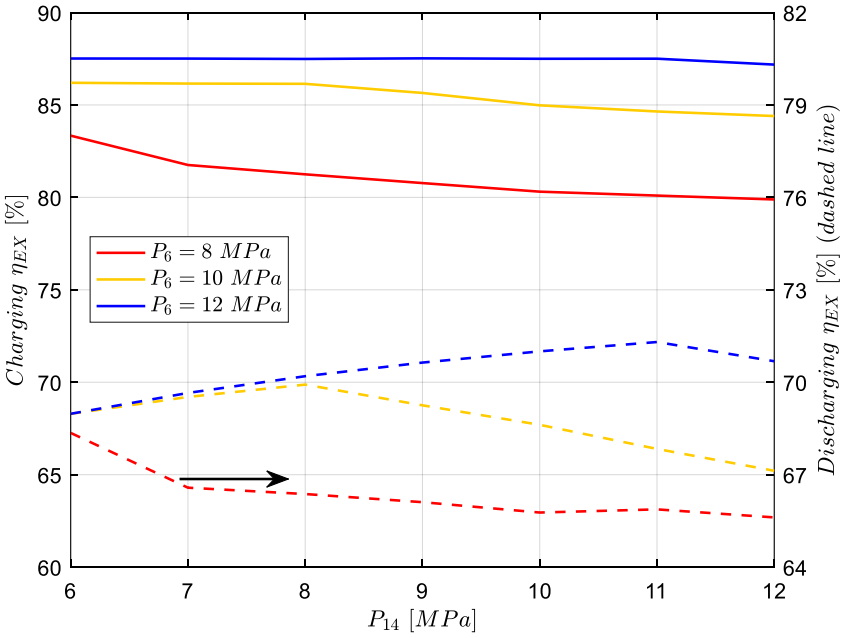

(b)

Figure 7.8 Influence of discharging pressure on the performance of the LAES-LNG system; (a) round trip efficiency and liquid air yield; (b) exergy efficiency of the charging and discharging cycles.

7.3.6 Simulation results of the LAES-LNG-CS system

A large-scale LAES-LNG-CS system with the same power consumption as the LAES-LNG system is simulated in this research, whose operating time is consisted of 8 hours for the charging cycle at off-peak hours and 8 hours for discharging cycle in an entire day. Three different operating times for LNG regasification unit are discussed, including at the off-peak time, at peak time and both. The default values of parameters of LAES-LNG-CE system are given in Table 7.1, where the majority of parameters are the same as that of the LAES-LNG system.

The setting pressure of charging cycle and discharging cycle are 14 MPa and 8 MPa respectively and the optimized performance of LAES-LNG-CS system is shown in Table 7.6, in terms of net work for charging and discharging cycles, mass flow rate of each cycles, exergy efficiencies, roundtrip efficiency and liquid air yield. For comparison purposes, the result of the LAES-LNG are also given in Table 7.6.

From Table 7.6, one can see that for the same quantity of liquid air, the LAES-LNG system gives more net output power during the discharging process due to the extra output power generated by the Brayton cycle. However, compared to the LAES-LNG system, the LAES-LNG-CS system can produce ~5.7% more electric energy during the LNG regasification process by only using ~48% of LNG. Although using different refrigerants in the charging process, the LAES-LNG-CS system and the LAES-LNG system can product same quantity of liquid air with consuming same amount of electric energy. The exergy efficiency of the LAES-LNG-CS discharging cycle is significantly higher than that of the LAES-LNG discharging cycle, which is mainly because that some of the cold energy from liquid air evaporation is also efficiently recovered by the low-grade cold store, compared with the lower thermal efficiency of the Brayton cycle (~50%) in the LAES-LNG system.

Table 7.6 Performance results of the LAES-LNG-CS and the LAES-LNG-CS systems.

Items	LAES-LNG		LAES-LNG-CS		
	Charging	Discharging	Charging	Discharging	LNG cycle
Net power (MW)	13.69	10.00	13.69	8.76	0.50
Air mass flow rate (kg/s)	22.52	20.13	22.52	20.13	-
Exergy efficiency	86.14%	68.16%	85.61%	79.70%	-
LNG mass flow rate (kg/s)	9.78		4.71		
Liquid air yield	0.8940		0.8940		
Round trip efficiency	73.05%		$\eta_{off\text{-}peak}$=66.43%; η_{peak}=67.66%; η_{all}= 70.25%		

The stream data of the LAES-LNG-CS system is listed in Table 7.7 and Table 7.8 respectively for the charging cycle and discharging cycle, and

Table 7.9 for other processed and cycles including the thermal fluid, the cold fluid, the LNG regasification cycle. The temperature-Entropy diagrams (*T*-*S*) for charging and discharging processes are quite similar to those in Figure 7.3 (a) and Figure 7.3 (b) and will not be repeated. The LNG cycle of LAES-LNG-CS system is illustrated in Figure 7.9. The optimal heat exchange diagrams for the cold box are presented in Figure 7.10.

Table 7.7 Stream data for the LAES-LNG system in the charging cycle.

	$\dot{m}$ [kg/s]	T [K]	P [MPa]	H [kJ/kg]	Fluid
1	22.52	293.00	0.10	293.27	Air
2	22.52	493.58	0.52	496.62	Air
3	22.52	303.00	0.51	302.42	Air
4	22.52	510.69	2.67	513.39	Air
5	22.52	303.00	2.64	297.81	Air
6	22.52	513.23	13.72	513.10	Air
7	22.52	303.00	13.58	277.18	Air
8	22.52	93.23	13.45	-90.03	Air
9	22.52	79.80	0.11	-103.59	Air
10	2.39	82.45	0.11	79.60	Air
11	2.39	268.28	0.11	268.37	Air
12	20.13	79.66	0.11	-124.88	Air

Table 7.8 Stream data for the LAES-LNG system in the discharging cycle.

	$\dot{m}$ [kg/s]	T [K]	P [MPa]	H [kJ/kg]	Fluid
13	20.13	79.66	0.11	-124.88	Air
14	20.13	83.13	8.00	-112.91	Air
15	20.13	141.13	7.92	14.50	Air
16	20.13	273.00	7.84	253.07	Air
17	20.13	466.24	7.76	464.35	Air
18	20.13	321.95	1.80	319.17	Air
19	20.13	466.24	1.78	467.68	Air

20	20.13	323.47	0.41	323.34	Air
21	20.13	466.24	0.41	468.57	Air
22	20.13	323.88	0.10	324.37	Air

Table 7.9 Stream data for thermal oil, propane, LNG cycle.

	$\dot{m}$ [kg/s]	T [K]	P [MPa]	H [kJ/kg]	Fluid
H1	43.17	293.00	0.10	422.83	Thermal oil
H2	43.17	489.89	0.10	759.34	Thermal oil
H3	35.67	489.89	0.10	759.34	Thermal oil
H4	35.67	317.74	0.10	457.70	Thermal oil
C1	23.89	88.13	0.10	-191.52	Propane
C2	23.89	143.13	0.10	-84.15	Propane
C3	22.92	146.01	1.00	-77.36	Propane
C4	22.92	253.14	1.00	151.92	Propane
C5	15.09	293.00	1.00	251.26	Propane
C6	15.09	151.13	1.00	-67.10	Propane
C7	8.57	293.00	1.00	251.26	Propane
C8	8.57	151.13	1.00	-67.10	Propane
L1	4.71	0.10	-5.79	-5.79	Methane
L2	4.71	20.00	55.93	55.93	Methane
L3	4.71	20.00	635.20	635.20	Methane
L4	4.71	20.00	728.54	728.54	Methane
L5	4.71	14.09	693.95	595.85	Methane
L6	4.71	14.09	770.74	876.47	Methane

L7	4.71	9.93	735.53	699.21	Methane
L8	4.71	9.93	809.75	904.87	Methane
L9	4.71	7.00	772.70	717.88	Methane

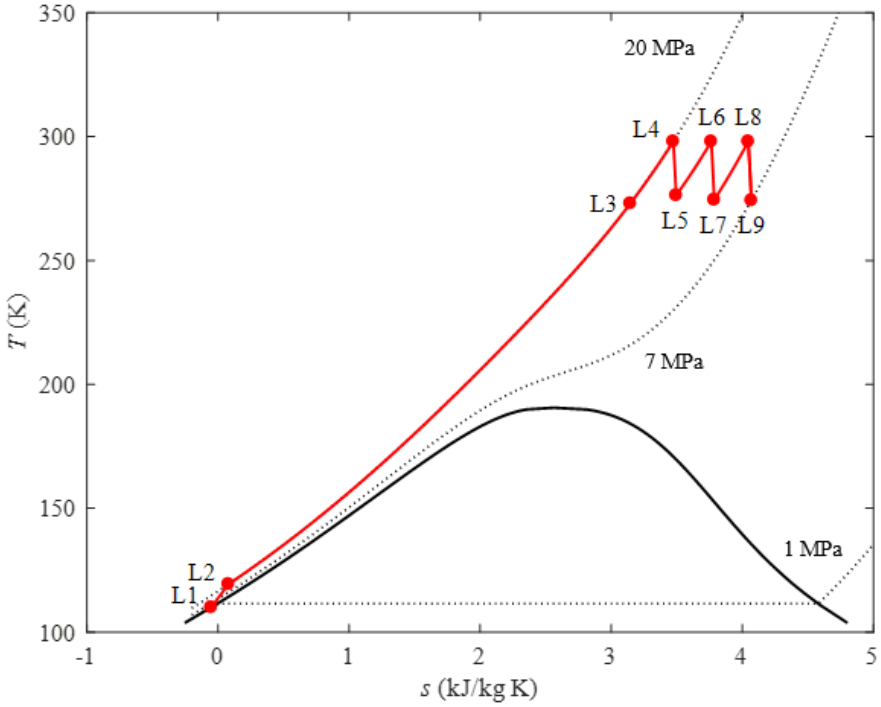

Figure 7.9 *T-S* diagrams for LNG cycle in the LAES-LNG-CS system.

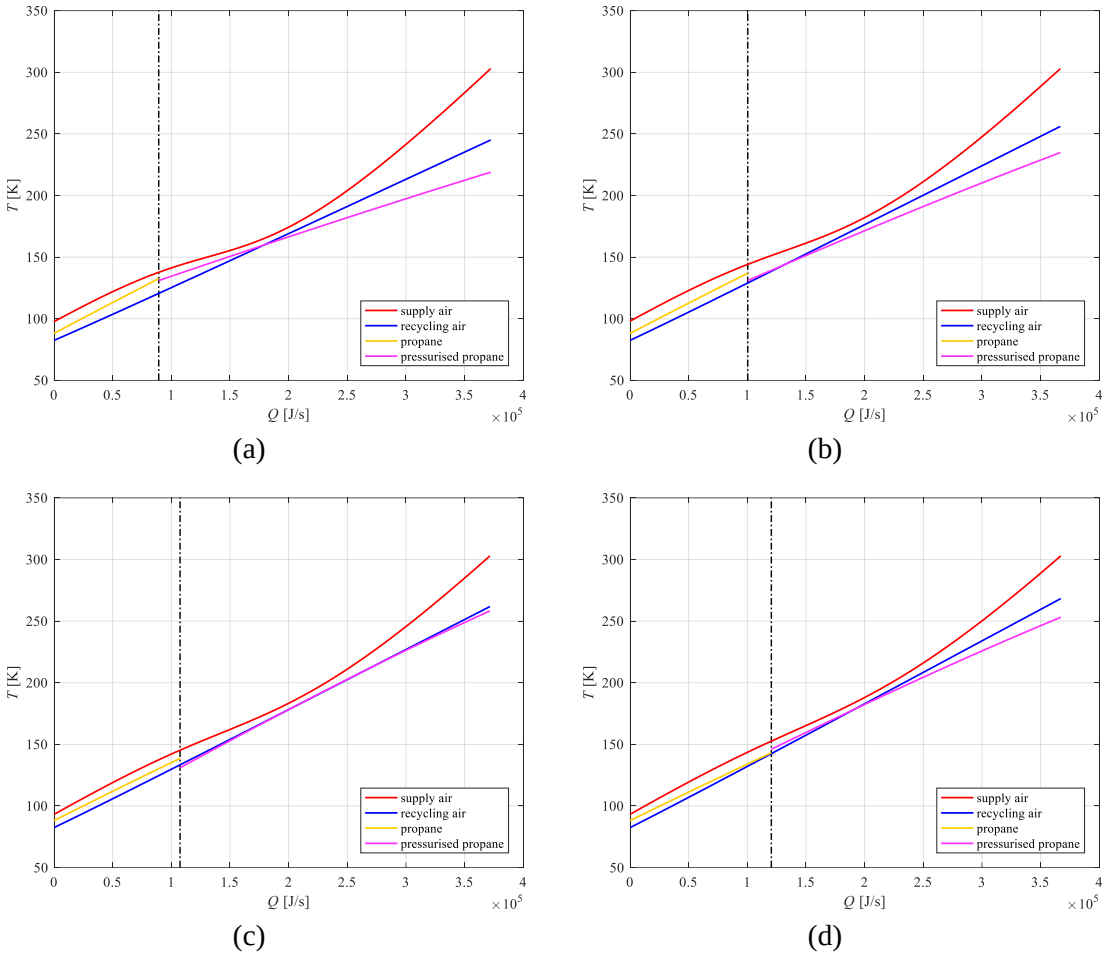

Figure 7.10 Optimal heat exchange diagrams for the cold box at P_{14} =8 MPa; (a) P_6=8 MPa; P_6=10 MPa; (c) P_6=12 MPa; (d) P_6=14 MPa.

7.3.7 Influence of LNG amount on the LAES-LNG-CS performance

Figure 7.11 illustrates how the mass flow rate ratio of the LNG input affects the LAES-LNG system performance, including the liquid air yield, the amount of the cold pressurised propane, the roundtrip efficiencies. Note that the mass flow rate of the LNG cannot directly affect the liquid air yield, but the change in the LNG inlet directly affects the quantity of the cold pressurised propane when cold energy is recovered from LNG evaporation. Such recovered cold is stored and reused in the charging process and hence both the direct and the indirect effects are illustrated in Figure 7.11. The horizontal axis represents the mass flow rate ratio of the LNG to the supplied air through

liquification. An increase in the LNG mass flow increases the amount of the cold pressurised propane until the ratio reaches to ~0.21, beyond which the rate of the increase drops slightly, and the increase shows a linear manner. This is mainly due to the amount of the cold pressurised propane produced from the liquid air evaporation is constant when the ratio over ~0.21, and all the rest comes from the LNG evaporation. Also, an increase in the LNG mass flow increases the liquid air yield first until the maximum of ~0.89, any further increases brings little benefit for liquid air yield can be seen, as shown in Figure 7.11 (a). The three round trip efficiencies show the same trends, as illustrated in Figure 7.11 (b), where an increase in the LNG mass flow increases round trip efficiencies, when the mass flow rate ratio is above ~0.21, there are slight increases in all the three different round trip efficiencies. All the further increases are coming from the LNG turbine generation, evidenced by the increase in the mass flow of cold pressurised propane but no more any changes in the liquid air yield. The all-day round trip efficiency is the highest one among the three. This is because the power generated by LNG turbines not only increases the net output in the discharging process, but decreases the power consumption in the charging process, as illustrated in Eq. 7.9. Compared with the round trip efficiency at off-peak hour and that at peak hour, the power generated by the LNG turbines is better to increase the net output at peak hour than to decrease the power consumption at off-peak hour. It should also be noticed that exaggerated increase in LNG mass flow rate leads to the infinite increase in the round trip efficiencies, and it brings excess cold energy for liquefication. To avoid this, the optimal round trip efficiency here refers to the lowest round trip efficiency when liquid air yield reaches its maximum.

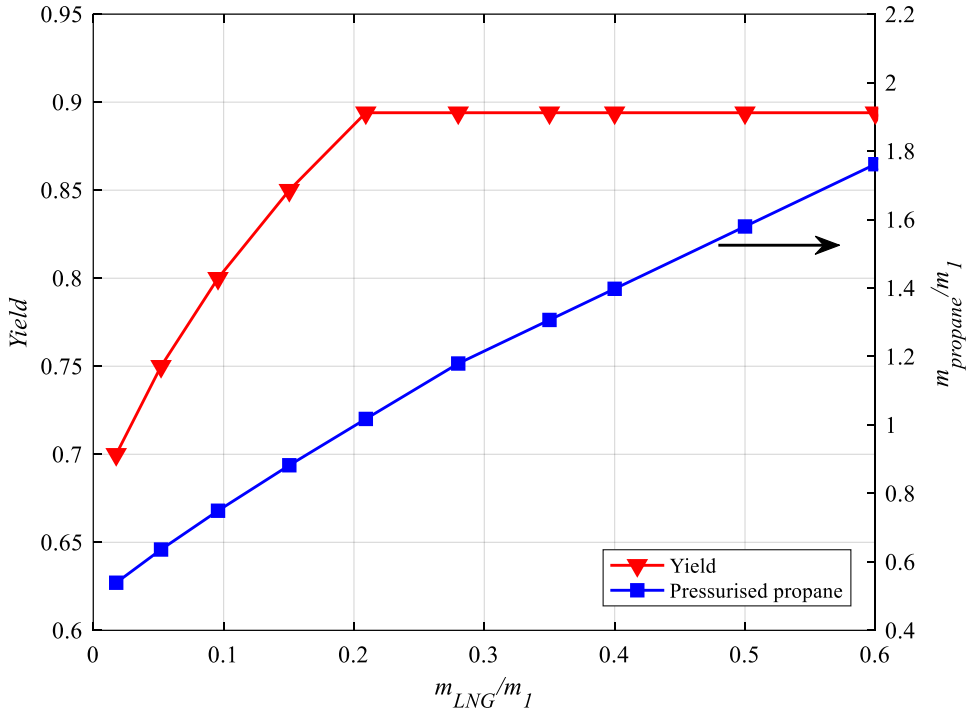

(a)

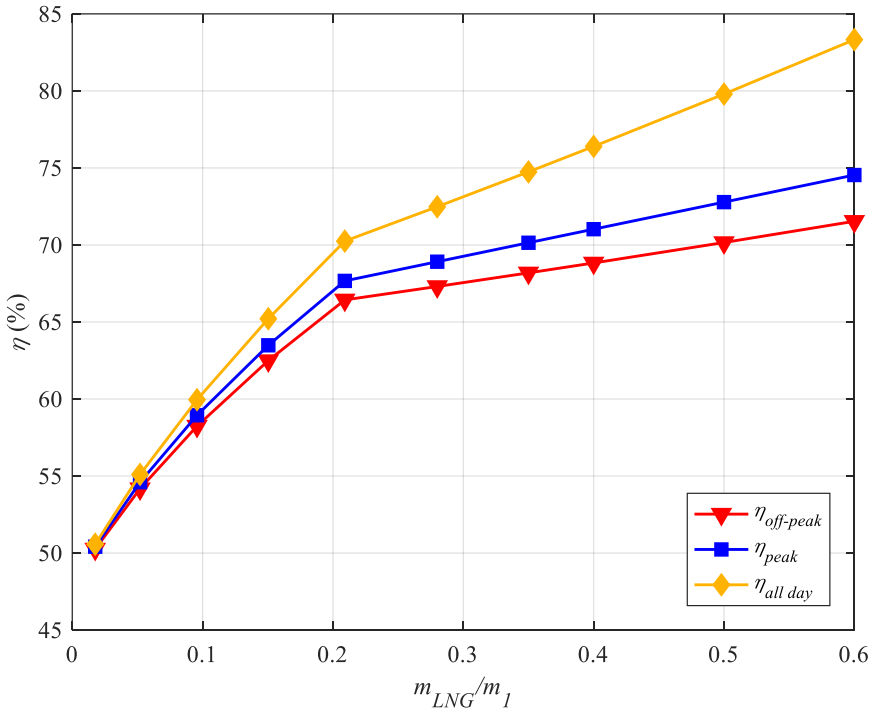

(b)

Figure 7.11 Influence of LNG flowing to the cold box on liquid air yield, amount of pressurised propane, roundtrip efficiency, $P_{charging}$ =14 MPa, $P_{discharging}$ =8 MPa.

7.3.8 Influence of thermal losses of the heat and cold storage

Thermal dissipation to the environment is inevitable during energy storage processes. In the LAES-LNG-CS system, high-grade cold energy is stored in the propane while the low-grade is stored in the pressurise propane (1 MPa). Energy losses lead to the temperature increase of the propane, but the amount of fluids in the cold stores does not change. Figure 7.12 illustrates the effect of energy losses of the fluids on the liquid air yield and off-peak hour round trip efficiency of the LAES-LNG-CS system with a charging pressure of 14 MPa and a discharging pressure of 8 MPa. Note that the performance of the off-peak hour, peak hour and all-day hour round trip efficiencies are similar, here just use off-peak hour for example. One can see from the Figure 7.12 (a) that an increase in the high-grade cold energy leads to a significant decrease in the liquid air yield while the low-grade cold energy loss gives little benefit for the maximum liquid air yield. This is because that the maximum yield is determined by the charging pressure, the amount and the temperature of the high-grade cold (propane). The optimal round trip efficiency presents a significant drop from 66.4% to 65.7% as the high-grade cold loss increase. However, the optimal round trip efficiency increase from 66.4% to 67.6% as the low-grade cold loss as the low-grade cold loss increase from 0 to ~5%. It is mainly due to more LNG is used to provide the cold energy to meet the cold shortage in the air liquefication caused by the energy loss, and hence the power output increases in the LNG regasification cycle. Excellent thermal insulation of the cold stores is therefore more essential to the high-grade cold store than the low-grade one for performance improvement for the LAES-LNG-CS system.

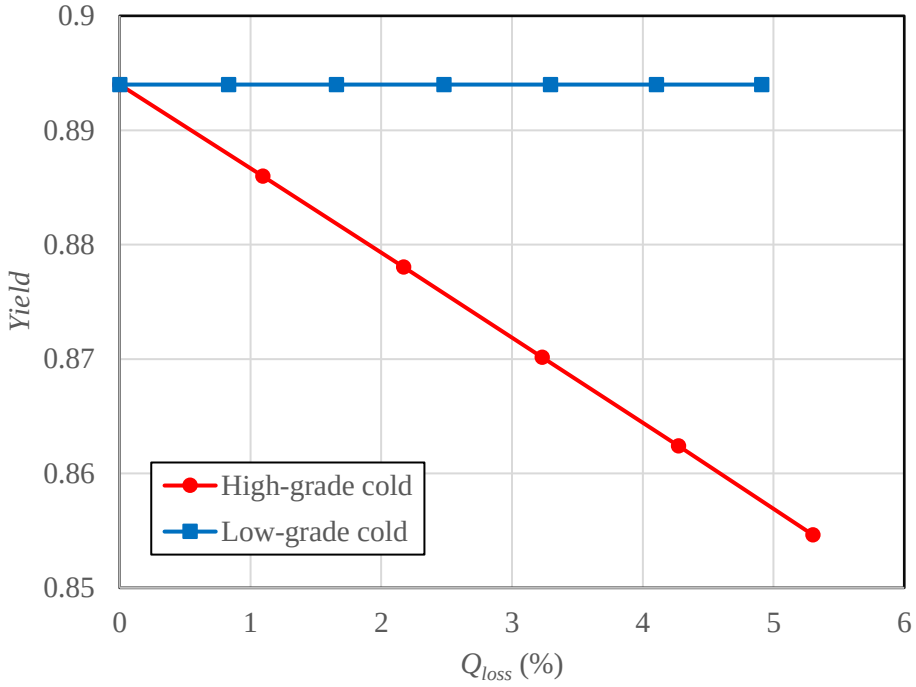

(a)

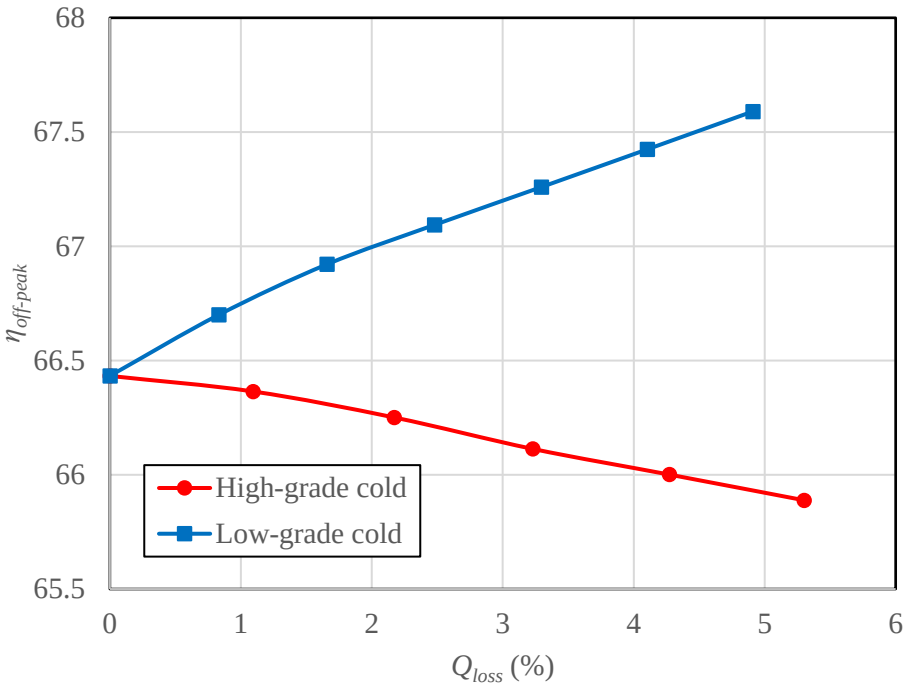

(b)

Figure 7.12 Effect of energy losses of the high-grade cold fluid (propane) and low-grade cold fluid (pressurised propane) in energy stores on (a) the liquid air yield and (b) off-peak hour round trip efficiency, $P_{charging}$ =14 MPa, $P_{discharging}$ =8 MPa.

7.4 Conclusions of Chapter 7

This chapter investigates into the use of external cold sources, such as LNG, through integration to enhance the LAES efficiency. Two integrated LAES systems, LAES-LNG and LAES-LNG-CS are proposed. The main conclusions are as follow:

- The use of the cold from LNG regasification could give a higher round trip efficiency of the LAES system, ~75-85%. This is ~15-35% higher than the current standalone LAES system. One of the reasons for the enhancement is due to a higher liquid air yield of up to 0.87.

- The changes in the charging pressure does not give a significantly effect on the liquid air yield due to the use of high-grade cold energy from the LNG regasification.

- The increase in the charging pressure decreases in the round trip efficiency, whereas the increase in the discharging pressure increases the output power of turbines and hence increases the round trip efficiency.

- The LAES-LNG-CS system is a more flexible and feasible system than the LAES-LNG system due to a cold store to store LNG cold energy, meeting the instability of LNG regasification. The LAES-LNG-CS system can produce ~5.7% more electric energy during the LNG regasification process by only using ~48% of LNG. The exergy efficiency of the LAES-LNG-CS discharging cycle is significantly higher (~20%) than that of the LAES-LNG discharging cycle.

- The increase in mass flow rate of LNG can indirectly increase the round trip efficiency of the LAES-LNG-CS system, but it is unavailable to continually increase the liquid yield by increase the LNG inlet.

- The effect of the energy losses in high-grade cold store is much more crisis than that in low-grade cold store in the LAES-LNG-CS system. Therefore, good thermal insulation of the stores is needed, particularly for the high-grade cold store, to ensure a good system performance.

Chapter 8 Conclusions and Suggestion for Further Research

This chapter first summarizes the main conclusions of this work. Recommendations are then given for the future work based on this study.

8.1 Summary of the main conclusions

This Ph.D. work focuses on four aspects associated with the Liquid Air Energy Storage (LAES) technology:

(1) The development of a standalone LAES model for understanding the optimal operation conditions of future implementation of the LAES plants.

(2) The operation of the pilot plant to obtain actual parameters for comparison with modelling.

(3) The in-depth investigation into the thermal energy transfer and conversion in the LAES system for guiding the LAES performance.

(4) The integration of the LAES with other cycles/processes including Organic Rankine Cycle (ORC), Vapor Compression Refrigeration Cycle (VCRC), Absorption Refrigeration Cycle (ARC) and LNG regasification for further enhancing LAES performance.

The main conclusions are as follow:

(1) The experimentally measured output power of the LAES pilot plant correlates well with the mass flow rate, for a given set of pressure and temperature before turbine. The inter-stage reheating temperature significantly affects the output power: an increase of 1℃ contributes to an increase of ~1 kW in output power. The LAES pilot plant gives an excellent dynamic response, which could bring ~70% of maximum power output in 2 minutes.

(2) The modelling results show that energy losses of the cold and hot energy stores significantly affect the performance of a standalone LAES. The extent of performance decrease caused by the cold energy losses is ~7 times that caused by the hot energy losses under given operating conditions. The high-grade cold energy recovered from the evaporation of liquid air in the discharging process is insufficient to achieve the maximum liquid air yield in the charging process, which provides an opportunity for the use external cold sources, such as waste cold from the regasification of liquified natural gas. The hot energy generated during air compression in the charging process is ~20-45% in excess which cannot be efficiently used in the discharging process. The use of such excess heat provides more opportunities to increase the round trip efficiency of the LAES. Thus, LAES is suitable to integrate with other processes/cycles to improve the performance.

(3) The round trip efficiency of the LAES-ORC-VCRC could be higher than 60%, which is 9-12% higher than that of the LAES system. The exergy efficiencies of the discharging cycle and the integrated discharging cycle of the LAES-ORC-VCRC are ~9.6% and ~6.5% higher on average than that of the discharging cycle of the LAES, respectively; The LAES-ORC-VCRC system has an excellent economic performance with a payback period of 2.7 years and a savings to investment ratio of 3.08 under the given project life-span of 15 years. Although a higher discount rate or inflation rate decreases both the net present value and the savings to investment ratio, the discount rate has a much more significant effect on the economic benefit than the inflation rate.

(4) Using the excess heat to drive an (ORC) for power generation is a possible solution. The integrated LAES-ORC and LAES-ORC-ARC systems are more efficient than the standalone LAES system with highest improvements of ~17% and ~13% respectively for the round trip efficiency. The LAES-ORC shows a better performance than the LAES-

ORC-ARC and has a simpler configuration. The LAES-ORC system is more efficient than the LAES-ORC-ARC system.

(5) The use of the cold from LNG regasification could give a higher round trip efficiency of the LAES system, ~75-85%. This is ~15-35% higher than the current standalone LAES system due to a higher liquid air yield. The changes in the charging pressure does not give a significantly effect on the liquid air yield due to the use of high-grade cold energy from the LNG regasification. The increase in the charging pressure decreases in the round trip efficiency, whereas the increase in the discharging pressure increases the output power of turbines and hence increases the round trip efficiency.

(6) The LAES-LNG-CS system is a more flexible and feasible system than the LAES-LNG system due to a cold store to store LNG cold energy, meeting the instability of LNG regasification. The LAES-LNG-CS system can give an improved system performance with an efficiency of at least ~67%, by using less LNG than the LAES-LNG system. There could be a significant improvement in the round trip efficiency if more amount of LNG can be used to drive LNG turbines. Although the LNG input can indirectly increase the round trip efficiency of the LAES-LNG-CS system, it is unavailable to continually increase the liquid yield.

8.2 Recommendations for the future works

Although interesting and very promising results have been obtained in this Ph.D. study, there are still numerous aspects that need further investigation. Some of the major ones are summarised in the following:

(1) The work reported in this dissertation is restricted to steady state operation of the energy storage systems. The electricity demand and supply various drastically, depending on different time of the day, week, month and season, or different users. The availability of

renewable energy is also intermittent and unpredictable. Therefore, a possible approach to improve the performance of the LAES system is dynamic operation.

(2) To address the energy losses which remarkably weaken the performance of the LAES especially to cold energy, the breakthrough in the low-temperature energy storage material and the novel TES components with excellent thermal insulation are predicted and recommended.

(3) The LAES integration system is in the initial stages of development and there are still many areas can be combined together, such as off-shore wind power station. Liquid air can also regard as the ‘fuel’ for small-scale devices if mechanical restrictions disappear.

Appendix APublications

Journal paper:

1) Peng X, She X, Cong L, Zhang T, Li C, Li Y, et al. Thermodynamic study on the effect of cold and heat recovery on performance of liquid air energy storage. Applied Energy 2018;221:86–99.

2) Peng X, She X, Li Y, Ding Y. Thermodynamic analysis of Liquid Air Energy Storage integrated with a serial system of Organic Rankine and Absorption Refrigeration Cycles driven by compression heat. Energy Procedia, vol. 142, 2017, p. 3440–6.

3) She X, Peng X, Nie B, Leng G, Zhang X, Weng L, et al. Enhancement of round trip efficiency of liquid air energy storage through effective utilization of heat of compression. Applied Energy 2017:0–1.

4) She X, Li Y, Peng X, Ding Y. Theoretical analysis on performance enhancement of stand-alone liquid air energy storage from perspective of energy storage and heat transfer. Energy Procedia, vol. 142, 2017, p. 3498–504.

5) Peng X, She X, Nie B, Li C, Li Y, Ding Y. Liquid Air Energy Storage with LNG cold recovery for air liquefaction improvement. Energy Procedia. (accepted)

Patent:

1) Yulong Ding, Xiaohui She, ***Xiaodong Peng***, Binjian Nie, Lin Cong, Zhu Jiang, et al. An integrated liquid air energy storage and battery system for black start and frequency regulation of power grids, China Patent No. 201710491478.2, filed Feb 2018.

2) Xiaohui She, Yulong Ding, ***Xiaodong Peng***, Likui Weng, Binjian Nie, Jiuliang Chen, Lin Cong, Guanghui Leng, et al. A device and method for enhancing round trip efficiency of liquid air energy storage system, China Patent No. 201710491411.9, filed Feb 2018.

3) Yulong Ding, Xiaohui She, Tongtong Zhang, ***Xiaodong Peng***, Li Wang, Lige Tong. A cold-heat-power trigeneration system based on liquid air energy storage. (Submitted)

4) Yulong Ding, Xiaohui She, Yuanye Meng, ***Xiaodong Peng***. An advanced off-shore renewable energy transportation method based on liquid air energy storage. (Submitted)

Bibliography

[1] Kadiri M, Ahmadian R, Bockelmann-Evans B, Rauen W, Falconer R. A review of the potential water quality impacts of tidal renewable energy systems. Renew Sustain Energy Rev 2012;16:329–41. doi:10.1016/J.RSER.2011.07.160.

[2] Manzano-Agugliaro F, Alcayde A, Montoya FG, Zapata-Sierra A, Gil C. Scientific production of renewable energies worldwide: An overview. Renew Sustain Energy Rev 2013;18:134–43. doi:10.1016/J.RSER.2012.10.020.

[3] OCDE & IEA. Market Report Series: Renewables 2017, analysis and forecats to 2022. J Qual Particip 2017;104:20142–20142. doi:10.1073?pnas.0603395103.

[4] Buckley T, Nicholas S. China's global renewable energy expansion. 2017.

[5] International Renewable Energy Agency. Renewable Energy Prospects: United States of America. 2015.

[6] International Renewable Energy Agency (IRENA). Renewable Energy Prospects for Poland. 2015.

[7] International Energy Agency (IEA). World Energy Outlook 2017. 2017.

[8] Strbac G, Aunedi M, Pudjianto D, Djapic P, Teng F, Sturt A, et al. Strategic Assessment of the Role and Value of Energy Storage Systems in the UK Low Carbon Energy Future 2012.

[9] Hendry S. Renewable Energy Technologies. Energy 1994;3:220–272.

[10] Milborrow D. IMPACTS OF WIND ON ELECTRICITY SYSTEMS WITH PARTICULAR REFERENCE TO ALBERTA. 2004.

[11] Weisser D, Garcia RS. Instantaneous wind energy penetration in isolated electricity grids:

Concepts and review. Renew Energy 2005;30:1299–308. doi:10.1016/j.renene.2004.10.002.

[12] Li Y. Cryogen Based Energy Storage : Process Modelling and Optimisation 2011.

[13] Data explorer | National Grid UK n.d. https://www.nationalgrid.com/uk/electricity/market-operations-and-data/data-explorer (accessed March 7, 2018).

[14] Chen H, Cong TN, Yang W, Tan C, Li Y, Ding Y. Progress in electrical energy storage system: A critical review. Prog Nat Sci 2009;19:291–312. doi:10.1016/j.pnsc.2008.07.014.

[15] Hamidi V, Li F, Robinson F. Demand response in the UK's domestic sector. Electr Power Syst Res 2009;79:1722–6. doi:10.1016/j.epsr.2009.07.013.

[16] Time-of-Use Rates for Residential Customers 2017:2016–9.

[17] Rodrigues EMG, Godina R, Santos SF, Bizuayehu AW, Contreras J, Catalão JPS. Energy storage systems supporting increased penetration of renewables in islanded systems. Energy 2014;75:265–80. doi:10.1016/J.ENERGY.2014.07.072.

[18] Ge Z, Li Y, Li D, Sun Z, Jin Y, Liu C, et al. Thermal energy storage: Challenges and the role of particle technology. Particuology 2014;15:2–8. doi:10.1016/J.PARTIC.2014.03.003.

[19] Strahan D. Liquid Air in the energy and transport systems. 2013.

[20] Chen H, Ding Y, Peters T, Berger F. Energy storage and generation, 2009.

[21] Ding Y, Tong L, Zhang P, Li Y, Radcliffe J, Wang L. Chapter 9 – Liquid Air Energy Storage. Elsevier Inc.; 2016. doi:10.1016/B978-0-12-803440-8.00009-9.

[22] Smith EM. Storage of Electrical Energy Using Supercritical Liquid Air. Proc Inst Mech

Eng 1977;191:289–98. doi:10.1243/PIME_PROC_1977_191_035_02.

[23] Hasegawa K, Kishimoto K. Development of Generator of Liquid Air Storage Energy System. MhiCoJp n.d.

[24] Tanaka T, Ishikawa A, Aoyama K, Kishimoto K, Yoshida Y, Toda K, et al. Gas Turbine Inlet Air Cooling System With Liquid Air. Vol. 4 Heat Transf. Electr. Power; Ind. Cogener., ASME; 1998, p. V004T10A020. doi:10.1115/98-GT-449.

[25] Chino K, Araki H. Evaluation of energy storage method using liquid air. Heat Transf - Asian Res 2000;29:347–57. doi:10.1002/1523-1496(200007)29:5<347::AID-HTJ1>3.0.CO;2-A.

[26] Araki H, Nakabaru M, Chino K. Simulation of heat transfer in the cool storage unit of a liquid-air energy storage system. Heat Transf - Asian Res 2002;31:284–96. doi:10.1002/htj.10035.

[27] Cold heat reused air liquefaction/vaporization and storage gas turbine electric power system 2002.

[28] Vandor D. System and method for liquid air production, power storage and power release 2011.

[29] Bash E. Refrigeration Systems and Applications. vol. 1. 2015. doi:10.1017/CBO9781107415324.004.

[30] Cammarata G, Fichera A, Guglielmino D. Optimization of a liquefaction plant using genetic algorithms. Appl Energy 2001;68:19–29. doi:10.1016/S0306-2619(00)00041-6.

[31] Kanoglu M, Dincer I, Rosen MA. Performance analysis of gas liquefaction cycles. Int J Energy Res 2008;32:35–43. doi:10.1002/er.1333.

[32] de Waele ATAM. Basics of Joule–Thomson Liquefaction and JT Cooling. J Low Temp Phys 2017;186:385–403. doi:10.1007/s10909-016-1733-3.

[33] Maytal B. Cool-down periods similarity for a fast Joule - Thomson cryocooler. Cryogenics (Guildf) 1992;32:653–8. doi:10.1016/0011-2275(92)90298-O.

[34] Maytal BZ. Maximizing production rates of the Linde-Hampson machine. Cryogenics (Guildf) 2006;46:49–54. doi:10.1016/j.cryogenics.2005.11.004.

[35] Syed MT, Sherif SA, Veziroglu TN, Sheffield JW. Second law analysis of hydrogen liquefiers operating on the modified Collins cycle. Int J Energy Res 2001;25:961–78. doi:10.1002/er.733.

[36] Barron R. Cryogenic Systems. 1966.

[37] Jensen JB, Skogestad S. Optimal operation of a mixed fluid cascade LNG plant. Comput Aided Chem Eng 2006;21:1569–74. doi:10.1016/S1570-7946(06)80271-3.

[38] Barclay MA, Gongaware DF, Dalton K, Skrzypkowski MP. Thermodynamic Cycle Selection for Distributed Natural Gas Liquefaction. AIP Conf. Proc., vol. 710, AIP; 2004, p. 75–82. doi:10.1063/1.1774669.

[39] Engineering NK-C and P, 2004 undefined. Analysis of modern natural gas liquefaction technologies. Springer n.d.

[40] Kanoğlu M. Exergy analysis of multistage cascade refrigeration cycle used for natural gas liquefaction. Int J Energy Res 2002;26:763–74. doi:10.1002/er.814.

[41] Process for nitrogen liquefaction 1999.

[42] Chang H-M, Chung MJ, Lee S, Choe KH. An efficient multi-stage Brayton–JT cycle for liquefaction of natural gas. Cryogenics (Guildf) 2011;51:278–86.

doi:10.1016/J.CRYOGENICS.2010.10.006.

[43] Aminyavari M, Najafi B, Shirazi A, Rinaldi F. Exergetic, economic and environmental (3E) analyses, and multi-objective optimization of a CO2/NH3 cascade refrigeration system. Appl Therm Eng 2014;65:42–50. doi:10.1016/J.APPLTHERMALENG.2013.12.075.

[44] Krasae-in S, Stang JH, Neksa P. Development of large-scale hydrogen liquefaction processes from 1898 to 2009. Int J Hydrogen Energy 2010;35:4524–33. doi:10.1016/J.IJHYDENE.2010.02.109.

[45] Valenti G, Macchi E. Proposal of an innovative, high-efficiency, large-scale hydrogen liquefier. Int J Hydrogen Energy 2008;33:3116–21. doi:10.1016/J.IJHYDENE.2008.03.044.

[46] Finn AJ, Johnson GL TT. Development in natural gas liquefaction. Hydrocarb Process 1999;78.

[47] Lizarte R, Palacios-Lorenzo ME, Marcos JD. Parametric study of a novel organic Rankine cycle combined with a cascade refrigeration cycle (ORC-CRS) using natural refrigerants. Appl Therm Eng 2017;127:378–89. doi:10.1016/J.APPLTHERMALENG.2017.08.063.

[48] Jiang L, Lu H, Wang R, Wang L, Gong L, Lu Y, et al. Investigation on an innovative cascading cycle for power and refrigeration cogeneration. Energy Convers Manag 2017;145:20–9. doi:10.1016/J.ENCONMAN.2017.04.086.

[49] Lee GC, Smith R, Zhu XX. Optimal synthesis of mixed-refrigerant systems for low-temperature processes. Ind Eng Chem Res 2002;41:5016–28. doi:10.1021/ie020057p.

[50] Cao L, Liu J, Xu X. Robustness analysis of the mixed refrigerant composition employed in the single mixed refrigerant (SMR) liquefied natural gas (LNG) process. Appl Therm

Eng 2016;93:1155–63. doi:10.1016/J.APPLTHERMALENG.2015.10.072.

[51] Bosma P, Nagelvoort RK. Liquefaction Technology; Developments through History. Proc. 1st Annu. Gas Process. Symp., Elsevier; 2009, p. 19–31. doi:10.1016/B978-0-444-53292-3.50006-7.

[52] Yoon J, Lee H, Oh S, Lee S, Science KC-WA of, 2009 undefined. Characteristics of cascade and C3MR cycle on natural gas liquefaction process. WasetOrg n.d.

[53] Li QY, Ju YL. Design and analysis of liquefaction process for offshore associated gas resources. Appl Therm Eng 2010;30:2518–25. doi:10.1016/J.APPLTHERMALENG.2010.07.001.

[54] Mortazavi A, Alabdulkarem A, Hwang Y, Radermacher R. Novel combined cycle configurations for propane pre-cooled mixed refrigerant (APCI) natural gas liquefaction cycle. Appl Energy 2014;117:76–86. doi:10.1016/J.APENERGY.2013.11.056.

[55] Hwang J-H, Roh M-I, Lee K-Y. Determination of the optimal operating conditions of the dual mixed refrigerant cycle for the LNG FPSO topside liquefaction process. Comput Chem Eng 2013;49:25–36. doi:10.1016/J.COMPCHEMENG.2012.09.008.

[56] Tan H, Shan S, Nie Y, Zhao Q. A new boil-off gas re-liquefaction system for LNG carriers based on dual mixed refrigerant cycle. Cryogenics (Guildf) 2018;92:84–92. doi:10.1016/J.CRYOGENICS.2018.04.009.

[57] Khan MS, Karimi IA, Lee M. Evolution and optimization of the dual mixed refrigerant process of natural gas liquefaction. Appl Therm Eng 2016;96:320–9. doi:10.1016/j.applthermaleng.2015.11.092.

[58] Nibbelke R, Kauffman S, Pek B. Double mixed refrigerant LNG process provides viable alternative for tropical conditions. Oil Gas J 2002.

[59] Bukowski J, Liu YN, Boccella SJ, Kowalski L. Innovations in natural gas liquefaction technology. Int. Gas Union Res. Conf. 2011, 2011.

[60] Barclay M, Shukri T. Enhanced single mixed refrigerant process for stranded gas liquefaction, n.d., p. 1–10.

[61] IGU IGU. World LNG Report. vol. 53. 2017. doi:10.1017/CBO9781107415324.004.

[62] Miller J, Luyben WL, Blouin S. Economic incentive for intermittent operation of air separation plants with variable power costs. Ind Eng Chem Res 2008;47:1132–9. doi:10.1021/ie070593n.

[63] Timmerhaus KD, Flynn TM. Cryogenic Process Engineering. Boston, MA: Springer US; 1989. doi:10.1007/978-1-4684-8756-5.

[64] Chang H-M, Chung MJ, Lee S, Choe KH. An efficient multi-stage Brayton–JT cycle for liquefaction of natural gas. Cryogenics (Guildf) 2011;51:278–86. doi:10.1016/J.CRYOGENICS.2010.10.006.

[65] LNG production using dual independent expander refrigeration cycles 2001.

[66] Bracha M, Lorenz G, Patzelt A, Wanner M. Large-scale hydrogen liquefaction in Germany. Int J Hydrogen Energy 1994;19:53–9. doi:10.1016/0360-3199(94)90177-5.

[67] Nandi TK, Sarangi S. Performance and optimization of hydrogen liquefaction cycles. Int J Hydrogen Energy 1993;18:131–9. doi:10.1016/0360-3199(93)90199-K.

[68] Kanoglu M, Yilmaz C, Abusoglu A. Geothermal energy use in absorption precooling for Claude hydrogen liquefaction cycle. Int J Hydrogen Energy 2016;41:11185–200. doi:10.1016/J.IJHYDENE.2016.04.068.

[69] Thomas RJ, Ghosh P, Chowdhury K. Exergy analysis of helium liquefaction systems

based on modified Claude cycle with two-expanders. Cryogenics (Guildf) 2011;51:287–94. doi:10.1016/J.CRYOGENICS.2010.12.006.

[70] Quack H. Conceptual design of a high efficiency large capacity hydrogen liquefier. AIP Conf. Proc., vol. 613, AIP; 2002, p. 255–63. doi:10.1063/1.1472029.

[71] Li Y, Wang X, Ding Y. An optimal design methodology for large-scale gas liquefaction. Appl Energy 2012;99:484–90. doi:10.1016/J.APENERGY.2012.04.040.

[72] Chang H-M, Lim HS, Choe KH. Thermodynamic design of natural gas liquefaction cycles for offshore application. Cryogenics (Guildf) 2014;63:114–21. doi:10.1016/J.CRYOGENICS.2014.03.007.

[73] Gadhiraju V. Cryogenic Mixed Refrigerant Processes. New York, NY: Springer New York; 2008. doi:10.1007/978-0-387-78514-1.

[74] Abstracts MS-F and E, 2002 undefined. Second law analysis of hydrogen liquefiers operating on the modified Collins cycle. Elsevier n.d.

[75] Yu X, Yuan G, Su S, Jiang Y, Chen G. Theoretical study on the ideal open cycle of the liquid nitrogen engine. J Zhejiang Univ A n.d.;3:258–62. doi:10.1007/bf03396449.

[76] Knowlen C, Mattick A, Bruckner A, Hertzberg A. High efficiency energy conversion systems for liquid nitrogen automobiles 1998.

[77] Knowlen C, Hertzberg A, Mattick A. Automotive propulsion using liquid nitrogen. 30th Jt. Propuls. Conf. Exhib., Reston, Virigina: American Institute of Aeronautics and Astronautics; 1994, p. AIAA# 94-3349. doi:10.2514/6.1994-3349.

[78] Plummer MC, Koehler CP, Flanders DR, Reidy RF, Ordonez CA. Cryogenic Heat Engine Experiment. Adv. Cryog. Eng., vol. 64, Boston, MA: Springer US; 1998, p. 1245–52. doi:10.1007/978-1-4757-9047-4_155.

[79] Knowlen C, Williams J, Mattick AT, Deparis H, Hertzberg A. Quasi-Isothermal Expansion Engines for Liquid Nitrogen Automotive Propulsion. SAE Electr. Veh. Altern. Powerplants, Energy Manag. Batter. Technol. - SP-1284, 1997, p. SAE Technical Paper # 972649. doi:10.4271/972649.

[80] Ordonez CA, Plummer MC. Cold thermal storage and cryogenic heat engines for energy storage applications. Energy Sources 1997;19:389–96. doi:10.1080/00908319708908858.

[81] Kim H. Review on Economical Efficiency of Lng Cold Energy Use in South Korea. 23rd World Gas Conf., vol. 5, 2006, p. 2870–85.

[82] BAI F, ZHANG Z. Integration of Low-level Waste Heat Recovery and Liquefied Nature Gas Cold Energy Utilization. Chinese J Chem Eng 2008;16:95–9. doi:10.1016/S1004-9541(08)60044-0.

[83] Qiang W, Yanzhong L, Jiang W. Analysis of power cycle based on cold energy of liquefied natural gas and low-grade heat source. Appl Therm Eng 2004;24:539–48. doi:10.1016/J.APPLTHERMALENG.2003.09.010.

[84] Szargut J, Szczygiel I. Utilization of the cryogenic exergy of liquid natural gas (LNG) for the production of electricity. Energy 2009;34:827–37. doi:10.1016/J.ENERGY.2009.02.015.

[85] Bisio G, Tagliafico L. On the recovery of LNG physical exergy. Collect Tech Pap 35th Intersoc Energy Convers Eng Conf Exhib 2000;1:309–17. doi:10.1109/IECEC.2000.870703.

[86] Bisio G, Tagliafico L. On the recovery of LNG physical exergy by means of a simple cycle or a complex system. Exergy, An Int J 2002;2:34–50. doi:10.1016/S1164-0235(01)00037-1.

[87] Kim D, Giametta REH, Gundersen T. Optimal Use of Liquefied Natural Gas (LNG) Cold Energy in Air Separation Units. Ind Eng Chem Res 2018:acs.iecr.7b04282. doi:10.1021/acs.iecr.7b04282.

[88] Deng S, Jin H, Cai R, Lin R. Novel cogeneration power system with liquefied natural gas (LNG) cryogenic exergy utilization. Energy 2004;29:497–512. doi:10.1016/J.ENERGY.2003.11.001.

[89] Zhang N, Lior N. A novel near-zero CO2 emission thermal cycle with LNG cryogenic exergy utilization. Energy 2006;31:1666–79. doi:10.1016/J.ENERGY.2005.05.006.

[90] Wei D, Lu X, Lu Z, Gu J. Performance analysis and optimization of organic Rankine cycle (ORC) for waste heat recovery. Energy Convers Manag 2007;48:1113–9. doi:10.1016/J.ENCONMAN.2006.10.020.

[91] Liu B-T, Chien K-H, Wang C-C. Effect of working fluids on organic Rankine cycle for waste heat recovery. Energy 2004;29:1207–17. doi:10.1016/J.ENERGY.2004.01.004.

[92] Drescher U, Brüggemann D. Fluid selection for the Organic Rankine Cycle (ORC) in biomass power and heat plants. Appl Therm Eng 2007;27:223–8. doi:10.1016/J.APPLTHERMALENG.2006.04.024.

[93] Madhawa Hettiarachchi HD, Golubovic M, Worek WM, Ikegami Y. Optimum design criteria for an Organic Rankine cycle using low-temperature geothermal heat sources. Energy 2007;32:1698–706. doi:10.1016/J.ENERGY.2007.01.005.

[94] Chintala V, Kumar S, Pandey JK. A technical review on waste heat recovery from compression ignition engines using organic Rankine cycle. Renew Sustain Energy Rev 2018;81:493–509. doi:10.1016/j.rser.2017.08.016.

[95] Agazzani A, Massardo AF, Korakianitis T. An Assessment of the Performance of Closed

Cycles With and Without Heat Rejection at Cryogenic Temperatures. J Eng Gas Turbines Power 1999;121:458. doi:10.1115/1.2818495.

[96] Na Z, Weiwei L, - CR, 2003 U. Thermodynamic Analysis of Closed Brayton Cycle Working on LNG Cryogenic Exergy and Waste Heat Utilization. CHINESE Soc … n.d.

[97] Romero Gómez M, Ferreiro Garcia R, Romero Gómez J, Carbia Carril J. Review of thermal cycles exploiting the exergy of liquefied natural gas in the regasification process. Renew Sustain Energy Rev 2014;38:781–95. doi:10.1016/J.RSER.2014.07.029.

[98] Kaneko K, Ohtani K, Tsujikawa Y, Fujii S. Utilization of the cryogenic exergy of LNG by a mirror gas-turbine. Appl Energy 2004;79:355–69. doi:10.1016/j.apenergy.2004.02.007.

[99] Otsuka T. Evolution of an LNG terminal: Senboku terminal of Osaka GAS. 23rd World Gas Conf., vol. 3, 2006, p. 1516–28.

[100] Oliveti G, Arcuri N, Bruno R, De Simone M. A rational thermodynamic use of liquefied natural gas in a waste incinerator plant. Appl Therm Eng 2012;35:134–44. doi:10.1016/J.APPLTHERMALENG.2011.10.015.

[101] Meng X, Bai F, Yang F, Bao Z, Zhang Z. Study of integrated metal hydrides heat pump and cascade utilization of liquefied natural gas cold energy recovery system. Int J Hydrogen Energy 2010;35:7236–45. doi:10.1016/J.IJHYDENE.2010.02.008.

[102] Shi X, Che D. A combined power cycle utilizing low-temperature waste heat and LNG cold energy. Energy Convers Manag 2009;50:567–75. doi:10.1016/J.ENCONMAN.2008.10.015.

[103] Dispenza C, Dispenza G, La Rocca V, Panno G. Exergy recovery during LNG regasification: Electric energy production – Part one. Appl Therm Eng 2009;29:380–7. doi:10.1016/J.APPLTHERMALENG.2008.03.036.

[104] Dispenza C, Dispenza G, Rocca V La, Panno G. Exergy recovery during LNG regasification: Electric energy production – Part two. Appl Therm Eng 2009;29:388–99. doi:10.1016/J.APPLTHERMALENG.2008.03.035.

[105] BAI F, ZHANG Z. Integration of Low-level Waste Heat Recovery and Liquefied Nature Gas Cold Energy Utilization** Supported by the Science and Technology Foundation of Shaanxi Province (No.2002K08-G9). Chinese J Chem Eng 2008;16:95–9. doi:10.1016/S1004-9541(08)60044-0.

[106] Hisazumi Y, Yamasaki Y, Sugiyama S. Proposal for a high efficiency LNG power-generation system utilizing waste heat from the combined cycle. Appl Energy 1998;60:169–82. doi:10.1016/S0306-2619(98)00034-8.

[107] Rao W-J, Zhao L-J, Liu C, Zhang M-G. A combined cycle utilizing LNG and low-temperature solar energy. Appl Therm Eng 2013;60:51–60. doi:10.1016/J.APPLTHERMALENG.2013.06.043.

[108] Morosuk T, Tsatsaronis G. Comparative evaluation of LNG – based cogeneration systems using advanced exergetic analysis. Energy 2011;36:3771–8. doi:10.1016/J.ENERGY.2010.07.035.

[109] Strahan D. Liquid Air in the energy and transport systems. 2013.

[110] Morgan R, Nelmes S, Gibson E, Brett G. Liquid air energy storage – Analysis and first results from a pilot scale demonstration plant. Appl Energy 2015;137:845–53. doi:10.1016/J.APENERGY.2014.07.109.

[111] Morgan R, Nelmes S, … EG-P of the I, 2015 undefined. An analysis of a large-scale liquid air energy storage system. EprintsBrightonAcUk n.d.

[112] Abdo RF, Pedro HTC, Koury RNN, Machado L, Coimbra CFM, Porto MP. Performance

evaluation of various cryogenic energy storage systems. Energy 2015;90:1024–32. doi:10.1016/j.energy.2015.08.008.

[113] Borri E, Tafone A, Romagnoli A, Comodi G. A preliminary study on the optimal configuration and operating range of a “microgrid scale” air liquefaction plant for Liquid Air Energy Storage. Energy Convers Manag 2017;143:275–85. doi:10.1016/J.ENCONMAN.2017.03.079.

[114] Guizzi GL, Manno M, Tolomei LM, Vitali RM. Thermodynamic analysis of a liquid air energy storage system. Energy 2015;93:1639–47. doi:10.1016/j.energy.2015.10.030.

[115] Chino K, Araki H. Evaluation of energy storage method using liquid air. Heat Transf Res 2000;29:347–57. doi:10.1002/1523-1496(200007)29:5<347::AID-HTJ1>3.0.CO;2-A.

[116] Antonelli M, Barsali S, Desideri U, Giglioli R, Paganucci F, Pasini G. Liquid air energy storage: Potential and challenges of hybrid power plants. Appl Energy 2017;194:522–9. doi:10.1016/J.APENERGY.2016.11.091.

[117] Krawczyk P, Szabłowski Ł, Karellas S, Kakaras E, Badyda K. Comparative thermodynamic analysis of compressed air and liquid air energy storage systems. Energy 2018;142:46–54. doi:10.1016/J.ENERGY.2017.07.078.

[118] Kantharaj B, Garvey S, Pimm A. Compressed air energy storage with liquid air capacity extension. Appl Energy 2015;157:152–64. doi:10.1016/J.APENERGY.2015.07.076.

[119] Kantharaj B, Garvey S, Pimm A. Thermodynamic analysis of a hybrid energy storage system based on compressed air and liquid air. Sustain Energy Technol Assessments 2015;11:159–64. doi:10.1016/J.SETA.2014.11.002.

[120] Hamdy S, Morosuk T, Tsatsaronis G. Cryogenics-based energy storage: Evaluation of cold exergy recovery cycles. Energy 2017;138:1069–80.

doi:10.1016/J.ENERGY.2017.07.118.

[121] Gil A, Medrano M, Martorell I, … AL-… and SE, 2010 undefined. State of the art on high temperature thermal energy storage for power generation. Part 1—Concepts, materials and modellization. Elsevier n.d.

[122] Medrano M, Gil A, Martorell I, … XP-… and SE, 2010 undefined. State of the art on high-temperature thermal energy storage for power generation. Part 2—Case studies. Elsevier n.d.

[123] Peng H, Dong H, Ling X. Thermal investigation of PCM-based high temperature thermal energy storage in packed bed. Energy Convers Manag 2014;81:420–7. doi:10.1016/J.ENCONMAN.2014.02.052.

[124] Barbour E, Mignard D, Ding Y, Li Y. Adiabatic Compressed Air Energy Storage with packed bed thermal energy storage. Appl Energy 2015;155:804–15. doi:10.1016/J.APENERGY.2015.06.019.

[125] Peng H, Li R, Ling X, Dong H. Modeling on heat storage performance of compressed air in a packed bed system. Appl Energy 2015;160:1–9. doi:10.1016/J.APENERGY.2015.09.029.

[126] Coutier JP, Farber EA. Two applications of a numerical approach of heat transfer process within rock beds. Sol Energy 1982;29:451–62. doi:10.1016/0038-092X(82)90053-6.

[127] Adeyanju AA, Manohar K. Theoretical and experimental investigation of heat transfer in packed beds 2009;4:166–77.

[128] Villatoro FR, Pérez J, Santander JLG, Borovsky MA, Ratis YL, Izzheurov EA, et al. Perturbation analysis of the heat transfer in porous media with small thermal conductivity. J Math Anal Appl 2011;374:57–70. doi:10.1016/J.JMAA.2010.08.038.

[129] Peng H, Yang Y, Li R, Ling X. Thermodynamic analysis of an improved adiabatic compressed air energy storage system. Appl Energy 2016;183:1361–73. doi:10.1016/J.APENERGY.2016.09.102.

[130] Peng H, Shan X, Yang Y, Ling X. A study on performance of a liquid air energy storage system with packed bed units. Appl Energy 2018;211:126–35. doi:10.1016/J.APENERGY.2017.11.045.

[131] Sciacovelli A, Vecchi A, Ding Y. Liquid air energy storage (LAES) with packed bed cold thermal storage – From component to system level performance through dynamic modelling. Appl Energy 2017;190:84–98. doi:10.1016/J.APENERGY.2016.12.118.

[132] Li Y, Cao H, Wang S, Jin Y, Li D, Wang X, et al. Load shifting of nuclear power plants using cryogenic energy storage technology. Appl Energy 2014;113:1710–6. doi:10.1016/J.APENERGY.2013.08.077.

[133] Lee I, Park J, Moon I. Conceptual design and exergy analysis of combined cryogenic energy storage and LNG regasification processes: Cold and power integration. Energy 2017;140:106–15. doi:10.1016/J.ENERGY.2017.08.054.

[134] Kim J, Noh Y, Chang D. Storage system for distributed-energy generation using liquid air combined with liquefied natural gas. Appl Energy 2018;212:1417–32. doi:10.1016/J.APENERGY.2017.12.092.

[135] Pinch Technology: Basics for Beginners - Heat Transfer - Articles - Chemical Engineering - Frontpage - Cheresources.com n.d. http://www.cheresources.com/content/articles/heat-transfer/pinch-technology-basics-for-beginners?pg=3 (accessed May 23, 2018).

[136] Linnhoff B, Flower JR. Synthesis of heat exchanger networks: I. Systematic generation of energy optimal networks. AIChE J 1978;24:633–42. doi:10.1002/aic.690240411.

[137] Linnhoff B, Flower JR. Synthesis of heat exchanger networks: II. Evolutionary generation of networks with various criteria of optimality. AIChE J 1978;24:642–54. doi:10.1002/aic.690240412.

[138] Linnhoff B. Thermodynamic Analysis in the Design of Process Networks 1979.

[139] Linnhoff B, Hindmarsh E. The pinch design method for heat exchanger networks. Chem Eng Sci 1983;38:745–63. doi:10.1016/0009-2509(83)80185-7.

[140] Ebrahim M, Kawari A-. Pinch technology: an efficient tool for chemical-plant energy and capital-cost saving. Appl Energy 2000;65:45–9. doi:10.1016/S0306-2619(99)00057-4.

[141] Kemp I. Pinch analysis and process integration: a user guide on process integration for the efficient use of energy. 2011.

[142] Asante NDK, Zhu XX. An automated approach for heat exchanger network retrofit featuring minimal topology modifications. Comput Chem Eng 1996;20:S7–12. doi:10.1016/0098-1354(96)00013-0.

[143] Nist. NIST reference fluid thermodynamic and transport properties-REFPROP. … Chem Prop … 2002.

[144] Energy storage-a revolution in the air. Mod Power Syst 2013:32. http://viewer.zmags.com/publication/388070e3# /388070e3/32 (accessed April 19, 2018).

[145] Bindra H, Bueno P, Morris JF, Shinnar R. Thermal analysis and exergy evaluation of packed bed thermal storage systems. Appl Therm Eng 2013;52:255–63. doi:10.1016/J.APPLTHERMALENG.2012.12.007.

[146] Zanganeh G, Pedretti A, Zavattoni S, Barbato M, Steinfeld A. Packed-bed thermal storage for concentrated solar power – Pilot-scale demonstration and industrial-scale design. Sol Energy 2012;86:3084–98. doi:10.1016/J.SOLENER.2012.07.019.

[147] Morgan R, Nelmes S, Gibson E, Brett G. Liquid air energy storage – Analysis and first results from a pilot scale demonstration plant. Appl Energy 2015;137:845–53. doi:10.1016/j.apenergy.2014.07.109.

[148] Morgan R. An analysis of a large-scale liquid air energy storage system n.d. doi:10.1680/ener.14.00038.

[149] Kantharaj B, Garvey S, Pimm A. Thermodynamic analysis of a hybrid energy storage system based on compressed air and liquid air. Sustain Energy Technol Assessments 2014. doi:10.1016/j.seta.2014.11.002.

[150] Feidel BJ. Investment performance measurement. J. Wiley; 2003.

[151] Salehin S, Ferdaous MT, Chowdhury RM, Shithi SS, Rofi MSRSRB, Mohammed MA. Assessment of renewable energy systems combining techno-economic optimization with energy scenario analysis. Energy 2016;112:729–41. doi:10.1016/j.energy.2016.06.110.

[152] Gas & Electricity Energy for your Home | npower n.d. http://www.npower.com/home/ (accessed April 19, 2018).

[153] Du S, Wang RZ, Xia ZZ. Optimal ammonia water absorption refrigeration cycle with maximum internal heat recovery derived from pinch technology. Energy 2014;68:862–9. doi:10.1016/J.ENERGY.2014.02.065.

[154] Su W, Zhao L, Deng S, Xu W, Yu Z. A limiting efficiency of subcritical Organic Rankine cycle under the constraint of working fluids. Energy 2018;143:458–66. doi:10.1016/J.ENERGY.2017.11.003.

[155] Şevik S. An analysis of the current and future use of natural gas-fired power plants in meeting electricity energy needs: The case of Turkey. Renew Sustain Energy Rev 2015;52:572–86. doi:10.1016/j.rser.2015.07.102.

[156] Smil V. Natural Gas: Fuel for the 21st Century. 2015.

[157] Wei L, Geng P. A review on natural gas/diesel dual fuel combustion, emissions and performance. Fuel Process Technol 2016;142:264–78. doi:10.1016/j.fuproc.2015.09.018.

[158] Mokhatab S, Mak J, Valappil J, Wood D. Handbook of liquefied natural gas. 2013.

[159] Kumar S, Kwon HT, Choi KH, Hyun Cho J, Lim W, Moon I. Current status and future projections of LNG demand and supplies: A global prospective. Energy Policy 2011;39:4097–104. doi:10.1016/j.enpol.2011.03.067.

[160] Qi C, Wang W, Wang B, Kuang Y, Xu J. Performance analysis of submerged combustion vaporizer. J Nat Gas Sci Eng 2016;31:313–9. doi:10.1016/j.jngse.2016.03.003.

[161] Kanbur BB, Xiang L, Dubey S, Choo FH, Duan F. Cold utilization systems of LNG : A review 2017;79:1171–88. doi:10.1016/j.rser.2017.05.161.

[162] Sun H, Zhu H, Liu F, Ding H. Simulation and optimization of a novel Rankine power cycle for recovering cold energy from liquefied natural gas using a mixed working fluid. Energy 2014;70:317–24. doi:10.1016/j.energy.2014.03.128.

[163] Lee U, Kim K, Han C. Design and optimization of multi-component organic rankine cycle using liquefied natural gas cryogenic exergy. Energy 2014;77:520–32. doi:10.1016/j.energy.2014.09.036.

[164] Shi X, Agnew B, Che D, Gao J. Performance enhancement of conventional combined cycle power plant by inlet air cooling, inter-cooling and LNG cold energy utilization. Appl Therm Eng 2010;30:2003–10. doi:10.1016/j.applthermaleng.2010.05.005.

[165] Shi X, Che D. Thermodynamic analysis of an LNG fuelled combined cycle power plant with waste heat recovery and utilization system. Int J Energy Res 2007;31:975–98. doi:10.1002/er.1293.

[166] Salimpour MR, Zahedi @bullet M A. Proposing a novel combined cycle for optimal exergy recovery of liquefied natural gas n.d. doi:10.1007/s00231-012-0977-y.

[167] Zhang N, Lior N. Configuration Analysis of a Novel Zero CO. Adv. Energy Syst., vol. 2003, ASME; 2003, p. 333–43. doi:10.1115/IMECE2003-41958.

[168] Deng S, Jin H, Cai R, Lin R. Novel cogeneration power system with liquefied natural gas (LNG) cryogenic exergy utilization. Energy 2004;29:497–512. doi:10.1016/j.energy.2003.11.001.

[169] Messineo A, Panno D. Potential applications using LNG cold energy in Sicily. Int J Energy Res 2008;32:1058–64. doi:10.1002/er.1411.

[170] Messineo A, Panno G. LNG cold energy use in agro-food industry: A case study in Sicily. J Nat Gas Sci Eng 2011;3:356–63. doi:10.1016/j.jngse.2011.02.002.

[171] Uwitonze H, Han S, Jangryeok C, Hwang KS. Design process of LNG heavy hydrocarbons fractionation: Low LNG temperature recovery. Chem Eng Process Process Intensif 2014;85:187–95. doi:10.1016/j.cep.2014.09.002.

[172] Tuo H, Li Y. Exergy Analysis of Combined Cycle of Air Separation and Natural Gas Liquefaction. World Acad Sci Eng Technol 2011;5:569–75.